



City Research Online

City, University of London Institutional Repository

Citation: Rackham, J. W. (1992). The design of haunched composite beam frames for buildings. (Unpublished Doctoral thesis, City, University of London)

This is the accepted version of the paper.

This version of the publication may differ from the final published version.

Permanent repository link: <https://openaccess.city.ac.uk/id/eprint/29257/>

Link to published version:

Copyright: City Research Online aims to make research outputs of City, University of London available to a wider audience. Copyright and Moral Rights remain with the author(s) and/or copyright holders. URLs from City Research Online may be freely distributed and linked to.

Reuse: Copies of full items can be used for personal research or study, educational, or not-for-profit purposes without prior permission or charge. Provided that the authors, title and full bibliographic details are credited, a hyperlink and/or URL is given for the original metadata page and the content is not changed in any way.

**THE DESIGN OF
HAUNCHED COMPOSITE BEAM FRAMES
FOR BUILDINGS**

**Dissertation submitted to the City University
in fulfilment of the requirement for the
Degree of Doctor of Philosophy**

by

James William RACKHAM

Department of Civil Engineering

August, 1992

CONTENTS

TITLE PAGE	1
CONTENTS	2
LIST OF FIGURES	8
LIST OF TABLES	16
LIST OF DIAGRAMS	18
ACKNOWLEDGEMENTS	20
DECLARATION	21
ABSTRACT	22
NOTATION	23
REFERENCES	29
1. INTRODUCTION	34
1.1 General Background and Terminology	34
1.1.1 Historical Development and Alternative Systems	34
1.1.2 Use of Haunches and their Manufacture	36
1.1.3 Other Terminology	38
1.2 Aims of This Research	38
1.3 Outline of This Thesis	38
2. DEVELOPMENT OF THE PROPOSED DESIGN METHODS	40
2.1 Consideration of Sway	40
2.2 Design Philosophy	40
2.2.1 General Design Principles	40
2.2.2 Plasticity in the Columns	41
2.2.3 Plasticity within the Haunch Length	41
2.2.4 Premature Failure of Non-Beam Elements	43
2.3 Frame Design using Plastic Principles at the Ultimate Limit State	43
2.3.1 Design Assumptions and Related Research Work	43
2.3.1.1 Lateral Buckling	44
2.3.1.2 Local Buckling	44
2.3.1.3 Hinge Rotation Capacity	45
2.3.2 Design Process using Plastic Principles	49
2.3.3 Haunch Length Optimisation for Plastic Design	51
2.3.4 Restraint of Plastic Hinges	55

2.4	Frame Design Using Elastic Global Analysis and Moment Redistribution Principles at the Ultimate Limit State	56
2.4.1	Introduction	56
2.4.2	The Phenomenum of Moment Redistribution	56
2.4.3	Limitations on Moment Redistribution	57
2.4.4	Application to Haunched Composite Beams	58
2.4.5	Design Process using Elastic Global Analysis	59
2.5	Column Design	62
2.6	Checks at the Serviceability Limit State	64
2.6.1	Stresses and Deflections	64
2.6.2	Dynamic Sensitivity	66
2.7	Connections	69
3.	LATERAL TORSIONAL INSTABILITY	71
3.1	Introduction	71
3.2	Proposed Lateral Distortional Buckling Design Method	72
3.2.1	Determination of the Elastic Critical Buckling Moment	72
3.2.2	Determination of Equivalent Slenderness	84
3.2.3	Effect of Reinforcement in the Concrete Slab	88
3.2.4	Shear Connection Flexibility and Concrete Slab Flexibility	89
3.2.5	Allowance for Varying Moments	96
3.2.6	Modification for Tapered Sections	97
3.2.7	Critical Buckling Length	98
3.2.8	Summary of Lateral Distortional Buckling Check	102
3.3	Comparison of Proposed Method with other Methods	103
3.3.1	Method of Bradford and Johnson	103
3.3.2	Method of Weston, Nethercot and Crisfield	107
3.3.3	Method of Roik, Hanswille and Kina	108
3.3.4	Comparison between Design Methods	112
4.	EXPERIMENTAL WORK: THE SUB-ASSEMBLY TEST	115
4.1	Introduction	115
4.2	Test Design Considerations	116
4.2.1	General Test Arrangement	116
4.2.2	Steel Beams	116
4.2.3	Columns	117
4.2.4	Cuttings	117
4.2.5	Stiffening and Restraint at the Haunch Toe	118
4.2.6	Floor Slab	119
4.2.7	End Connections	119
4.3	Construction	120

4.4	Loading Assembly	121
4.5	Instrumentation	121
4.5.1	Measurement of Haunch Connection Bolt Strains	121
4.5.2	Measurement of Strains in Beams and Knee Braces	122
4.5.3	Measurement of Beam Compression Flange Torsional Rotation	122
4.5.4	Measurement of Flange Lateral Displacements	123
4.5.5	Measurement of Vertical Displacements under the Point Loads	123
4.5.6	Other Displacement Measurements	123
4.5.7	Measurement of the Spread of Plasticity	124
4.6	Material Properties	124
4.7	Sub-Assembly Test Results	126
4.7.1	Bedding-In Test	126
4.7.2	Working Load Test	126
4.7.3	Ultimate Load Test 1	127
4.7.4	Ultimate Load Test 2	128
4.7.5	Ultimate Load Test 3	130
4.7.6	Connection Behaviour	132
4.7.7	Behaviour of the Knee Brace	133
4A.	MEASUREMENT OF AXIAL FORCE IN THE SUB-ASSEMBLY TEST KNEE BRACE FROM STRAIN GAUGE READINGS	135
5.	COMPARISON OF THE SUB-ASSEMBLY TEST RESULTS WITH THEORY	136
5.1	Elastic Stiffness	136
5.2	Maximum Strengths	137
5.3	Lateral Distortional Buckling	138
5.4	Moment/Rotational Characteristics and Haunch Toe Stiffening	144
6.	EXPERIMENTAL WORK: THE MAIN BEAM TEST	148
6.1	Introduction	148
6.2	Design Considerations	148
6.2.1	General Test Arrangement	148
6.2.2	Design of the Test Frame	149
6.2.3	Haunch Design	151
6.2.4	Main Beam Stiffening and Lateral Stability	151
6.2.5	Haunch Heel Connections	152
6.2.6	Column Stiffening	152
6.2.7	Floor Slab	152

6.2.8	Secondary Beams	153
6.2.9	Shear Connector Layout and Longitudinal Shear Reinforcement	153
6.2.10	Reactant Frames	154
6.2.11	Column Base Supports	154
6.3	Construction	154
6.4	Loading Assembly	157
6.5	Instrumentation	157
6.5.1	Equipment Specification	157
6.5.2	Measurement of Strains in the Steel Members	158
6.5.3	Measurement of Displacements	159
6.5.4	Measurement of Strains in the Concrete Slab	159
6.5.5	Measurement of Column Verticality	160
6.5.6	Measurement of Vertical Loads	160
6.5.7	Measurement of the Spread of Plasticity	161
6.6	Material Properties	161
6.7	Main Beam Test Results	163
6.7.1	The Dynamic Test	163
6.7.2	Bedding-In Test	163
6.7.3	Working Load Test 1	164
6.7.4	Working Load Test 2	165
6.7.5	Ultimate Load Test 1	167
6.7.6	Ultimate Load Test 2	168
6A.	ANALYSES OF MAIN BEAM DYNAMIC TEST	172
6A.1	Natural Frequency	172
6A.2	Logarithmic Decrement	172
6A.3	Damping Ratio	173
7.	COMPARISON OF THE MAIN BEAM TEST RESULTS WITH THEORY	174
7.1	Dynamic Behaviour	174
7.2	Elastic Behaviour	176
7.3	Plastic Behaviour	178
7.3.1	Haunch Toe Strength	178
7.3.2	Mid-Span Composite Strength	179
7.3.3	Frame Strength	180
7.A	MAIN BEAM TEST ELASTIC SECTION PROPERTIES	183
7A.1	Short-Term Uncracked Composite Stiffness	183
7A.2	Composite Uncracked Section - Elastic Neutral Axis Position	184

7.B	MAIN BEAM TEST PLASTIC SECTION PROPERTIES - USING MEASURED DIMENSIONS	185
7B.1	Bare Steel Section-Plastic Neutral Axis Position	185
7B.2	Bare Steel Section-Plastic Moment of Resistance	186
7B.3	Combined Section (Steel Beam, Decking and Mesh) - Plastic Neutral Axis Position	187
7B.4	Combined Section (Steel Beam, Decking and Mesh) - Plastic Moment of Resistance	189
7B.5	Composite Section at Mid-Span - Plastic Neutral Axis Position	190
7B.6	Composite Section at Mid-Span - Plastic Moment of Resistance	191
8.	COMPUTER STUDIES	192
8.1	Introduction	192
8.2	Analysis of the Sub-Assembly Tests	193
8.2.1	Elastic Numerical Model and Analyses	193
8.2.2	Elasto-Plastic Numerical Model	194
8.2.3	Elasto-Plastic Results and Discussion	195
8.3	Analysis of the Main Beam Test	197
8.3.1	Numerical Model	197
8.3.2	Results of the Main Beam Test Analysis	198
8.4	Haunch Parametric Study	198
8.4.1	Introduction	198
8.4.2	Numerical Model	199
8.4.3	Results of Haunch Parametric Study	199
8.4.4	Work by Other Researchers	202
8.4.5	Design Recommendations from Parametric Study . . .	203
9.	CONCLUSIONS, RECOMMENDATIONS AND FUTURE WORK .	206
9.1	Conclusions and Recommendations	206
9.1.1	General	206
9.1.2	Dynamic Behaviour of the Main Beam Test	206
9.1.3	Elastic Behaviour of the Tests	206
9.1.4	Section Classification	207
9.1.5	Hogging Region Moment Capacity	207
9.1.6	Sagging Region Moment Capacity	208

9.1.7	Local and Lateral Buckling	208
9.1.7.1	Test Behaviour	208
9.1.7.2	Comparison of Test Behaviour with Theory	208
9.1.7.3	Comparison of the Proposed Method with Other Methods	209
9.1.7.4	Influence of Slab Flexibility	209
9.1.8	Moment/Rotation Characteristics	210
9.1.9	Computer Studies	210
9.1.9.1	Moment/Rotation Characteristics	210
9.1.9.2	Element Forces at the Haunch Toe . . .	211
9.1.10	Beam to Column Connections	212
9.2	Design Example	212
9.3	Future Work	213
9.3.1	Computer Studies	213
9.3.2	Future Testing	213
9A.	DESIGN EXAMPLE	214

LIST OF FIGURES

- 1.1 Some Alternative Composite Beam Structural Forms used in Buildings
- 1.2 Different Configurations of Haunched Composite Beams
- 1.3 Summaries of Frame Weights and Opening Sizes of Various Structural Systems based on a 6-storey 15m Single-Bay Building

- 2.1 Haunch Design Moment versus Capacity based on a 457 x 191 UB 67 Beam and Cutting
- 2.2 Haunch Length Optimisation for a Haunched Beam subject to a UDL
- 2.3 Relationship Between the Bending Resistances of the Haunch Heel and the Beam
- 2.4 Ratio of Plastic Moment Capacity of the Composite Section to that of the Steel Section
- 2.5 Frequency Modification Factor for a Single-Storey Symmetrical Sub-Frame subject to Symmetric Loading

- 3.1 Equivalent Slenderness Values for a 457 x 152 UB 82 Section Grade 50, According to Various Buckling Design Methods
- 3.2 Design Strength Ratio versus Slenderness for a 457 x 152 UB 82 Section Grade 50, According to Various Buckling Design Methods

- 4.1 Sub-Assembly Test - Specimen General Arrangement
- 4.2 Sub-Assembly Test - Beam B2 Haunch Knee Brace Detail
- 4.3 Sub-Assembly Test - Erected Structure
- 4.4 Sub-Assembly Test - Prior to Pouring the Slab

- 4.5 Sub-Assembly Test - Pouring the Concrete Slab
- 4.6 Sub-Assembly Test - As-Built Dimensions
- 4.7 Sub-Assembly Test - Loading Frame Assembly
- 4.8 Sub-Assembly Test - Typical Jacking System
- 4.9 Sub-Assembly Test - Strain-Gauged Bolt Layout
- 4.10 Sub-Assembly Test - Strain-Gauged Bolt
- 4.11 Sub-Assembly Test - Strain Gauge Arrangement for Beams B1 and B2
- 4.12 Sub-Assembly Test - Strain Gauge Arrangement for Beams B3 and B4
- 4.13 Sub-Assembly Test - Torsional Rotation Measurement Gauges
- 4.14 Sub-Assembly Test - Positioning the Graded Staff for Lateral Displacement Measurement
- 4.15 Sub-Assembly Test - Torsional Rotation and Lateral Movement measurement Arrangement
- 4.16 Sub-Assembly Test - Displacement Gauge Arrangement for Beams B1 and B2
- 4.17 Sub-Assembly Test - Displacement Gauge Arrangement for Beams B3 and B4
- 4.18 Sub-Assembly Test - Haunch Moment/Rotation Behaviour of Beam 1
- 4.19 Sub-Assembly Test - Haunch Moment/Rotation Behaviour of Beam 2
- 4.20 Sub-Assembly Test - Haunch Moment/Rotation Behaviour of Beam 3
- 4.21 Sub-Assembly Test - Haunch Moment/Rotation Behaviour of Beam 4
- 4.22 Sub-Assembly Test - Comparison of Compression Flange Lateral Movement at the Haunch Toe Positions
- 4.23 Sub-Assembly Test - Comparison of the Relative Lateral Displacements Between the Tension and Compression Flanges at Selected End Slopes

- 4.24 Sub-Assembly Ultimate Load Test 1 - Local Flange Buckle in Beam B2
- 4.25 Sub-Assembly Ultimate Load Test 2 - Cracking in the Concrete slab Above Beams B1 and B3
- 4.26 Sub-Assembly Ultimate Load Test 2 - Cracking in the Concrete slab Above Beams B2 and B4
- 4.27 Sub-Assembly Ultimate Load Test 2 - Cracking in the Slab Above the Haunch Toe of Beam B1
- 4.28 Sub-Assembly Ultimate Load Test 2 - Local Buckling of Beam B2 and Shearing of Knee Brace Connections
- 4.29 Sub-Assembly Ultimate Load Test 2 - Local Buckling Beyond the Haunch Toe of Beam B3
- 4.30 Sub-Assembly Ultimate Load Test 2 - Local Buckling Beyond the Haunch Toe of Beam B4
- 4.31 Sub-Assembly Ultimate Load Test 2 - Local Web and Flange Buckling of Beam B1
- 4.32 Sub-Assembly Ultimate Load Test 2 - Local Web and Flange Buckling of Beam B3
- 4.33 Sub-Assembly Ultimate Load Test 3 - Local Buckling of Beam B1
- 4.34 Sub-Assembly Ultimate Load Test 3 - Local Buckling of Beam B2 and Shearing of the Knee Brace Connections
- 4.35 Sub-Assembly Ultimate Load Test 3 - Buckling of Beam B3
- 4.36 Sub-Assembly Ultimate Load Test 3 - Buckling of Beam B4
- 4.37 Sub-Assembly Ultimate Load Test 3 - Detail of Local Buckling of Beam B1
- 4.38 Sub-Assembly Ultimate Load Test 3 - Detail of Local Buckling of Beam B2
- 4.39 Sub-Assembly Ultimate Load Test 3 - Lateral Distortional Buckling of Beam B2

- 4.40 Sub-Assembly Ultimate Load Test 3 - Final Deformation of Test Structure
- 4.41 Sub-Assembly Ultimate Load Test 1 - Haunch Connection Bolt Force Growth in Beam B1
- 4.42 Sub-Assembly Ultimate Load Test 2 - Haunch Connection Bolt Force Growth in Beam B1
- 4.43 Sub-Assembly Ultimate Load Test 3 - Haunch Connection Bolt Force Growth in Beam B1
- 4.44 Sub-Assembly Ultimate Load Test 1 - Haunch Connection Bolt Force Profiles
- 4.45 Sub-Assembly Ultimate Load Test 2 - Haunch Connection Bolt Force Profiles
- 4.46 Sub-Assembly Ultimate Load Test 3 - Haunch Connection Bolt Force Profiles
- 4.47 Sub-Assembly Load Ultimate Load Tests 1 and 2 - Growth in Knee Brace Force with Haunch Toe Moment for Beam B2
- 4.48 Sub-Assembly Ultimate Load Tests 1 and 2 - Horizontal Component of Knee Brace Expressed as a Percentage of the Haunch Toe Compression Flange Force in Beam B2, against the Beam End Slope
- 5.1 Sub-Assembly Test - Progressive Lowering of the Neutral Axis on Beam B1 with Beam Deformation
- 5.2 Sub-Assembly Test - Comparison of Non-Linear Moment/Rotation Behaviour
- 6.1 Main Beam Test - Multi-Storey Frame Arrangement Modelled by the Test
- 6.2 Main Beam Test - Specimen General Arrangement
- 6.3 Main Beam Test - Reactant Frame General Arrangement
- 6.4 Main Beam Test - Column Base Support Assembly
- 6.5 Main Beam Test - Structure Prior to Casting Floor

- 6.6 Main Beam Test - Sockets for Loading Frame Pull-Down Rods
- 6.7 Main Beam Test - Floor Detail Around a Column
- 6.8 Main Beam Test - Casting the Slab
- 6.9 Main Beam Test - The As-Built Dimensions
- 6.10 Main Beam Test - Arrangement of the Loading Systems
- 6.11 Main Beam Test - The Central Loading Frame and one of the Outer Loading Frames
- 6.12 Main Beam Test - Electrical Resistance Strain Gauge Layout
- 6.13 Main Beam Test - Frame Displacement and Column Verticality Measurement Arrangements
- 6.14 Main Beam Test - Vibrating Wire Strain Gauge Layout
- 6.15 Main Beam Test - A Vibrating Wire Strain Gauge
- 6.16 Main Beam Test - Graded Staff Arrangement for Column Verticality Check
- 6.17 Main Beam Test - Dynamic 'Heel Drop' Test Plot
- 6.18 Main Beam Test - Growth of Horizontal Column Reactions with Span Loading
- 6.19 Main Beam Working Load Test 1 - Span Loading versus Central Deflection
- 6.20 Main Beam Test - Span Load versus Central Deflection
- 6.21 Main Beam Test - Haunch Toe B5 Moment Rotation Characteristics
- 6.22 Main Beam Test - Haunch Toe B6 Moment/Rotation Characteristics
- 6.23 Main Beam Test - Typical Longitudinal Strain Profiles for Half of the Span
- 6.24 Main Beam Working Load Test 2 - Cracking in the Slab above the Haunches
- 6.25 Main Beam Test - Degree of Span Load Supported by the Main Columns

- 6.26 Main Beam Ultimate load Test 1 - Buckling and Yielding Adjacent to the Haunch Toes
- 6.27 Main Beam Ultimate Load Tests 1 & 2 - Hinge Moments versus Mid-Span Deflection
- 6.28 Main Beam Ultimate Load Test 1 - Growth in Moments at the Hinge Positions with Span Loading
- 6.29 Main Beam Ultimate Load Tests 1 & 2 - Typical Bending Moment Profiles
- 6.30 Main Beam Ultimate Load Test 1 - Growth of Horizontal Column Reactions with Span Loading
- 6.31 Main Beam Ultimate Load Test 2 - Cracking in the Slab
- 6.32 Main Beam Ultimate Load Test 2 - Diagonal Cracking in the Slab Close to Column C4
- 6.33 Main Beam Ultimate Load Test 2 - Concrete Longitudinal Strain Contours on Half of the Span
- 6.34 Main Beam Ultimate Load Test 2 - Transverse Profiles of Longitudinal Concrete Strain
- 6.35 Main Beam Ultimate Load Test 2 - Transverse Concrete Strain Profiles
- 6.36 Main Beam Ultimate Load Test 2 - Growth in Moments at the Hinge Positions with Span Loading
- 6.37 Main Beam Ultimate Load Test 2 - Buckling and Yielding Adjacent to the Haunch Toes
- 6.38 Main Beam Ultimate Load Test 2 - Beam Deformation Near the Haunches
- 6.39 Main Beam Ultimate Load Test 2 - Growth of Horizontal Column Reactions with Span Loading
- 6.40 Main Beam Ultimate Load Test 2 - Final Deformation of Test Structure

- 7.1 Typical Cross-Sectional Strain Diagrams for Selected Positions Along the Main Beam
- 7.2 Cross-Sectional Strain Diagram at the Main Beam Mid-Span Position

- 8.1 Computer Studies - Typical Finite Element Model for Elastic Analysis of the Sub-Assembly Tests
- 8.2 Computer Studies - Typical Finite Element Model for Non-Linear Analysis of the Sub-Assembly Tests
- 8.3 Sub-Assembly Tests - Initial Imperfections used in the Non-Linear Analysis
- 8.4 Computer Studies - Model Stress/Strain Curves for Sub-Assembly Test Beam B1
- 8.5 Computer Studies - Model Stress/Strain Curves for Sub-Assembly Test Beam B2
- 8.6 Computer Studies - Model Stress/Strain Curves for Sub-Assembly Test Beam B3
- 8.7 Computer Studies - Model Stress/Strain Curves for Sub-Assembly Test Beam B4
- 8.8 Computer Results - Haunch Toe Moment/Rotation Comparison for Sub-Assembly Test Beam B1
- 8.9 Computer Results - Haunch Toe Moment/Rotation Comparison for Sub-Assembly Test Beam B2
- 8.10 Computer Results - Haunch Toe Moment/Rotation Comparison for Sub-Assembly Test Beam B3
- 8.11 Computer Results - Haunch Toe Moment/Rotation Comparison for Sub-Assembly Test Beam B4
- 8.12 Computer Results - Influence of Maximum Imperfection on the Behaviour of Sub-Assembly Test Beam B2

- 8.13 Computer Results - The Deformed Shape of Beam B4
- 8.14 Computer Results - Moment/Lateral Displacement Comparisons for Sub-Assembly Test Beams B2 & B4
- 8.15 Computer Results - Moment/Lateral Displacement Comparisons for Sub-Assembly Test Beams B1 & B3
- 8.16 Computer Results - Comparison of Lateral Displacement Profiles for the Compression Flanges in the Sub-Assembly Beam Tests
- 8.17 Computer Studies - Main Beam Test Finite Element Model
- 8.18 Computer Studies - Haunch Toe Force Ratios $F1/F0$ and $F4/F0$ versus the Cutting Depth/Length Ratio
- 8.19 Computer Studies - Haunch Toe Force Ratios $F2/F0$ and $F3/F0$ versus the Cutting Depth/Length Ratio
- 8.20 Computer Studies - Maximum Cutting Weld Stress Relationship with the Cutting Depth/Length Ratio
- 8.21 Computer Studies - Cutting Web Weld Stress Profile - Case $L_c = D$
- 8.22 Computer Studies - Cutting Web Weld Stress Profile - Case $L_c = 2D$
- 8.23 Computer Studies - Cutting Web Weld Stress Profile - Case $L_c = 3D$
- 8.24 Computer Studies - Cutting Web Weld Stress Profile - Case $L_c = 4D$

LIST OF TABLES

- 2.1 Maximum Redistribution of Support Moments in Continuous Composite Beams According to Section Classification

- 3.1 Factor 'r' for Various Beam Conditions

- 3.2 Example 1 - British Rolled Steel Sections for which Torsional Restraint to the Top Flange Cannot be Assumed

- 3.3 Example 2 - British Rolled Steel Sections for which Torsional Restraint to the Top Flange Cannot be Assumed

- 4.1 Sub-Assembly Test - Steel Beam Material Properties

- 4.2 Sub-Assembly Test - Average Concrete Cube Compressive Strengths and Cylinder Tensile Strengths

- 4.3 Sub-Assembly Test - Mesh Reinforcement Properties (Type A142)

- 4.4 Sub-Assembly Ultimate Load Test 1 - Growth in Concrete Cracking over Beams B1 and B3

- 5.1 Sub-Assembly Test - Maximum Haunch Toe Moments Compared with Predicted Plastic Strengths

- 5.2 Sub-Assembly Test - Theoretical and Test Values of Lateral Distortional Buckling Length

- 5.3 Sub-Assembly Test - Predicted Buckling Moment Values Using Method of Chapter 3

- 5.4 Sub-Assembly Test - Modified Values of the Predicted Buckling Moments using Actual Test Buckling Lengths

- 5.5 Sub-Assembly Test - Modification Factors for v_t Necessary to Ensure that $\lambda_{LT} = 30$ for the Test Beams

- 5.6 Sub-Assembly Test - Comparison of Various Theoretical Buckling Moment Resistances in kNm
- 5.7 Sub-Assembly Test - Model Factors for the Various Theoretical Buckling Moment Resistances
- 5.8 Sub-Assembly Test - Comparison of Haunch Toe Beam Strengths at a Rotation of 3°
- 5.9 Sub-Assembly Test - Available Haunch Toe Rotations

- 6.1 Main Beam Test - Main Steel Beam Material Properties
- 6.2 Main Beam Test - Concrete Slab Material Properties
- 6.3 Main Beam Test - Mesh Reinforcement Properties (Type A193)
- 6.4 Main Beam Test - Shear Reinforcement Properties (T16's)
- 6.5 Main Beam Test - Decking Material Properties

- 8.1 Computer Studies - Results from the Main Beam Analysis
- 8.2 Computer Haunch Parametric Study - Design Values of τ/σ at the Haunch Heel for Various Haunch Lengths

LIST OF DIAGRAMS

- 1.1 A Typical 'Cutting' Fabrication Plan
- 1.2 A Typical Haunch/Column Detail

- 2.1 Postulated Moment/Rotation Relationship for a Composite Sagging Region Section (Johnson and Hope-Gill {22})
- 2.2 Postulated Moment/Rotation Relationship for a Hogging Region Section in a Continuous Composite Beam (Johnson and Hope-Gill {22})
- 2.3 The Plastic Collapse Bending Moment Diagram for a Typical Single-Span 'Sub-Frame'
- 2.4 Example of a Sub-Frame for the Elastic Global Analysis of a Beam
- 2.5 Design Moments and Ultimate Moment Resistance Envelope for a Beam within a Typical Single-Span Sub-Frame
- 2.6 Typical Sub-Frame for the Design of a Column Element

- 3.1 Beam Element and Cross-sectional Deformation
- 3.2 Element for Calculating Web Bending Energy
- 3.3 Element for Calculating Web Torsional Energy
- 3.4 Element and Stress Distribution for Calculating the Work Done by the Forces in the Web
- 3.5 Buckled Shape of Two Adjacent Beams with a Connecting Single-Span Concrete Floor Slab
- 3.6 Elastic Critical Buckling Moment versus the Beam Buckled Length

- 4A.1 Sub-Assembly Test - Strain Gauge Arrangements in Knee Brace

- 7.1 Plastic Collapse Equilibrium Diagram for one Half of the Main Beam Span

- 7B.1 Main Beam Test - Bare Steel Section

- 7B.2 Main Beam Test - Combined Section (Steel Beam + Decking + Mesh)

- 7B.3 Main Beam Test - Composite Section at Mid-Span

- 8.1 Haunch Forces Determined by Computer Study

ACKNOWLEDGEMENTS

I would first like to thank my supervisor Dr L F Boswell for his support and guidance throughout the duration of this work and, in particular, for his assistance in arranging and co-ordinating the experimental programme. Thanks are also due to Dr Boswell for arranging for Dr Li to carry out the computer analysis of the tests and for providing him with technical guidance. I am grateful to Dr Li for allowing me to quote the results of his work, which are duly acknowledged in the text.

I am also greatly indebted to my industrial supervisor from the Steel Construction Institute, Dr R M Lawson. It has been a privilege to work with Dr Lawson and I am enormously appreciative of his encouragement and technical advice. The Steel Construction Institute has provided me with financial support as well as placing their facilities at my disposal, and for this I would like to thank its director, Dr G W Owens, and his staff.

I would also like to acknowledge the financial support given to the project by the Science and Engineering Research Council and the British Steel Market Development Fund, which has enabled the full-scale testing to be carried out. Materials from the tests were kindly donated by several companies and thanks are due to Messrs F R Fox and D M Drane of Bourne Steel Limited, Mr N J Day of Quikspan Construction Limited, Mr W Tosh of Haywood Engineering and Mr D Smith of Delta Structural Services.

A special mention should be made of the technical staff within the structures group at City University, including the Departmental Superintendent, Mr W A R Jones and his staff: Mr A Bonomini, Mr L Ansdale, Mr V Bullemor, Mr J Rose and Mr P K Mennell.

Finally, I would like to thank my wife Carol for her continued moral support during the course of this work and my good friend Mr S V Payne for his help in proof-reading the thesis.

DECLARATION

I wish to declare that the contents of this thesis are my own original work, except where specifically acknowledged otherwise. The work has not been submitted previously to any University for a degree, diploma or other qualification. The work was carried out at City University, and the Steel Construction Institute between 1987 and 1992.

I grant powers of discretion to the City University Librarian to allow single copies of this thesis to be made without further reference to me.

J W Rackham

ABSTRACT

This thesis examines the design and overall behaviour of haunched composite beam frames braced against sidesway. It has been compiled as a result of both a theoretical and an experimental study.

A detailed design method is presented, which incorporates options for plastic or elasto-plastic analysis at the Ultimate Limit State. A method for checking the susceptibility to lateral instability in the hogging regions of composite beams is also presented, and it has been developed by using elastic energy theory. The design method is intended to be applied in conjunction with the British Standard for the design of steel-framed building structures, BS5950 Parts 1 and 3, although the engineering principles involved could be used with other countries' codes. A detailed design example is also included to demonstrate the application of the method. A review of other relevant experimental and theoretical work has also been undertaken and is critically appraised where appropriate.

The experimental programme carried out as part of this work involved two full-scale tests, and these are described. Particular attention was given to the stiffening details at the shallow end of the haunches, and several options were tested. The most successful proved to be that where full-depth web stiffeners were fitted at this position. Analyses of the tests are included and they show that the theoretical predictions are generally slightly conservative.

A finite element model of the hogging region of a haunched composite beam was also developed, and this was applied to one of the tests. The results of this are presented. It is intended that this particular work will enable further computer simulations to be carried out.

To enable early dissemination of the ideas developed in this thesis, during the course of this work an interim design guide, written jointly by this author and his industrial supervisor, Dr R M Lawson, was published by the Steel Construction Institute.

NOTATION

a	Distance of lateral restraint above the steel beam neutral axis
A	Cross-sectional area of steel beam section
A_c	Area of concrete slab
A_f	Area of one steel beam flange
A_r	Area of concrete slab longitudinal reinforcement
b	Span of the concrete floor slab, ie, distance between haunched beams
b_f	Steel beam flange width (= B)
B	Steel beam flange width
B_e	Effective breadth of concrete floor slab
c	A buckling parameter for tapered sections
C_4	A property of the distribution of the bending moments along the beam
d	Depth of web
d_n	Distance above upper steel beam flange to the neutral axis of the concrete slab
D	Beam depth
D_c	Cutting depth
D_h	Haunch heel depth
D_p	Overall depth of profiled decking
D_s	Depth of concrete floor slab
E	Young's modulus of steel
E_{cn}	Young's modulus of concrete
$E_1, E_2 \text{ etc}$	Energy quantities
f	Beam natural frequency
f_{cu}	Cube strength of concrete
f_o	Simply-supported beam frequency
$F_0, F_1 F_2 \text{ etc}$	Forces in the haunch elements
G	Shear modulus of steel
h	Storey height
h_D	Haunch depth
h_s	Distance between steel beam flange shear centres

H	Column horizontal reactions in the Main Beam Test
I	Second moment of area
I_{afz}	Second moment of area of bottom steel beam flange about the minor axis, ie, $I_{afz} \approx I_y / 2$
I_c	Second moment of area of column
I_{cn}	Second moment of area of concrete floor slab
I_g	Second moment of area of uncracked beam section
I_w	Second moment of area per unit depth of steel beam web (= $t_w^3 / 12$)
I_x	Major axis second moment of area of steel beam
I_y	Minor axis second moment of area of steel beam
J	1: torsional constant of steel beam section
J	2: load on beam from one jack in the Main Beam Test
J_f	Torsional constant of bottom steel beam flange
J_w	Torsional constant of steel beam web
k_c	Geometric property of steel beam cross-section
k_f	Frequency modification factor
k_s	Transverse stiffness per unit length of beam including effect of concrete slab
L	Beam span
L_c	Length of cutting
L_{cr}	Critical buckling length
L_o	Quarter-wave buckling length
M_b	Buckling resistance moment
M_b^*	Modified buckling resistance moment based on test buckling lengths
$M_{b(0.77)}$	Buckling resistance moment with moment modification factor $n_t = 0.77$
M_c	Plastic moment of resistance of composite section at sagging region hinge
M_{cr}	Elastic critical buckling moment
M_{dl}	Buckling resistance moment according to European codes EC3 and EC4

M_{d2}	Buckling resistance moment according to method of Weston et al
M_h	Unmodified plastic design moment on column centre-line
M_{hc}	Haunch heel (ie, beam to column) connection strength
M_{he}	Elastic haunch heel strength
M_{max}	Maximum moment of resistance recorded in the test
M_n	Plastic moment of resistance at haunch toe
M_o	Maximum free bending moment
M_p	Plastic moment of resistance
$M_{p(A)}$	Plastic moment of resistance of steel section alone
$M_{p(B)}$	Plastic moment of resistance of steel beam and reinforcing mesh
$M_{p(design)}$	Plastic moment of resistance of steel section according to BS 5950 Part 1
M_s	Bare steel beam plastic moment of resistance
$M_{support}$	Moment at the support
M_u	Component of moment applied to knee brace in Sub-Assembly Test
M_v	Component of moment applied to knee brace in Sub-Assembly Test
M_1 & M_2	1: Beam end bending moments
M_1, M_2 etc	2: Resistance moments along buckling check length
n	number of dynamic cycles
n_t	Slenderness correction factor for moments
N_E	The greater of applied moment value N_1 and N_5 (see below)
N_s	The greater of applied moment values N_2, N_3 and N_4 (see below)
N_1, N_2 etc	Applied moments along buckling check length
p_b	Steel beam bending strength
p_y	Steel yield stress
q	Ratio of tapered beam length to buckling check length
r	1: concrete floor slab flexibility factor
r	2: number of halfwaves in buckled length

r_a	Available rotation at a particular cross-section, e.g. at a plastic hinge position
r_r	Required available rotation at a particular cross-section, e.g. at a plastic hinge position
r_y	Minor axis radius of gyration
r_{yb}	Minor axis radius of gyration of bottom steel flange only
R	Ratio of greater depth to lesser depth of the steel beam section over the buckling check length
S_x	Major axis plastic modulus of steel beam
t_w	Steel beam web thickness
T_f	Steel beam flange thickness
$T_1, T_2 \text{ etc}$	Vibrating wire strain gauge readings
u	1: lateral displacement of steel beam web, during buckling
u	2: buckling parameter of steel beam section
v	Lateral displacement of steel beam flange during buckling
v_t	Slenderness factor of steel beam section
v_l	Lateral displacement of bottom steel beam flange due to floor slab flexibility
V	Amplitude of lateral buckle of steel beam flange
W	load
$W_1, W_2 \text{ etc}$	Beam loads
x	1: a distance measured along the beam
x	2: torsional index of the steel beam section
x_p	Distance to plastic neutral axis from underside of bottom steel flange
x_r, x_{r+p}	Dynamic displacement magnitudes
y	Maximum short term beam deflection due to self-weight of the structure that the beam is supporting
y_g	Depth of elastic neutral axis below top of concrete slab in an uncracked composite beam condition
z	A distance measured down steel beam web
Z_e	Elastic steel beam modulus about bottom steel flange centroid
Z_{er}	Elastic modulus of reinforced beam section about bottom steel flange centroid

Z_p	Plastic modulus of steel section
α	Ratio of haunch length to beam span
α_e	Modular ratio of steel to concrete
α_x	Angle of twist of steel beam web at a distance z down web
β	1: ratio M_c / M_n
β	2: slenderness ratio ($= \lambda_{LT} \sqrt{p_y/355}$)
γ	1: ratio M_h / M_n
γ	2: dynamic damping ratio
γ_{f3}	Partial safety factor
γ_m	Partial safety factor
δ	Dynamic logarithmic decrement
δ_c	Maximum beam deflection
δ_o	Maximum deflection of a simply-supported beam
$\delta_{(x,z)}$	Initial imperfection function
δ_{10}	Maximum beam deflection when support moments have been reduced by 10%
Δ	Amplitude of initial imperfection
ϵ	Strain
ϵ_u	Strain in the Sub-Assembly Test knee brace due to moment component M_v
η_{LT}	Perry coefficient
θ	1: angle of twist of beam during buckling
θ	2: haunch toe cutting angle
$\bar{\theta}$	Amplitude of angle of twist of beam during buckling
θ_c	Rotation assuming cracked section properties, minus θ_e
θ_e	Rotation assuming uncracked section properties
θ_p	Total inelastic rotation, minus ($\theta_c + \theta_e$)
θ_s	Angle of rotation of steel beam due to floor slab flexibility
λ	Slenderness ($= L/r_y$)
λ_{LT}	Equivalent slenderness ratio ($= (M_p \pi^2 E / M_{cr} p_y)^{0.5}$)
$\bar{\lambda}_{LT}$	Equivalent slenderness ratio ($= (M_p / M_{cr})^{0.5}$)
ν_a	Poisson's ratio for steel
ρ	Density

σ	Longitudinal stress
σ_{cr}	Elastic critical buckling stress
σ_d	Yield stress in steel profile decking
σ_f	Yield stress in steel beam flange
σ_{li}	Basic limiting stress
σ_m	Yield stress in reinforcing mesh
σ_w	Yield stress in steel beam web
τ	Cutting web to beam flange shear stress
ϕ	Angle of twist of buckled steel beam flange
ϕ_c	Stiffness parameter ($I_c L/I_g h$)
χ	A geometric property of the beam incorporating the transverse stiffness
χ_{LT}	Buckling parameter which is a function of the equivalent slenderness $\bar{\lambda}_{LT}$
ψ	A frame moment parameter

REFERENCES

1. CP117 'Composite construction in structural steel and concrete: Part 1 Simply-supported beams in building', British Standards Institute, 1965.
2. CP117 'Composite construction in structural steel and concrete: Part 2 Beams for bridges', British Standards Institute, 1967.
3. Johnson, R. P., 'Composite structures of steel and concrete Vol. 1', Constrado Monograph, Crosby Lockwood Staples, 1975.
4. Lawson, R. M., 'Composite beams and slabs with profiled sheeting', CIRIA Report No. 99, 1983.
5. Gray, B. A., Mullett, D. L. and Walker, H. B., 'Design recommendations for composite floors and beams using steel decks. Section 1. Structural', Constrado, 1983.
6. Calder, I., 'Grand Buildings, Trafalgar Square, London WC2', Steel Construction Today, Vol. 1, No. 6, p180-182, 1990.
7. 'Services in Buildings', Report to be published, Steel Construction Institute.
8. Horne, M. R., 'Determination of the shape of fixed-ended beams for maximum economy according to the plastic theory', Prelim. Pubn. 4th Congr. Intern. Assn. Bridge and Structural Engng., 111. Cambridge, 1952.
9. Lawson, R. M., and Rackham, J. W., 'Design of haunched composite beams in buildings', Steel Construction Institute, 1989.
10. Morris, L. T., and Randall, A. L., 'Plastic design', Constrado, 1975.

11. BS 5950 'Structural use of steelwork in building: Part 1 Code of practice for design in simple and continuous construction: hot rolled sections', British Standards Institution, 1985.
12. BS ENV 1993-1-1 'Eurocode 3: Design of steel structures: Part 1.1: General rules and rules for buildings', to be published Sept 1992.
13. Andrade, S. A. L., and Morris, L. J., 'The influence of stress levels on the behaviour of steel haunched members', 10th Australian Conf. on the Mechanics and Structures and Materials, Australia, 1986.
14. BS 5950 'Structural use of steelwork in building: Part 3 Design in composite construction: Section 3.1: Code of practice for design in simple and continuous composite beams', British Standards Institution, 1990.
15. BS ENV 1994-1-1 'Eurocode 4: Design of steel and composite structures: Part 1.1: General rules and rules for buildings', to be published Jan 1993.
16. Ansourian, P., 'Experiments on continuous composite beams', Proc. Instn. Civ. Engrs, Part 2, 1981, Vol 71, Dec., p25-51.
17. Barnard, P. R. and Johnson, R. P., 'Ultimate strength of composite beams', Proc. Instn. Civ. Engrs, 1965, Vol 32, Oct., p161-179.
18. Barnard, P. R. and Johnson, R. P., 'Plastic behaviour of continuous composite beams', Proc. Instn. Civ. Engrs, 1965, Vol 32, Oct., p180-197.
19. Johnson, R. P. and Hope-Gill, M. C., 'Applicability of simple plastic theory to continuous composite beams, Proc. Instn. Civ. Engrs, Part 2, 1976, Vol 61, Mar., p367-381.
20. Hope-Gill, M. C. and Johnson, R. P., 'Tests on three three-span continuous composite beams', Proc. Instn. Civ. Engrs, Part 2, 1976, Vol 61, June, p367-381.

21. Lawson, R. M., 'Composite beams - appraisal of BS 5950 Part 3.1', Internal Report No. SCI-RT-095, November 1989, Steel Construction Institute.
22. Hope-Gill, M. C., 'Redistribution in composite beams', The Structural Engineer, Vol 57B, No. 1, March 1979.
23. 'Fully rigid multi-storey welded steel frames', 2nd Joint Report, Institution of Structural Engineers and the Welding Institute, May 1971.
24. BS 6399 'Loadings for buildings: Part 1 Code of practice for dead and imposed loads', British Standards Institution, 1984.
25. Brett, P. R., Nethercot, D. A. and Owens, G. W., 'Continuous construction in steel for roofs and composite floors', The Structural Engineer, Vol 65A, No. 10, October 1987.
26. Wyatt, T. A., 'Design guide on the vibration of floors', Steel Construction Institute, 1989.
27. Johnson, R. P. and Bradford, M. A., 'Distortional lateral buckling of unstiffened composite bridge girders', Proc. Conf. Instability and Plastic Collapse of Steel Structures, ed. L. J. Morris, Granada, 1983, p569-580.
28. Weston, G. and Nethercot, D. A., 'Continuous composite bridge beams - Stability of the steel compression flange in hogging bending', ECCS Colloquium on Stability of Plate and Shell Structures 1987, ed. P. Dubas and D. Vandepitte, p47-52.
29. Weston, G., Nethercot, D. A. and Crisfield, M. A., 'Lateral buckling in continuous composite bridge girders', The Structural Engineer, Vol 69, No. 5, March 1991.

30. Singh, K. P., 'Ultimate behaviour of laterally supported beams', PhD thesis, University of Manchester, 1969.
31. Horne, M. R., Shakir-Khalil, H. and Akhtar, S., 'The stability of tapered and haunched beams', Proc. Instn. Civ. Engrs, Part 2, 1979, Vol. 67, Sept., p677-694.
32. Morris, L. J. and Nakane, K., 'Member stability in portal frames', Steel Framed Structures - Stability and Strength, ed. R Narayanan, Elsevier, 1985, p307-336.
33. BS 5400 'Steel, concrete and composite bridges: Part 3 Code of practice for design of steel bridges', British Standards Institution, 1982.
34. Bradford, M. A. and Johnson, R. P., 'Inelastic buckling of composite bridge girders near internal supports', Proc. Instn. Civ. Engrs, Part 2, 1987, Vol. 83, March, p143-159.
35. Roik, K., Hanswille, G. and Kina, J., 'Nachweis gegen Biegedrillknicken bei Verbundträgern', Der Stahlbau, 1990.
36. Roik, K., Hanswille, G. and Kina, J., 'Background document on Eurocode 4, Clause 4.6.2 and Annex B: Lateral torsional buckling', Report EC4/9/90, Research report for the harmonisation of the European Construction Codes, Eurocodes 3, 4 and 8/part 3, Nr.: RS II 2-674102-88.17, Bochum, April 1990.
37. Johnson, R. P. and Fan, C. K. R., 'Distortional lateral buckling of continuous composite beams', Proc. Instn. Civ. Engrs, Part 2, 1991, Vol. 91, March, p131-161.
38. Madros, M. S. Z., 'The structural behaviour of composite stub-girder floor systems', PhD Thesis, University of Cambridge, 1989.

39. BS EN 10 002-1 'Testing of metallic materials: Part 1 Method of test at ambient temperature', British Standards Institution, 1990.
40. Kemp, A. R. and Dekker, N. W., 'Available rotation capacity in steel and composite beams', *The Structural Engineer*, Vol. 69, No. 5, March 1991.
41. Bs 8110 'Structural use of concrete: Part 1, Code of practice for design and construction', British Standards Institution, 1985.
42. 'Guide to the structural use of lightweight aggregate concrete', Institution of Structural Engineers and The Concrete Society, 1987.
43. Warburton, G. B., 'The dynamical behaviour of structures', 2nd Edition, Pergamon Press, 1976.
44. Boswell, L. F. and Qiao, L. 'Inelastic buckling of haunched composite beams', *Structural Integrity Assessment*, Elsevier Applied Science, ed. P. Stanley, 1992, p413-423.
45. BS 5400 'Steel concrete and composite bridges: Part 6, Specification for materials and workmanship, steel', British Standards Institution, 1980.
46. Andrade, S. A. L. and Morris, L. J., 'The influence of stress levels on the behaviour of steel haunched members', 10th Australian Conference on the Mechanics of Structures and Materials, Adelaide, August 1986.
47. Andrade, S. A. L. and Morris, L. J., 'Limited studies of non-linear behaviour of haunched members', *Advances in design and construction of steel structures*, ed. R Narayanan, Eslevier, 1987, p355-365.
48. Morris, L. J. and Nakane, K., 'Experimental behaviour of haunched members', *Proc. Conf. Instability and Plastic Collapse of Steel Structures*, ed. L. J. Morris, Granada, 1983, p 547-559.

CHAPTER 1

INTRODUCTION

1.1 GENERAL BACKGROUND AND TERMINOLOGY

1.1.1 Historical Development and Alternative Systems

Composite construction was pioneered principally by Britain and America, and Codes of Practice for its design started to appear in the late 1960's {1,2}. In its earliest form, this type of construction involved the use of timber shuttering, on which was cast a solid concrete slab, and when the concrete had set, the shuttering was removed. Shear studs were welded to the upper flange of each steel beam and they became encased by the concrete when the slab was cast, and so provided a shear connection.

In Britain, this type of construction became popular for bridges, but not for buildings. Although further comprehensive design guidance became available {3}, it was only after the development of the use of rolled profiled steel decking as a permanent shutter to the concrete slab that attitudes changed. This was because the system offered much faster construction times without the need for propping the slab. This idea originated in America and, as a result of studying American practice, the system was adopted in Britain and British design guidance was developed {4,5}. At this time, however, it only applied to simply supported building structures.

In more recent times there has been a surge of interest in composite construction and this has largely been fuelled by the overall economy of the system compared with other structural forms. Experience of its use and the number of specialist sub-contractors and decking manufacturers in this competitive market has made it very attractive to developers and architects alike, who especially appreciate the short erection times. In addition to this drive for speed of erection, clients have become more demanding in their requirements for buildings, in terms of uninterrupted floor areas and the provision of services. This has led to the need for long-span structures capable of providing flexibility for the installation of services within a shallow floor depth.

Several composite beam systems have recently been developed to meet these requirements and some are shown in Figure 1.1. These include:

- (i) beams with circular or rectangular web openings cut in them.
- (ii) tapered beams with services passing under the shallow part of the taper
- (iii) stub girders where the services pass between the stubs
- (iv) castellated beams where a fixed pattern of castellations is provided for services
- (v) trusses, either within the floor zone, or over a storey height
- (vi) parallel beam grillage systems where the composite secondary beams lie across the primary beams, the services being incorporated between both sets of beams.

These systems have been used to a greater or lesser extent, and design guidance for them is either available, or is currently being developed.

A further option to the above systems is that of the haunched beam, which is the subject of this thesis. Several forms are envisaged and these are shown in Figure 1.2. In this system very shallow beams can be achieved because of the use of rigid connections to the columns, and this provides structural continuity. The space between the haunches is then a large void which is available under the beam for services. The various framing arrangements shown in the figure include two basic types. Firstly, there are those where the haunched beams are relatively close together and the floor is designed to span transversely on to them. Secondly, there are those where the floor is designed to span parallel to the haunched beams, and onto secondary beams. It is considered that this latter option will prove to be the more popular because of the limiting capability of current steel decking profiles to about 3.5m^{span}. The economic span range for haunched composite beams is considered to be from about 12m to 20m.

Haunched beams have been used for many years in non-composite single-storey portal frame structures as roofing members, but only recently as composite beams in multi-storey structures. In fact, this author knows of only one such structure that has been reported, and that is 'Grand Buildings' at Trafalgar Square in London {6}. The reason why a greater number of structures has not been built with

this system is no doubt its novelty and the lack of specific design guidance. The building industry is generally cautious, and rightly so, but in a recent report {7} various structural steel options for a generic 15.0m span single-bay 6-storey office building were compared. It was found that the least overall weight solution was that of the haunched composite beam frame. A summary of the weights of the different systems and the size of openings available for services, which was based on a floor zone depth of 1250mm, is reproduced from the report in Figure 1.3 by kind permission of the publishers. The figure shows that the service area for the haunched composite beam system is the greatest.

1.1.2 Use of Haunches and their Manufacture

The considerations for stiffening up selected parts of a structure to make it more efficient is a typical structural engineering activity, and with the advent of plastic design methods, this practice has greatly developed. One of the early papers on the subject of optimum strengthening for economy using plastic design was published in 1952 by Horne {8}, who examined the benefits of discrete strengthening of a fixed-ended beam. The provision of a haunch follows this philosophy because it allows the beam to be shallower than it would otherwise need to be. As previously stated, the use of haunches in non-composite portal frames is well-established and the haunches normally take the form of deep tapered sections close to the eaves, where they form part of the beam rather than the column. The haunch is much shorter in a composite floor beam in order to avoid failure of the columns. This will be discussed later.

It is useful to explain how a typical haunch is manufactured. At the outset, it should be noted that the term 'haunch' is used by different people in different ways, but in this thesis it refers to the combined beam and tapered section. Normally the tapered section is cut from a similar beam section, in which case it is referred to as a 'cutting'. Diagram 1.1 shows a typical 'cutting' fabrication plan and it can be seen that two cuttings are neatly manufactured from a short length of beam.

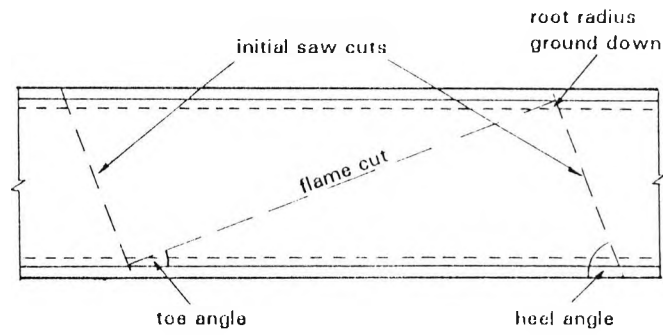


Diagram 1.1 A Typical 'Cutting' Fabrication Plan

A typical haunch/column detail is shown below in Diagram 1.2.

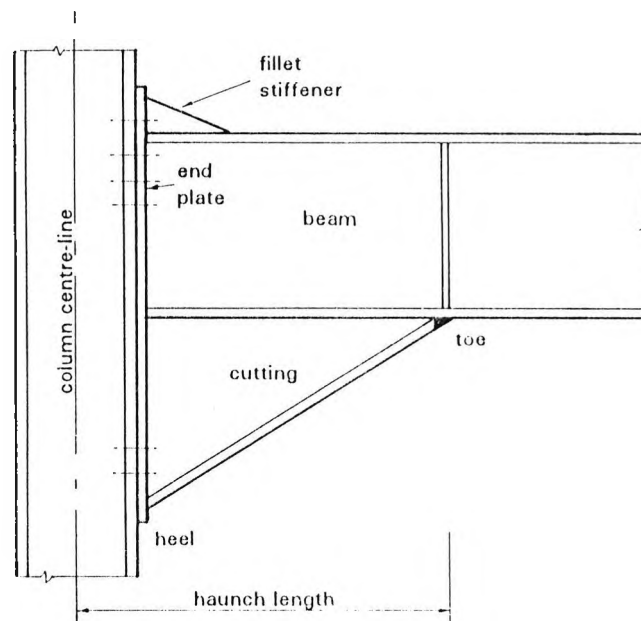


Diagram 1.2 A Typical Haunch/Column Detail

The 'haunch length' is defined as the length from the shallow tapered end of the cutting, known as the 'toe', to the column centre-line. The haunch 'heel' is the deepest part of the cutting, next to the column. The cutting is welded to the beam section, and an end plate is added. A fillet stiffener can also be provided, as shown, to facilitate a further pair of bolts above the top flange so as to enhance the connection strength.

1.1.3 Other Terminology

In order to reflect the practice of recent codes, the terms 'sagging' and 'hogging' are also referred to as 'positive' and 'negative' respectively when dealing with moments or moment regions in beams.

It should also be noted that some symbols, ie, 'x', 'u' and 'v' have more than one definition, but they are used in such a way that confusion should not occur.

1.2 AIMS OF THIS RESEARCH

The principal aim of this research was to develop a suitable method for the design of haunched composite beam frames and, also, by carrying out a full-scale laboratory test programme, to validate the method and so encourage the adoption of the system. In order to provide early guidance, as stated in the Abstract, it was decided that the results of the initial studies should be published. An interim design guide {9} written by this author together with his industrial supervisor, Dr R M Lawson, was therefore issued.

1.3 OUTLINE OF THIS THESIS

Following the introduction in this chapter, the design philosophy and general design methods are developed in Chapter 2. These have been developed from a combination of theoretical studies by the author, other research and design information, and cautious engineering practice.

An area of particular interest was that of the stability of hogging regions of composite beams and a new method of checking for instability is presented in Chapter 3. Other related methods are also considered in detail and compared with the proposed method.

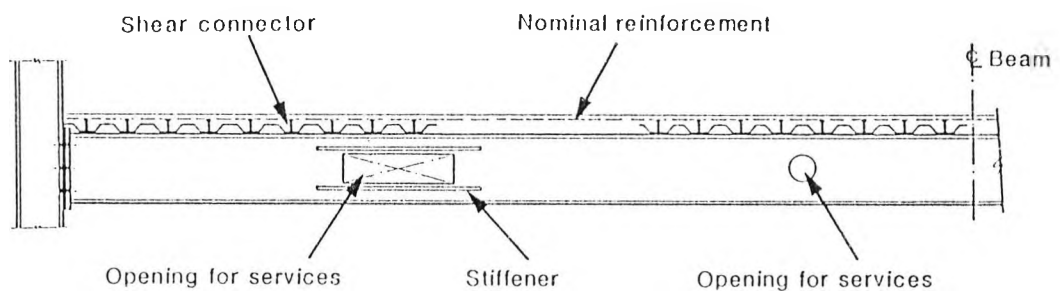
Chapter 4 describes the first part of the experimental programme, referred to as the Sub-Assembly Test. This test was designed to examine the problem of buckling in hogging moment regions and, in particular, restraint to the haunch toe,

where several alternative methods were tested. A further objective of this test was to provide information on the moment-rotation characteristics of this region, and one of the more slender sections suitable for plastic design was used. The results of this test are compared with theory in Chapter 5, where the validity of the proposed buckling check is examined.

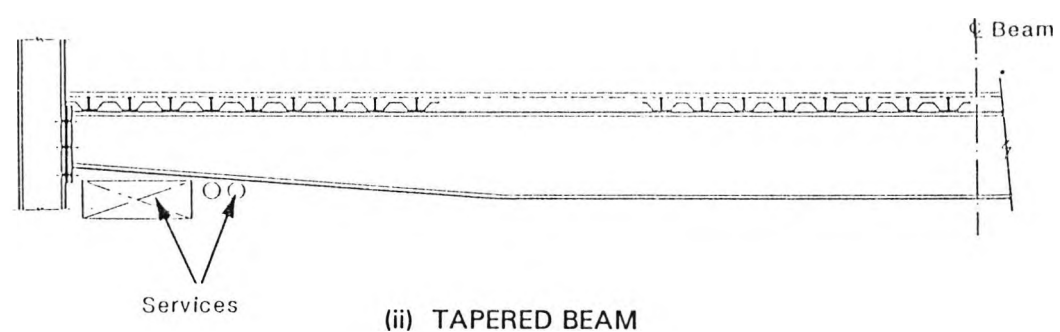
Chapter 6 describes the second part of the experimental programme, referred to as the Main Beam Test. This was devised to examine the overall behaviour of a haunched beam within a sub-frame. The results of this test are compared with the theory in Chapter 7.

The computer studies are included in Chapter 8, where the finite elements used in the analysis of the tests are described. Further computer simulations, by varying the restraint and imperfection parameters etc, on the Sub-Assembly Test, are also explained in detail in this chapter.

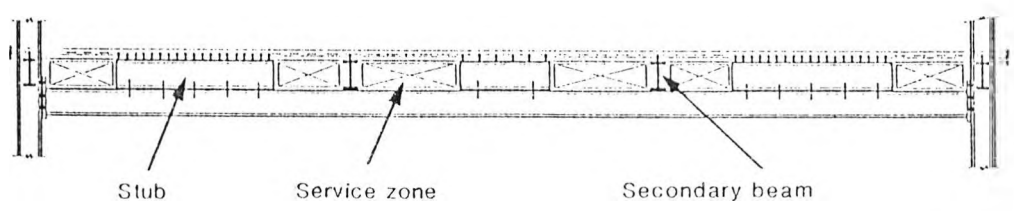
The conclusions from the work are presented in Chapter 9, where design recommendations are made. Suggested areas for future computer work and further theoretical study, together with ideas for possible future testing, are also given in this Chapter.



(i) BEAM WITH WEB OPENINGS

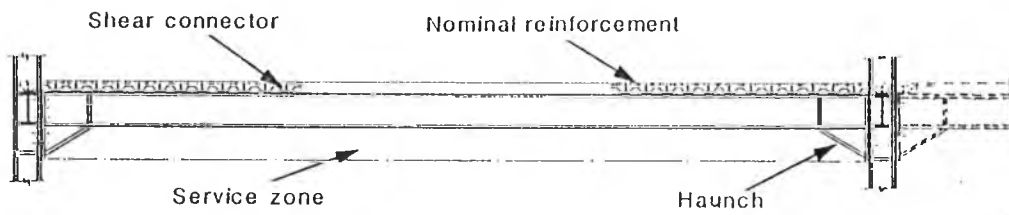


(ii) TAPERED BEAM

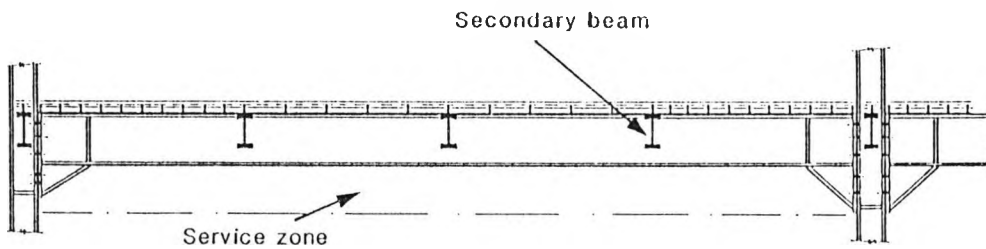


(iii) STUB GIRDER

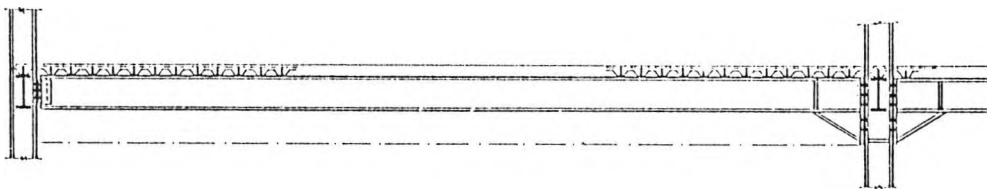
Figure 1.1 Some Alternative Composite Beam Structural Forms used in Buildings



(i) HAUNCHED BEAM SUPPORTING COMPOSITE SLAB - SINGLE OR MULTI-BAY FRAME



(ii) HAUNCHED BEAM SUPPORTING SECONDARY BEAMS - SINGLE OR MULTI-BAY FRAME



(iii) SINGLE SIDED HAUNCHED BEAM - MULTI-BAY FRAME



(iv) HAUNCHED BEAM CONNECTED TO SPINE BEAM

Figure 1.2 Different Configurations of Haunched Composite Beams

Structural Option	WEIGHT (kg/m ²)		
	Primary Beams	Including Secondary Beams	Including Allowance for Columns
Universal Beams with Openings	26.9	35.2	45.7
Cellular Beams	23.3	31.6	42.1
Truss MK1 - Ts and RSAs	26.4	34.7	45.2
Truss MK1 - Hollow sections	21.2	29.5	40.0
Truss MK2 - Ts and RSAs	25.8	34.1	44.6
Truss MK2 - Hollow sections	20.8	29.1	39.6
Haunched Beam	13.7	22.0	36.0
Stub Girder Mk1	22.9	35.9	46.4
Stub Girder Mk2	26.3	34.6	45.1
Tapered Beam	22.3	30.7	41.2
Dual Plane Grillage	24.8	40.2	45.8
Conventional 6 x 7.5m grid with universal beams	8.0	20.3	32.0

STRUCTURAL OPTION	BEAM SIZE	GROSS OPENING SIZE
Universal Beam with Stiffened Holes	686 x 254UB170 OR 686 x 254UB152 ¹	3 @ 485 x 1000 3 @ 450 x 1100
Cellular Beam	835 x 229 cut from 610 x 229UB140	500 dia @ 750 ctrs = 18
Truss Mk1	1000 o/all depth	1 @ 570 x 1500 i6 @ 300 dia
Truss Mk2	1000 o/all depth	1 @ 570 x 1500 8 @ 300 dia 4 @ 200 x 1000 OR 4 @ 400 dia
Haunched Beam	457 x 191UB82	1 @ 450 x 13000
Stub Girder Mk1	305 x 305UC118 plus 406 x 140UB39 stubs	10 @ 400 x 750
Stub Girder Mk2	254 x 254UC89 plus 610 x 229UB101 stubs	1 @ 600 x 1200 2 @ 600 x 1000 2 @ 600 x 750
Tapered Beam	250 wide x 750 deep max	2 @ 400 to 775 x 7500
Dual Plane Grillage ²	610 x 305UB149 406 x 140UB46	plus 3 @ 400 x 3000 2 @ 400 x 1500 1 @ 600 x 1200

¹ reduced hole depth prohibits use of VAV system

² based on 12m x 12m grid. Hole sizes refer to orthogonal directions.

Figure 1.3 Summaries of Frame Weights and Opening Sizes of Various Structural Systems based on a 6-Storey 15m Single-Bay Building

CHAPTER 2

DEVELOPMENT OF THE PROPOSED DESIGN METHODS

2.1 CONSIDERATION OF SWAY

The haunched composite beam building structure is a continuous frame structure by virtue of the full-moment connections between the beams and the columns. It may therefore be designed to be used to resist sway moments, ie, in a sway condition, or it can be used in conjunction with bracing which resists these moments, ie, in a no-sway condition.

multi-storey

Traditionally, sway frames have been designed elastically to prevent the possibility of P- Δ effects in the columns, which could otherwise precipitate catastrophic failure of the structure. This author believes that, unless designers have both the access to, and the desire to use, highly sophisticated elasto-plastic frame programs which can handle these effects, this situation will continue. Caution suggests that it should. However, there is scope to design frames of this type by allowing a degree of plasticity in the beam elements, provided that the structure is braced against side-sway. Bracing against lateral forces is frequently provided in simply supported structures by using the floors as diaphragms which are connected to stiff cores, such as lift or staircase areas. This option is also available for continuous structures, and the development of the design methods, which now follow, assumes the no-sway condition in the design of the frame.

2.2 DESIGN PHILOSOPHY

2.2.1 General Design Principles

Two alternative methods of design of haunched composite beam frames are presented, but both adopt the principle that the weakest link in the frames must always be the beams. This is obviously to prevent the extensive collapse that could occur in the event of premature failure of any column. A further principle is that any

beam failure should be gradual, ie, plastic, so that ample physical warning would be given prior to collapse. With these principles in mind it is considered appropriate to prevent hinges from occurring in the columns, and to restrict plasticity within the haunches to close to the toe. These design principles were also adopted by Morris and Randall, who, 13 years ago, published an important guide on the plastic design of non-composite structures {10} which has been widely used in the industry.

2.2.2 Plasticity in the Columns

With regard to the design of the columns, current design codes {11,12} actually permit the full strength to be utilised up to the plastic moment of resistance, M_p , which, by definition, implies a degree of plasticity. It should be remembered, however, that, although the column may be permitted to reach M_p , this would be associated with a relatively small strain of about three times the yield strain which would also occur over a relatively short length because of the steep moment gradient that normally occurs in columns. Therefore, the plastic rotation associated with this strain, ie, the integral of the strain, would be very small. By comparison, the strain associated with a hinge is of the order of twenty times the yield strain, and consequently a large rotation occurs. It is then clear that merely reaching M_p does not necessarily imply development of a plastic hinge, and that there is therefore no contradiction within the design philosophy.

2.2.3 Plasticity Within the Haunch Length

With regard to the stresses permitted in the haunch at the design collapse condition, there has been much research in this area relevant to single-storey non-composite portal frames. The guide by Morris and Randall recommended that the eaves haunch should remain elastic to prevent instability occurring within the haunch. This was based on the reasoning that, should a hinge occur at the haunch toe, then, because of the steep moment gradient, the tapering section would suffer a considerable spread of plasticity, which would cause instability. Morris subsequently carried out tests and computer analyses on haunched beams which led him to make further recommendations {13}. These included the recommendation that, when a structure is designed with a plastic hinge at the haunch toe, the haunch should be

proportioned so that the haunch heel moment is less than 0.75 times the heel resistance moment at yield. This was to allow for the deleterious effect of residual stresses on the stability of the haunch.

There are, however, important differences between the non-composite frame haunch details which were considered by Morris et al and haunch details appropriate for haunched composite beam construction. Firstly, the length of the haunch as a proportion of the span is much less for a haunched composite beam, (see later paragraph 2.3.3), and this leads to a much steeper haunch taper. This has the effect of limiting the spread of plasticity into the haunch to just beyond the haunch toe. To illustrate this point, a typical frame has been analysed and the results are shown in Figure 2.1. The design moment has been superimposed over the elastic and plastic haunch capacities in the figure, and it can be seen that, even with a plastic hinge at the toe, the extent of the yielding is only 15% into the haunch length. It is also seen that, where yielding occurs, the elastic capacity is only marginally exceeded.

The second major difference between composite beams and the non-composite beams considered by Morris is that, with composite beams, the top flange of the steel beam is connected to the floor by shear connectors, and this provides torsional restraint to the section. The short haunches associated with composite beams also enable the column to have a much greater influence on the torsional stability of the haunch, and when the haunch toe is reinforced by fitting full-depth web stiffeners, as is recommended later, this leads to a very torsionally stiff element.

The current relevant British Code {11} permits hinges at the haunch toes of non-composite frames provided the compression flange is sufficiently laterally braced, and also, provided that the section is sufficiently stocky. For the above reasons it is recommended that a plastic hinge should be permitted at the haunch toes in composite frames under certain conditions, as will also be discussed later.

With regard to the stress level at the haunch heel, despite Morris's caution, it is current practice to permit the haunch heel to reach yield, and, because of the other favourable reasons given above, this author believes that this would be appropriate for haunched composite beams. It might be added that this restriction

will rarely be critical if bolted connections are used. This is concluded because it was found that, from ^{an unpublished} study of practical haunch connection details, ^{by this author} the connection strength normally lay between 60% and 110% of the haunch section strength, with a typical value of 80%.

2.2.4 Premature Failure of Non-Beam Elements

In order to satisfy the criterion of collapse ductility, it is important to ensure that elements where yielding is not specifically designed to take place do not suffer excessive deformation. For example, should a slight under-estimate of the beam strength be made, the increased moment that would then be necessary to cause collapse should not unduly deform the connections, haunches and columns. Clearly the use of an appreciably over-strength beam could result in considerable deformation of these elements, but that could only occur at a much higher loading. It is therefore recommended that, until further test evidence becomes available, a margin of strength should be provided in the haunch heel, the connections and the columns, according to the degree of plasticity required for collapse. This is outlined in more detail later but it is also recommended that the column section should at least be able to sustain its plastic moment of resistance, ie, it should be either a 'compact' or 'plastic' section as defined by the codes {11,12} - see later paragraph 2.3.1.2.

2.3 FRAME DESIGN USING PLASTIC PRINCIPLES AT THE ULTIMATE LIMIT STATE

2.3.1 Design Assumptions and Related Research Work

In this method, a plastic collapse mechanism is designed to be achieved in the beam, with hinges forming at the haunch toes and in the sagging region of the span. The method, as with most plastic methods, assumes an idealised behaviour, and several important assumptions are made. These include:

- i. lateral instability does not occur
- ii. local buckling does not occur

- iii. sufficient hinge rotation is available to enable the plastic collapse load to be supported.

2.3.1.1 Lateral Buckling

Lateral buckling in non-composite beams normally takes the form of lateral torsional buckling, where torsion of the section as a whole occurs. Lateral buckling of composite beams involves distortion of the section, and this is known as lateral distortional buckling. These concepts are explained more fully in Chapter 3, but suffice it to say here that both types can occur either in the form of 'premature' buckling, ie, before the full moment of resistance is reached, or they can occur after this and during hinge rotation. The former case should be prevented, but the latter case may be tolerated in certain circumstances, provided the associated decline in strength is sufficiently gradual.

Current design practice to prevent lateral buckling in non-composite construction is to provide restraints in the form of diagonal 'knee' braces to the compression flange at the hinge positions. The full-scale experiments carried out by the author, and reported in this thesis, showed that it may be possible to omit this bracing in certain conditions. A design method which checks for lateral instability is developed in Chapter 3 and it is shown that assumption (i) can be accepted.

2.3.1.2 Local Buckling

Local buckling is not the wholesome movement of the section out-of-plane, but, rather, the individual buckling of an element within the section, eg., the compression flange or the part of the web in compression. It is caused by the level of strain in the element reaching a point where the lateral stiffness of the elements can no longer restrain it from lateral movement. If the element dimensions are such that it is 'thin' then this might occur in elastic state, but normally it occurs in the elasto-plastic state. In order to categorise the characteristics of the behaviour of different sections in this respect, a section classification system has been adopted in codes {11,12}. This can be summarised in such a way that the following can be assumed without the possibility of local buckling:

‘plastic’	the section can sustain its plastic moment of resistance with a degree of hinge rotation
‘compact’	the section can attain its plastic moment of resistance
‘semi-compact’	the section can attain its yield moment of resistance
‘slender’	the section cannot attain its yield moment of resistance.

The above categories, which are also referred to as classes 1 to 4 in the European Code {12}, are largely based on the moment of resistance that can be achieved by assuming the small degree of rotation that is normally associated with the design of non-composite structures. In composite structures, however, the degree of rotation required can be considerably higher, and even the criteria for the ‘plastic’ classification can be insufficient, so a modified criteria has been adopted for the design of composite structures in the British Code {14}.

Of course, ‘plastic’ sections will still develop local buckling at very large rotations, as the author’s tests subsequently showed, but the important factor is not whether a buckle occurs, but the degree of loss of strength associated with it if it does so. This was also confirmed in tests on continuous composite beams carried out by Ansourian {16}. He reported that local buckling limited the maximum load in some tests but to a level still above the plastic collapse load, because of strain hardening.

Further restrictions, however, do need to be applied when designing continuous composite beam structures using plastic principles, as discussed next, but local buckling can be limited by the use of ‘plastic’ sections only.

2.3.1.3 Hinge Rotation Capacity

The third assumption listed is an all-embracing one which really incorporates the first two. The assumption is made that each hinge is capable of the the rotation that is necessary for plastic collapse without loss of strength. As explained, early buckling of plastic hinges in hogging regions of composite beams can

be prevented, but, in certain circumstances, there can be a necessity for hinges in the composite sagging regions to rotate, and this may not be possible.

This phenomenon was appreciated by Barnard and Johnson {17} who investigated the strength and moment-rotation characteristics of composite sagging hinges in simply-supported beams. They found that the stress-strain characteristics of the concrete had a major effect on the moment-rotation relationship for the hinge but, for a given value of maximum stress, no effect on the hinge strength. In another study {18} they compared the typical moment-rotation relationship of a composite section in the sagging region with that of a section in the hogging region of a continuous composite beam. They found that, after M_p had been attained in composite sagging regions, there was a significant drop-off in strength, as shown in Diagram 2.1. They defined this type of hinge characteristic as strain-softening. However, with hogging region hinges, provided premature buckling was prevented, they recorded an increase in strength after M_p had been reached due to strain hardening, and only a drop-off below that at a much larger rotation, as shown in Diagram 2.2.

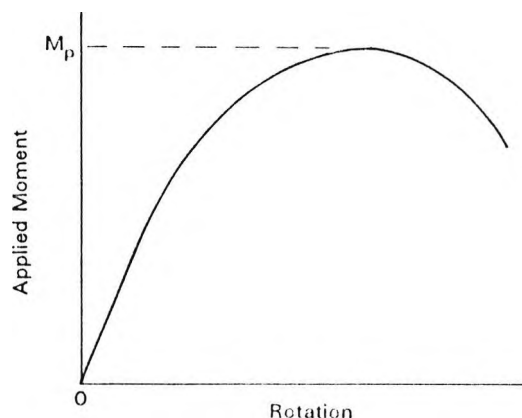


Diagram 2.1 Postulated Moment-Rotation Relationship for a Composite Sagging Region Hinge (Johnson and Hope-Gill {19})

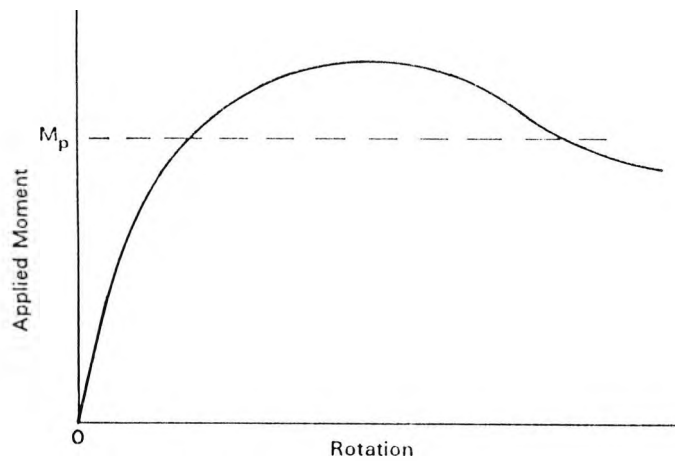


Diagram 2.2 **Postulated Moment-Rotation Relationship for a Hogging Region Hinge in a Continuous Composite Beam (Johnson and Hope-Gill {19})**

in continuous composite beams Bernard and Johnson defined the formation of a plastic collapse mechanism as that stage 'where the rate of loss of strength in the strain softening hinges is exactly balanced by the rate of gain in strength of the strain hardening hinges'. In this they were assuming that the 'strain hardening' hinges were invariably operating in the strain hardening region which, in some cases, might require the provision of web stiffening. The important conclusion, therefore, is that, since there is always a falling branch to the moment-rotation resistance curve of any hinge, composite or otherwise, and, since plastic hinges form around a structure at different load levels, it cannot be relied upon that all the hinges necessary for plastic collapse will achieve their maximum resistance at the same time.

Following the above conclusion, it is then necessary to identify under which circumstances the point when this 'balance' is achieved before the collapse load level has been reached. This was specifically investigated by Johnson and Hope-Gill {19} in relation to continuous composite beams on simple supports. The problem involved considering multi-span beams containing different span lengths and stiffnesses, as well as various loading types. Mathematical models were developed by them to describe the moment-rotation performance, including the falling branches, of both types of hinge. They carried out several computer simulations and followed this up by tests on some of the more severe cases {20}. They found two main failure types and categorised these as either 'sagging' or 'hogging'. 'Sagging' was defined as that occurring when the sagging hinge in the span was able to reach its maximum

capacity, irrespective of the state of the hogging region hinges and 'hogging' as the reverse of this. They discovered that the interplay between the moment-rotation performances of the various hinges, for a given beams, strongly influenced the failure modes but not so much the collapse load. They also found from the test results that the performance of the sagging region hinge was rather better than they had anticipated, and that there was a degree of strain-hardening accompanied by a larger rotation capacity.

From a study of all these results the authors developed a set of design conditions. These were based on the principle that it was better to exclude from the use of plastic design those cases where the plastic collapse load could not be achieved, rather than develop specific methods to accommodate them. These conditions included that:

- i. steel members should be grade 43 or 50 (ie. to the British Code {11})
- ii. the concrete slab should be of a concrete grade between 22.5 and 45 (N/mm²)
- iii. the plastic neutral axis of the sagging region of each span should lie within the concrete slab or the compression flange of the steel member, but not in the web
- iv. the length of an end span simply-supported at one end should not exceed that of an adjacent span by more than 15%
- v. not more than half of the design ultimate load for any span should be concentrated within a length of span/5.

The more recent tests by Ansourian {16} confirmed the theory and approach of Johnson and Hope-Gill, and the above conditions have now been incorporated in the British code for the design of composite beams {14}. However, by way of further study, the author of this thesis carried out an analysis of several reported tests on continuous composite beams in accordance with this code, and the

results of this have been reported in {21}. Conventional plastic analysis was applied and the test model factors in each case deduced. It was found that they varied between 0.99 and 1.98, although the upper limit of this range was reduced to 1.53 when all the test reinforcement was included (ie, including that beyond the theoretical effective breadth) and when the steel section was assumed to be unaffected by the level of shear.

Of course, the situation with haunched composite beams is more favourable than with continuous composite beams on simple supports. This is because the presence of the columns limits the extreme bending moment conditions forming from one span to another by providing a degree of fixity at the supports. However, until further research is produced, it is recommended that the above conditions should still apply to haunched composite beams.

2.3.2 The Design Process Using Plastic Principles

The plastic collapse equation, whereby the work done by the loads is made equal to the work done by the plastic hinges during rotation, applies to haunched composite beams in the normal way. However, to limit premature deformation of the haunch connection and column due to possible over-strength of the beam, as discussed earlier in paragraph 2.2.4, the plastic design moment for these elements should be increased by a value equal to ^{say,} 10% of the applied hinge moment at the haunch toe. An example is now given.

The case of a typical single-span frame subject to a UDL is shown below in Diagram 2.3.

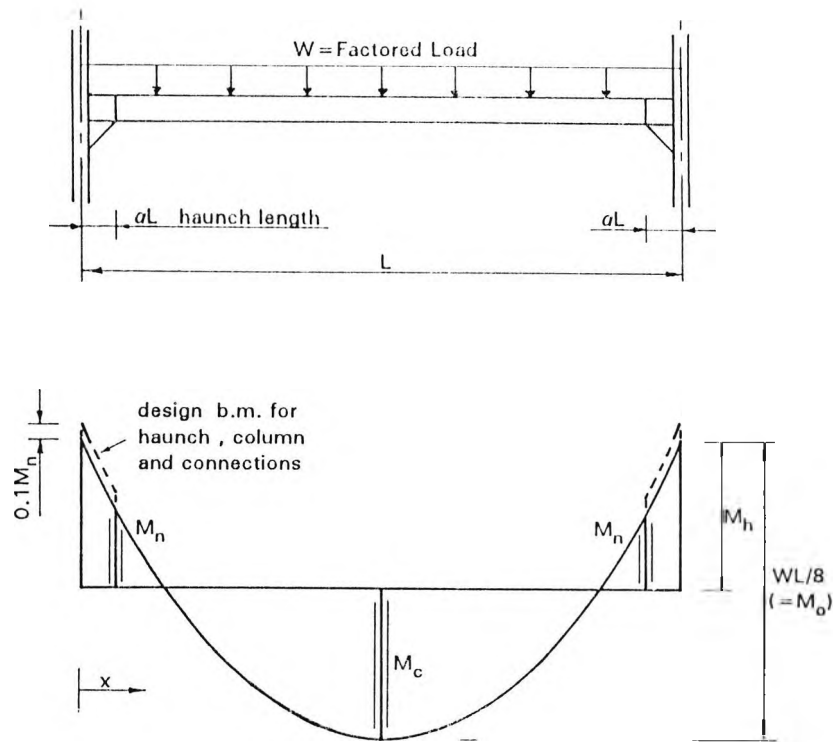


Diagram 2.3 The Plastic Collapse Bending Moment Diagram for a Typical Single-Span Sub-Frame

The plastic design bending moments are shown in the diagram and the plastic design equation can be written as:

$$M_n + M_c = \frac{WL}{8} (1 - 2\alpha) \quad (2.1)$$

- where
- L = beam span
 - αL = haunch length (measured from centre-line of column)
 - M_n = plastic moment of resistance at the haunch toe ie, in hogging (negative) bending
 - M_c = plastic moment of resistance of the hinge in the sagging (positive bending) region
 - W = plastic collapse load

Also, for future reference, it is useful to define here:

M_h	=	unmodified plastic design moment on the column centre-line
M_o	=	maximum free bending moment
x	=	a distance measured along the beam from the column centre-line.

The design process then involves checking that the collapse load is greater than the applied load. The elastic haunch heel strength and the connection strength should, of course, be based on $M_h + 0.1M_n$.

2.3.3 Haunch Length Optimisation for Plastic Design

For design economy, it is necessary to choose an appropriate haunch length because it greatly influences the beam and column design moments. From the initial design philosophy, if plastic collapse is to be confined to the beam, the haunch must be short enough to ensure that this occurs. In theory, a very short haunch would give rise to high beam design moments, and hence a deep beam would be required. For practical reasons this may be unacceptable because it might leave little room beneath it for services. Conversely, a long haunch would give rise to high column moments, and so a heavy column section would be required. Clearly, a designer would have to balance these two considerations, but it is useful to have some estimate of the implications of a particular haunch length for preliminary design purposes, and this is now attempted.

An all-embracing formula expressed in the form of a minimum weight function is not considered appropriate because the shape of the haunch is not just based on strength, but also on practical limitations. The haunch needs to be deep enough to enable the connection strength to be achieved, but not so shallow as to make fabrication impractical. The optimum length will depend on the conditions of a particular case but simple relationships can be found which define the haunch length at the point when the haunch toe hinge, the span hinge, and the haunch heel all reach their maximum design strengths simultaneously.

The example of the single-span frame, referred to earlier and illustrated in Diagram 2.3, is now given. It is to be noted that, for simplicity, it is assumed that the applied moment on the column centre-line is used to determine the haunch heel and connection design. By referring to the plastic moments in Diagram 2.3, and, by initially ignoring the extra design moment of $0.1M_n$ applied beyond the haunch toe, the following equilibrium equation can be derived:

$$M_o = M_h + M_c = \frac{WL}{8} \quad (2.2)$$

Also, the haunch toe moment is given by:

$$M_n = M_h - \frac{W\alpha L}{2} (1 - \alpha) \quad (2.3)$$

By combining these two equations to eliminate W , and by putting $\beta = \frac{M_c}{M_n}$ and

$\gamma = \frac{M_h}{M_n}$, the following solution can be obtained:

$$\gamma = \frac{4\alpha\beta(1 - \alpha) + 1}{(1 - 4\alpha(1 - \alpha))} \quad (2.4)$$

This equation is in the form $\gamma = m.\beta + C$ and is therefore a family of straight lines of γ against β , where the gradient depends on α . This family of lines is shown in Figure 2.2. As a point of interest, the lines all pass through the point $(\beta, \gamma) = (-1, 1)$. It can also be seen from the above equations that the haunch toe strength is given by:

$$M_n = \frac{M_o}{(\beta + \gamma)} \quad (2.5)$$

and when there is no hogging region reinforcement,

$$M_s = \frac{M_o}{(\beta + \gamma)} \quad (2.6)$$

where M_s = bare steel beam plastic moment of resistance.

The case above refers to a UDL, but, from analysis of the more onerous case with a central point load, the following equation can be derived:

$$\gamma = \frac{2\alpha\beta + 1}{(1 - 2\alpha)} \quad (2.7)$$

This also represents a family of straight lines through the same point as the above family, but it produces values of α of the order of twice those from equation 2.4. In other words, the haunch length for a central point load case will need to be roughly twice that of a similar UDL case. In practice, most frames will contain secondary beams and therefore the optimum haunch lengths will be somewhere between these two cases.

A further case was also analysed by way of completion, and that was that of a propped cantilever subject to UDL. This case would apply, say, when the outer columns of a two-span frame are deliberately designed to be pin-connected to the beams to keep the columns slim. The following equation then applies:

$$\beta = \frac{[(\gamma - \alpha\gamma - 1) - \alpha\gamma(1 - \alpha)]^2}{4\alpha(1 - \alpha)(\gamma - \alpha\gamma - 1)} \quad (2.8)$$

Optimum haunch lengths from this equation are found to be about 10% longer than for the symmetric UDL case, ie, equation 2.4.

The required strength of the haunch toe is then given by

$$M_n = \frac{4M_o}{\gamma^2} [2\beta + \gamma - 2\sqrt{\beta(\beta + \gamma)}] \quad (2.9)$$

Of course, M_h is not the value of the design moment for the haunch heel and haunch connection because, as stated, this is $(M_h + 0.1M_n)$. Hence, for design,

$$(M_h + 0.1M_n) \leq M_{he}, M_{hc} \quad (2.10)$$

where M_{he} = elastic haunch heel strength
 M_{hc} = haunch heel connection strength

Therefore, when calculating the haunch toe strength ^{from} the above equations, ^(2.4 to 2.9) a deduction of $0.1M_n$ should be made.

It is appropriate at this stage to consider the practical range of β and γ in order to determine a practical range of α , ie, the haunch length. An unpublished parametric study was carried out by the author to determine a relationship between the elastic haunch heel strength, M_{he} , and the plastic haunch toe strength, M_n . For the purpose of the study the haunch was assumed to be non-composite, ie, unreinforced, hence $M_n = M_s$. After considering the available British rolled sections, a lower-bound design relationship was found, whereby:

$$\frac{M_{he}}{M_s} = 0.17 \left[\frac{D_h}{D} \right]^2 + 0.7 \left[\frac{D_h}{D} \right] \quad (2.11)$$

where D_h = haunch heel depth
 D = beam depth

The curve of this equation is illustrated in Figure 2.3.

If, typically, a haunch heel depth of twice the beam depth is used, it can be seen that $M_{he}/M_s = 2.1$, and hence, for a bolted end connection achieving, say, 80% of the elastic haunch heel strength, it can be seen that $M_{hc} = 1.7M_s$. Therefore, for an unreinforced haunch, from equation 2.10,

$$M_h = 1.7M_s - 0.1M_s = 1.6M_s, \text{ ie., } \gamma = 1.6$$

From a further study of the ratio of composite to non-composite strength of practical sagging region sections it was found that for most beams the ratio varied between 1.4 and 2.4, but was typically around 1.6 for the beams considered most likely to be used in this structural system. A plot of beam weight against composite strength is shown in Figure 2.4. This has been taken from reference {9} and is reproduced by kind permission of the SCI. Hence, referring to Figure 2.2, for an unreinforced beam subject to a UDL, and with $\beta = 1.6$ and $\gamma = 1.6$, it can be seen that an optimum haunch length would be about 5% of the span.

The above percentage is roughly half the length normally used for non-composite haunched single-storey portal frames, but this is because in that case hinges are permitted in the columns. The optimum lengths for other load cases, as discussed, would be correspondingly higher, but it can be concluded that the ideal haunch lengths for haunched composite beams are quite short. In practice, haunches with cutting toe angles greater than 45° are likely to be impractical and inefficient, and some designs might be governed by this limit. As a general rule, it is anticipated that most designs using plastic analysis would use haunches between 4% and 7% of the span length, and a practical range is indicated in Figure 2.2.

2.3.4 Restraint of Plastic Hinges

As stated, it is a requirement in current codes to provide a torsional restraint at the location of plastic hinges in order to allow the necessary hinge rotation for plastic collapse to take place. In conventional portal frames this takes the form of a diagonal knee brace from the purlin or side rail to the compression flange of the member, and this can readily be inserted at the steel erection stage. Restraint to composite beams, however, is more difficult because, unless a secondary member is located near the hinge position, there is nothing to connect the brace to at the erection stage. Therefore, to install bracing at this stage, extra secondary steelwork would be required. However, fortunately, bracing for the construction loading is not normally necessary, but, in order to brace the composite condition, if extra steelwork is to be avoided, it would be necessary to make the brace connection to the cured concrete slab. This would be inconvenient because it would be mean that a

further steelwork erection operation would be required at a much later stage, and this would be costly.

With regard to restraining the hinge position at the haunch toe in the composite stage, it was postulated at the outset of this research that, because the haunch lengths in this system were likely to be short, it might be possible to omit a restraint here altogether and rely on web stiffening. This is because the cutting flange would form a direct load path to the column and, in conjunction with, say, full-depth web stiffeners, might provide sufficient torsional restraint. The experimental program was designed to investigate this and the finite element study, described in Chapter 9, also compared various restraint options.

2.4 FRAME DESIGN USING ELASTIC GLOBAL ANALYSIS FOLLOWED BY MOMENT REDISTRIBUTION PRINCIPLES AT THE ULTIMATE LIMIT STATE

2.4.1 Introduction

This method is not so much a beam design method as a frame design method because it involves the calculation of elastic moment values in the beam, which, in turn, are influenced by the stiffness of the columns. It is applicable to beams of all classifications and may be more suitable than the plastic design method when serviceability conditions are likely to govern.

2.4.2 The Phenomenon of Moment Redistribution

At low levels of loading, a frame will behave elastically, but, with increasing load, the most highly stressed areas will start to behave inelastically, ie, the moments will increase at a lower rate than dictated by elastic principles. The effect of this is that, for equilibrium to be maintained, there will be other points where the moments will need to increase at a higher rate than that dictated by elastic principles. With further increasing load, there will eventually be a sufficient number of points yielding, or losing strength, to cause the maximum load capability to be reached, and collapse will occur. Therefore, during this process it is as if moments

are redistributed from highly stressed areas to less stressed areas, and hence the term 'moment redistribution'. The 'percentage redistribution' is then defined as the difference between the theoretical elastic moment, based on the collapse load value, and the actual moment at the collapse condition. This is normally expressed as a percentage drop from the elastic value. The amount of redistribution occurring in a given case is then simply a function of the elastic bending moment diagram and the ultimate strength envelope.

The behaviour described is, of course, precisely that which leads to a plastic collapse, irrespective of how a particular frame is designed. However, the difference between the redistribution approach and plastic design is that with the redistribution method the 'percentage redistribution' can be specified at the design stage according to the particular moment-rotation characteristics of the sections used. The collapse load can then be based on this design condition. This method will therefore always be a more conservative ^{method} relative to the plastic design method.

2.4.3 Limitations on Moment Redistribution

Moment redistribution is achieved by two main effects in continuous composite beams. It normally occurs first by cracking in the hogging regions, followed by yielding and, possibly, by local buckling of the section. The degree to which a particular section can undergo rotation and, hence, redistribution of moments, is governed by the shape of the cross-section. The section classification system, described earlier, can be used in this regard, although it is mainly intended to be used to determine only a specific value of design strength, ie, that which can be achieved without premature buckling. It is therefore necessary to define the limit of rotation or, rather, the degree of redistribution that can be tolerated without undue loss of strength for each classification band.

Work on this topic has been done by Hope-Gill {22} who re-used the computer models developed as part of his earlier work with Johnson {19} and applied them to 32 further cases of multi-span continuous composite beams. A variety of loading patterns, span/length ratios, neutral axis depths etc. were included, but the steel sections were 'compact'. He correlated the degree of redistribution to the load

design factor to determine the limits when the factor became less than 1.0. He also compared the difference between the degree of distribution required when the elastic bending moments were based on 'uncracked' hogging regions as opposed to 'cracked' sections, ie, where concrete cracking was assumed to extend 15% into the span. Clearly, if cracking is assumed, this is then equivalent to assuming an initial degree of redistribution.

As a result of Hope-Gill's work, limits to the amount of redistribution that can be permitted from the supports in a continuous composite beam have been specified in the British Code {14} and are shown below in Table 2.1.

Global Analysis	Classification of flange at support				
	Class 4 Slender	Class 3 Semi-compact	Class 4 Compact	Class 1 Plastic	
				Generally	Non-reinforced
Uncracked section	10%	20%	30%	40%	50%
Cracked section	0%	10%	20%	30%	40%

Table 2.1 Maximum Redistribution of Support Moments in Continuous Composite Beams According to Section Classification

2.4.4 Application to Haunched Composite Beams

With haunched composite beam frames, the positions where redistribution of moments is normally designed to occur is at the haunch toes and not the supports. For a given frame, if the ultimate strength of the section is plotted along the beam and the theoretical elastic moments, based on the collapse load, are superimposed, the degree of redistribution that is required to reduce the elastic values down to the ultimate strength can be seen at once. Clearly, a redistribution to below the ultimate strength cannot be permitted and occasionally no redistribution will actually be found to be necessary, and so the frame will behave elastically, ie, in these cases the envelope of strength will actually encompass the elastic bending moment diagram.

The limits of redistribution quoted in Table 2.1 were not derived for haunched beams and, as mentioned before, the presence of columns reduces the potential for extreme bending moment conditions such as those that can occur in continuous beams on simple supports. However, until further research suggests otherwise, these values should be used for haunched composite beams.

As with the plastic design method, it is necessary to allow for the possibility of a slightly over-strength beam, which could lead to higher moments occurring at the haunch toe and in the hogging region before redistribution begins. If, then, the design were to be based purely on the design collapse moment condition, the haunch, haunch connection and column could be over-loaded. To avoid this it is proposed that these elements should be designed for a slightly higher moment. If the percentage redistribution at the haunch toe is 10% or less, then it is proposed that the full elastic value should be used. If it is more than 10%, a level of moment based on a percentage of redistribution equal to the actual value of collapse, minus 10%, should be used. For example, if the redistribution at the haunch toe at collapse was 40%, a moment diagram based on $40\% - 10\% = 30\%$ should be used for the design of the haunch heel, connection and column.

2.4.5 Design Process Using Elastic Global Analysis

The process of design initially involves the calculation of the global elastic bending moments based on the ultimate loading. This requires an estimate of the column and beam sizes. The columns of this structural system are likely to be heavier than those in simple construction. Preliminary studies by the author showed that, for buildings up to six storeys high, 70% of the column capacity may be required to resist the bending. Also, to satisfy serviceability requirements, it was found that the beam would normally need to have a span to overall depth ratio of between 24 and 28.

The beam and column are then considered as part of an appropriate sub-frame, eg., as shown below in Diagram 2.4 for the case when the column ends are fixed.

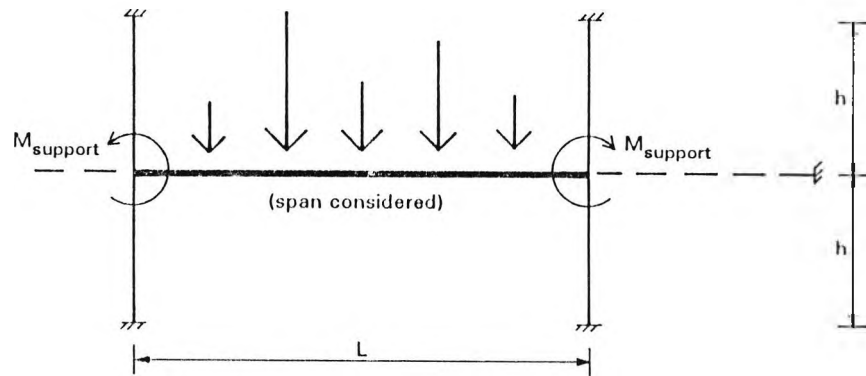


Diagram 2.4 Example of a Sub-Frame for the Elastic Global Analysis of a Beam

The support moment for a single-span symmetric frame with a symmetric loading can then be shown {23} to be:

$$M_{\text{support}} = \text{F.E.M.} \times \frac{4\phi_c}{(4\phi_c + 1)} \quad (2.12)$$

where F.E.M = fixed end moment

and $\phi_c = I_c \cdot L / I_g \cdot h$

where h = storey height

I_c = second moment of area of column

I_g = second moment of area of uncracked beam section

L = span

M_{support} = moment at the support

For completeness, other cases are presented thus:

- i. as above, but for columns with pinned ends

$$M_{\text{support}} = \text{F.E.M} \times \frac{3\phi_c}{(3\phi_c + 1)} \quad (2.13)$$

ii. as above, but for columns pinned at one end, fixed at the other

$$M_{\text{support}} = \text{F.E.M} \times \frac{7\phi_c}{(7\phi_c + 1)} \quad (2.14)$$

Following the calculation of the elastic bending moment, it can be compared with the strength, or moment resistance envelope, to determine the percentage of redistribution necessary. This value should lie within the limits given in Table 2.1. The elastic moments and ultimate moment resistance envelope for a beam within a typical single-bay multi-storey frame are shown below in Diagram 2.5.

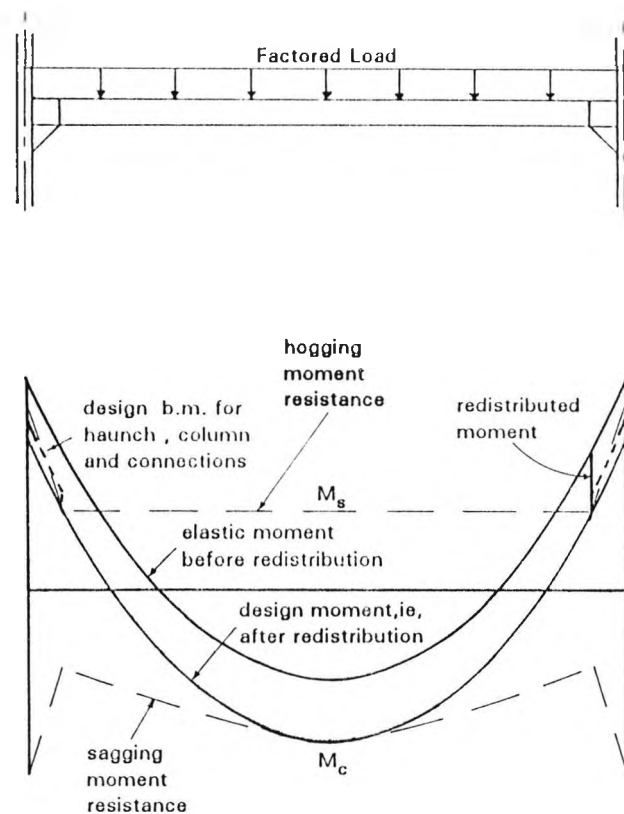


Diagram 2.5 Design Moments and Ultimate Moment Resistance Envelope for a Beam within a Typical Single-Span Sub-Frame

One drawback with the method is that, because the elastic global moments are dependent on the stiffness of the sections chosen, any change to satisfy, say, strength requirements, will also change the global moments. Hence a new set of global moments would need to be calculated, so some iteration may be necessary. An example of the use of this method is given in reference {9}.

2.5 COLUMN DESIGN

The design of the columns is normally determined by the ultimate limit state condition, according to which of the two frame methods is applied. In a multi-storey building it is sufficient to consider the loading on an appropriate sub-frame for the design of each column element. A typical sub-frame is shown below in Diagram 2.6.

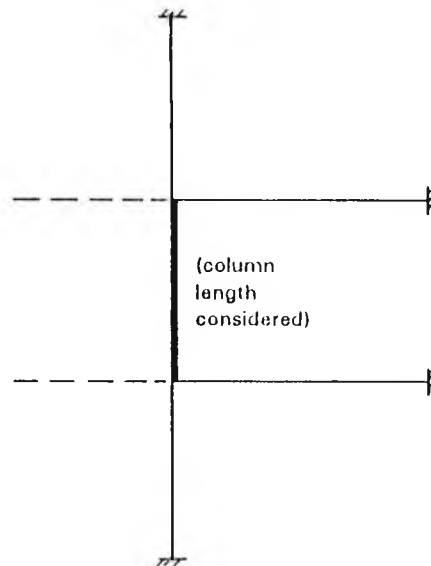


Diagram 2.6 Typical Sub-Frame for the Design of a Column Element

There may be many possible combinations of pattern loading on these sub-frames, each of which may cause yielding, or even hinges, in some beams whilst not in others. This can result in a multitude of design cases for consideration. However, these cases can normally be reduced to three basic combinations of loading for the design of each column element, as follows:

- i. that which produces the largest moment, plus the associated axial load, ie, for a capacity check.
- ii. that which produces the most onerous moment shape, plus the associated axial load, ie, for a buckling check.
- iii. that which produces the largest axial load, plus the associated moments, ie, for capacity and buckling checks.

From a study of the analysis of medium-rise buildings by the author it was found that it is likely that case (i) will govern the design, and that the simple method of calculating the design moments, which follows, is sufficient. This involves the assumption that beams within the appropriate design sub-frame which induce the most onerous moment conditions in a given column length should be fully loaded and, if plastic analysis is applied, they will therefore have plastic hinge moment values at the haunch toes. It would also be appropriate to assume composite properties for these beams. In addition, beams relieving these moment conditions should be loaded only with dead load, but should be assumed to have non-composite properties.

It is to be noted that when applying a probability-type reduction factor according to the number of floors loaded, such as that in {24}, only the axial force should be reduced and not the moments. This is, of course, because the moments in a given column element length will largely be influenced by the loadings on only one or two floors.

Where the structure has bolted beam end connections to the columns, the choice of column section will also be influenced by its susceptibility to local flange bending. For efficient connection design with minimal stiffening, it^{is} unlikely that the thinner flanged columns, within a given serial size, will be suitable. As stated earlier, it is also recommended that only columns with a section classification of 'compact' or 'plastic' be specified, to ensure that there is no loss of strength in the columns.

2.6 CHECKS AT THE SERVICEABILITY LIMIT STATE

2.6.1 Stresses and Deflections

At the serviceability limit state it is necessary to check the stresses so as to have confidence in the deflection calculations. An initial elastic moment distribution is appropriate for this, based on a beam sub-frame, and using composite beam stiffnesses. It is often adequate to calculate the composite stiffness by using a modular ratio which assumes that two-thirds of the imposed load is short-term and that the remainder is long-term. To determine the serviceability conditions, it is necessary to consider several factors, namely:

- i. pattern loading
- ii. the cracking of concrete in the hogging region
- iii. the potential for alternating plasticity and shake-down effects
- iv. yielding at the supports.

To allow for pattern loading in continuous beams designed to the British composite design code {14}, only one load case of imposed load, applied equally to all spans, need be considered. The support moments are then calculated and redistributed by up to 30% for buildings of normal usage, and up to 50% for buildings subject to heavy loads, such as warehouses. This takes account of both the effects of pattern loading and the reduction in stiffness in hogging regions due to concrete cracking. In haunched beams there is a major difference, in that framing into the columns reduces the influence of pattern loading. An equivalent approach to that in reference {14} is to analyse the structure under the most probable loading at the serviceability limit state. For buildings of normal usage, it is suggested by Lawson {9} that this may be taken as the full unfactored imposed loading on the span under consideration and one-third imposed load on the adjacent spans. For buildings or floors potentially subject to highly variable loads, more extreme pattern loads should be considered. No additional reduction in support moment is necessary, however, to allow for the reduction in stiffness of the hogging regions due to concrete cracking, when pattern loads of the above forms are included.

When checking deflections in single-bay haunched composite beams, it is necessary to redistribute the initial elastic moment at the supports to allow for concrete cracking, and a theoretical study by the author indicated that a value of 10% was appropriate. This was to be confirmed later by the test results.

There is also the possibility of plastic rotation at the supports in buildings. This applies to buildings subject to heavy or highly variable imposed loads, where repeated loading can cause alternating plasticity or 'shakedown'. This can lead to permanent moments and deformations at the plastic hinge locations, and hence, to permanent deflections of the beam, which should be added to the elastic deflections on further cycling. To allow for these effects a more detailed analysis is required, which is explained in reference {9}.

There is also a further situation when yield is likely at the supports or, rather, the haunch toes. This is when the degree of redistribution of moments at the ultimate limit state is so high that a considerable rotation at the haunch toe hinges is required before the sagging region span hinge forms. This is likely to mean that, at the serviceability limit state, moments greater than M_p will theoretically occur at the support hinges. In these cases, which are unlikely to arise unless the redistribution is over 40%, further redistribution must be undertaken so that M_p is not exceeded.

The above procedures are designed to limit the extent of yielding which might occur at the haunch toes, but the idea that yield anywhere in the structure may be tolerated at working load is contrary to traditional practice. However, now, in certain circumstances, it is considered acceptable. The reasoning is that if, when the support moments are redistributed to allow for yielding and the span moments are consequently increased, the sagging region of the structure remains elastic, then there will still be an acceptable degree of residual stiffness. This principle was adopted by Brett et al {25} in the design of 'parallel beam' structures and has now been included in the British Code {14}.

It is therefore not necessary to check the serviceability stresses at the haunch toe positions if the above procedures are adopted, but the deflections and stress in the sagging region can be checked from the same moment diagram. The

stress calculations will need to consider both the non-composite and composite stages, and the current limitations {14} on the stresses are $0.5 f_{cu}$ for the concrete and p_y for the steel. It is to be noted that the European Code {15} does not require a serviceability stress check, even in sagging regions, because it is considered that a slight overstress will not seriously effect the reliability of the deflection calculations.

2.6.2 Dynamic Sensitivity

A further consideration of the serviceability limit state is that of dynamic sensitivity. This is necessary to avoid the problem which arises when the impulses given to a floor by the process of walking generate uncomfortable movements around the structure. This is possible when the natural frequency of the floor is relatively close to the walking pace. Further conditions for this discomfort to occur usually include that the mass of the structure must be low enough to allow large accelerations and that the inherent damping of the structure must be low enough to be unable to prevent the strength of the motion from dying away quickly. A detailed study of this problem is given in reference {26} which also gives a recommended design approach. In short, a floor frequency below 3Hz is deemed unacceptable but frequencies down to this level may be permitted according to the value of a human 'response factor' which attempts to define the degree of human tolerance.

With haunched composite beams there is a benefit over simply supported beams because the rigid end conditions reduce the effective span. This is relevant because the natural frequency is proportional to $1/(\text{span})^2$ and hence the frequency is less likely to be in the sensitive range. The frequency is also proportional to the square root of the beam stiffness, ie, \sqrt{EI} , and since this check is for instantaneous impulse loading, it is appropriate to use the dynamic modulus for the concrete, which may increase the beam stiffness by about 10%. For the same reason, it is also appropriate to ignore the concrete cracking in the hogging region, and so there should be no consequential reduction in support moments for this check.

It is interesting to observe the effect that end continuity has on the natural frequency and this is now examined in relation to some typical cases. If the value of the natural frequency of a beam with end continuity is 'f' and the value without it,

ie, for a simply-supported beam, is 'f_o', then a frequency modification factor 'k_f' can be introduced such that

$$f = f_o \times k_f \quad (2.15)$$

Values of k_f can then be found for each individual case and this is now done for the example of a symmetric single-span sub-frame with fixed-ended columns, subject to a symmetric load.

A good approximation for the calculation of the natural frequency of any beam is given in reference {26} as

$$f = \frac{18}{\sqrt{y}} \text{ (Hz)} \quad (2.16)$$

where y = maximum short-term deflection due to the self-weight of the structure that the beam is supporting, expressed in millimetres.

The maximum deflection, δ_c , of a beam with fixity at the supports and subject to a symmetric loading can be approximated by the formula quoted in the code {14}, as follows:

$$\delta_c = \delta_o (1 - 0.6 (M_1 + M_2)/M_o) \quad (2.17)$$

where δ_o = maximum deflection of a similar simply supported beam with the same loading

and where M_1 , M_2 and M_o are the support moments and the maximum free bending moment respectively.

For this example $M_1 = M_2$ but, from before (equation 2.12), the support moments are given by

$$M_{\text{support}} = \frac{WL}{12} \times \frac{4\phi_c}{(4\phi_c + 1)} \quad (2.18)$$

where W = beam load
L = beam span

Therefore, from equation 2.17, it can be shown that

$$\delta_c = \delta_o \frac{(0.8\phi_c + 1)}{(4\phi_c + 1)} \quad (2.19)$$

The natural frequency of a similar simply-supported beam can then be expressed as

$$f_o = \frac{18}{\sqrt{\delta_o}} \quad (2.20)$$

Hence if y is put equal to δ_c in equation 2.16, from equations 2.19 and 2.20, it follows that

$$f = f_o \sqrt{\frac{(4\phi_c + 1)}{(0.8\phi_c + 1)}} \quad (2.21)$$

ie,
$$k_f = \sqrt{\frac{(4\phi_c + 1)}{(0.8\phi_c + 1)}}$$

The relationship for a similar case with pin-ended columns is

$$f = f_o \sqrt{\frac{(3\phi_c + 1)}{(0.6\phi_c + 1)}} \quad (2.22)$$

and the similar case with columns pinned at one end and fixed at the other is

$$f = f_o \sqrt{\frac{(7\phi_c + 2)}{1.4\phi_c + 2}} \quad (2.23)$$

All the above cases are shown graphically in Figure 2.5, where it can be seen that the maximum possible modification factor is 2.236, ie, for a fully fixed-ended beam. For typical values of ϕ_c of 0.9 to 1.5 the frequency is seen to increase by around 1.7, which still represents a significant improvement.

2.7 CONNECTIONS

The beam to column connections need to mobilise high bending moments by virtue of the fact that the structural system is a rigid frame. Fully-welded end connections can be provided and bolted connections introduced at the haunch toes or point of contraflexure. However it is believed that, in common with traditional practice, the use of bolted connections at the haunch heel positions will be more popular. In that case it will normally be found that the depth of the connection, and hence the depth of the haunch, will be determined from the strength of the connection rather than the strength of the haunch. In fact, as stated earlier, this author carried out a study of appropriate connection designs for beams of 400mm depth and above, with the haunch depth assumed to be twice the beam depth. It was found that the ratio of the connection strength to the elastic haunch strength varied from 0.48 to 1.04 for grade 50 sections, and some 15% to 20% greater for grade 43 sections. A typical value for grade 50 sections was 80%.

A design procedure for bolted haunch heel connections was developed as part of this work and is explained in detail in reference {9}. The method is also used in the worked example in Chapter 9. In short, the method assumes that the lower bolt group resists the shear and the upper bolt group, together with the compression zone, resists the moment. The point of rotation is determined from equilibrium by

assuming that the forces in the upper group bolt are proportional to the distance of each bolt from this point. However, where bolts are provided above the top beam flange, and where the end plate is stiffened there by a fillet stiffener, the bolts immediately above and below the flange are assumed to have the same forces. The end plate and column flange are checked for local bending, using yield line analysis, and the influence of the axial load on the column is also included.

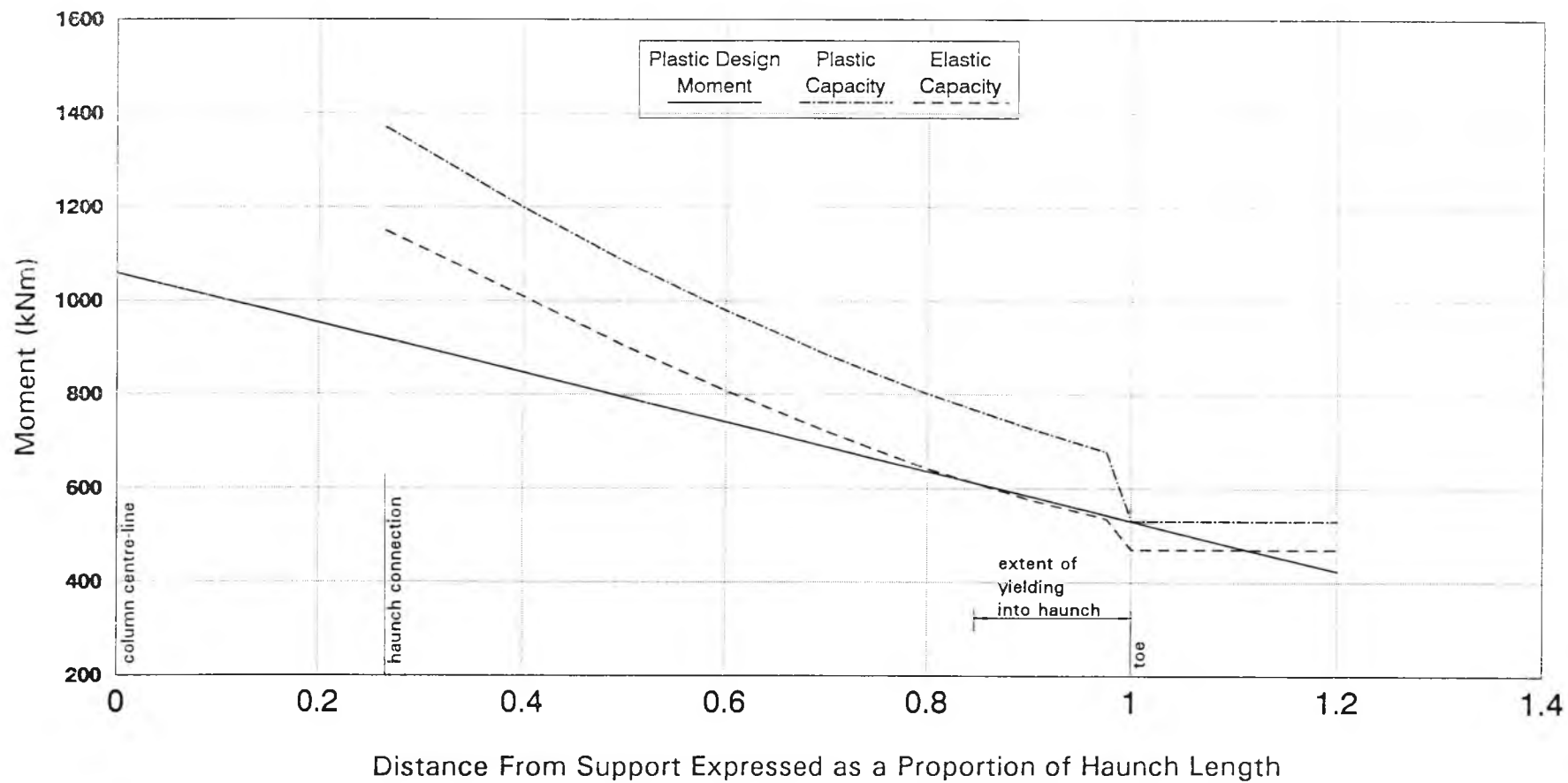


Figure 2.1 Haunch Design Moment versus Moment Capacity based on a 457x191UB 67 Beam and Cutting

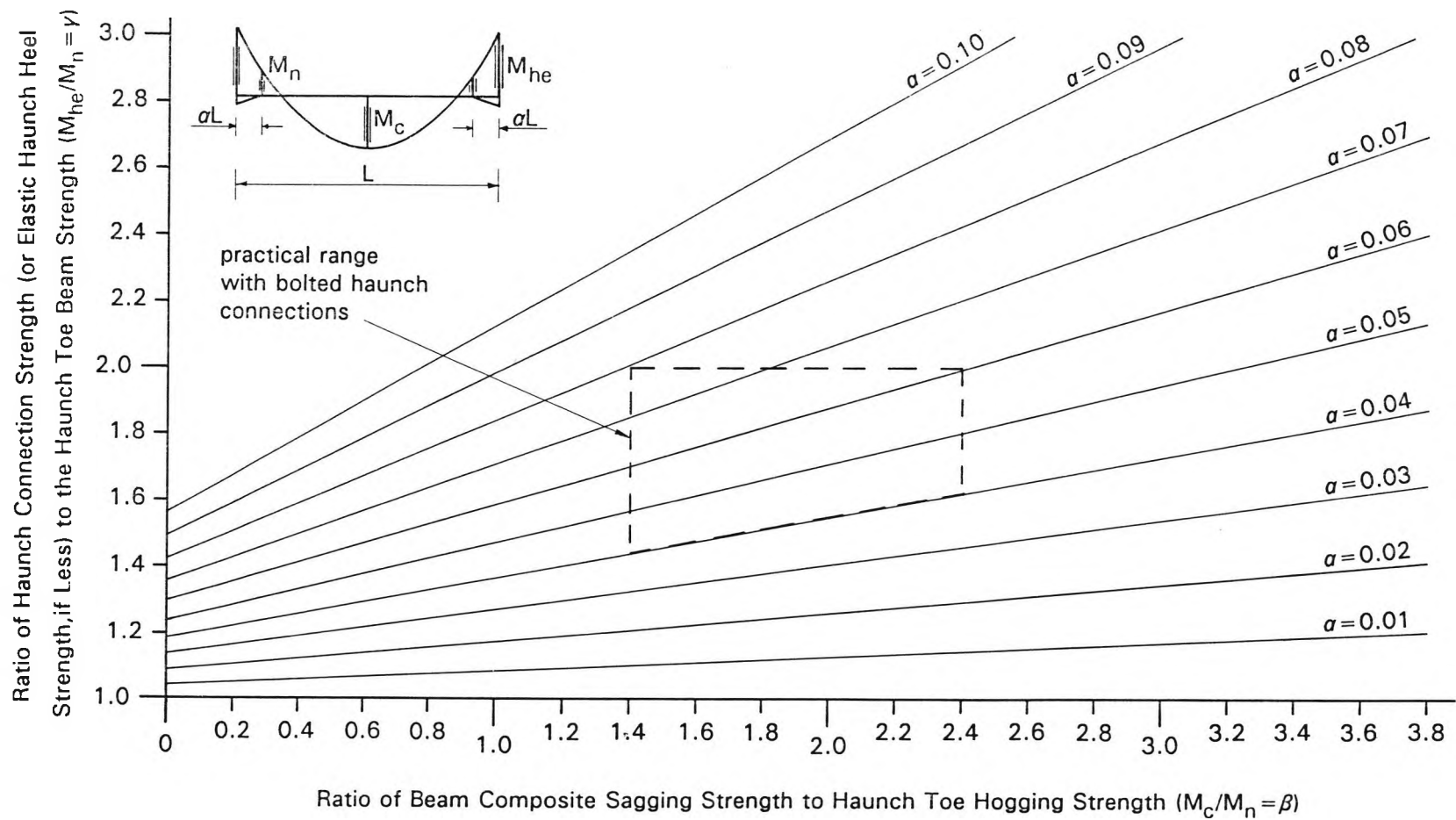


Figure 2.2 Haunch Length Optimisation for a Haunched Beam Subject to a UDL

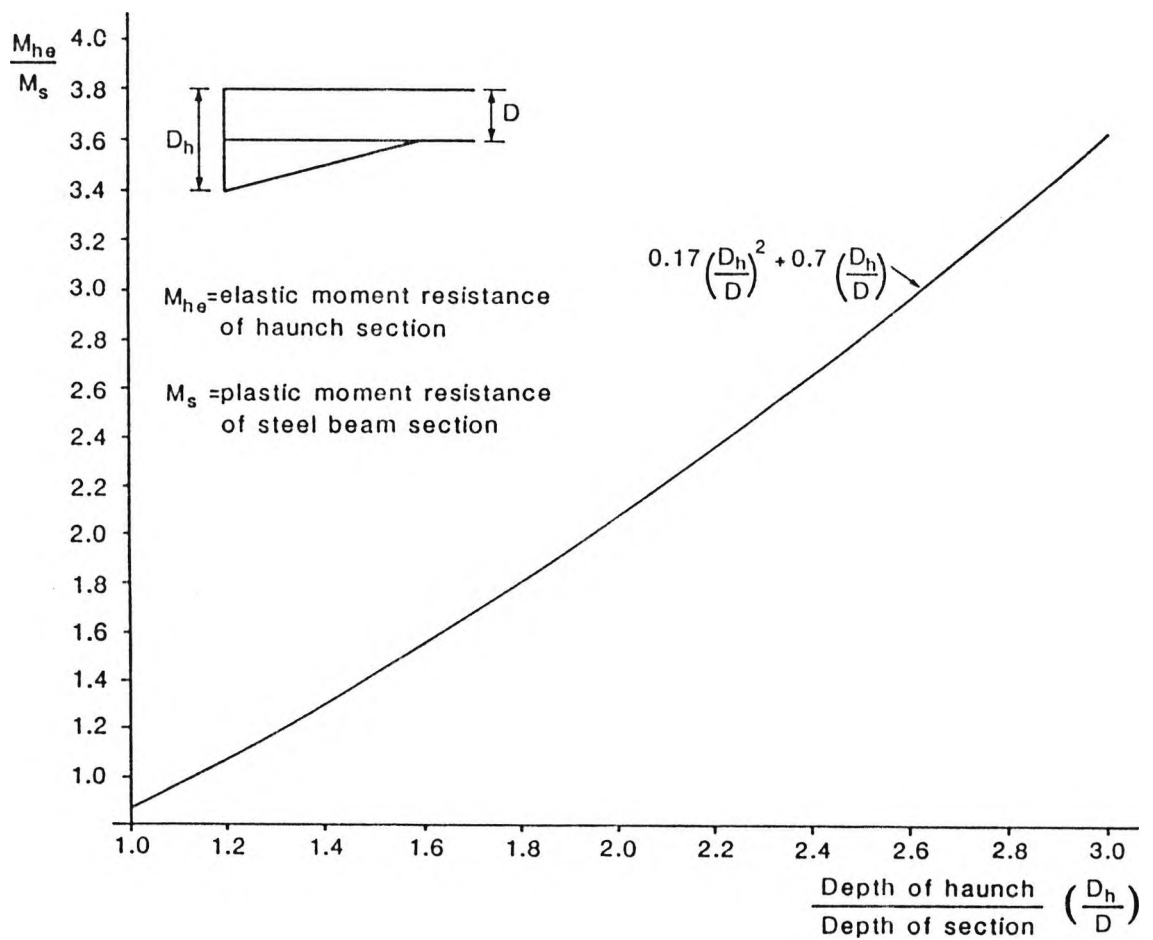


Figure 2.3 Relationship Between the Bending Resistances of the Haunch Heel and the Beam

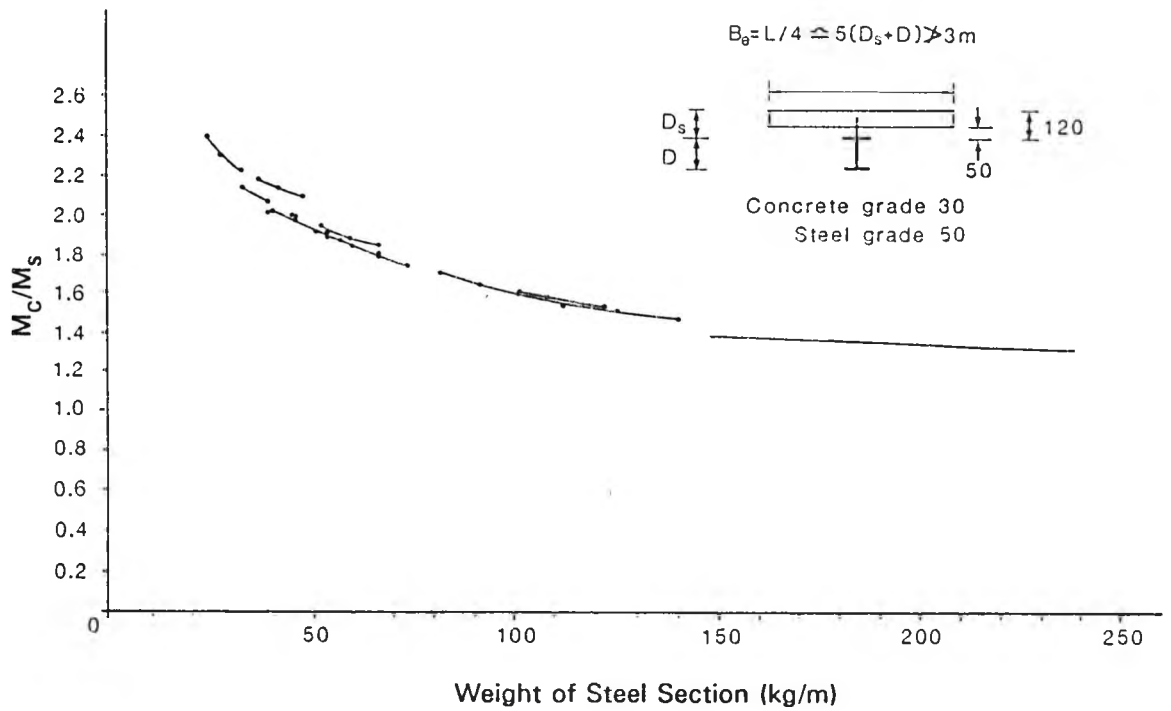


Figure 2.4 Ratio of Plastic Moment Capacity of the Composite Section to that of the Steel Section

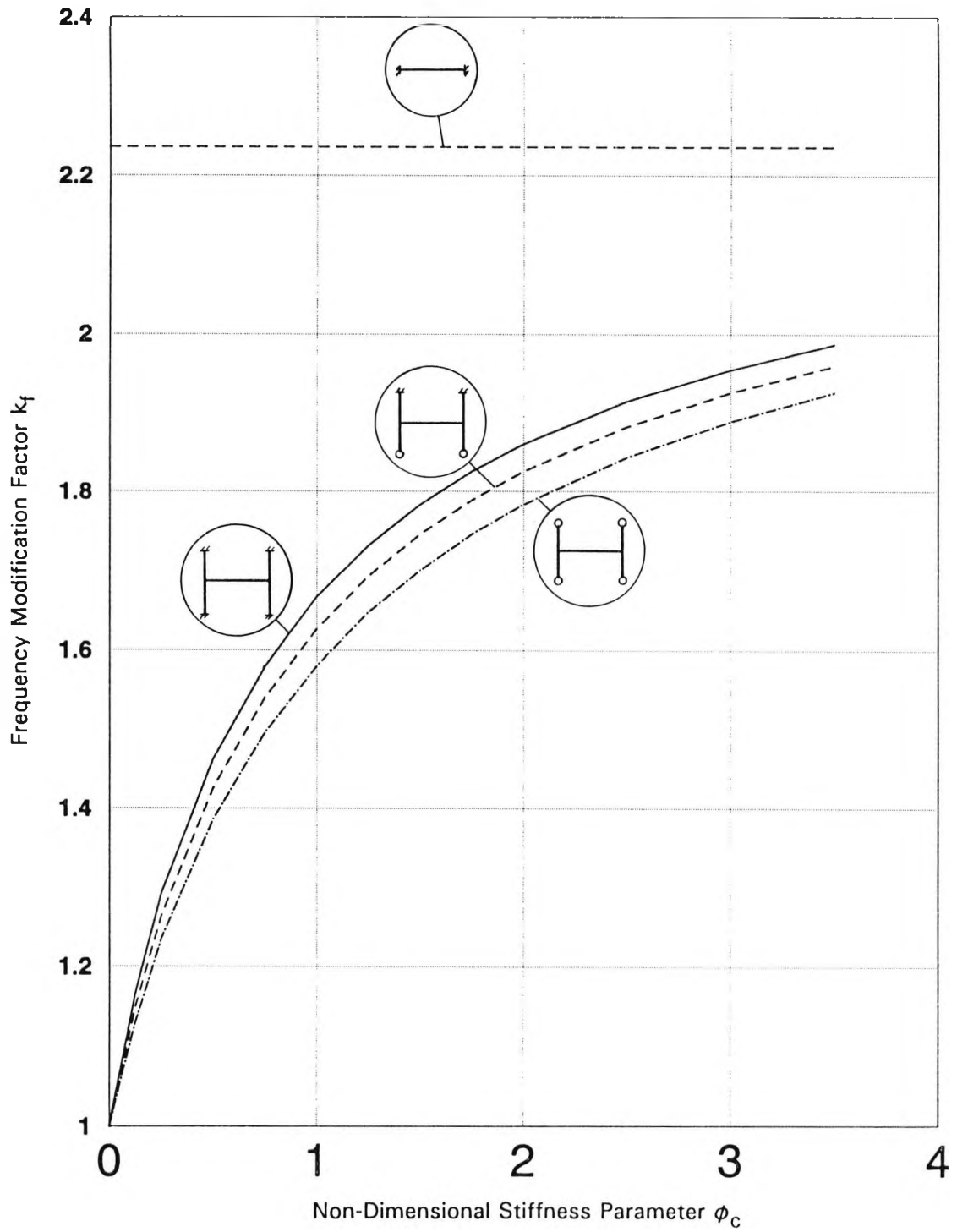


Figure 2.5 Frequency Modification Factor for a Single-Storey Symmetrical Sub-Frame subject to Symmetric Loading

CHAPTER 3

LATERAL TORSIONAL INSTABILITY

3.1 INTRODUCTION

When designing a non-composite steel-framed structure, it is necessary to ensure that premature buckling will not occur before the full design capacity of the structure is reached. For beams, two types of buckling normally apply. One is 'local buckling' which, as discussed earlier in Chapter 2, can be limited by the selection of a beam with an appropriate 'section classification'. The other is 'lateral torsional buckling' which involves both the rotation and displacement of the cross-section as a whole. This can be prevented by the appropriate choice of the member section or by the provision of lateral and torsional restraints. Design guidance for this is well established in the Codes {11} and {12}.

The behaviour of a composite beam is different to that of a steel beam because of the continuous connection provided by the shear connectors between the concrete floor and the beam. This provides both torsional and lateral restraint to the upper flange of the beam and, provided the slab is sufficiently stiff, which is normally the case, lateral or torsional movement of the top flange is prevented and buckling can only involve deformation of the web and bottom flange. For simply-supported beams and sagging (positive moment) regions of continuous beams, the restrained flange is the compression flange and so buckling is prevented. In hogging (negative moment) regions of continuous beams, however, the compression flange is not so restrained and buckling is possible. A typical buckled shape for this region is shown in Diagram 3.1. It can be seen that the cross-section is not merely displaced, but is distorted, and hence this kind of buckling is referred to as 'lateral distortional buckling'. It requires more energy to induce than lateral torsional buckling because it involves distortion of the cross-section.

When the author began his research into this problem, there was little other relevant published work available, and that which existed was largely based on computer parametric studies {27}, {28}. It was also directed at bridge structures where thin webs are used in deep beam sections. Empirical design formulae, which

are discussed in more detail later, were proposed for these methods. It was therefore necessary to develop a method suitable for the typical sections used in buildings, and this is now presented. The method is expressed in a form which makes it readily usable with the British Code {11}, but it can be adapted for use with other codes.

3.2 PROPOSED LATERAL DISTORTIONAL BUCKLING DESIGN METHOD

This method enables a uniform symmetric unreinforced 'I' beam, which is attached by shear connectors to a concrete floor slab, to be checked for its susceptibility to lateral distortional buckling. The method leads to the comparison of a 'buckling resistance moment' with the maximum moment occurring within a potential buckling length. The buckling resistance moment takes account of the value of the 'elastic critical moment' and the 'plastic moment of resistance' in a Perry-Robertson formulation which allows for dimensional imperfections and residual stresses in the same manner as is used in the checking of beams for lateral torsional buckling. This, of course, makes the assumption that these effects are the same for both lateral distortional buckling and lateral torsional buckling which, in the absence of direct evidence to the contrary, is considered reasonable and this assumption was also made in the other research {27}, {29}. The method was developed in close collaboration with my industrial supervisor, Dr R M Lawson, and advice was also obtained from Professor R P Johnson of the University of Warwick.

3.2.1 Determination of the Elastic Critical Buckling Moment

The elastic critical (hogging) buckling moment, M_{cr} , is now derived for a beam length by equating the work done by the forces during buckling to the energy absorbed by deforming the section. The effects of restrained warping and the transverse flexibility of the concrete slab oppose one another and are neglected. The upper steel section flange is assumed to be laterally and torsionally restrained by the concrete slab which is, itself, assumed to be unreinforced.

Consider a beam element, length 'L', restrained as described and subjected to a uniform hogging moment, ie, M_{cr} , which just causes buckling. The beam

element and cross-section will then deform as shown in Diagram 3.1. Let the distance between the shear centres (or centroids in this case) of the flanges of the steel section be ' h_s ', and the lateral displacement of the bottom flange shear centre, at distance ' x ' along the beam, be ' v '. Let also the rotation of the bottom flange shear centre relative to the top flange shear centre be ' θ ', and the rotation of the bottom flange relative to its initial position be ' ϕ ', as shown in the diagram.

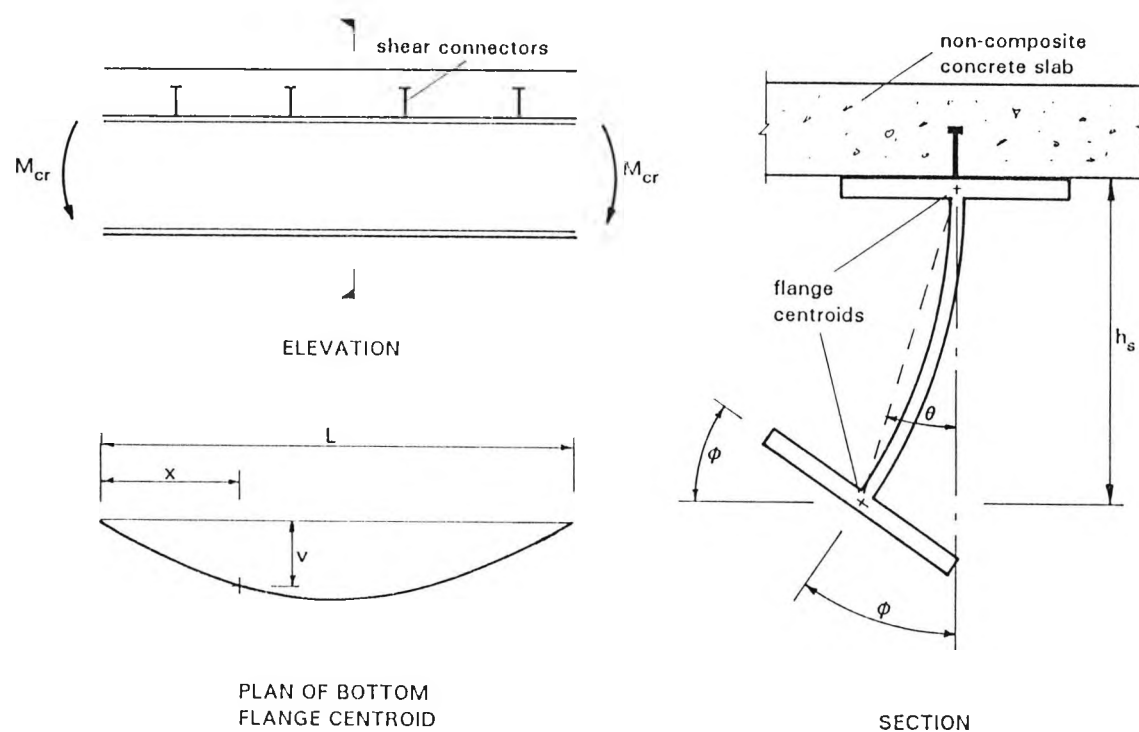


Diagram 3.1 **Beam Element and Cross-Sectional Deformation**

The energy absorbed in deforming the section can be considered as the algebraic summation of separate energies associated with separate deformations, such that, when they are all superimposed, the final deformed state closely resembles the actual deformation. It is therefore an approximate method but it can, nevertheless, give a close approximation. This summated energy can be expressed as the quantity $(E_1 + E_2 + E_3 + E_4)$ where:

- E_1 = strain energy absorbed in lateral bending of the bottom flange
- E_2 = torsional energy absorbed in twisting the bottom flange

$$\begin{aligned}
 E_3 &= \text{bending energy absorbed in displacing the web} \\
 E_4 &= \text{torsional energy absorbed in twisting the web.}
 \end{aligned}$$

The above energies can be equated to the work done which can be defined as ($E_5 + E_6$), where:

$$\begin{aligned}
 E_5 &= \text{work done by the compressive force in the bottom flange} \\
 E_6 &= \text{work done by the forces in the web}
 \end{aligned}$$

Hence,

$$E_1 + E_2 + E_3 + E_4 = E_5 + E_6 \quad (3.1)$$

Let the buckled plane shape of the shear centre of the bottom flange be a sine wave such that the lateral displacement, v , is given by:

$$v = V \sin \frac{\pi x}{L} \quad (3.2)$$

where V is the maximum value of v , ie, the amplitude.

Consider energy quantity E_1 :

$$\text{In general, energy due to bending} = \frac{1}{2} EI \int_0^L \left(\frac{d^2 v}{dx^2} \right)^2 .dx$$

where EI = flexural stiffness of the member

For the bottom flange only, $I = \frac{I_y}{2}$. I_y is not assumed to be affected by the rotation of the flange

$$\therefore E_1 = \frac{1}{2} \frac{EI_y}{2} \int_0^L \left(\frac{d^2 v}{dx^2} \right)^2 dx$$

but
$$\frac{d^2v}{dx^2} = - \frac{\pi^2 V}{L^4} \sin \frac{\pi x}{L}$$

$$\therefore E_1 = \frac{1}{2} \frac{EI_y}{2} \int_0^L \frac{\pi^4 V^2}{L^4} \sin^2 \frac{\pi x}{L} .dx$$

$$= \frac{1}{2} \frac{EI_y}{2} \frac{\pi^4 V^2}{L^4} \frac{L}{2}$$

$$E_1 = \frac{EI_y \pi^4 V^2}{4L^3} \tag{3.3}$$

Consider energy quantity E_2 :

The general equation for the energy due to twisting of a beam, when warping is neglected, is:

$$= \frac{1}{2} GJ \int_0^L \left[\frac{d\phi}{dx} \right]^2 dx$$

- where ϕ = angle twist at a distance x along the beam
 G = shear modulus
 J = torsional constant

Since most of the destabilising compressive force throughout the cross-section lies in the bottom flange, it is reasonable to assume that the deflected shape of the web takes the form of a point-loaded cantilever. It can then be shown that the rotation of the bottom flange, ie, at the tip of the cantilever, is equal to $3\theta/2$, where θ was defined earlier. Therefore, for the bottom flange only

$$E_2 = \frac{1}{2} GJ_f \int_0^L \left[\frac{d(3\theta/2)}{dx} \right]^2 dx$$

where $J_f =$ torsional constant of the bottom flange
 $= \frac{1}{3} B \cdot T_f^3$

where $B =$ steel flange width
 $T_f =$ steel flange thickness

$$\therefore E_2 = \frac{1}{2} GJ_f \frac{9}{4} \int_0^L \left[\frac{d\theta}{dx} \right]^2 dx$$

but for small angles of θ , $v = h_s \theta$

$$\theta = \frac{V}{h_s} \sin \frac{\pi x}{L} \tag{3.4}$$

$$\frac{d\theta}{dx} = \frac{V\pi}{h_s L} \cos \frac{\pi x}{L}$$

Hence $E_2 = \frac{1}{2} GJ_f \frac{9}{4} \int_0^L \frac{V^2 \pi^2}{h_s^2 L^2} \cos^2 \frac{\pi x}{L} dx$

$$= \frac{1}{2} GJ_f \frac{9}{4} \frac{V^2 \pi^2}{h_s^2 L^2} \frac{L}{2}$$

$$\therefore E_2 = \frac{1}{2} \frac{9}{8} \frac{GJ_f V^2 \pi^2}{h_s^2 L} \tag{3.5}$$

Consider energy quantity E_3 :

The bending energy associated with the bending of the web may be considered by first calculating the bending energy of a cantilever element, width dx , and then, by integrating all these elements along the potential buckling length, L . Let the lateral

displacement of the element be 'u' at a distance 'z' down the web from the top steel flange centroid, as shown in Diagram 3.2 below:

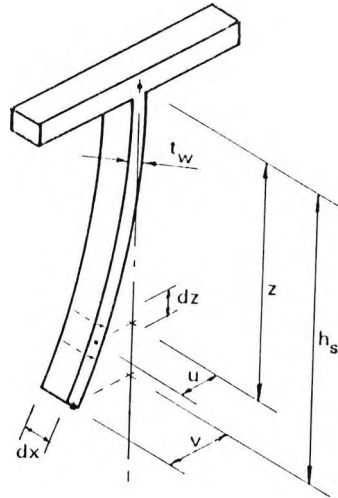


Diagram 3.2 Element for Calculating Web Bending Energy

It can be shown that the deflected shape of the cantilever element can be expressed as:

$$u = \frac{3v}{2h_s^3} \left[h_s z^2 - \frac{z^3}{3} \right] \quad (3.6)$$

Then the bending energy per element

$$E_3/\text{element} = \frac{1}{2} E I_w dx \int_0^{h_s} \left[\frac{d^2 u}{dz^2} \right]^2 dz$$

where $I_w = \frac{1}{12} t_w^3$, and $t_w =$ web thickness

$$\text{but } \frac{d^2 u}{dz^2} = \frac{3v}{h_s^3} (h_s - z)$$

$$\begin{aligned}
\therefore E_3/\text{element} &= \frac{1}{2} EI_w dx \int_0^{h_s} \frac{9v^2}{h_s^6} (h_s^2 - 2h_s z + z^2) dz \\
&= \frac{1}{2} EI_w dx \times \frac{9v^2}{h_s^6} (h_s^3 - h_s^3 + h_s^3/3) \\
&= \frac{1}{2} \times \frac{3EI_w v^2}{h_s^3} dx
\end{aligned}$$

Integrating along the buckling length, it follows that:

$$\begin{aligned}
E_3 &= \int_0^L \frac{1}{2} \times \frac{3EI_w v^2}{h_s^3} dx \\
&= \frac{3EI_w}{2h_s^3} v^2 \int_0^L \sin^2 \frac{\pi x}{L} dx \\
\therefore E_3 &= \frac{1}{2} \times \frac{3EI_w v^2 L}{2h_s^3} \tag{3.7}
\end{aligned}$$

Consider energy quantity E_4 :

The torsional energy associated with the twisting of the web can be calculated by considering the web as a series of longitudinal strips, length L , and width ' dz '. Let the angle of twist of each element be ' α_x ' at a distance ' x ' along the beam, as shown in Diagram 3.3.

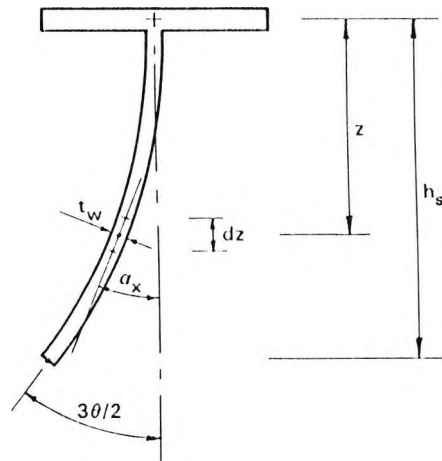


Diagram 3.3 Element for Calculating Web Torsional Energy

By again assuming that the web deforms like a point-loaded cantilever, it can be shown that the twist at depth 'z' of an element is given by:

$$\alpha_x = \frac{3\theta}{h_s^2} \left[(h_s z - \frac{z^2}{2}) \right] \quad (3.8)$$

Then the strain energy per element

$$E_{4/\text{element}} = \frac{1}{2} G \frac{J_w}{h_s} dz \int_0^L \left[\frac{d\alpha_x}{dx} \right]^2 dx$$

where $J_w = \frac{1}{3} h_s t_w^3$

By substituting equation 3.4 in equation 3.8

$$\alpha_x = \frac{3V}{h_s^3} \left[h_s z - \frac{z^2}{2} \right] \sin \frac{\pi x}{L}$$

$$\therefore \frac{d\alpha_x}{dx} = \frac{3\pi V}{h_s^3 L} \left(h_s z - \frac{z^2}{2} \right) \cos \frac{\pi x}{L}$$

$$\begin{aligned} \therefore E_4/\text{element} &= \frac{1}{2} G \frac{J_w}{h_s} dz \int_0^L \frac{9\pi^2 V^2}{h_s^6 L^2} \left(h_s z - \frac{z^2}{2} \right)^2 \cos^2 \frac{\pi x}{L} dx \\ &= \frac{1}{2} G \frac{J_w}{h_s} dz \frac{9\pi^2 V^2}{h_s^6 L^2} \left(\frac{h_s z - z^2}{2} \right)^2 \frac{L}{2} \end{aligned}$$

By integrating down the web:

$$\begin{aligned} E_4 &= \frac{1}{2} G J_w \frac{9\pi^2 V^2}{2h_s^7 L} \int_0^{h_s} \left(h_s^2 z^2 - h_s z^3 + \frac{z^4}{4} \right) dz \\ &= \frac{1}{2} \times \frac{9 G J_w \pi^2 V^2}{2 h_s^7 L} \left[\frac{h_s^2 z^3}{3} - \frac{h_s z^4}{4} + \frac{z^5}{20} \right]_0^{h_s} \end{aligned}$$

which reduces to

$$E_4 = \frac{1}{2} \times \frac{3 G J_w \pi^2 V^2}{5 h_s^2 L} \quad (3.9)$$

Consider energy quantity E_5 :

The work done by the force in an element is equal to the force times the distance through which the force moves. The latter quantity is the shortening of the distance between the ends of the element and, neglecting any axial compressive shortening, this is the difference between the shortened length of the buckled shape and its initial

length. It can be shown that for a longitudinal element of length 'ds', which has buckled out of plane a distance 'v' and now has a projected length of 'dx' on the initial longitudinal axis, the shortened projected length is given by:

$$ds - dx \approx \frac{1}{2} \left[\frac{dv}{ds} \right]^2 \cdot dx$$

Hence for a member, length L, the total shortening is given by:

$$\int_0^L \frac{1}{2} \left[\frac{dv}{ds} \right]^2 dx \quad (3.10)$$

The force in the bottom flange is the elastic critical buckling load and this can be expressed in terms of an elastic critical stress, σ_{cr} , where

$$\text{flange force} = \sigma_{cr} B T_f$$

It is convenient to consider the destabilising energy in terms of stress so that the contributions of the web and flange may be considered separately. In preliminary studies {9} this was not done.

If the elastic critical buckling moment is M_{cr} , then the elastic critical stress in the bottom flange can be expressed as $\frac{M_{cr}}{Z_e}$, where Z_e = elastic steel beam modulus of the centroid of the bottom flange

$$\text{Hence, } E_s \quad = \frac{1}{2} \frac{M_{cr}}{Z_e} B T_f \int_0^L \left[\frac{dv}{dx} \right]^2 dx$$

but from before, for sinusoidal movement of the flange, $v = V \sin \frac{\pi x}{L}$

$$\begin{aligned} \therefore E_5 &= \frac{1}{2} \frac{M_{cr}}{Z_e} B T_f \int_0^L \frac{\pi^2 V^2}{L^2} \cos^2 \frac{\pi x}{L} dx \\ E_5 &= \frac{1}{2} \times \frac{M_{cr} B T_f \pi^2 V^2}{2 Z_e L} \end{aligned} \quad (3.11)$$

Consider energy quantity E_6 :

The work done by the forces in the web can be calculated by considering a series of longitudinal elements, width 'dz' down the web, whereby each element is subject to a force according to the stress distribution down the web. Each element also undergoes a degree of shortening, which varies according to its lateral deformation. Assuming that there is no reinforcement in the slab and that the concrete has no tensile strength, then the stress distribution at the elastic critical buckling moment in a symmetric 'I' section will vary linearly, from $-M_{cr}/Z_e$ at the centroid of the top steel flange, to $+M_{cr}/Z_e$ at the centroid of the bottom steel flange, as shown in Diagram 3.4. The deflected shape of the web is again assumed as that of a point-loaded cantilever, and each longitudinal element is assumed to have a lateral deflection of 'u' at a distance 'z' down from the centroid of top flange, and at a distance 'x' along the beam, as shown in the diagram.

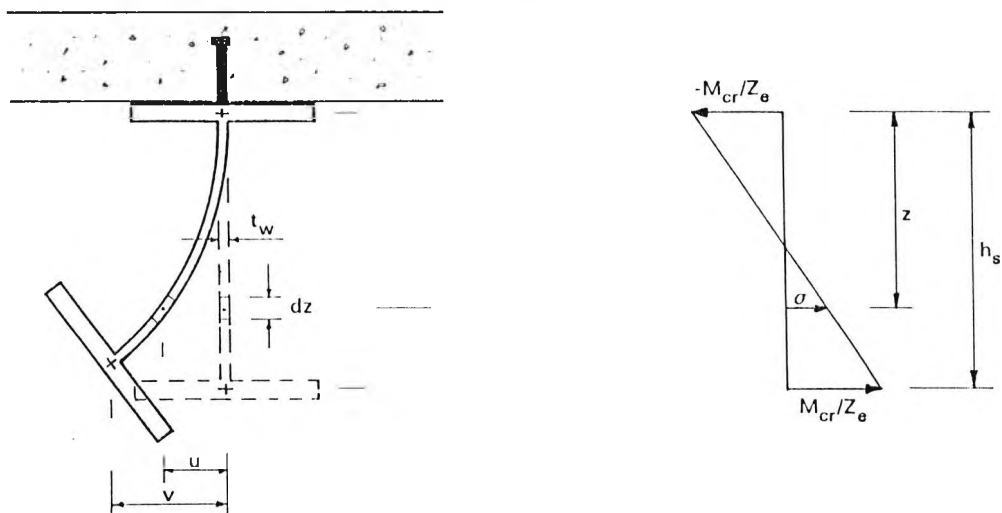


Diagram 3.4 Element and Stress Distribution for Calculating the Work Done by the Forces in the Web

The elastic stress, σ , at depth z , when the elastic critical moment is applied, is given by:

$$\sigma = \frac{2 M_{cr}}{h_s Z_e} z - \frac{M_{cr}}{Z_e} \quad (3.12)$$

The force on an element = $\sigma t_w dz$, and the work done by this force is then

$$\frac{1}{2} \sigma t_w dz \int_{x=0}^{x=L} \left(\frac{du}{dx} \right)^2 dx \quad (3.13)$$

The total work done on the web is then the integral of this down the web, ie,

$$E_6 = \int_{z=0}^{z=h_s} \left\{ \frac{1}{2} \sigma t_w dz \int_{x=0}^{x=L} \left(\frac{du}{dx} \right)^2 dx \right\}$$

By using the equation for the vertically deflected shape, 3.6, and that for the longitudinal deflected shape, 3.2, and then differentiating, the following result is obtained:

$$\left(\frac{du}{dx} \right)^2 = \left(\frac{dv}{dx} \right)^2 \times \frac{9}{4 h_s^6} \left(h_s z^2 - \frac{z^3}{3} \right)^2 \quad (3.14)$$

Hence:

$$E_6 = \int_{z=0}^{z=h_s} \left\{ \frac{1}{2} \left[\frac{2M_{cr}}{h_s Z_e} z - \frac{M_{cr}}{Z_e} \right] t_w dz \cdot \int_{x=0}^{x=L} \frac{9 \pi^2 V^2}{4 L^2 h_s^6} \left(h_s z^2 - \frac{z^3}{3} \right) \cos^2 \frac{\pi x}{L} dx \right\}$$

$$\therefore E_6 = \frac{1}{2} \int_{z=0}^{z=h_s} \frac{9 \pi^2 V^2 M_{cr} t_w}{4 L^2 h_s^6 Z_e} \left[\frac{2z}{h_s} - 1 \right] \left[h_s^2 z^4 + \frac{z^6}{9} - \frac{2 h_s z^5}{3} \right] \frac{L}{2} dz$$

After integrating and rearranging, this reduces to

$$E_6 = \frac{1}{2} \times \frac{83 \pi^2 V^2 M_{cr} t_w h_s}{1120 L Z_e} \quad (3.15)$$

Hence from equation 3.1, by equating the energies, multiplying throughout by $\frac{4 L}{\pi^2 V^2}$ and collating terms, the elastic critical buckling equation is obtained thus:

$$\frac{M_{cr}}{Z_e} \left[B T_f + \frac{83}{560} h_s t_w \right] = \frac{EI_y}{2} \left[\frac{\pi}{L} \right]^2 + \frac{2G}{h_s^2} \left[\frac{9J_f}{8} + \frac{3J_w}{5} \right] + \frac{3EI_w}{h_s^3} \left[\frac{L}{\pi} \right]^2 \quad (3.16)$$

3.2.2 Determination of Equivalent Slenderness

The analysis so far has been based purely on elastic principles without the inclusion of imperfections. It has also not considered the limitation of the yield strength or the effect of residual stresses. These are now considered in the way that they are treated in the British Code {11} but the equation for the elastic critical moment (3.16) could be adapted in other ways, according to different codes, to allow for these effects.

The British Code introduces the concept of 'equivalent slenderness', λ_{LT} , which is used to determine the 'buckling resistance moment', M_b , mentioned earlier, which can be compared with the applied, or rather, 'design' moment. For a uniform design moment, λ_{LT} merely quantifies the degree of restraint and the cross-sectional properties which relate to the susceptibility to buckling. λ_{LT} is related in the code to M_{cr} and the plastic moment of resistance, M_p , as follows:

$$M_{cr} = \frac{M_p \pi^2 E}{\lambda_{LT}^2 p_y} \quad (3.17)$$

where $p_y = \text{yield stress}$

The imperfections and residual stresses are incorporated in a Perry coefficient ' η_{LT} ' which appears in the formula for the calculation of M_b , where M_b is the smaller root of:

$$(M_{cr} - M_b) (M_p - M_b) = \eta_{LT} M_{cr} M_b \quad (3.18)$$

For the proposed method, λ_{LT} can be obtained from equations 3.16 and 3.17 and, by putting $M_p = S_x p_y$, where S_x is the major axis plastic modulus, the following equation is derived:

$$\lambda_{LT} = \frac{\left\{ \frac{2S_x L^2}{h_s I_y} \right\}^{0.5} \left\{ \frac{h_s}{Z_e} \left[BT_f + \frac{83}{560} h_s t_w \right] \right\}^{0.5}}{\left\{ 1 + \frac{4GL^2}{h_s^2 \pi^2 EI_y} \left[\frac{9J_f}{8} + \frac{3J_w}{5} \right] + \frac{6I_w L^4}{\pi^4 h_s^3 I_y} \right\}^{0.5}} \quad (3.19)$$

The first numerator term can be rewritten as:

$$\left\{ \frac{2S_x}{A h_s} \right\}^{0.5} \lambda$$

where $A = \text{area of steel section}$

and $\lambda = L/r_y$,

where r_y = minor axis radius of gyration

Now $\left\{ \frac{2S_x}{Ah_s} \right\}^{0.5}$ is a section parameter, but a buckling parameter 'u' is defined in

the code {11}, for flanged sections symmetrical about their minor axis, as

$$u = \left\{ \frac{2S_x}{Ah_s} \right\}^{0.5} \left\{ 1 - \frac{I_y}{I_x} \right\}^{0.25} \quad (3.20)$$

and it can be seen that for normal 'I' sections, when $I_y \ll I_x$, the right hand side term reduces to unity and the quantities become the same.

The second numerator term in equation 3.19 can be reduced to

$$\left\{ \left[BT_f + \frac{83}{560} h_s t_w \right] / \left[BT_f + \frac{93}{560} h_s t_w \right] \right\}^{0.5}$$

which can also be conservatively approximated to unity. The term $\left[\frac{9J_f}{8} + \frac{3J_w}{5} \right]$

can be conservatively approximated to $J/2$, where J is the torsional constant for the whole steel section, ie,

$$\text{where } J = 2J_f + J_w$$

By putting $G = E/2.6$, ie, the value for steel, equation 3.19 can be simplified to

$$\lambda_{LT} = \frac{u \lambda}{\left\{ 1 + \frac{2JL^2}{2.6 \pi^2 h_s^2 I_y} + \frac{6I_w L^4}{\pi^4 h_s^3 I_y} \right\}^{0.5}}$$

and by introducing a further torsional parameter 'x' into the second denominator term, where 'x' is also defined in the code {11} for flanged sections symmetrical about their minor axis, as

$$x = 0.566 h_s (A/J)^{0.5}, \quad (3.21)$$

the above equation can be reduced to:

$$\lambda_{LT} = \frac{u\lambda}{\left[1 + \frac{1}{40.05} \left(\frac{\lambda}{x} \right)^2 + \frac{1}{16.23} \left(\frac{L}{h_s} \right)^3 \frac{LI_w}{I_y} \right]^{0.5}}$$

For ease of use, this equation can be conservatively simplified by substituting the depth of the steel section, D, for h_s . By rounding terms, the following result is then obtained, which has been quoted in {9}:

$$\lambda_{LT} = \frac{u\lambda}{\left[1 + \frac{1}{40} \left(\frac{\lambda}{x} \right)^2 + \frac{1}{16} \left(\frac{L}{D} \right)^3 \frac{LI_w}{I_y} \right]^{0.5}} \quad (3.22)$$

The right-hand side of the above equation can be considered as $u v_t \lambda$, where ' v_t ' is referred to in the code as a slenderness factor. The value of ' v_t ', above, can be compared with the value quoted in the code for the case when the tension flange is continuously restrained laterally, but not torsionally, along its length. For a uniform section subject to a constant moment, v_t is quoted in the British Code {11} in clause G.3.3, as

$$v_t = \left[\frac{\frac{4a}{h_s}}{1 + \left[\frac{2a}{h_s} \right]^2 + \frac{1}{20} \left[\frac{\lambda}{x} \right]^2} \right]^{0.5} \quad (3.23)$$

where a = distance of lateral restraint above the neutral axis. For the comparison, by putting $a = h_s/2$, equation 3.23 can be reduced to

$$v_t = \frac{1}{\left[1 + \frac{1}{40} \left[\frac{\lambda}{x} \right]^2 \right]^{0.5}} \quad (3.24)$$

which is exactly the same as equation 3.22 without the last denominator term for the bending of the web.

3.2.3 Effect of Reinforcement in the Concrete Slab

The analysis so far presented assumes that there is no reinforcement in the concrete slab. If reinforcement is provided, this will increase the major axis strength of the member but the neutral axis will also be raised. This means that the web will be subjected to compression over a greater depth, which will increase instability. If a limit to the position of the neutral axis is taken to be the centroid of the top steel flange, then the energy terms can be re-calculated and compared.

The equation for the stress with depth, formally equation 3.12, would become

$$\sigma = \frac{M_{cr}}{Z_{er}} z$$

where Z_{er} = elastic modulus of reinforced section about the centroid of the bottom flange.

By integrating over the full depth, as before, the following revised energy quantity E_6 is obtained thus:

$$E_6 = \frac{1}{2} \times \frac{107.5 \pi^2 V^2 M_{cr} t_w h_s}{1120L Z_{er}}$$

It can be seen that the numerical multiplier is 30% greater than in equation 3.15, but, by inspection, the second numerator term in the equation for the effective slenderness, 3.19, can still be approximated to unity with very little error. The first numerator term, however, could take advantage of the reinforced section strength, if desired. It can therefore be concluded from the analysis that the destabilising effect due to the addition of reinforcement is likely to be minimal and that the buckling strength will, in fact, be enhanced by the increased bending strength that the reinforcement provides.

3.2.4 Shear Connection Flexibility and Transverse Concrete Slab Flexibility

For simplicity, the buckling analysis developed so far assumes that the top flange of the steel beam is rigidly restrained by the shear connection and the concrete floor slab. Of course, this is not strictly true, because the shear connectors will deform to a degree during buckling and the concrete slab will also develop a slight curvature. Therefore, the top steel flange will not be entirely prevented from rotating.

With regard to the flexibility of the shear connection, the stress regime around a connector is complex, and any calculation of flexibility would need to include the bending of the connector, the compression of the concrete and the bending of the steel flange around the connector. Other researchers in the field {27}, as discussed later in Section 3.2, have analysed this behaviour and found that it was at least an order of magnitude less than the slab flexibility, and could be ignored. They

considered that the slab flexibility, on the other hand, did have an influence on the buckling strength in some cases. This author's review of the other research, however, found only one method that proposed a precise allowance for it.

To maintain the simplicity of the method developed in this thesis, it is not proposed to calculate an 'exact' buckling moment taking the slab flexibility into account, but, rather, it is proposed to assess the transverse flexibility in a given case, to check whether it is beyond a prescribed limit. If it is, then it is suggested that only lateral restraint to the top flange be assumed. This approach was initially suggested by Professor Johnson in correspondence, and he proposed that the condition for this should be based on the relative extra lateral displacement of the bottom flange due to the slab flexibility. He suggested that torsional restraint should only be assumed when this additional displacement was less than 10% of the value calculated by assuming a rigid top flange. The case where least restraint is provided is that where two adjacent beams buckle simultaneously, and where both are connected to the same single-span floor slab, and this case is now analysed.

Consider the bottom beam flanges such that each is subject to a lateral unit destabilising force, as shown in Diagram 3.5. Let the lateral displacement of the bottom beam flanges due to the slab flexibility alone be ' v_1 ', and, as before, let the lateral displacement due to bending of the web be ' v '. Also, let the rotation of the steel member due to the slab flexibility be θ_s .

**Diagram 3.5 Buckled Shape of Two Adjacent Beams with a Connecting
Single-Span Concrete Floor Slab**

It is noted that the displacements v and v_1 are not co-linear, but, for simplicity, they are defined as shown in the diagram. 'v' is then given by

$$v = \frac{1 \times h_s^3}{3 E I_w} \quad (3.25)$$

where terms have been defined earlier

The unit force applies end moments to the slab of $1 \times (h_s + d_n)$, where d_n is the distance from the neutral axis in the slab to the centroid of the top steel flange. The end rotation in the slab is then

$$\theta_s = \frac{1 \times (h_s + d_n) b}{2 E_{cn} I_{cn}} \quad (3.26)$$

Where b = the span of the concrete slab
 E_{cn} = Young's modulus of concrete
 I_{cn} = the second moment of area of the concrete slab

For small θ_s

$$v_1 = (h_s + d_n) \theta_s$$

$$\therefore v_1 = \frac{(h_s + d_n)^2 b}{2 E_{cn} I_{cn}} \quad (3.27)$$

The condition that the slab flexibility should be neglected is when

$$\frac{v_1}{v} \leq 0.1$$

$$\text{i.e.} \quad \left\{ \frac{10 (h_s + d_n)^2 b}{E_{cn} I_{cn}} \right\} / \left\{ \frac{h_s^2}{3 E I_w} \right\} \leq 1$$

$$\therefore \frac{30 (h_s + d_n)^2 b E I_w}{h_s^3 E_{cn} I_{cn}} \leq 1 \quad (3.28)$$

This applies to the unusually onerous case of a single-span concrete slab but most beams will be supporting a multi-span continuous slab. For these latter situations the flexibility will be less and, therefore, so will the beam rotations and lateral displacements. In general, equations 3.26 and 3.27 can be re-written as

$$\theta_s = \frac{r (h_s + d_n) b}{E_{cn} I_{cn}}$$

$$\text{and} \quad v_1 = \frac{r (h_s + d_n)^2 b}{E_{cn} I_{cn}}$$

where r is a factor depending on the particular case, and values are given below in Table 3.1.

No. of continuous spans of floor slab	1	2	3 or more
Edge Beam	0.5	0.417	0.4
Intermediate Beam	-	0.333	0.3

Table 3.1 Factor 'r' for Various Beam Conditions

Hence, the general condition becomes

$$\frac{30r (h_s + d_n)^2 b E I_w}{h_s^3 E_{cn} I_{cn}} \quad (3.29)$$

Further simplifications to this can be made, as follows:

$\frac{E}{E_{cn}} = 10$ for normal weight concrete or 15 for lightweight concrete,

$I_{cn} \approx \frac{(0.9 D_s)^3}{12}$, where $D_s =$ the depth of the concrete slab,

also $h_s \approx D$ and $d_n \approx D_s/2$.

By putting $I_w = t_w^3/12$, equation 3.29 can then be simplified for normal weight concrete to

$$t_w \leq \frac{0.9 D D_s}{\sqrt[3]{300 r b (D + D_s/2)^2}} \quad (3.30)$$

and for lightweight concrete to

$$t_w \leq \frac{0.9 D D_s}{\sqrt[3]{450 r b (D + D_s/2)^2}} \quad (3.31)$$

Therefore, if the web thickness of the beam is less than the value given by equation 3.30 (or 3.31 as appropriate), or, in other words, if the ratio of the concrete slab stiffness to the steel beam web stiffness is sufficiently large, then torsional restraint may be assumed.

To quantify how restrictive these conditions are, it is appropriate to consider examples. For example 1, consider a lightweight multi-span concrete slab with $b = 3000\text{mm}$ and $D_s = 130\text{mm}$. The condition for an internal beam then becomes

$$t_w \leq \frac{1.58 D}{\sqrt[3]{(D + 65)^2}} \quad (\text{mm})$$

By examining the range of British rolled sections, the following table showing beams failing the condition has been derived. These are the heavier beams in each serial size range.

UB Serial Size	356 x 171	406 x 140	406 x 178	457 x 152	457 x 191	533 x 210	610 x 229	610 x 305	686 x 254	762 x 267	838 x 292	914 x 305	914 x 419
Maximum t_w (mm)	10.0	10.6	10.6	11.2	11.2	11.5	12.5	12.5	13.1	13.7	14.2	14.7	14.7
No. of sections failing condition	None	None	None	None	1 out of 5	2 out of 5	1 out of 4	2 out of 3	2 out of 4	2 out of 3	2 out of 3	All	All

Table 3.2 Example 1 - British Rolled Steel Sections for which Torsional Restraint to the Top Flange Cannot be Assumed

It is considered that this example represents the most likely case in practice and the above table shows that only a few sections fail the criterion, and those that do are the heavy sections.

For example 2, consider a lightweight single-span condition, with other values as before. The criterion then becomes

$$t_w \leq \frac{1.33 D}{\sqrt[3]{(D + 65)^2}} \text{ (mm)}$$

and Table 3.3 shows the sections failing this condition.

UB Serial Size	356 x 171	406 x 140	406 x 178	457 x 152	457 x 191	533 x 210	610 x 229	610 x 305	686 x 254	> 686
Maximum t_w (mm)	8.4	8.9	8.9	9.4	9.4	10.0	10.6	10.6	11.1	> 11.1
No. of sections failing condition	1 out of 4	None	1 out of 4	2 out of 5	3 out of 5	4 out of 5	3 out of 4	All	All	All

Table 3.3 Example 2 - British Rolled Steel Sections for which Torsional Restraint to the Top Flange Cannot be Assumed

Since this case is the most onerous, as one might expect, it is much more restrictive than the previous example. However, it is an unlikely case, and yet, nevertheless, the table shows that the lightest section in most serial sizes up to 610 passes the criterion.

From the above analysis it can be seen that where heavy sections are chosen, and for external beams, this check may prove to be restrictive, but, for most situations, it will not be so. However, if a beam fails this check, it does not mean that it is unsuitable, but merely that more bracing may be required.

3.2.5 Allowance for Varying Moments

As for the treatment of imperfections and residual stresses, it seems reasonable to assume that the effect of a varying moment will be the same for both lateral torsional buckling and lateral distortional buckling. The method presented in Appendix G of the British Code {11}, based on work by Singh {30}, is considered appropriate. This takes the form of a factor, n_t , which is used to modify the equivalent slenderness such that

$$\lambda_{LT} = n_t u v_t \lambda \quad (3.31)$$

' n_t ' is found by a method involving numerical integration of the moment diagram and it is calibrated so as to reduce the equivalent slenderness to a level which produces an appropriate value of buckling resistance moment, M_b , for comparison with the maximum applied moment. In other words, its effect on a beam subject to varying design moments along its length is the same as reducing the value of the design moment, which is normally taken as the peak value, to an equivalent uniform moment which, in similar circumstances, would also just cause buckling.

n_t is defined in Appendix G of reference {11} by

$$n_t = \left[\frac{1}{12} \left\{ \frac{N_1}{M_1} + \frac{3N_2}{M_2} + \frac{4N_3}{M_3} + \frac{3N_4}{M_4} + \frac{N_5}{M_5} + 2 \left[\frac{N_s}{M_s} - \frac{N_E}{M_E} \right] \right\} \right]^{0.5} \quad (3.32)$$

N_1 and N_5 are the values of the applied moments at the ends of the potential buckling length under consideration and N_2 , N_3 and N_4 are the values at $\frac{1}{4}$ length intervals between these. N_s/M_s is the greater of N_2/M_2 , N_3/M_3 and N_4/M_4 , and N_E/M_E is the greater of N_1/M_1 and N_5/M_5 . Also, only positive values of $\left[\frac{N_s}{M_s} - \frac{N_E}{M_E} \right]$ are

included.

For tapered beams, or beams containing a haunch, the above method can be tedious because it entails the calculation of the section properties in the tapered length. An alternative simpler approach, which is conservative, is suggested for haunched composite beams where the haunch is relatively short. This is to treat the values of N_1 , N_2 , etc, as applied stresses and the values of M_1 , M_2 , etc, as the yield stress, p_y . When the applied moments are greater than that causing yield, the appropriate value of N can be replaced by p_y . A further simplification can be made, and that is to assume that the applied stress in the tapering haunch length is constant. For typical cases, if the section at the haunch heel is designed to remain elastic as recommended, then it will be found that the applied stress is likely to decrease towards the heel and the assumption is therefore conservative (see Chapter 2, Figure 2.1).

3.2.6 Modification for Tapered Sections

A further factor is introduced in the British Code to modify the equivalent slenderness for tapered or haunched beams. This is necessary because the elastic buckling resistance and the critical buckling length (see later paragraph 3.1.7) are normally calculated using the section properties of the shallowest part of the beam. It would seem appropriate, therefore, to apply a factor which would serve to lower the effective slenderness to reflect the increase in strength and the buckling length, owing to the presence of the haunch or taper. However, the modification for varying moments does not consider the absolute value of the moments and strengths, but merely the ratios of the two. Therefore, a fully stressed tapered beam will have the same n_t factor as a fully stressed uniform beam, even though the critical buckling length is likely to be shorter in the former case. It is because of the treatment of the moments and strengths in this way that it is necessary, in fact, to increase the effective slenderness in a tapered or haunched beam.

The method adopted by the code is based on that of Horne et al {31}. It involves the calculation of a factor 'c', which is defined as the ratio of the elastic critical buckling length of a uniform member, subjected to a uniform moment, which is just sufficient to cause yield in the extreme fibres at each cross-section, to the critical buckling length of a tapered or haunched member of the base section, which

is also loaded just to cause yield. [Note. - the reciprocal of this definition is actually given in reference {31}, which the author of this thesis believes to be incorrect.]

After a parametric study had been carried out by considering typical rolled sections, the authors proposed the following empirical formula

$$c = 1 + \frac{3}{\left[\frac{D}{T_f} \right] - 9} (R - 1)^{3/8} q^{1/2} \quad (3.33)$$

where R = ratio of the greater depth to the lesser depth of the section over the buckling length
 q = ratio of the tapered length to the buckling length.

The value of c is clearly equal to unity for uniform beams, and greater than that for tapered or haunched beams. It is applied in the code to the equivalent slenderness as follows:

$$\lambda_{LT} = n_t u c v_t \lambda \quad (3.34)$$

The method was originally derived for beams where the tapered section contained a deepening web and no middle or third flange, but remained as an 'I' section. In recent times, this type of construction has become less popular and it is now common practice to form the taper by adding a cutting of an I section to the beam, so that a cross-section containing 3 flanges is provided. The addition of this third flange has the effect of enhancing the lateral torsional stability, which led Morris and Nakane {32} to suggest that, for this case, it would even be conservative to put the value of c to unity, although this recommendation has not been adopted in the code.

3.2.7 Critical Buckling Length

The analysis so far has related an elastic critical buckling moment to a half-wave buckle, whatever the buckling length. Clearly this cannot be the full picture because beyond a certain length it will be easier for the beam to buckle in two or more halfwaves. In order to obtain a complete solution, the analysis would have to be repeated for all possible buckling modes, and the minimum buckling envelope obtained. It is clear, however, that the minimum buckling moment for these other modes cannot be less than that for the single half-wave mode and that the envelope of the minimum buckling moment will not be more onerous than that shown in Diagram 3.6

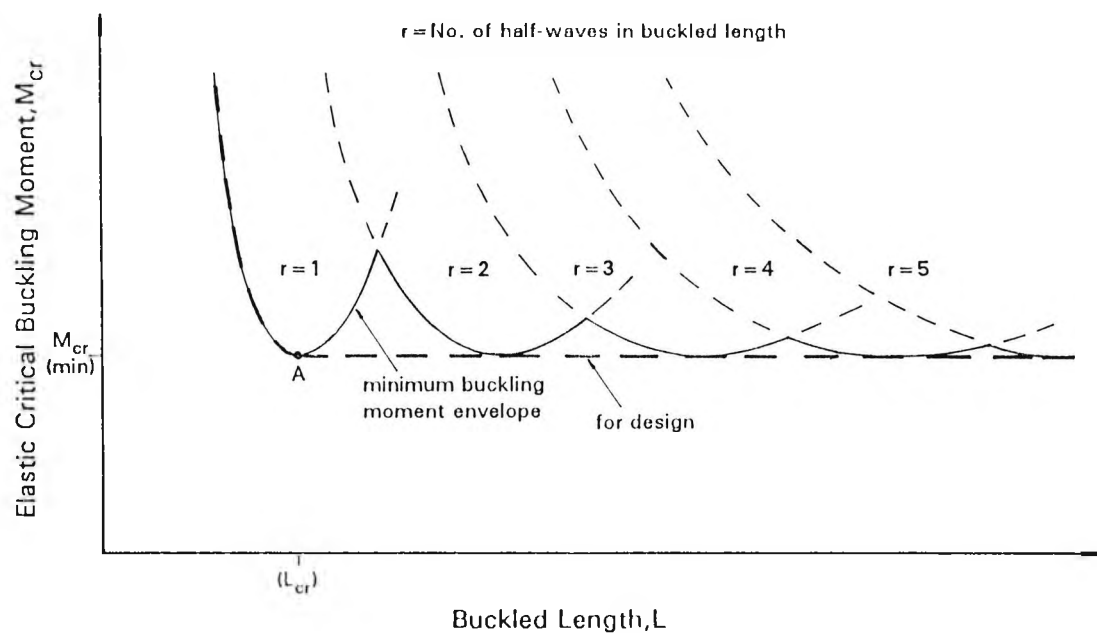


Diagram 3.6 **Elastic Critical Buckling Moment versus the Beam Buckled Length**

For simplicity of design, it is suggested that for lengths greater than that corresponding to the point where the minimum buckling moment occurs for a single half-wave buckle, ie, point 'A' in the above figure, it should be assumed that no further increase in the buckling moment occurs. The value of buckling length at this point is referred to as the critical buckling length, L_{cr} .

Of course, to be accurate, the important quantity is really the buckling resistance moment, M_b , and, for design, the envelope of the minimum of this value should really be plotted against the buckled length. L_{cr} would then be given by

$$\frac{\partial M_b}{\partial L} = 0$$

but this leads to a complicated expression and it is suggested that it is sufficient to consider

$$\frac{\partial \lambda_{LT}}{\partial L} = \frac{\partial (n_t u c v_t \lambda)}{\partial L}$$

The parameter ' n_t ' which, in effect, determines the equivalent elastic buckling moment, is likely to vary slightly with length but not necessarily in any regular way, since it depends on the actual moment diagram and it will be particularly complicated at the haunches. This is also true for the value of c in these cases. It is therefore considered reasonable for practical purposes, since the parameter ' u ' is a constant, to calculate L_{cr} from

$$\frac{\partial (v_t \lambda)}{\partial L}$$

Using equation 3.21,

$$\frac{\partial (v_t \lambda)}{\partial L} = \frac{\partial}{\partial L} \left[\frac{u/r_y}{\left\{ \frac{1}{L^2} + \frac{1}{40.05} \times \frac{1}{x^2 r_y^2} + \frac{1}{16.23} \times \frac{L^2 I_w}{D^3 I_y} \right\}^{0.5}} \right]$$

$$= \frac{-\frac{u}{r_y} \times 0.5 \left[\frac{-2}{L^3} + \frac{2}{16.23} \times \frac{L I_w}{D^3 I_y} \right]}{\left\{ \frac{1}{L^2} + \frac{1}{40.05} \times \frac{1}{x^2 r_y^2} + \frac{1}{16.23} \times \frac{L^2 I_w}{D^3 I_y} \right\}^{0.25}}$$

and for $\frac{\partial (v_t \lambda)}{\partial L} = 0,$

$$\left[\frac{-2}{L^3} + \frac{2}{16.23} \times \frac{L I_w}{D^3 I_y} \right] = 0$$

Hence $L^4 = 16.23 \frac{D^3 I_y}{I_w}$

and by putting $I_w = \frac{1}{12} t_w^3$, the critical buckling length is given by

$$L_{cr} = 3.74 \left\{ I_y \left[\frac{D}{t_w} \right]^3 \right\}^{0.25} \quad (3.35)$$

This length corresponds to the minimum value of the equivalent slenderness which, in turn, corresponds to the minimum value of the elastic critical moment (the simplifications having been accepted) - see Diagram 3.6. The minimum value of λ_{LT} , found by substituting equation 3.35 into equation 3.22, is given by

$$\lambda_{LT} = \frac{u \lambda}{\left[2 + \frac{1}{40} \left(\frac{\lambda}{x} \right)^2 \right]^{0.5}} \quad (3.36)$$

Hence a minimum value of the buckling resistance moment, M_b , can be obtained.

Therefore, for design, the potential buckling length, L , under consideration, can first be compared with L_{cr} . If it is less than L_{cr} , a value of M_{cr} greater than the minimum value will apply, for which the equivalent slenderness, λ_{LT} , can be calculated from equation 3.22 with modifications for moment (ie, 'n') and for taper (ie, 'c') where appropriate. If it is greater or equal to L_{cr} then the minimum elastic critical buckling moment will apply, for which λ_{LT} can be calculated from equation 3.36, with the appropriate modifications as described. Hence, in both cases, the buckling resistant moment, M_b , can be obtained and compared with the appropriate design moment occurring in the potential buckling length.

3.2.8 Summary of Lateral Distortional Buckling Check

1. Check, using equation 3.30 or 3.31, to see whether torsional restraint to the top steel flange can be assumed.

If the beam fails the condition, refer to a more rigorous method to include the flexibility, e.g. that of EC4, or assume lateral top flange restraint only using another method, e.g. that of BS 5950 Part 1, Appendix G.

If the beam passes the condition, continue.

2. Compare the potential buckling length L with L_{cr} , given by equation 3.35.

If $L < L_{cr}$, find λ_{LT} from equation 3.22.

If $L \geq L_{cr}$, find λ_{LT} from equation 3.36.

3. Modify λ_{LT} for moment (n_t factor) and section taper (c factor), calculated over the length of the buckle, ie, the lesser of L and L_{cr} .
4. Find p_b from Table 11, part 1 in the code {11}, and hence:
 - i. for uniform beams and tapered or haunched beams, where a constant stress has been assumed in the flange throughout the taper, calculate $M_b (= S_x \cdot p_b)$.
 - ii. for tapered or haunched beams, where a constant stress has not been assumed in the taper, calculate S_x at the cross-section along the beam where the ratio of the applied moment to S_x is considered to be greatest. Hence calculate M_b at this point.
5. Compare M_b with the appropriate design moment occurring in the check length L .

The use of the method is demonstrated in the design example given in Appendix 9A

3.3 COMPARISON OF PROPOSED METHOD WITH OTHER METHODS

It is instructive to review other work on lateral distortional buckling of composite beams and draw comparisons between the methods, but, as previously stated, most of the research that the author has discovered was specifically directed at bridge structures where the beams consist of deep sections with relatively thin webs.

3.3.1 Method of Bradford and Johnson

An important early contribution was made by the above authors {27} who investigated the potential buckling in the hogging region of bridge beams close to their supports. The authors approximated the most onerous likely condition of a heavy goods vehicle straddling the first internal support in a multi-span bridge to that

of a fixed-ended beam subjected to a uniformly distributed load. The beam section that they studied consisted of a steel beam rigidly fixed to a 220mm deep by 2000mm wide slab, containing two layers of reinforcement. The yield strength of the steel beam and the reinforcement was taken as 355N/mm^2 and 428N/mm^2 respectively. A parametric study was then carried out on this to investigate the factors influencing buckling. This study employed an elastic analysis using a finite element program. Results were presented in their paper for 20 beams which included 13 rolled and 8 non-standard sections, ranging in depth from 880mm to 950mm. The specific variables investigated were:

- (i) ratio of web depth to thickness (range $39 \leq d/t_w \leq 100$)
- (ii) ratio of bottom flange width to thickness, range $9.6 \leq B/T_f \leq 15$
- (iii) ratio of unbraced length (ie. span in this case) to the flange width, range $48 \leq \text{span}/B \leq 90$
- (iv) percentage of reinforcement in the slab, range $0.01 \leq A_r / A_c \leq 0.02$

where A_r = Area of reinforcement and A_c = Area of concrete

The authors discovered that the buckling strengths obtained were approximately double those predicted by the design methods quoted in the British bridge code {33}. This was suggested to be due to the assumption in the code method that the compressive flange was everywhere equal to its peak value at the internal support, and that the torsional stiffness of the concrete, and hence the torsional restraint, was negligible, owing to the tensile cracking of the concrete. The authors also concluded from their study that the flexibility of the shear connection and the transverse bending flexibility of the concrete slab were both very small.

The main finding from the study was that the elastic critical stresses at the onset of buckling depended principally on the ratio of d/t_w . A lower-bound design relationship which was readily usable with the code {33}, and which included a 10% conservative margin, was proposed as follows:

$$\beta = 3.4 (d/t_w)^{0.7} \quad (3.37)$$

where β is a slenderness parameter

This assumed a steel beam yield strength of 355N/mm², which was the value used in the study, but a more general expression would have been:

$$\beta = 3.4 (p_y / 355)^{0.5} (d/t_w)^{0.7} \quad (3.38)$$

This value of β was then to be substituted for the value of β given in the code as:

$$\beta = \lambda_{LT} (p_y / 355)^{0.5} \quad (3.39)$$

where λ_{LT} , as before, is an equivalent slenderness, from which a 'basic limiting stress' is found.

This design method can now be compared with the method proposed earlier in this thesis. In that method, the equivalent slenderness, λ_{LT} , which is comparable to β , is given by equation 3.36. That assumes that the beam is subjected to a constant moment and buckles over its critical buckling length. For a realistic comparison, equation 3.36 needs to be modified to represent the moment conditions approximated by Bradford and Johnson. This can be done by assuming a linear moment with a maximum value at one end, and reducing to zero at the other end of the buckling length. This is a reasonable approximation which leads to a value of $n_t = 0.77$, which then needs to be included. Referring to the equation and neglecting the denominator term in 'x', which is small, and, by putting $u = 0.9$, which is a typical value for normal rolled 'I' sections, the following expression is obtained:

$$\lambda_{LT} = 0.77 \times 0.636 \lambda = 0.49 \lambda$$

$$\text{But } \lambda = L_{cr} / r_y = 3.74 \frac{I_y^{0.25}}{r_y} \left[\frac{D}{t_w} \right]^{0.75}$$

$$\therefore \lambda_{LT} = 1.83 \left[\frac{A^2}{I_y} \right]^{0.25} \left[\frac{D}{t_w} \right]^{0.75} \quad (3.40)$$

$$\text{Also } I_y = \frac{B^3 T_f}{6} \text{ and } A = 2B T_f + D t_w,$$

$$\text{so the term } \left[\frac{A^2}{I_y} \right] = \frac{6}{B^3 T_f} (2Bt_f + Dt_w)^2$$

For most rolled I sections, $BT_f \approx D t_w$ and $B/T_f \approx 12$

$$\therefore \left[\frac{A^2}{I_y} \right] = 54 \frac{T_f}{B} = 4.5 \quad (3.41)$$

$$\therefore \lambda_{LT} = 2.67 \left[\frac{D}{t_w} \right]^{0.75} \quad (3.42)$$

It can thus be seen that this equation is very similar to the Bradford and Johnson design equation (3.37), without the 10% margin included.

A point made by the authors was that local buckling may, in reality, precipitate lateral buckling in a way not considered in their analysis and this was investigated in a later study by them {34}. This involved the modelling of a further 11 beams using the same type of structure, but this time they were analysed with an inelastic finite strip computer method. This led them to conclude that inelastic buckling always preceded lateral buckling in composite beams with a non-compact compression flange, whereas lateral buckling was likely to be the critical failure mode if the compression flanges were compact. The opinion of this author is that this is probably too simplistic, particularly for stocky shallow sections, where the strain

energy associated with lateral distortional buckling would be relatively high. This finding was also contradicted by others - see below (para 3.2.2). However, the authors re-affirmed their previously recommended design formula for checking for lateral distortional buckling, but suggested an additional section classification check for local buckling. The revised method then involved using the most onerous of these two checks to determine the beam strength.

3.3.2 Method of Weston, Nethercot and Crisfield

A further study of the stability of hogging regions in composite bridge beams at the supports was carried out by Weston, Nethercot and Crisfield {29}. They adopted the same bridge model and bending moment approximation as Bradford and Johnson {27} and carried out a similar parametric study using a large deflection, elasto-plastic finite element analysis. Nineteen beams were analysed and the parameters of each varied as follows:

- (i) ratio of web depth to thickness, range $39.4 \leq d/t_w \leq 160$
- (ii) ratio of bottom flange width to thickness, range $2.2 \leq B/T_f \leq 15$
- (iii) ratio of unbraced length (ie. the span) to the radius of gyration of the bottom flange, range $229 \leq \text{span}/r_{yb} \leq 1142$.

The authors considered span/r_{yb} to be a more relevant parameter than span/B , adopted earlier {27}.

Only two of the beams had 'compact' section classifications and some unrealistic sections were also specifically analysed to obtain a full picture of the behaviour. Rolled sections normally used for buildings have a d/t_w ratio between 35 and 60, and a B/T_f ratio between 10 and 16. Tentative calculations for haunched composite beams for buildings suggest a range of span/r_{yb} between 250 and 280, which is at the less slender end of the range considered.

The authors found that compact, or near-compact, sections were likely to fail by inelastic local buckling adjacent to the supports, but when the d/t_w ratio exceeded 60, failure was likely to be caused by lateral buckling of the compression flange. This contradicted earlier findings {27}, but it is consistent with the main beam test behaviour - see Chapter 6. The authors also investigated the influence of initial flange displacement, residual stresses, and concrete flange torsional rigidity, and all were found to have only a small effect on the ultimate capacity.

The most important parameters were considered to be the unrestrained length/ r_{yb} and the d/t_w ratios. From a plot of the results, a lower bound design curve was proposed thus:

$$\beta = 1.28 \left[\left[\frac{\text{Span}}{r_{yb}} \right]^{1/2} \left[\frac{d}{t_w} \right]^{1/8} \right] - 29 \quad (3.43)$$

This, like the previous design expression referred to earlier (equation 3.36), was then to be used by replacing the expression for β in the bridge code {33}.

Clearly both this method and the alternative methods reviewed so far apply to beams which have no bottom flange restraint over their span and are subjected to uniformly distributed loading. This may be appropriate for bridges but it is often not so for buildings because there are many cases where both the restraint and moment conditions cannot be realistically approximated by the above methods.

3.3.3 Method of Roik, Hanswille and Kina

A recent method has been developed by Roik et al {35, 36} specifically for buildings and can accommodate different restraint and moment conditions. The method is referred to in a paper by Johnson and Fan {37} and has been adopted into the European code for composite building structures {15}. Although independently derived, the derivation of the method follows the same elastic approach which was the basis of the method proposed in this thesis, and it produces similar results. It is

more general than that method because it caters for reinforced floor slabs as well as unreinforced slabs. In addition, it can also handle asymmetrical sections, and for these reasons it is more complicated. However, for symmetric sections with a cross-sectional classification of 2 or better, by neglecting the slab flexibility, it can be greatly simplified.

The method was developed by first deriving the 'elastic critical buckling' equation for two 'I' sections set apart and both connected to a reinforced concrete slab. This was done by assuming that the sections buckled in the shape of a sine wave defined by:

$$\theta = \bar{\theta} \sin \left[\frac{\pi x}{L} \right] \quad (3.44)$$

where the rotation θ included contributions from the transverse bending of the concrete slab and the distortion of the beam web. The local flexibility of the shear connection was considered and, as with earlier researchers, declared to be negligible. The elastic critical buckling moment, M_{cr} , was represented by the combined effect of suitably selected components. These consisted of a compressive force and a moment acting at the centroid of the steel member, and a tensile force and moment acting at the centroid of the concrete slab. The buckling equation was then derived and expressed as:

$$M_{cr} = \frac{k_c}{h_s} \left\{ E I_{afz} h_s^2 \left[\frac{\pi}{L} \right]^2 + G J + k_s \left[\frac{L}{\pi} \right]^2 \right\} \quad (3.45)$$

where k_c = a factor which includes the effect of the reinforcement
($k_c = 1$ for no reinforcement)

I_{afz} = second moment of area of the bottom flange about the
minor axis, ie, $I_{afz} \approx I_y / 2$

k_s = transverse stiffness per unit length of the beam.

NB. when the flexibility of the concrete is neglected:

$$k_s = \frac{1}{4} \frac{E}{(1 - \nu_a^2)} \frac{t_w^3}{h_s} \approx \frac{3E I_w}{h_s} \quad (3.46)$$

where ν_a = Poisson's ratio

By assuming the slab is unreinforced and by adopting the approximate terms for I_{afz} and k_s defined above, the buckling equation 3.45 can be compared with that for the proposed method (equation 3.16) and it will be seen that the two equations become identical.

Equation 3.45 was rearranged by the authors and a parameter C_4 introduced to account for the influence of the moment variation along the member. The elastic critical moment was then given as:

$$M_{cr} = \frac{k_c C_4}{L} \left\{ \left[G J + k_s \left(\frac{L}{\pi} \right)^2 \right] E I_{afz} \right\}^{0.5} \quad (3.47)$$

where C_4 depends on χ where:

$$\chi = \frac{E I_{afz} h_s^2}{\left[G J + k_s \left(\frac{L}{\pi} \right)^2 \right] L^2} \quad (3.48)$$

Graphs of C_4 for various moment shapes are given by the authors according to values of χ , and minimum values of C_4 are quoted, ie, because minimum values

of C_4 will result in minimum values of M_{cr} . However, it has been noted by this author that, beyond its minimum value, the value of C_4 continues to increase with increasing slenderness, so it would appear that the effect of multiple-wave buckles may not have been considered. Had this been so then it is suggested that the value of C_4 would have varied in a similar way to that of M_{cr} given by the minimum buckling moment envelope in Diagram 3.6.

As with methods for use with British Codes, M_{cr} is not used directly but in the form of an equivalent slenderness, defined by, $\bar{\lambda}_{LT}$. This differs from λ_{LT} used in the British Code {11} in that

$$\bar{\lambda}_{LT} = (M_p / M_{cr})^{0.5} \quad (3.49)$$

According to British Code, from equation 3.17

$$\lambda_{LT} = \left[\frac{M_p \pi^2 E}{M_{cr} p_y} \right]^{0.5}$$

hence
$$\lambda_{LT} = \bar{\lambda}_{LT} \left[\frac{\pi^2 E}{p_y} \right]^{0.5} \quad (3.50)$$

Having obtained $\bar{\lambda}_{LT}$, the method involves the determination of the buckling resistance in the same way as for non-composite beams, in accordance with EC3 {12}, which allows for imperfections and residual stresses.

A simplified conservative version of the above method is quoted in EC4 {15} for symmetric sections of class 2 or better, where the slab is unreinforced and its flexibility is neglected. The method is independent of the unrestrained length and so, presumably, must have assumed a value for the critical buckling length, but exactly how, this author could not prove, because of insufficient published information. The calculation of the elastic critical buckling length by this method without the consideration of the moment is, of course, identical to that in the

proposed method (equation 3.35) because the basic elastic buckling equations are the same (ie, after inclusion of the simplifications mentioned earlier).

The design equation for the method is given directly in terms of equivalent slenderness, such that

$$\bar{\lambda}_{LT} = \left[1 + \frac{t_w h_s}{4 b_f T_f} \right] \left[24 \left\{ \frac{(1 - \nu_a^2) \pi p_y}{E C_4} \right\}^2 \left\{ \frac{h_s}{t_w} \right\}^3 \left\{ \frac{T_f}{B} \right\} \right]^{0.5} \quad (3.51)$$

where the terms have been defined earlier

By putting this equation in terms of λ_{LT} and, as before, by assuming that for most rolled sections $t_w h_s = B T_f$, the following result is obtained

$$\lambda_{LT} = 4.41 \left\{ \frac{h_s}{t_w} \right\}^{0.75} \left\{ \frac{T_f}{B} \right\}^{0.25} \quad (3.52)$$

This equation can be compared with the similar equation in the proposed method when the beam is assumed to buckle over the critical buckling length, ie, equation 3.40. With the simplification incorporated from equation 3.41, the following result is obtained:

$$\lambda_{LT} = 4.96 \left\{ \frac{D}{t_w} \right\}^{0.75} \left\{ \frac{T_f}{B} \right\}^{0.25} \quad (3.53)$$

It can be seen that this is similar to equation 3.52, but is slightly more conservative.

3.3.4 Comparison Between Design Methods

For a direct comparison between the respective design methods, it is useful to consider an example. As the methods of Bradford and Johnson {27} and Weston et al {29} apply only to a fixed-ended beam loaded with a uniformly distributed load, it is necessary, as before, to consider the hogging region of a beam subjected to a linear bending moment which decreases to zero at the end of the buckling length. The ‘span’ in Weston et al’s method is then assumed to be equal to four times the hogging region.

The comparison between the methods is made by calculating the equivalent slenderness, λ_{LT} , for a range of slenderness, λ , where λ = the potential buckling length/ r_y . The results are presented in Figure 3.1 for a 457 x 152 UB 82 section, which is assumed to have a yield stress of 355N/mm². This section, although not commonly used, does have a stocky web and serves to emphasise the benefit of providing torsional restraint to the tension flange. The design equations used are summarised as follows:

proposed method	equation 3.34 with $n_t = 0.77$, incorporating the function for v_t from equation 3.22
Bradford and Johnson	equation 3.38
Weston et al	equation 3.43 with ‘span’ = 4 $r_y \lambda$
EC4 (Roik et al)	equation 3.47 with $k_c = 1$ and $L = r_y \lambda$
EC4 (simplified)	equation 3.51 with $C_4 = 11.1$.

For a further comparison, the method of BS 5950 part 1, Appendix G, has also been included, using equation 3.24, whereby only lateral tension flange restraint is assumed. The method of BS 5950 part 1, whereby no flange restraint is assumed, is also included for comparison.

The effect on design bending strength of the various methods is shown in Figure 3.2, where the ratio of this quantity to the yield strength is plotted against slenderness, λ . The bending strength was established by reference to the respective codes appropriate to each method by assuming that all partial safety factors were equal to unity.

The figures show that the EC4 method is slightly less conservative than the proposed method, ie, in the range for which data was available, and the design strength curve of the former method clearly shows the questionable increase in strength with slenderness referred to earlier. The EC4 (simplified) method is shown to be a safe lower-bound, in terms of strength, to the comprehensive EC4 method, but it is slightly less conservative than the proposed method for $\lambda > 80$. For $\lambda < 70$ it is shown to be up to 12% more conservative than all the methods. For this particular section, no reduction in strength is required by the method of Bradford and Johnson, whatever the slenderness, but the method of Weston et al shows a reduction only for $\lambda > 100$. Weston et al's method is also shown to be very conservative for high slendernesses but unconservative in the range $50 < \lambda < 130$. It must be questioned, therefore, whether these two methods, which were developed for bridges, are suitable for sections appropriate for buildings. This was also suggested by the Sub-Assembly Test results - see later, Chapter 5.

The BS 5950 (unrestrained) method is seen to be a safe lower-bound to most of the methods, as one would expect, but the benefit of torsional restraint, as well as lateral restraint to the tension flange, is clearly demonstrated. Lateral restraint is seen to have only a modest effect. For example, at a slenderness of 250, an increase in strength of 20% is recorded, but if torsional restraint is also provided, an increase of 140% is recorded. Hence, for economy, this additional strength should be utilised where possible and the proposed method of analysis of lateral distortional buckling is recommended.

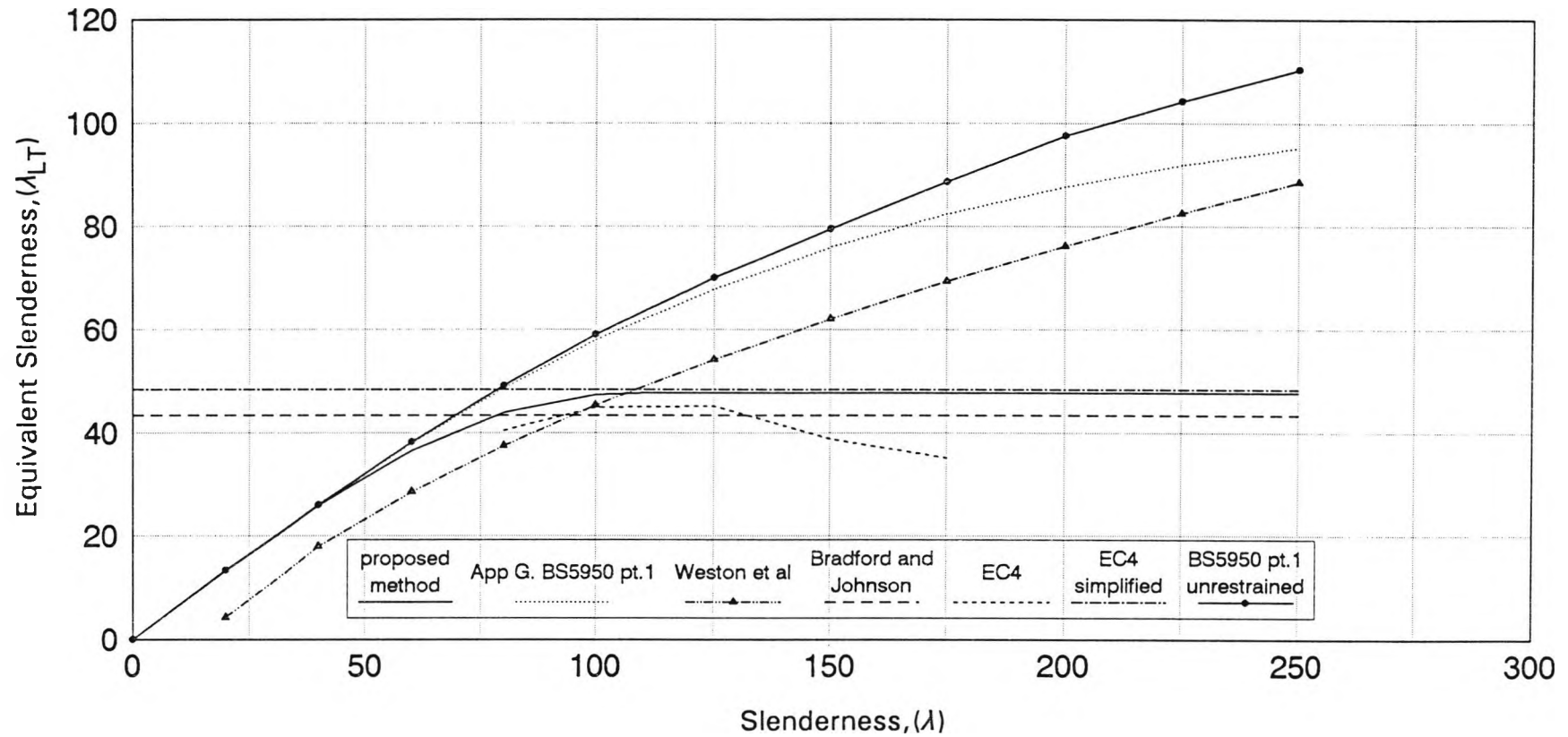


Figure 3.1 Equivalent Slenderness Values for a 457x152UB 82 Section Grade 50, According to Various Buckling Design Methods

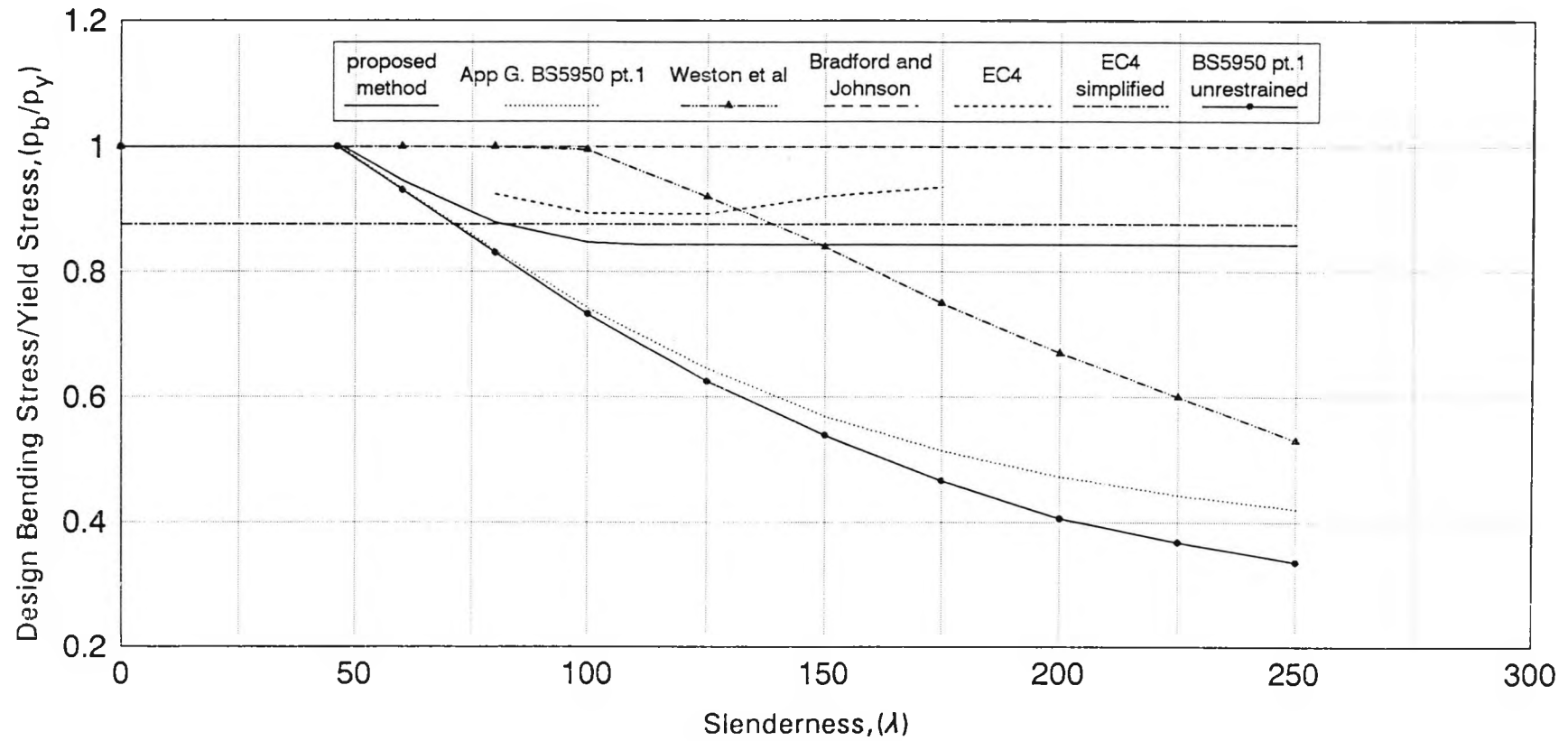


Figure 3.2 Design Strength Ratio versus Slenderness for a 457x152UB 82 Section Grade 50, According to Various Buckling Design Methods

CHAPTER 4

EXPERIMENTAL WORK: THE SUB-ASSEMBLY TEST

4.1 INTRODUCTION

The full scale experimental work consisted of two tests, namely a sub-assembly test modelling the hogging region of a haunched composite beam and a main beam test modelling a typical sub-frame within a single span multi-storey building.

The materials used in the experimental work were donated by several organisations. The fabricated structural steel test members were supplied by Bourne Steel Limited and the floor decking was supplied by Quikspan Construction Limited. The shear connectors were donated by Haywood Engineering and fixed by Delta Structural Services. Financial support was received from British Steel through their Market Development Fund administered by the Steel Construction Institute. The experimental work was also sponsored by the Science and Engineering Research Council.

The purpose of the sub-assembly test was to model the torsional restraint given to hogging moment regions by the floor slab and to investigate the susceptibility to lateral distortional buckling of the beam in this region. This restraint was not modelled accurately in the subsequent main beam test. The sub-assembly test was also carried out to compare practical structural options for providing restraint to the plastic hinge location at the haunch toe in order to achieve the best moment rotation characteristics.

4.2 DESIGN CONSIDERATIONS

4.2.1 The General Test Arrangement

To meet the above objectives, a balanced cantilevered test was designed consisting of two parallel frames. Each frame consisted of two cantilevered beams connected each side of a central column and the frames were mounted apart with a composite floor spanning between - see Figure 4.1.

4.2.2 The Steel Beams

Beams with a high ratio of bending strength to torsional strength were considered most likely to display lateral distortional instability, although there are a number of relevant parameters, including the web thickness, depth, etc., which determine their resistance to this behaviour, as explained in Chapter 3. From the available British sections the beam size 457 x 152 UB 52, grade 50, seemed most appropriate because it had a high torsional index value 'x', defined in reference {11}, where torsional resistance is proportional to $1/x$. It also had a large web d/t ratio, a high ratio of major axis second moment of area to the torsional constant (I_{xx}/J) and was within the range of practical sizes for haunched beam spans, the lower economic limit for haunched composite beams having been considered to be about 10m span. The chosen section was classified as 'plastic' in reference {11}, and therefore should have been capable of rotation at plastic hinge locations. Under normal office type U.D.L. conditions the beam should have been capable of spanning 15.0m.

The loaded length of each cantilevered beam needed to relate to the typical hogging moment region of a full scale beam and, for single span structures, this can be up to 20% of the span. In order to limit the influence of the structural restraint provided by the loading frame and to suit the arrangement of loading sockets cast into the laboratory floor, 4.0m cantilevers were chosen, with point loading positions set at 3.5m from the supports.

4.2.3 The Columns

The column section was determined by the flange thickness requirements for the haunch connections rather than by strength. For a beam end plate design thickness of 25mm (grade 50), the British Steel section 305 x 305 UC 158 kg/m was most appropriate. Being over designed for strength, the column would have been capable of supporting several storeys although no axial loads were to be applied in the test.

4.2.4 The Cuttings

It was assumed that most fabricators would prefer to make the haunch by welding to the beam a tapered segment of a rolled section, known as a 'cutting', and that this would be the same serial size as the beam. The haunch could of course have been made up partly or completely out of fabricated elements, but because of the extra work involved and the problem of residual stress, this option was assumed to be less popular, and so cuttings were designed for the tests.

A typical haunch length would be of the order of 5% to 7% of the span and for the chosen beam section this would be between 0.75m and 1.05m. Allowing for a column width of 300mm this would lead to cutting lengths of between 0.6m and 0.9m, ie, 1.33 to 2.0 times the steel beam depth D . It was therefore decided to consider two cases, one with a cutting length of D and the other of $2D$. The cutting depth was set at D for both cases, resulting in cutting toe angles of 45° and 26° . The reason for testing two different lengths was that there were opposing considerations for each. The steep cutting toe angle associated with a short cutting length would result in a high haunch toe flange force component being applied into the beam web, but a long cutting would put a high moment into the column because the lever-arm to the shear force at the haunch toe hinge position would increase. Movement of the hinge away from the column would also reduce the ability of the column to afford restraint to the hinge through the torsional rigidity of the haunch.

4.2.5 Stiffening and Restraint at the Haunch Toe

Preliminary calculations showed that web stiffeners were required for both cutting lengths to prevent web buckling due to the force from the cutting flange. These also showed that lateral restraints were required at the hinge locations, but since it is inconvenient to install lateral restraints within a composite floor, it was decided to investigate whether the web stiffening alone would provide sufficient torsional restraint, in view of the close proximity of the column. This is because these were relatively short haunches compared with conventional plastically designed portal frames, for which the code (reference {11}) clauses were intended to apply. To assist in the torsional restraint and to provide continuity to the cutting flange force, full strength welds were provided at each end of the cutting flange.

Five combinations of haunch and stiffening were devised as follows:

1. short haunch with full depth stiffeners both sides of web.
2. long haunch with full depth web stiffeners both sides of web.
3. short haunch with half depth web stiffeners both sides of web.
4. long haunch with no web stiffeners.
5. long haunch with one half depth web stiffener plus a knee brace restraint to the underside of the floor - see detail Figure 4.2.

Arrangements 4 and 5 were to be evaluated using the same beam by adding a stiffener and brace during the test programme. This was subsequently carried out but all stiffeners were made out of grade 43 steel because of the difficulty of obtaining grade 50 steel at the time. The beams were labelled B1 to B4 to identify the particular haunch/stiffening arrangement and the columns were labelled C1 and C2 (Figure 4.1).

4.2.6 Floor Slab

The floor slab design needed to reflect current practice and a 130mm thick, 25 N/mm²; lightweight concrete slab was specified. The mix chosen was a Lytag PFA/Sand mix of medium workability. The span of the floor, that is, the distance between the parallel test frames, needed to be set by consideration of the torsional stiffness afforded by a floor to an intermediate beam in a real structure. It can be shown that the effect of two adjacent floor spans on the middle beam can be modelled by providing one half-span floor. Assuming a slab span of 3.2m, the test frames were then set at 1.6m apart.

A re-entrant type steel decking 1.0mm thick was chosen with a profile depth of 50mm. Shear studs were specified as 19mm diameter x 100mm long. No specific guidance {14} was found for the spacing of studs in non-composite hogging regions when the beam is assumed to be torsionally restrained by the floor, but in other cases the lesser of 600mm and 4 x slab depth is stipulated. A decision was subsequently made to use a 300mm spacing, resulting in one stud every other trough. A light reinforcing mesh was also included, as it is in practice, for fire resistance purposes.

4.2.7 End Connections

The end connections were designed by assuming that the moment applied was determined by a 10% overstrength of the plastic hinge at the haunch toe. A bolt arrangement utilising M20 grade 8.8 bolts was selected, using the design method described in reference {9} and demonstrated in the design example given in Appendix 9A. The most practical layout resulted in an overcapacity of 10% for the long haunch case. For simplicity and to reduce the likelihood of connection failure, which was not the main area of investigation of the test, all connections were detailed the same. This resulted in an extra lower pair of bolts being provided for the short haunch connection and an over-design capacity of 30%. It was not, however, considered that this would significantly affect the buckling behaviour of the beam.

The end plate was designed by yield line analysis assuming prying action. Prying forces were not predicted but the design plastic modulus of the plate was taken as $t/5^2$ rather than $t/4^2$ per unit width to compensate for this. Grade 50 plate, 25mm thick, was initially specified but, as for the stiffeners, this was changed to 30mm thick, grade 43, because of the difficulty of obtaining grade 50 plate at the time.

4.3 CONSTRUCTION

All the structural steel elements were delivered prefabricated and erection began with the central columns being packed level off the strong floor and bolted down. The cantilever beams were then lifted using the overhead laboratory crane and bolted into position by hand torquing. The decking was then laid and fixed by shot fired nails into the steel beam. After trimming the decking, a cold formed steel edge trim was fixed to it using pop rivets.

Sockets were then prepared out of 100mm diameter plastic tube and positioned accurately to allow rods from the loading system to pass through the slab. The shear studs were then welded along the beams through the decking by the specialist subcontractor and checked for fixity. The mesh was then cut, laid on plastic reinforcement chairs and lapped along the centre line joining the columns. The structure was then substantially complete prior to preparation for casting the slab - see Figures 4.3 and 4.4.

The beam and column strain gauges were fixed at this point and protected with tape from water seepage. The concrete was then delivered ready-mixed to the laboratory and was poured by using a concrete skip, manoeuvred by the overhead crane. The concrete was mechanically vibrated and given a hand-tamped finish. When complete, the slab was covered with polythene to cure - see Figure 4.5.

The as-built dimensions of the structure are given in Figure 4.6.

4.4 **LOADING ASSEMBLY**

Each cantilevered beam was individually loaded from frames positioned at 3.5m from the central supports. The design of the loading frames was based on a system used at Cambridge University for the testing of stub girders, ref. {38} . This design enabled the beams to be pulled down to the strong floor, rather than have to be pushed down from a heavy overhead reaction structure - see Figure 4.7.

Each loading frame consisted of a beam held at 1m or so underneath the cantilever test beam by rods passing upwards through the slab and bolted to a cross-beam resting on the slab. As shown in the figure, the jack sat on the lower beam and pushed up against another beam, which was held at a fixed distance above the strong floor by further rods. Extension of the jack against this beam resulted in the lower beam moving down and a direct pull down force on the test structure. All the rods were continuously threaded, which offered the possibility of using locking nuts to fix the displacement of the frame and lock in the load displacement of the jack. Each jack was pressurised by its own hand-operated pump to ensure the complete independence of the loading systems - see Figure 4.8.

Each jacking system was independently calibrated so that the reading from the oil pressure gauge could be directly converted into a load. All the jacks were similar and of 90 tonnes capacity, with maximum stroke of 175mm.

4.5 **INSTRUMENTATION**

The instrumentation included the use of electrical resistance strain gauges, long and short-travel linear potentiometric displacement transducers (LPDT's), mechanical clock gauges and two theodolites with a graded staff.

4.5.1 **Measurement of Haunch Connection Bolt Strains**

Eight of the tension group bolts in the haunch connection of beams B1 and B2 were strain-gauged and labelled according to the layout in Figure 4.9. These bolts

were milled at three equidistant points around the circumference of the shank and electrical resistance gauges glued on. The wires from these were fed through a 2mm diameter hole drilled through the centre of the bolt and out from the head - see Figure 4.10. The gauges were connected in series so as to eliminate bending effects, and the outputs were fed into a data logger.

One bolt was tested to find the elastic limit and eventual failure load. The remainder were then individually calibrated to 80% of the elastic limit and all the calibrations proved to be virtually identical. All the strain gauged bolts were kindly donated by the Building Research Establishment.

4.5.2 Measurement of Strains in Beams and Knee Braces

Ninety-eight electrical resistance strain gauges were positioned around the structure to monitor the longitudinal strain in the beams and compressive strain in the column webs. Similar layouts were used for each beam and numbered accordingly, as shown in Figures 4.11 and 4.12. Two further gauges were placed at the mid-length of the knee brace and were positioned so that the axial force could be readily deduced - see Appendix 4A. All the electrical resistance gauges were Techni-Measure gauges type FLA-6-11 and the outputs were fed into an Intercole Spectra measurement control system, driven by a BBC micro-computer.

4.5.3 Measurement of Beam Compression Flange Torsional Rotation

Instrumentation was set up to measure the torsional rotation of the compression flanges of beams B1 and B2 but this proved to be unsuccessful. Tubular brackets were clamped to the bottom flange of four points along each of the two beams. The rotation of each bracket was measured by using two dial gauges set at a fixed vertical distance apart and attached to an independent frame - Figures 4.13 and 4.15. Although the bracket was likely to move in two planes at once, owing to bending and twisting of the beam, the magnitudes of the rotations anticipated were thought to be such that errors would be small, and that measurements would give a good indicative torsional profile.

From a study of the results, however, for various reasons, the readings could not be relied upon. It became clear that some of the gauges could not have been in initial contact and, with hindsight, it was unrealistic to expect so many clock gauges to be repeatedly read manually without error during test.

4.5.4 Measurement of Flange Lateral Displacements

The lateral displacement of the beam flanges was measured by the use of two theodolites. These were positioned so that two sight lines were established parallel to a line joining the ends of the test on each longitudinal side. The sight lines were 500mm or so clear of the steel beams and a graded staff was held horizontally at selected points along the beams - see Figures 4.14 and 4.15. The staff was rocked forward and backwards in the normal way to establish the minimum reading with an estimated accuracy of $\pm 0.5\text{mm}$.

4.5.5 Measurement of Vertical Displacements under the Load Points

The long-travel LPDT's were used for measuring the large displacements anticipated under the load points, to avoid the need for resetting. These transducers were SAKAE models 30HLP200 (3 No.) and 50LP300 (1 No.) with travels of 200mm and 300mm respectively, reading to the nearest mm. Their outputs were fed into individual monitors positioned at each individual loading station. The technicians used these monitors to control the pumping, according to displacement increments dictated by the author during the tests.

4.5.6 Other Displacement Measurements

A further 6 displacement measurements were taken per beam at positions labelled B1/1 to B1/6 etc., as shown in Figures 4.16 and 4.17. Readings from the LPDT's and gauges marked /1 were used to calculate the end slopes, while gauges /2 and /3 were used to confirm the deflected shape. Gauges marked /4 monitored vertical slip between the beam and column, while gauges marked /5 and /6 were to be used in calculating the end plate separation from the column. Horizontal movement of the columns, and thus tilting of the structure, was also measured, using

gauges labelled C11 to C22. All the gauges were either clock gauges or linear voltage displacement transducers, both reading to 0.01mm with 50mm travel.

4.5.7 Measurement of the Spread of Plasticity

An attempt was made to get a quantitative assessment of the spread of plasticity around the haunch regions using a white brush-applied paint normally used for whitening greenhouses, but this proved to be unsuccessful because it was insufficiently brittle. Proprietary products previously obtainable were no longer available because of dangerous fumes arising during their application.

4.6 MATERIAL PROPERTIES

Material property tests were carried out on the critical elements of the structure, including the beams, concrete and reinforcement. Coupons were machined from sections cut out of the webs and flanges of each beam from the relatively unstressed length at the end of each cantilever. The results are given in Table 4.1. Full stress/strain curves were obtained, from which mathematical model curves were drawn and used in the finite element analysis.

Beam	Location	Yield Stress (N/mm ²)	Ultimate Tensile Stress (N/mm ²)	Elongation %
B1	Flange	413	544	27.2 _{7.7}
	Web	430	546	26.3 _{7.7}
B2	Flange	407	553	28.7 _{8.2}
	Web	436	567	25.1 _{8.2}
B3	Flange	405	551	28.0 _{7.7}
	Web	427	538	26.7 _{7.7}
B4	Flange	413	563	28.0 _{8.2}
	Web	435	567	26.2 _{8.2}

Table 4.1 Sub-Assembly Test - Steel Beam Material Properties

N.B The elongation subscript number is the coefficient of proportionality 'k', where the gauge length = $k \times \sqrt{S_o}$, where S_o is the original cross-sectional area of the parallel length of the coupon, and this is defined in reference {39}.

The crushing strength of the concrete was measured using 100mm cubes and the tensile strength using 150mm diameter by 305mm long cylinders. The samples were cured by immersion in water and the test results are given in Table 4.2.

Age (days)	f_{cu} (N/mm ²)	Tensile Strength (N/mm ²)
7	32.4	
21	41.7	2.8
29	44.0	3.4
56	51.5	
117	59.0	
358/359	65.9	

Table 4.2 Sub-Assembly Test - Average Concrete Cube Compressive Strengths and Cylinder Tensile Strengths.

Samples from the mesh reinforcement were also tested and the results are shown in Table 4.3.

Sample Number	Young's Modulus (kN/mm ²)	Yield Stress (N/mm ²)	Ultimate Tensile Stress (N/mm ²)	Elongation (%)
1	215	500	680	7 _{19.3}
2	200	500	685	7 _{19.3}
Average	208	500	683	7 _{19.3}

Table 4.3 Sub-Assembly Test - Mesh Reinforcement Properties (Type A142)

One M20 grade 8.8 bolt was tested and failed at 194kN with an elastic limit of 167kN. As previously stated, 8 other strain gauged bolts were loaded to 80% of the elastic limit and calibrations were virtually identical.

4.7 THE SUB-ASSEMBLY TEST RESULTS

Five loading cases were carried out and referred to consecutively as: Bedding-In, Working Load and Ultimate Load Tests 1, 2 and 3.

4.7.1 Bedding-In Test

The Bedding-In test was conducted 15 days after casting the slab, to check the instrumentation. The assembly was loaded by balanced displacement increments (N.B. not balanced load - the load being determined by individual beam stiffness) of 2mm up to 6mm, followed by unloading. The maximum moment applied to any of the haunch toes occurred at beam B1, with a magnitude of 122kNm (design plastic moment of resistance of steel beam alone = 387kNm). No noticeable feature was observed during this relatively low loaded test and results are not included.

4.7.2 Working Load Test

The Working Load Test was carried out 19 days after casting and load increments were again of 2mm, up to a maximum deflection under the loading points of 18mm. At this deflection the haunch toe moments in beams B1 to B4 respectively were 241kNm, 195kNm, 232kNm and 216kNm, ie, at about 50% of the final maximum moments. Plots of the beam end rotations against haunch toe moments are presented for this and subsequent tests in Figures 4.18 to 4.21. The end rotations were defined as the measured beam slope beyond the loading point, with a correction included to allow for the overall tilt of the structure.

Parallel transverse cracking became noticeable in the slab above all beams when the haunch toe moments were 150kNm, 128kNm, 157kNm and 138kNm respectively. No other notable feature occurred and the load was released in controlled deflection increments. A reduction in stiffness with load was apparent, owing to the concrete cracking and a slight permanent set was recorded in each beam under the loading points of between 1mm and 3mm.

4.7.3 Ultimate Load Test 1

This was carried out 21 days after casting and a 4mm load displacement increment was initially applied, followed by 5mm increments up to a maximum displacement of 69mm. Referring to the Figures (4.18 - 4.21) it can be seen that all beams appeared to repeat the behaviour of the Working Load Test but with a slight increase in stiffness to make up for the permanent set. A gradual reduction in the stiffness is apparent up to the points where the yield strain was measured in the haunch toe strain gauges and this was undoubtedly due to the cracking of the concrete slab. Following this a rapid decrease in stiffness occurred, owing to the spread of plasticity.

The growth of the cracking over beams B1 and B3 is shown in Table 4.4.

Deflection under load (mm)	Haunch toe bending moments (kNm)				Crack width above haunch toe (mm)	Crack spacing generally (mm)
	B1		B3			
	Value	% of max.	Value	% of max.		
14	192	41.5	191	41.2	<0.5	-
24	298	64.4	286	61.6	0.5	300
34	380	82.1	368	79.3	1.0	200
44	433	93.5	420	90.5	1.3	150-200
54	458	98.9	453	97.6	1.5	150-200
64	463	99.4	464	100	2.0	150-200
69	460		464	100	3.0	150-200

Table 4.4 Sub-Assembly Ultimate Load Test 1 - Growth in Concrete Cracking Over Beams B1 and B3

Lateral distortional buckling became apparent in beam B2 when the haunch toe moment reached 400kNm (94% of max.) at an end slope of 1.1°. Following this, the lateral displacement of the bottom flange at the haunch toe developed rapidly with only a slight increase in moment resistance. This is clearly illustrated in Figure 4.22 which shows the growth in lateral displacement at the haunch toes for all

beams. It can be seen that lateral movement of the other beams was minimal until a haunch toe moment of about 460kNm was achieved, some 15% greater, and this is because of the absence of web stiffening on beam B2. Beam B1 showed an increase in lateral displacement from about 1.5° end slope, but beams B3 and B4, with the full depth web stiffeners, showed no appreciable lateral displacement during the test. Figure 4.23 shows the shape of the lateral distortional buckling and it can be seen that the buckling length for all beams was less than the cantilevered length and measured between 2.2m and 2.9m.

When the load displacement reached 69mm, a local flange buckle had developed in beam B2 at the haunch toe in the bottom flange. This occurred when the beam end slope was 1.5° and it can be seen clearly in Figure 4.24. Evidence of similar buckling could be seen on the other beams just beyond the toe, with half-wave amplitudes measuring 3mm (B1), 2mm (B3) and 1.5mm (B4). The end slopes were then 1.75° (B1), 1.75° (B3) and 1.6° (B4).

The test was terminated at this point because it was desired to preserve beam B2 from further damage for use in the next test, when a web stiffener and knee brace would be added. Beams B1 and B3 reached their maximum resistance during this test with haunch toe moments of 463kNm and 464kNm occurring at end slopes of 1.6° and 1.7° respectively. Beams B2 and B4 were clearly also close to that state because the stiffness was approaching zero. After the stepped unloading of the tests, permanent vertical sets at the ends of the beams of 33mm (B1), 27mm (B2), 33mm (B3) and 25mm (B4) were measured.

4.7.4. **Ultimate load test 2**

Ultimate Load Test 2 was carried out 29 days after casting the slab and was identical to the previous test except for the addition of one half depth stiffener welded to the haunch toe of beam B2. A knee brace was attached to the stiffener at one end and the other end was bolted to an angle which was rawl-bolted to the underside of the floor, which is shown in Figure 4.2. The displacement loading was carried out in 10mm increments up to 110mm, at which point the upper knee brace bolt sheared and the test was terminated.

Referring to Figure 4.18, it can be seen that for beam B1 a short plastic plateau of moment resistance of about 460 kNm at the haunch toe was achieved up to an end slope of 2.2° , after which a steady decline took place to 3.2° , when the test was terminated. The haunch toe moment by then had reduced to 355kNm, ie, 77% of the maximum strength. The light mesh reinforcement broke simultaneously over beams B1 and B3 above the haunch toes, and at end slopes of about 2° , ie, just beyond the point of maximum load. No consequential drop in moment resistance of either beam was apparent but this was to be expected because the area of the reinforcement was relatively small. The mesh broke over beams B2 and B4 above the haunch toes in the load increment following the similar breakage over the other beams. The end slopes when this occurred were 1.8° (B2) and 2° (B4).

The resistance shown by beam B2 (Figure 4.19) was less than the other beams and the maximum haunch toe moment of 425kNm was achieved only after the reinforcement broke, and at an end slope of 2.1° . An apparently longer plateau of constant moment resistance was measured at 415kNm for this beam but this is a reflection of the addition of the web stiffener. At 2.8° end slope the knee brace bolt broke and this was accompanied by a sudden weakening of the beam, thus proving the benefit of the brace. The knee brace bolts were actually undersized at grade 4.6 although they sustained the brace design force before failing - see later para 4.7.7. Grade 8.8 bolts were, however, fitted for the following test.

Beam B3 (Figure 4.20) displayed a long plateau of moment resistance of about 460 kNm up to 2.5° end slope, after which it declined gradually. At the end of the test, when the end slope was 3.2° , it had only dropped to 400kNm (86% of maximum). The maximum haunch toe moment in beam B4 was achieved during this test at a value of 489kNm and at an end slope of 1.8° (Figure 4.21). A relatively short plateau of resistance of about 470 kNm was measured up to 2.4° end slope, followed by a gradual decline in strength down to 3.0° , when the test was terminated. The drop-off in load was marginally the least of all the beams, to a value of 425kNm (87% of maximum).

The transverse cracking in the slab worsened throughout the test up to the stages when the reinforcement broke. The cracks where the reinforcement failed

were about 8mm wide at failure, but, with further load displacement during the test, they opened to 10mm. These cracks are shown dramatically in Figures 4.25 to 4.27. Other cracks were actually observed to close up when reinforcement fracture occurred, but this was logical because not only did the load decline, but the strain energy stored in the slab in those other areas was released.

The lateral distortional buckling, initiated in the previous test, also worsened but, despite the addition of the knee brace to beam B2, it was again most severe in that beam. This is confirmed by reference to Figures 4.22 and 4.23 which show that the lateral displacement at the haunch toe of beam B2 was nearly twice that of beam B1 and well over 3 times that of beams B3 and B4, for roughly the same end slope. This clearly demonstrates the beneficial effect of providing full depth web stiffeners.

The local buckling also became more severe during the test and was again most pronounced in beam B2 - see Figures 4.28 to 4.30. It was also accompanied by web buckling, which was worse in beams B1 and B2 with the half depth stiffeners, but was apparent in all beams. The buckled shape involved the raising of the bottom flange on one side of the beam and the lowering of it on the other. The web buckle was in a direction in sympathy with this rotation of the flange. This can be observed in Figures 4.31 and 4.32 which show the local buckling of beams B1 and B3.

4.7.5 Ultimate Load Test 3

Prior to carrying out this test a replacement knee brace was made and fitted to beam B2. This was because the deformation of this beam during the previous test, after the knee brace bolt broke, was too great ^{to} refit the former brace. As previously mentioned, grade 8.8 bolts were fitted this time and not grade 4.6 bolts which were used before.

The test was carried out 76 days after casting and over a period of two days, with the first stage loading being locked-in overnight. Increments were mainly of 10mm up to a maximum displacement of 105mm. Whilst loading the sixth increment (ie. to 60mm), the jack on beam B4 completely unloaded without warning

or obvious cause. The hydraulic circuits were checked and it was found that a release valve had leaked the pressure back to the reservoir in the pump. The valve was made secure and the previous deflection reinstated. There was some relieving of load on the other jacks owing to the out-of-balance effect, but on reloading to the next increment the behaviour had apparently been restored. There was also a slight drop in load overnight but again, on reloading, the behaviour was restored. The test was actually again terminated because of the failure of the upper knee brace bolt, despite using the higher grade. The lower bolt also appeared close to shearing and this is shown in Figure 4.34.

Referring to Figures 4.18 to 4.21, the loading characteristics at the start of this test can be seen to vary between beams, with beam B4 reloading virtually linearly up to the previous load termination point. From there, a gradual decline in strength was observed down to a haunch toe moment of 375kNm (80% of maximum) at test termination, with an end slope of 4.6°. The response of beam B1 followed the previous test behaviour and sustained a moment of 290kNm (63% of maximum) at the termination of the test, with an end slope again of 4.6°. Beam B2 showed greater weakness on reloading with a marked reduction in resistance. When the knee brace bolt broke, a haunch toe moment of only 265kNm (62% of maximum) was recorded at an end slope of 4.2°. This time beam B3 showed marginally the best performance with a slight reduction in strength to 375kNm (81% of maximum) at an end slope, at termination, of 4.6°. Again, the superior performance of the beams with the full depth stiffeners was demonstrated.

The lateral distortional buckling and local buckling continued to worsen during this test, but no lateral displacement readings were taken, because that operation was very time consuming and all the buckling had been initiated and observed in the earlier tests. The only difference this time was that the magnitude was greater. Figures 4.33 to 4.38 show the final state of the local buckling and Figure 4.39 shows the end cross-section of beam B2 which clearly exhibits the deformed shape associated with lateral distortional buckling.

Deformation of the concrete again reduced during the test but the cracks above the haunch toes continued to widen. In fact, three quite distinct slopes to the

floor slab could be seen along its length, with steps occurring at the haunch toes, ie, the hinge positions. The final deformed state of the structure showing this feature can be seen in Figure 4.40. The slab had actually prized itself off the steel beam at these positions because gaps could be seen between the top flanges and the decking (Figure 4.34). This occurred between successive shear connectors but on demolition of the test no significant deformation of the connectors was observed anywhere. There was no other distortion of the decking except that the edge trim had buckled at the points of change in the slope of the slab. The trim had also suffered deformation at lap positions.

The cumulative displacements for all the tests under the load points just prior to unloading were 210mm (B1), 195mm (B2), 217mm (B3) and 189mm (B4).

4.7.6 Connection Behaviour

As previously stated, the haunch connections were all identical and had a design capacity of 640kNm without including the reinforcement. The maximum connection moments achieved during the tests were 542kNm (B1), 590kNm (B2), 542kNm(B3) and 680kNm (B4). Despite these high values relative to the design strength, no noticeable bending of the plates occurred and their separation from the column flanges was limited to the order of 1mm. Negligible slip was also measured at the connection during the tests.

A loss of output from the strain gauge in bolt 'A' (Figure 4.9) of beam B2 occurred so results have only been plotted for beam B1. The growth of the bolt forces with connection moment is plotted for the three ultimate load tests in Figures 4.41 to 4.43. The results presented are the bolt loads relative to the start of each test and do not include dead load effect. The cumulative bolt loads are not considered because, for practical reasons, it was not possible to obtain the absolute zero point with sufficient accuracy during the erection stage. The behaviour is seen to be reasonably linear but with a slight reduction in the rate of increase of bolt load with moment, particularly for bolts with the greatest lever-arm. The reduction in bolt force recorded near the end of Ultimate Load Tests 2 and 3 is due to the weakening

of the beams, and hence the dropping of the load. The fracture of the reinforcement during load increments 5 and 6 of Ultimate Load Test 2 made little difference to the behaviour, confirming its minimal contribution to the connection strength. No evidence of substantial bolt preload is indicated and no prying force is apparent, which is to be expected because the connection was loaded to well below its ultimate capacity.

The bolt forces have also been plotted according to connection depth (Figures 4.44 to 4.46) and the profiles obtained are essentially linear, except for some equalisation of the forces in the upper two bolt rows, which became more noticeable as the tests proceeded. The neutral axis, however, is shown to lie above the middle of the connection and moved little during the tests, thus indicating that the connection was, indeed, relatively low loaded.

4.7.7 Behaviour of the Knee Brace

As previously explained, after Ultimate Test 1 a half depth stiffener was welded to beam B2 and a 50 x 50 x 6L knee brace was fitted to it using M12, grade 4.6 bolts. The force in the brace was deduced from strain gauge readings (para. 4.5.2) and is plotted against the haunch toe moment in Figure 4.47 for Ultimate Load Tests 2 and 3. The special unloading effect due to the failure of the jack on B4 has been omitted for clarity. In both tests the brace was in tension and the graph shows a modest increase in the brace force during Ultimate Test 2, up to when the maximum strength beam B2 was approached. After this, the force increased rapidly with no further increase in the moment until the upper brace bolt failed at which point the lower bolt was also close to failure (Figure 4.28). This rapid increase was also accompanied by a similar increase in lateral displacement at the haunch toe (Figure 4.22).

As mentioned earlier, it was necessary to renew the brace prior to Ultimate Test 3 and grade 8.8 bolts were used this time. The response during this test showed a more rapid growth in the knee brace force, reflecting the further increase in the lateral displacement, which was only 12mm at the start of Ultimate Test 2 but was 38mm prior to this test. Despite the higher bolt grade, the test was again terminated

because the upper knee brace bolt sheared. The force in the brace, however, was actually lower at failure than in Ultimate Load Test 2, which may have been due to increased local moments, low ductility or just under-performance. There did not appear to be any large deformations at the brace connections, which suggests that the latter reasons are more likely.

The horizontal component of the knee brace force can also be expressed as a percentage of the force in the steel beam compression flange at the haunch toe. This value has been plotted against beam end slope and is shown in Figure 4.48. It can be seen that during Ultimate Test 2 the percentage dropped from about 2% at low loadings, down to a minimum of 1% as the flange reached yield conditions, after which it climbed to about 3% when the brace bolt failed. In Ultimate Load Test 3 the behaviour was similar, but the percentages were generally higher because of the effect of the increased lateral displacement. The value at yield conditions was about 2% but had reached 2.6% when failure of the brace bolt occurred.

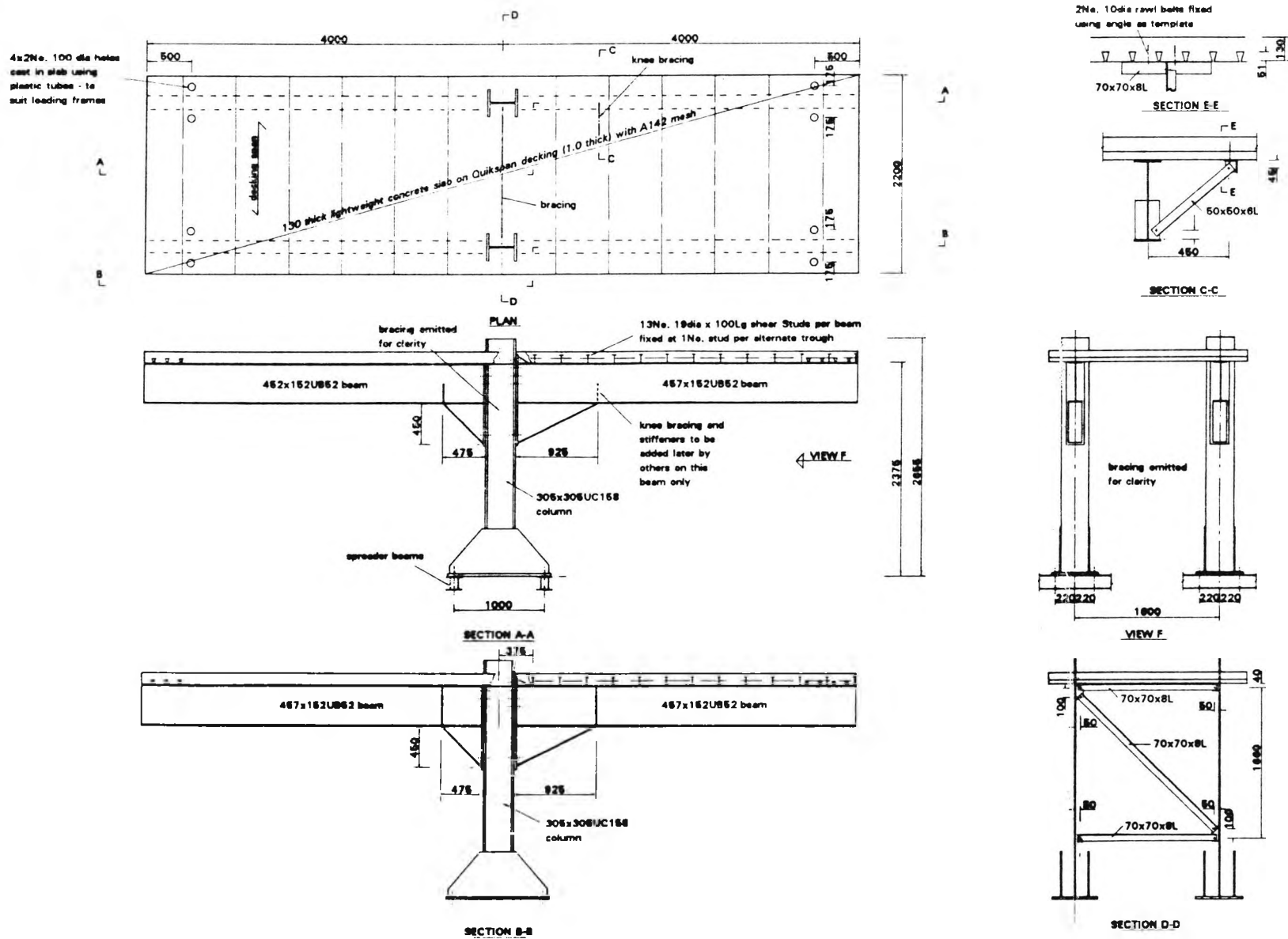


Figure 4.1 Sub-Assembly Test - Specimen General Arrangement

2No. rawl bolts fixed
using angle as template

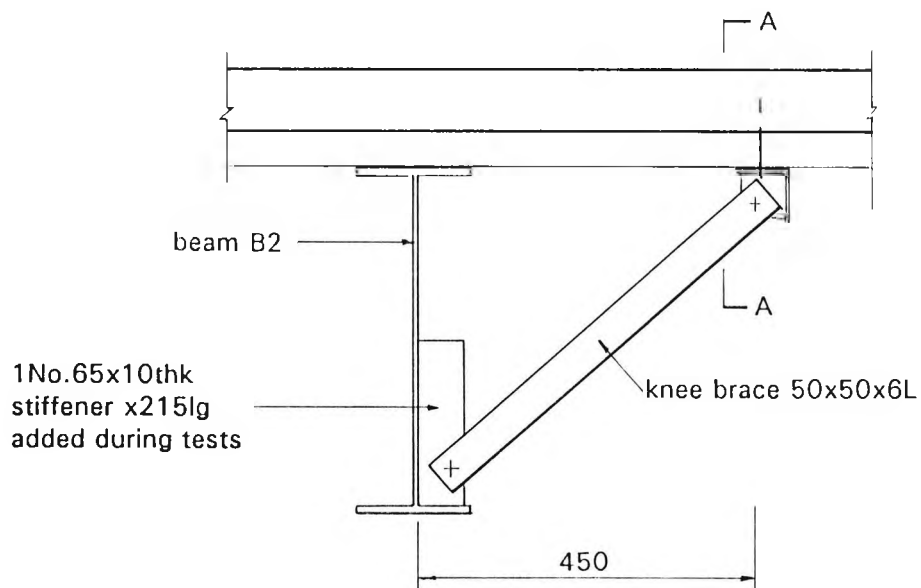
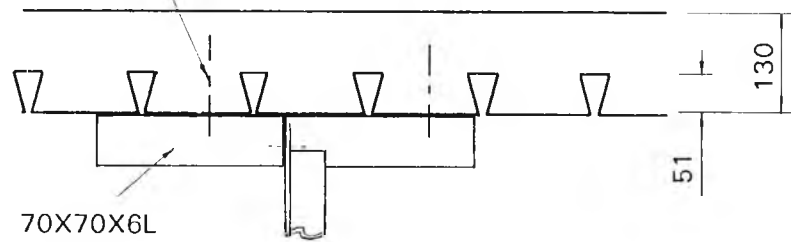


Figure 4.2 Sub-Assembly Test - Beam B2 Haunch Knee Brace Detail

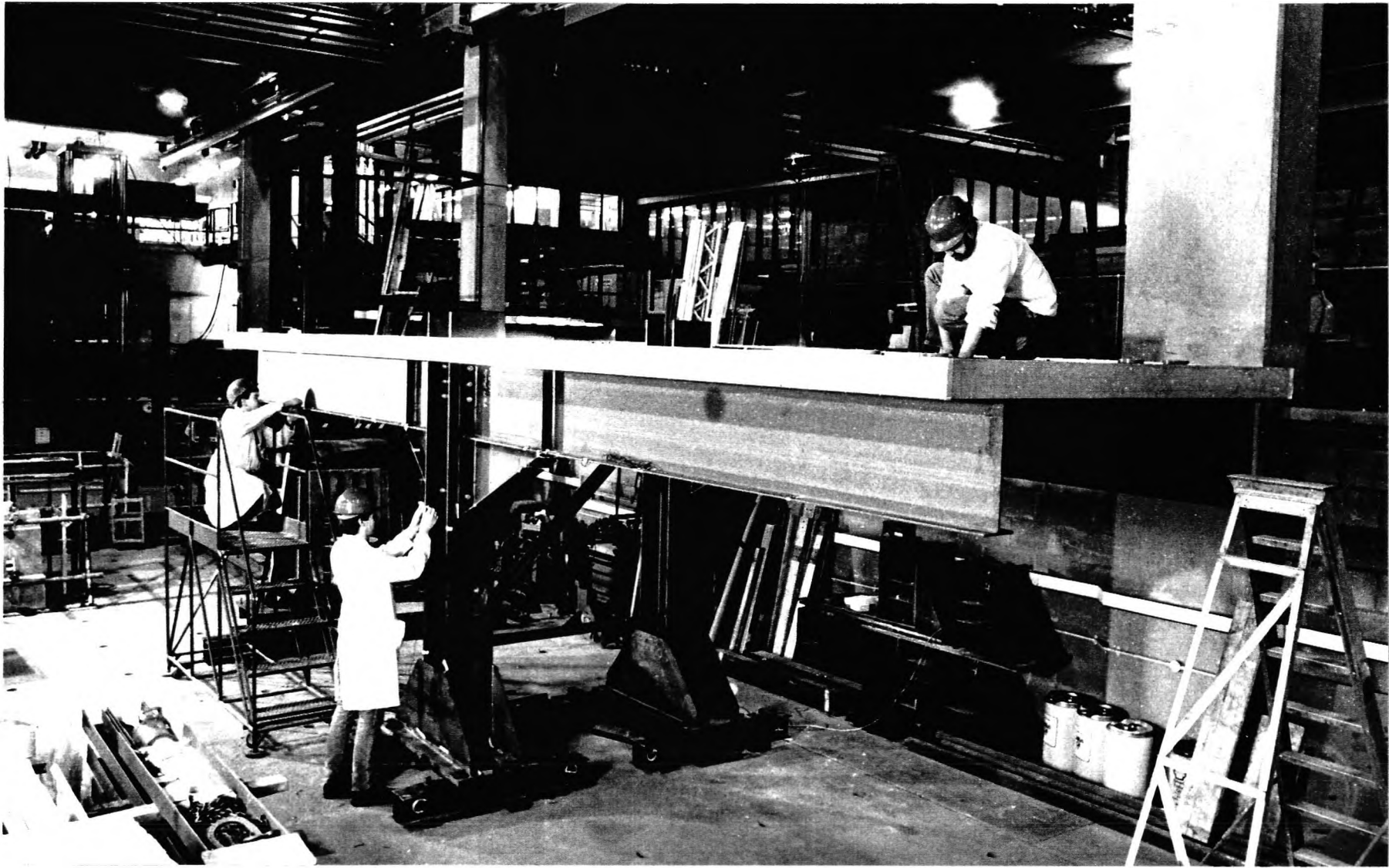


Figure 4.3 Sub-Assembly Test - Erected Structure



Figure 4.4 Sub-Assembly Test - Prior to Pouring the Concrete Slab

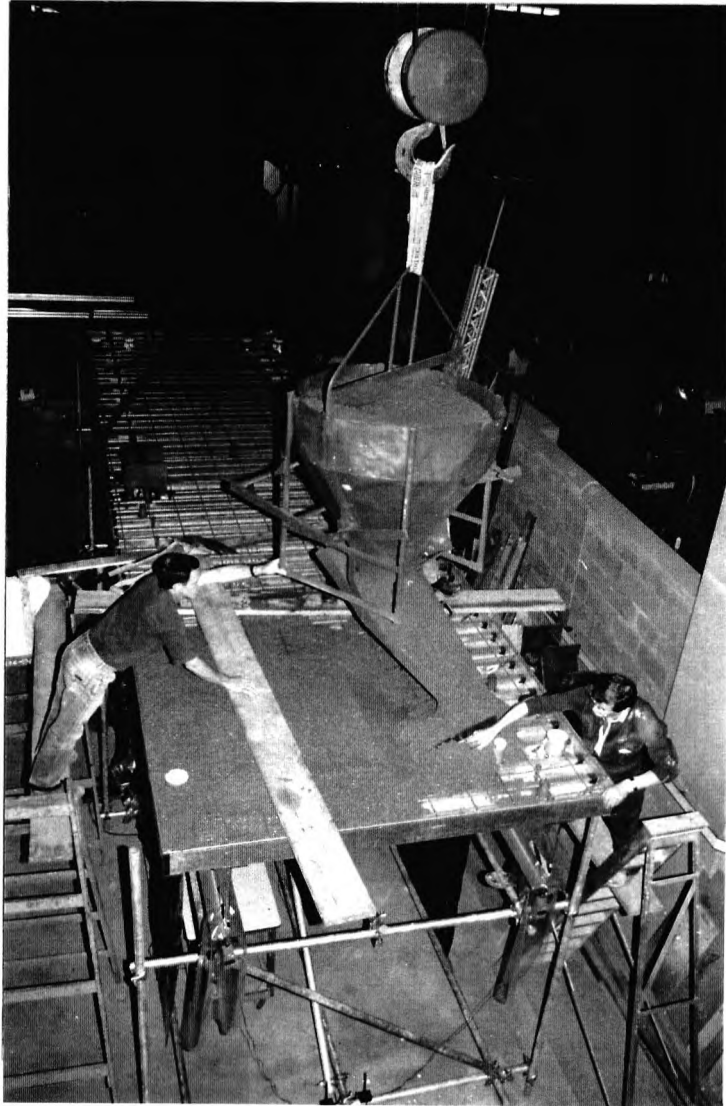
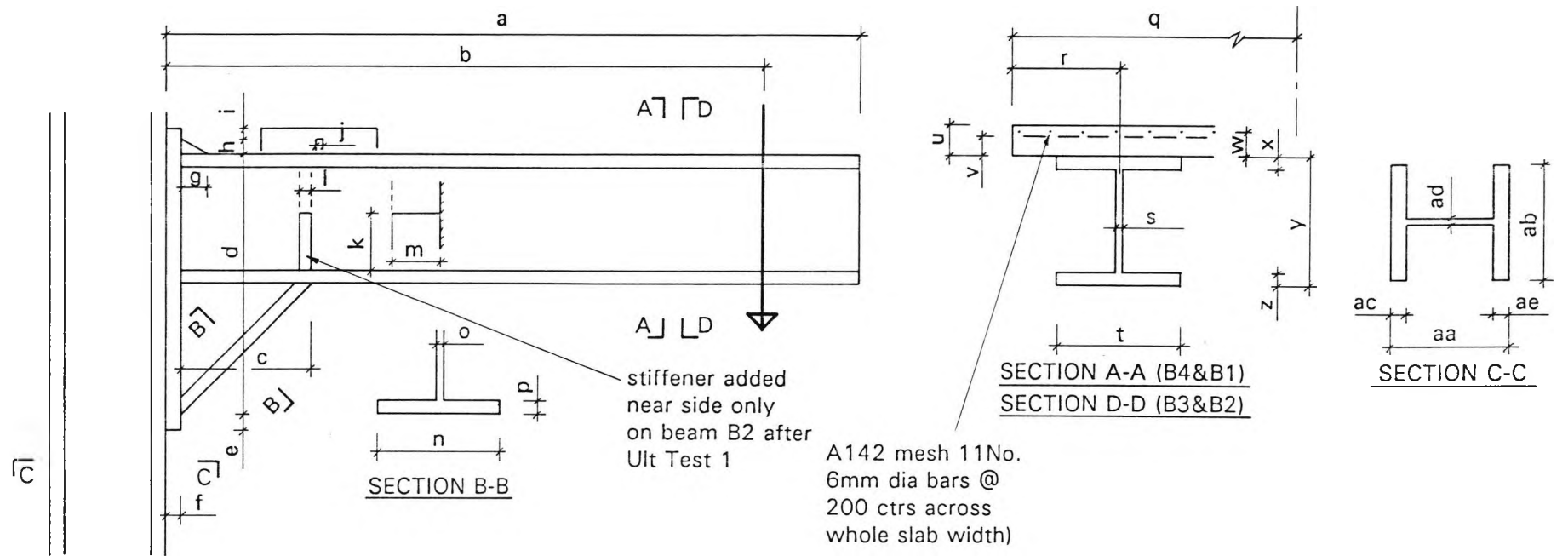


Figure 4.5 Sub-Assembly Test - Pouring the Concrete Slab



Beam	a	b	c	d	e	f	g	h	i	j	k	l	m	n	o	p	q	r	s	t	u	v	w	x	y	z
B1	3845	3330	487	911	16	30	100	80	18	8	HALF 216	9.9	68	152.5	9.3	10.8	1103	297	7.6	154	130	51	95	10.2	450	10.6
B2	3845	3350	940	900	20	30	100	80	25	8	HALF 205	9.7	70	153.7	8.5	10.7	1103	302	8.0	153	130	51	95	10.2	448	10.3
B3	3840	3350	487	907	15	30	100	80	23	8	FULL 428	10.0	68	153.7	8.1	10.7	1103	301	8.1	152	130	51	95	10.0	449	10.3
B4	3825	3350	940	905	17	30	100	80	23	8	FULL 430	10.1	67	153.2	8.0	10.9	1103	298	8.0	152	130	51	95	10.3	452	10.3
Col	aa	ab	ac	ad	ae	Beams B1 and B2 attached to Col C1 Beams B3 and B4 attached to Col C2																				
C1	329	312	22.5	18.4	24.3																					
C2	333	312	22.7	18.0	22.7																					

Figure 4.6 Sub-Assembly Test - As-Built Dimensions

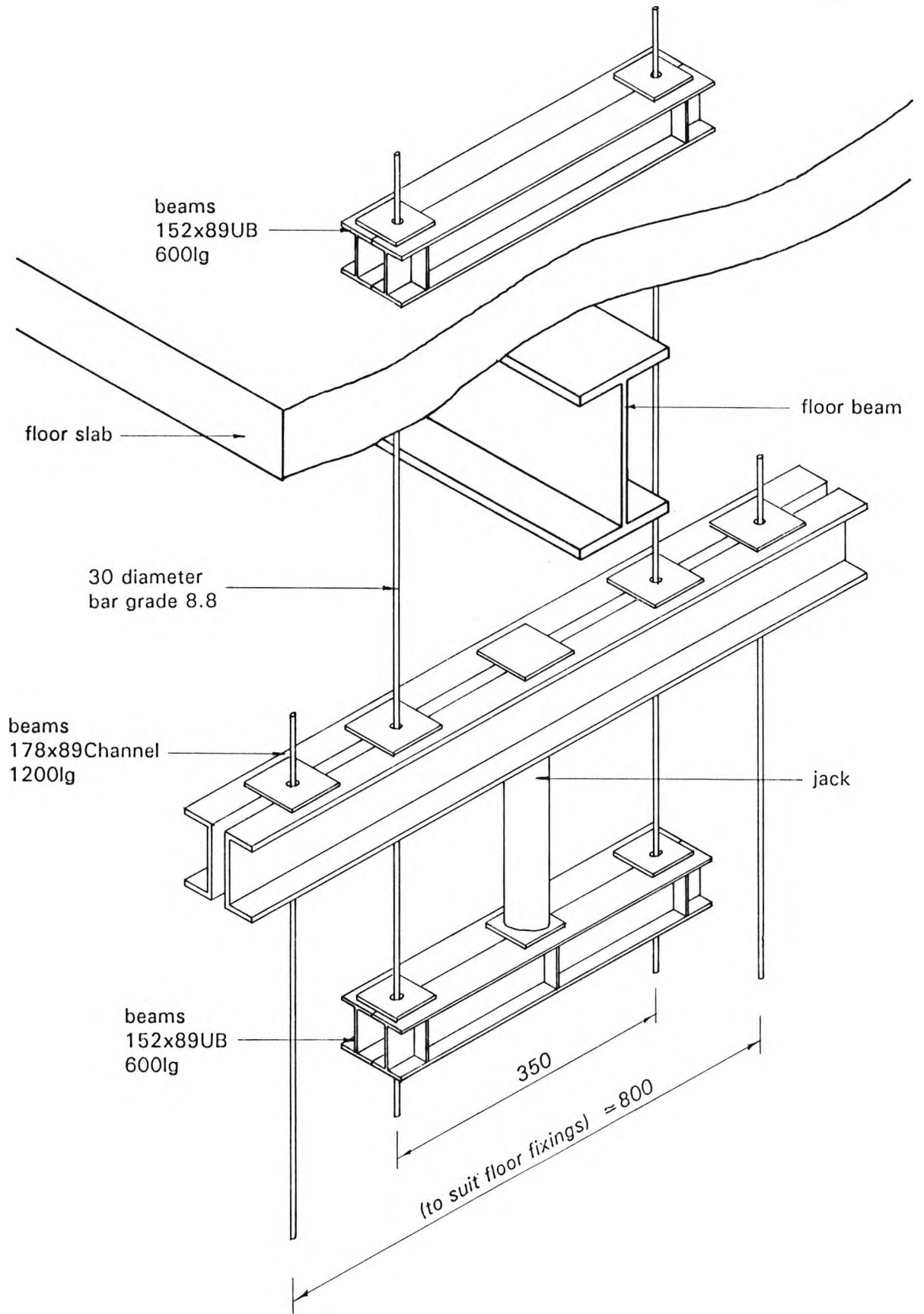


Figure 4.7 Sub-Assembly Test - Loading Frame Assembly

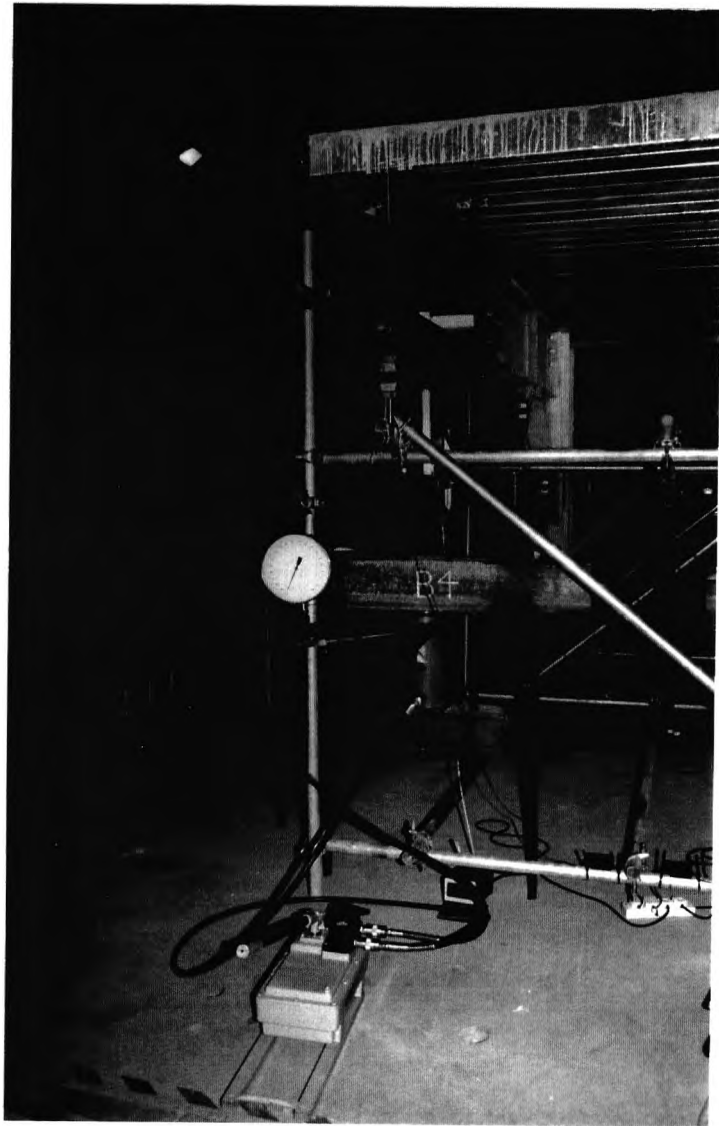


Figure 4.8 Sub-Assembly Test - Typical Jacking System

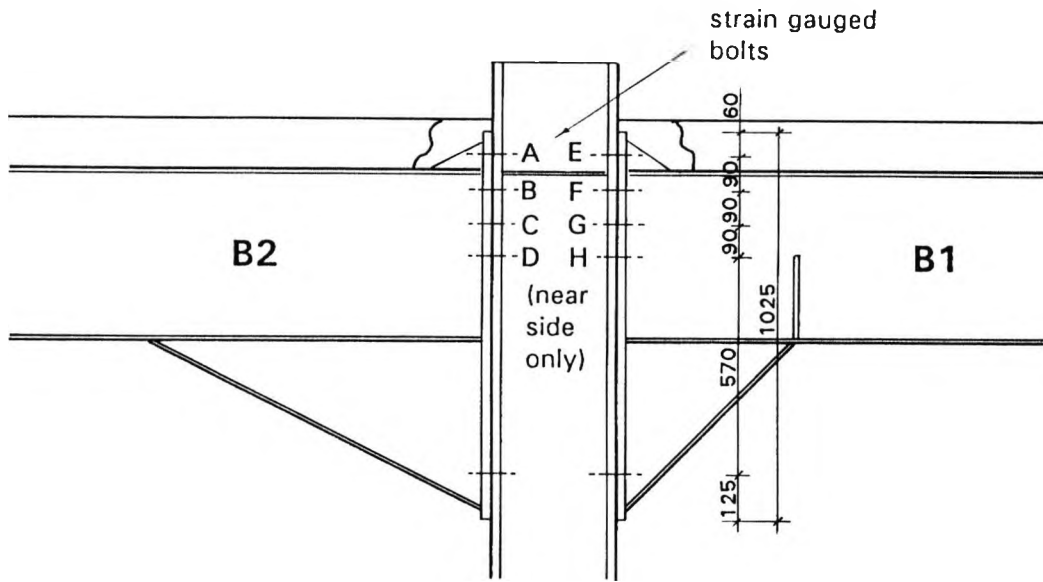


Figure 4.9 Sub-Assembly Test - Strain-Gauged Bolt Layout

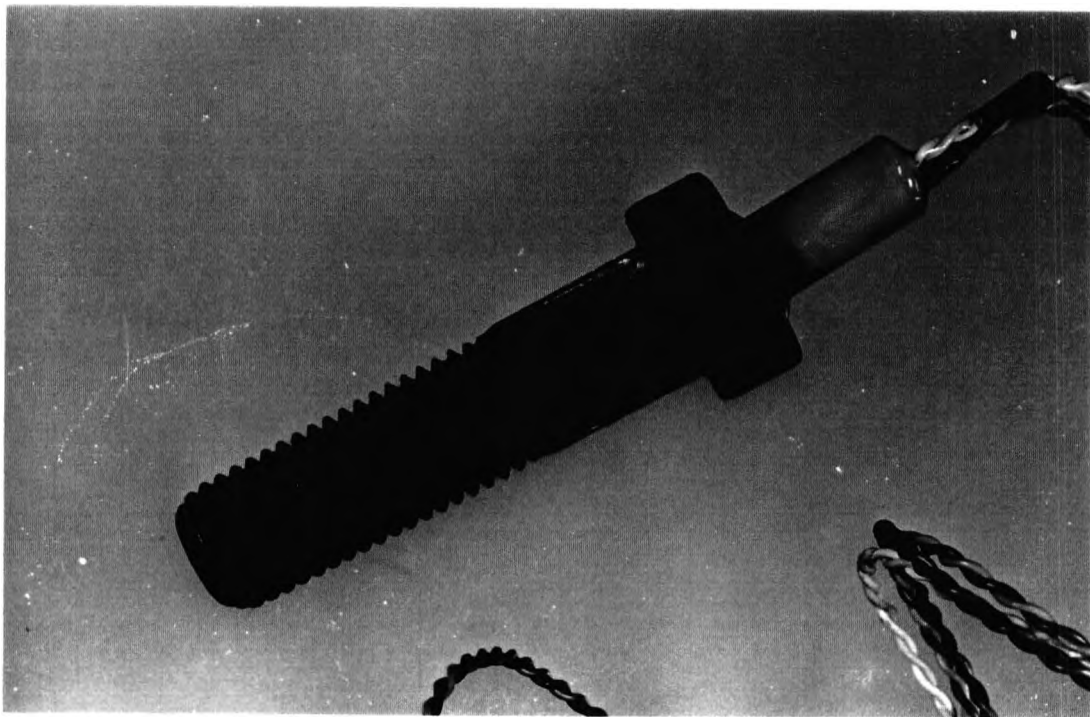


Figure 4.10 Sub-Assembly Test - Strain-Gauged Bolt

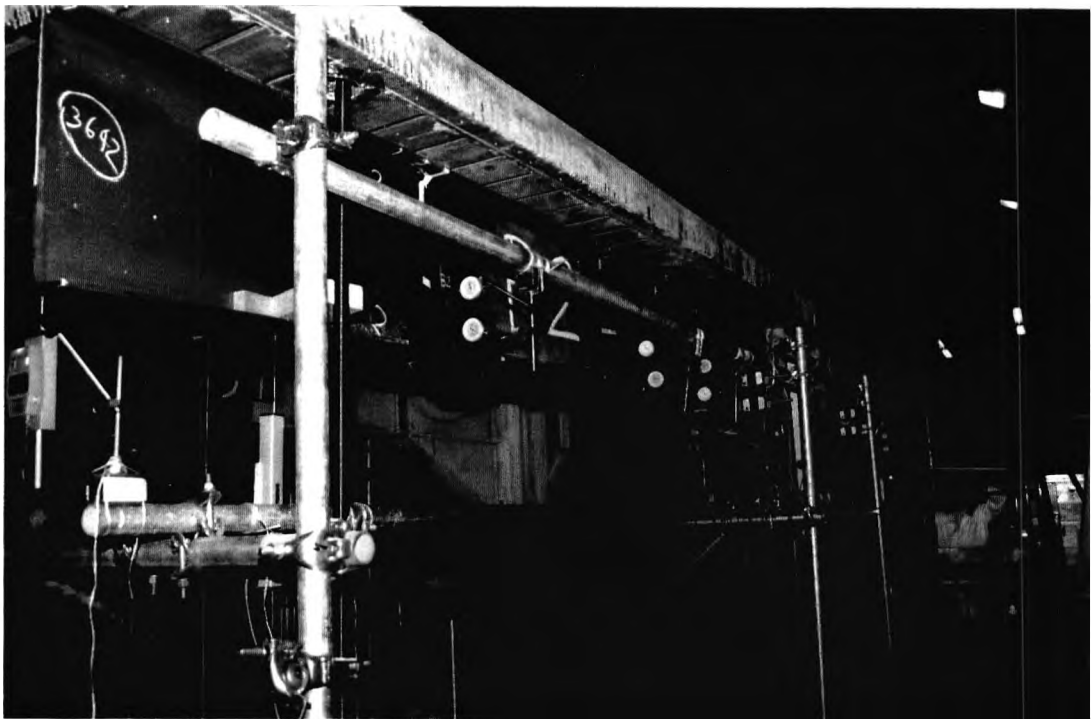
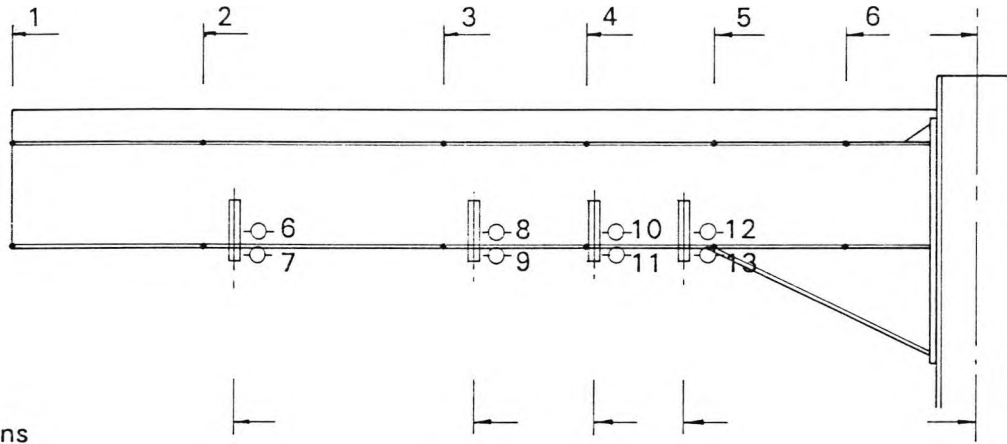


Figure 4.13 Sub-Assembly Test - Torsional Rotation Measurement Gauges

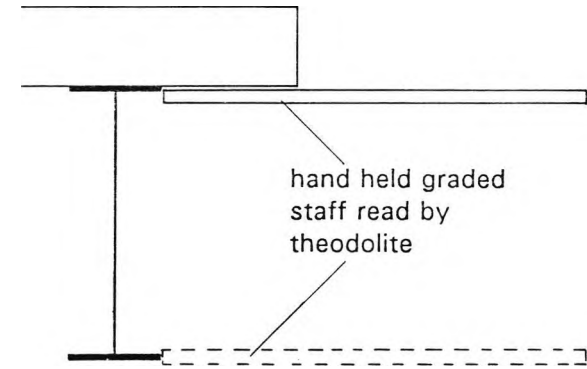


Figure 4.14 Sub-Assembly Test - Positioning the Graded Staff for Lateral Displacement Measurement

lateral movement measurement points

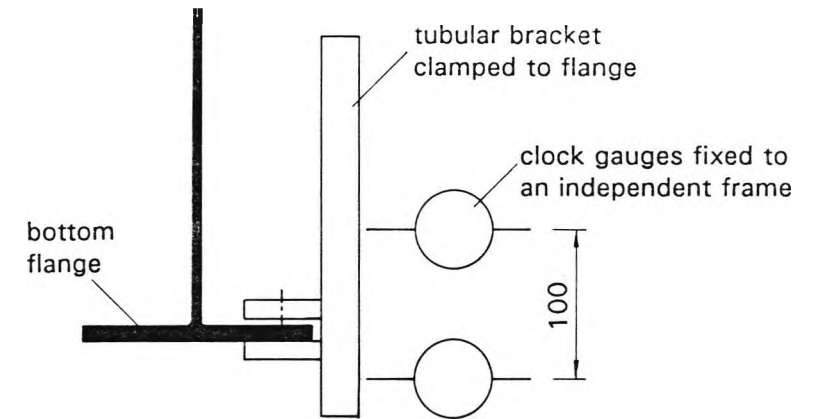


torsional movement measurement positions



Lateral movement measurement

Lateral movement measurement: position dimensions						
Beam	1	2	3	4	5	6
B1	4.000	2.744	1.744	1.149	0.859	0.424
B2	4.000	3.209	2.209	1.614	1.109	0.504
B3	4.000	2.651	1.646	1.151	0.856	0.426
B4	4.000	3.121	2.111	1.608	1.121	0.596
Torsional movement measurement: position dimensions						
Beam	6/7	8/9	10/11	12/13		
B1	2.809	1.809	1.114	0.759		
B2	3.074	2.074	1.579	1.204		



Torsional movement measurement

Figure 4.15 Sub-Assembly Test - Torsional Rotation and Lateral Movement Measurement Arrangement

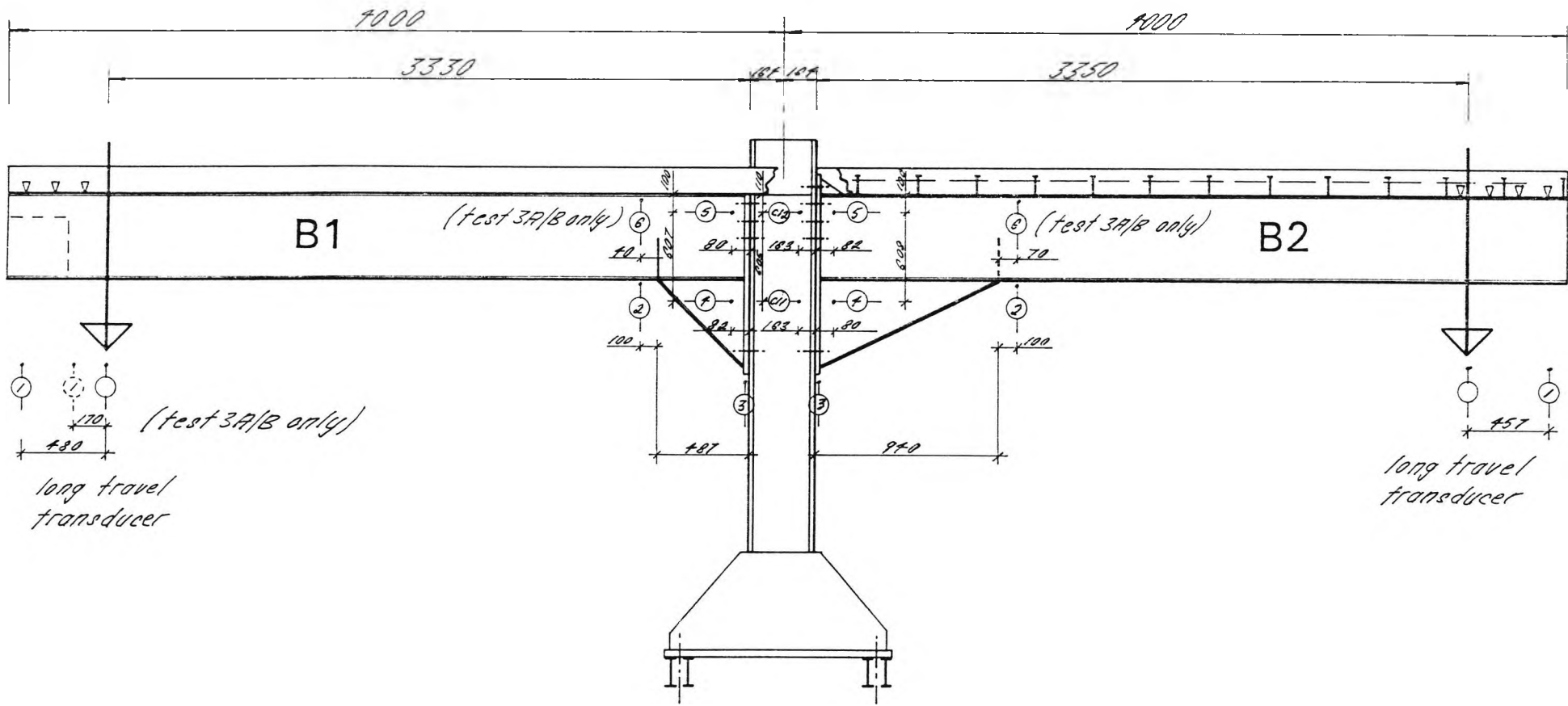


Figure 4.16 Sub-Assembly Test - Displacement Gauge Arrangement for Beams B1 and B2

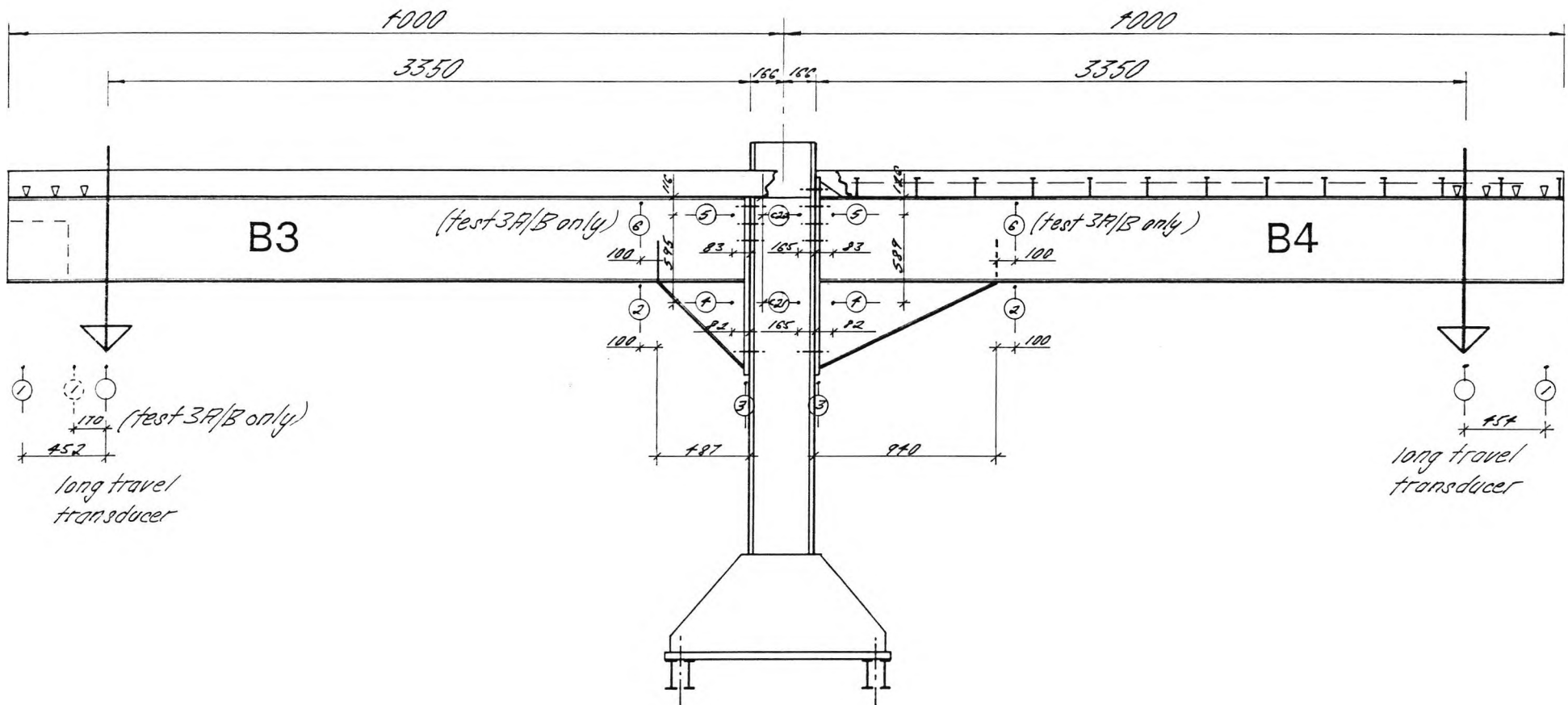


Figure 4.17 Sub-Assembly Test - Displacement Gauge Arrangement for Beams B3 and B4

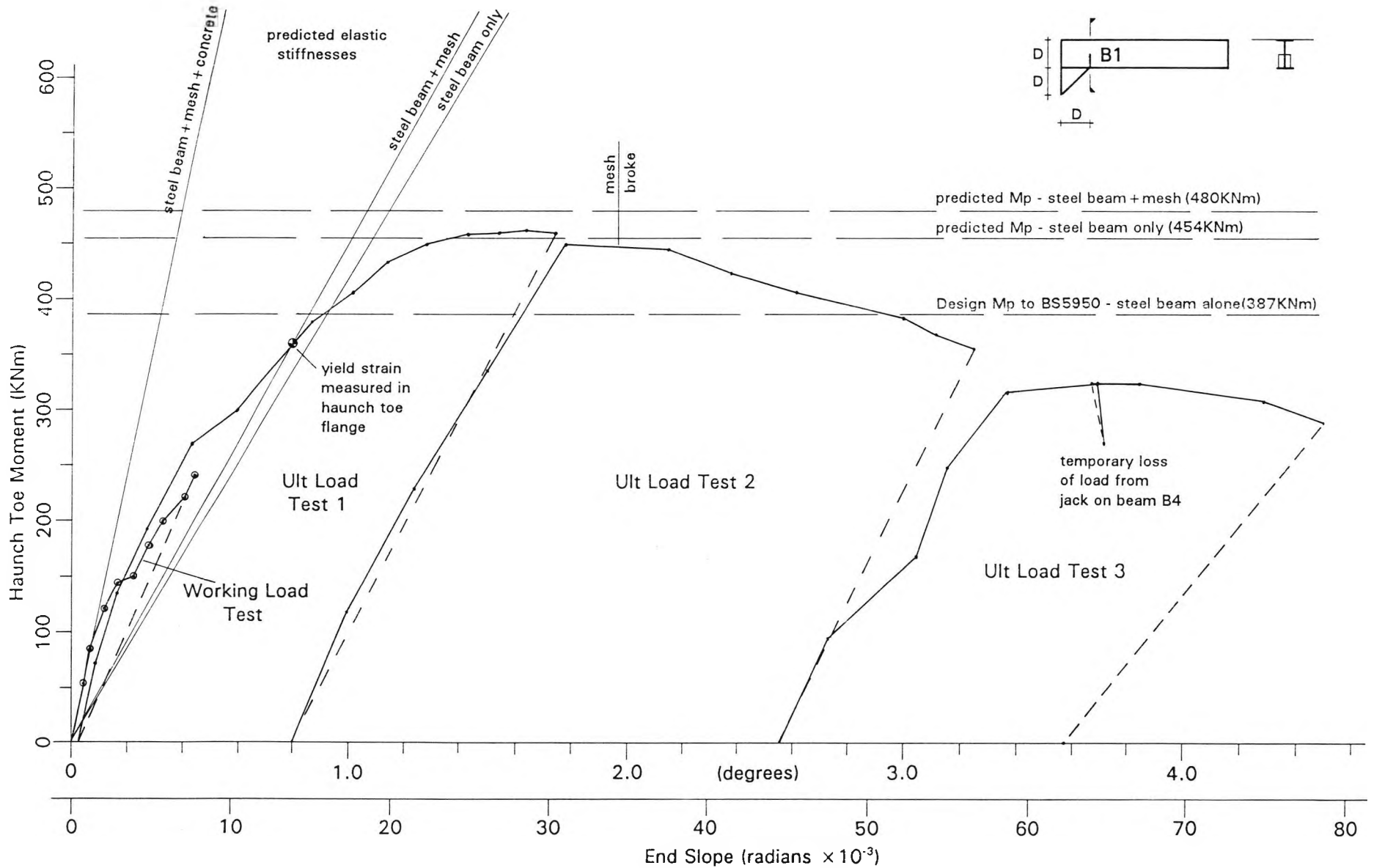


Figure 4.18 Sub-Assembly Test - Haunch Moment/Rotation Behaviour of Beam B1

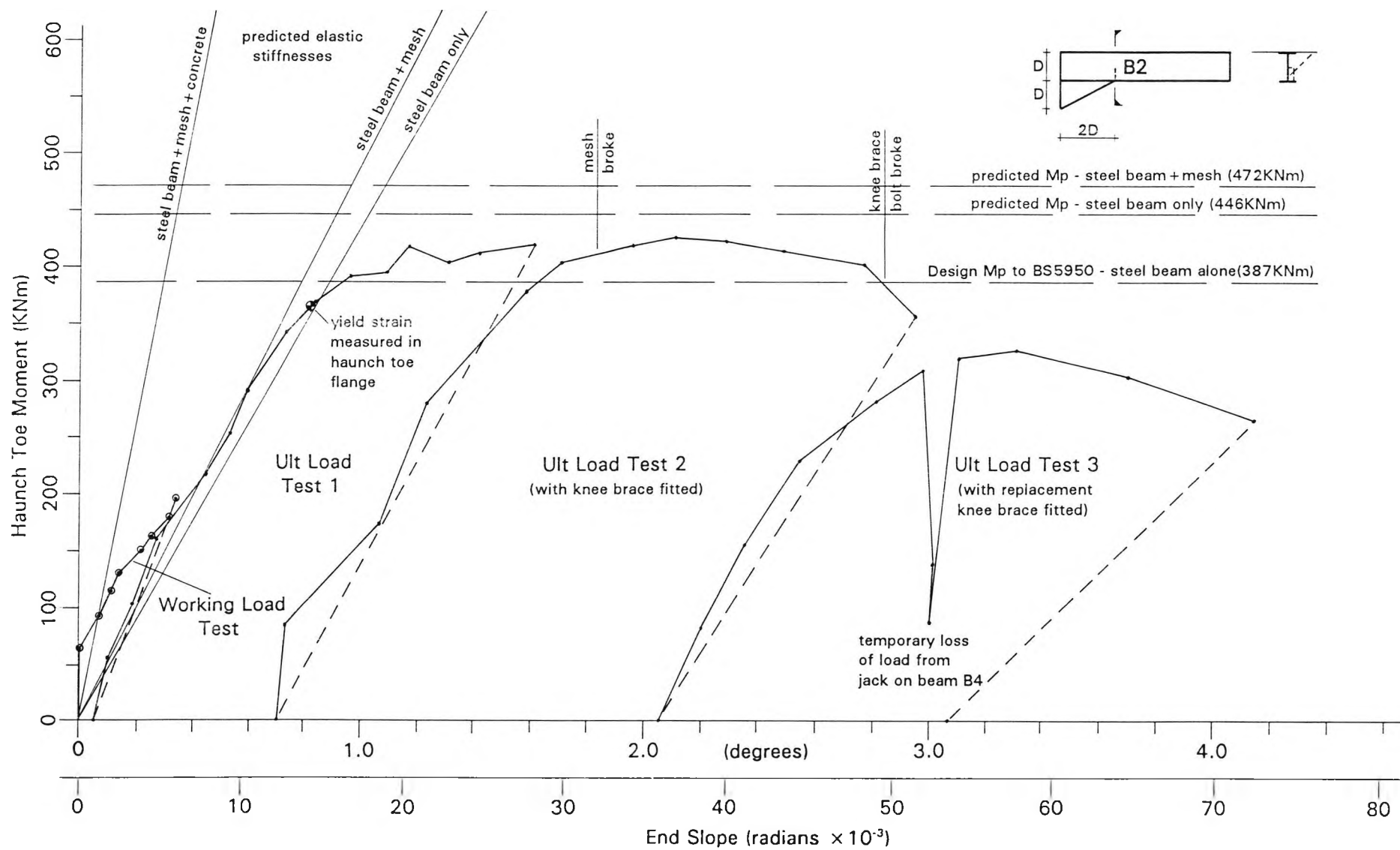


Figure 4.19 Sub-Assembly Test - Haunch Moment/Rotation Behaviour of Beam B2

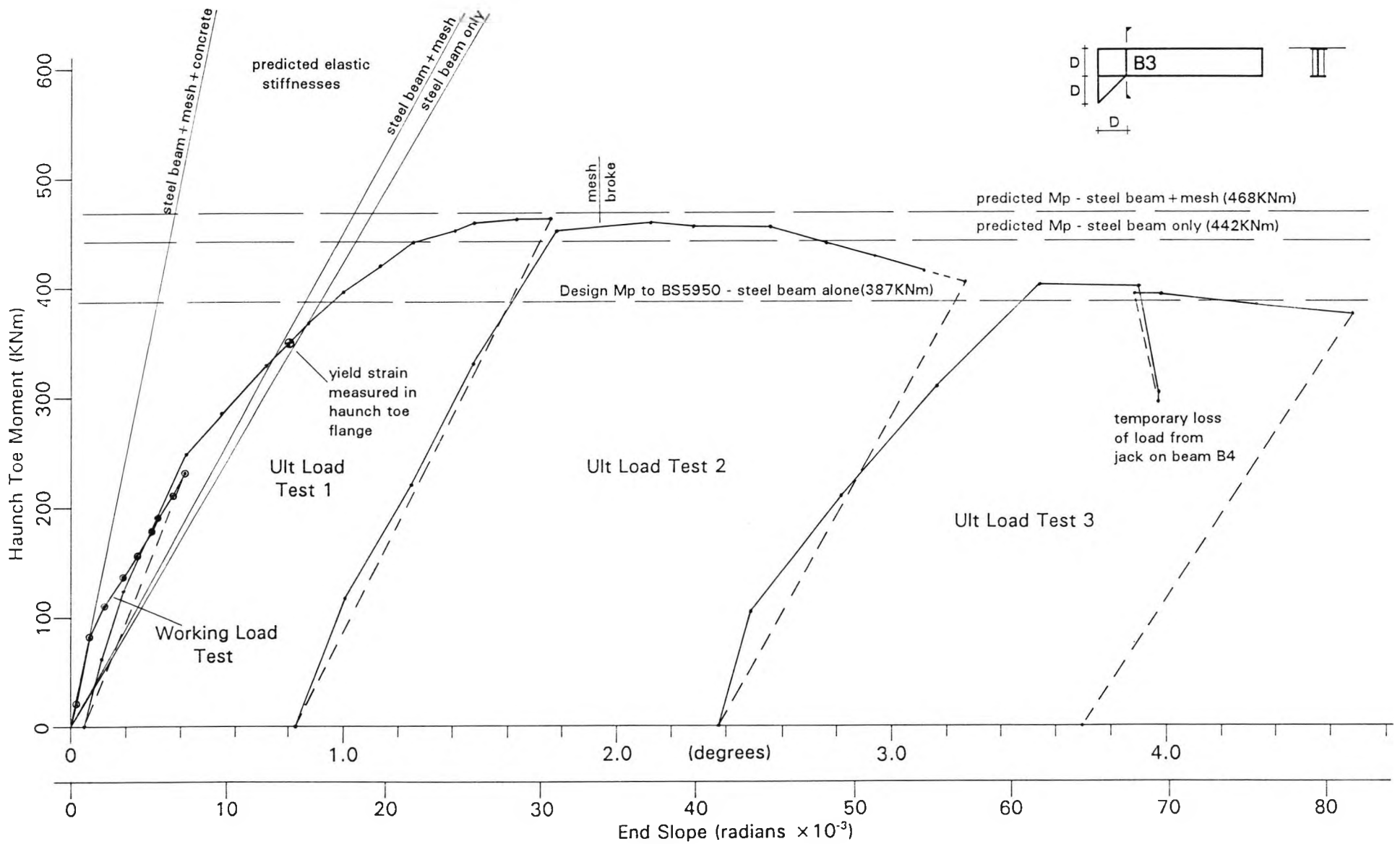


Figure 4.20 Sub-Assembly Test - Haunch Moment/Rotation Behaviour of Beam B3

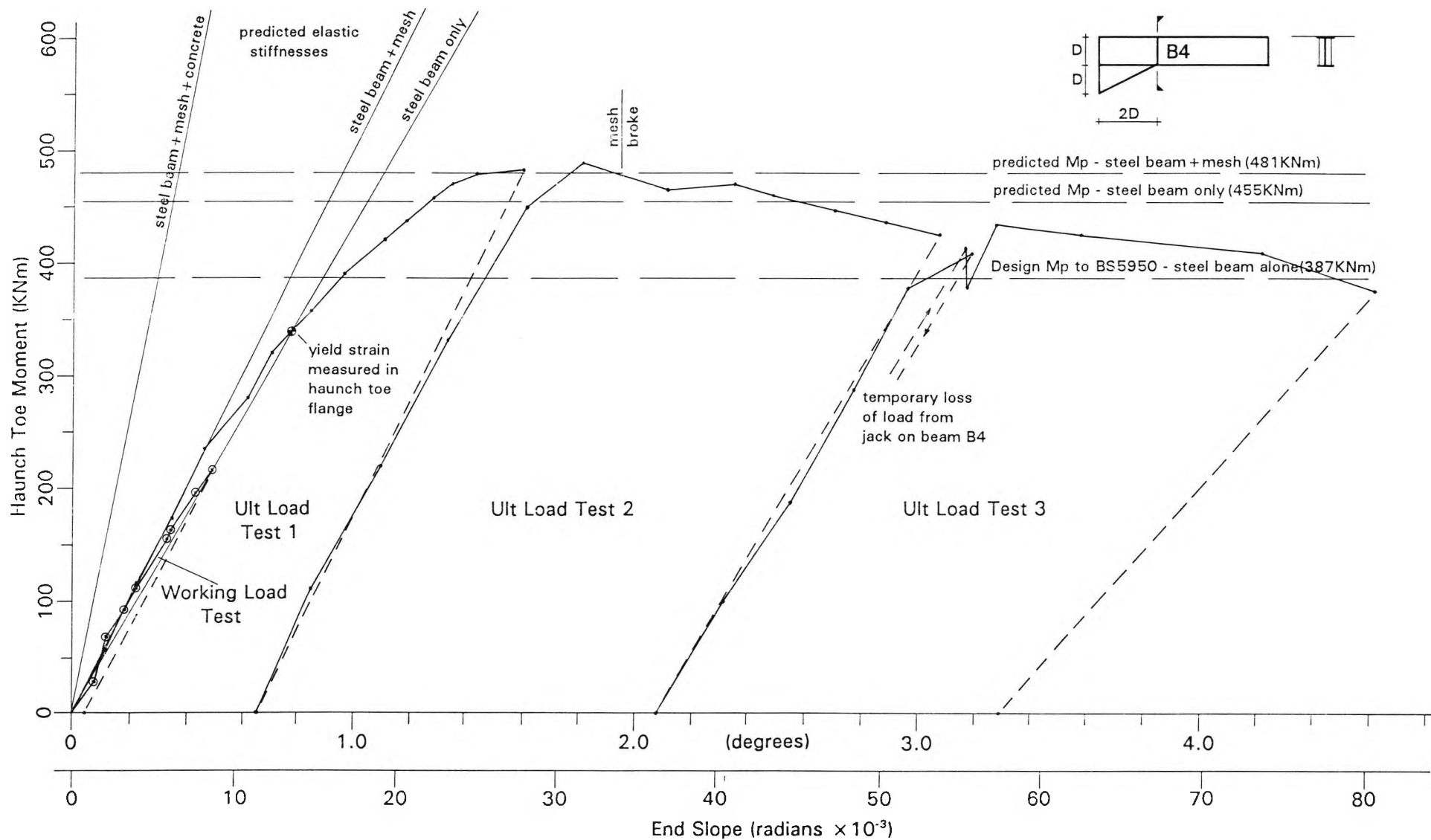


Figure 4.21 Sub-Assembly Test - Haunch Moment/Rotation Behaviour of Beam B4

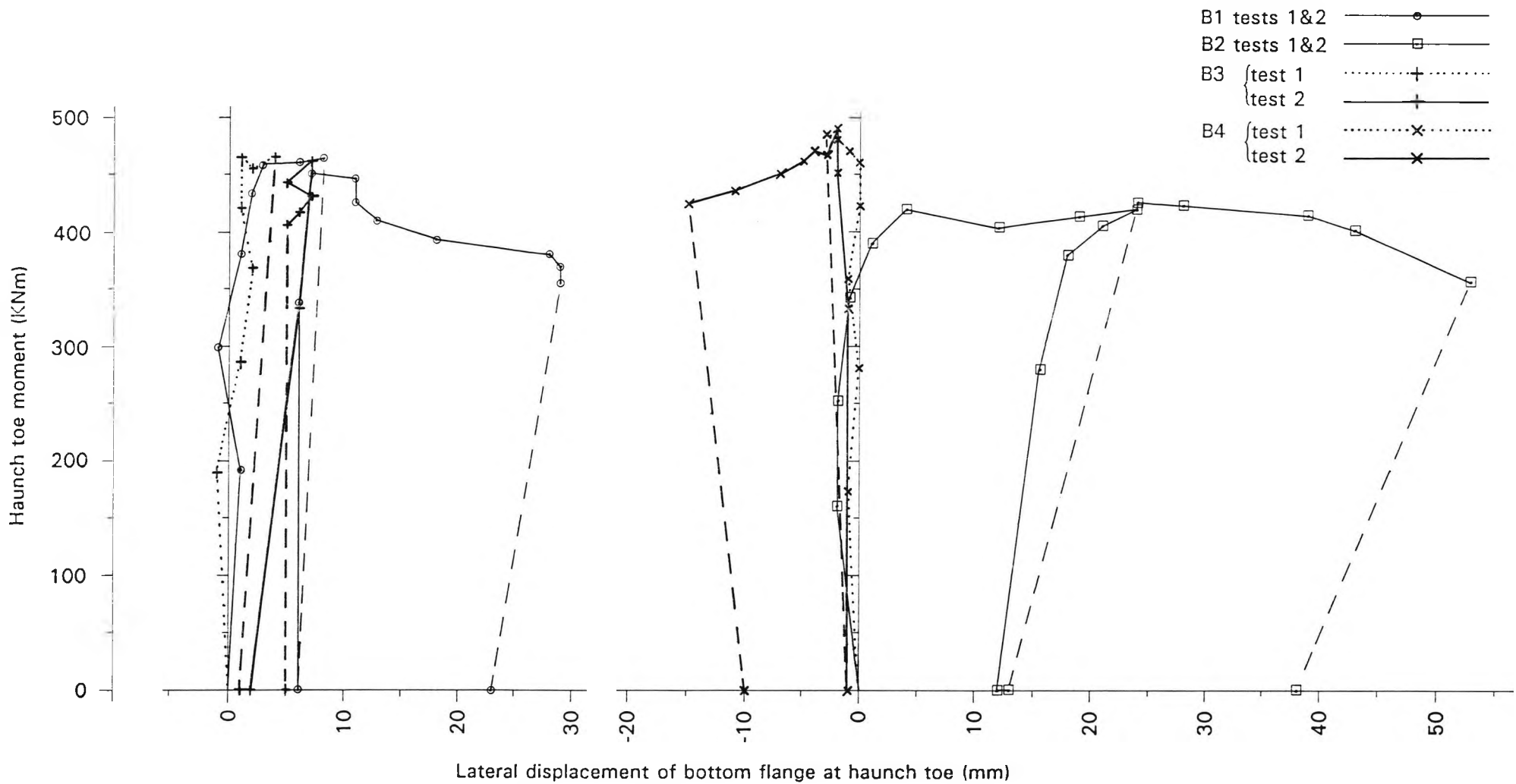


Figure 4.22 Sub-Assembly Test - A Comparison of Compression Flange Lateral Movement at the Haunch Toe Positions

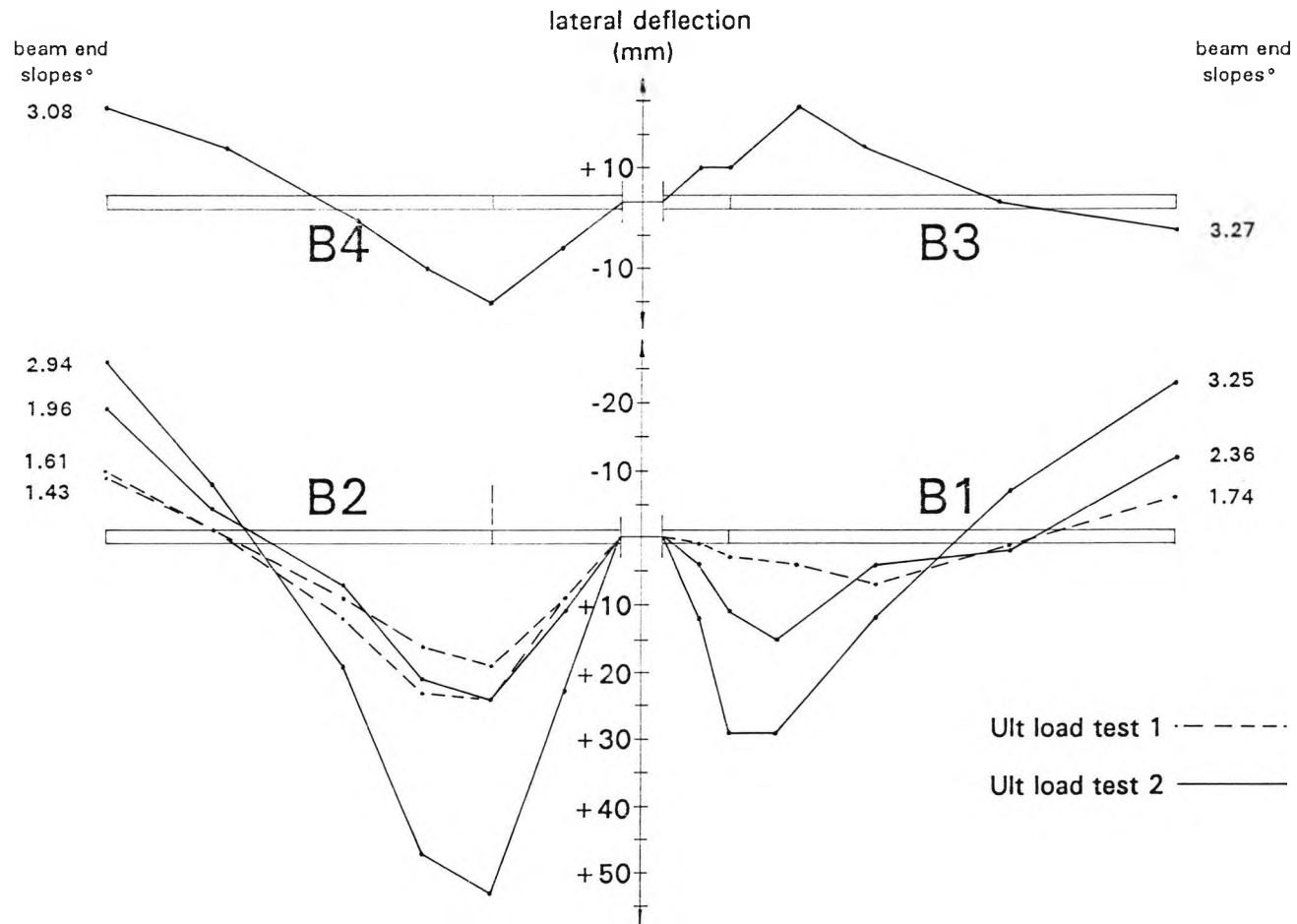
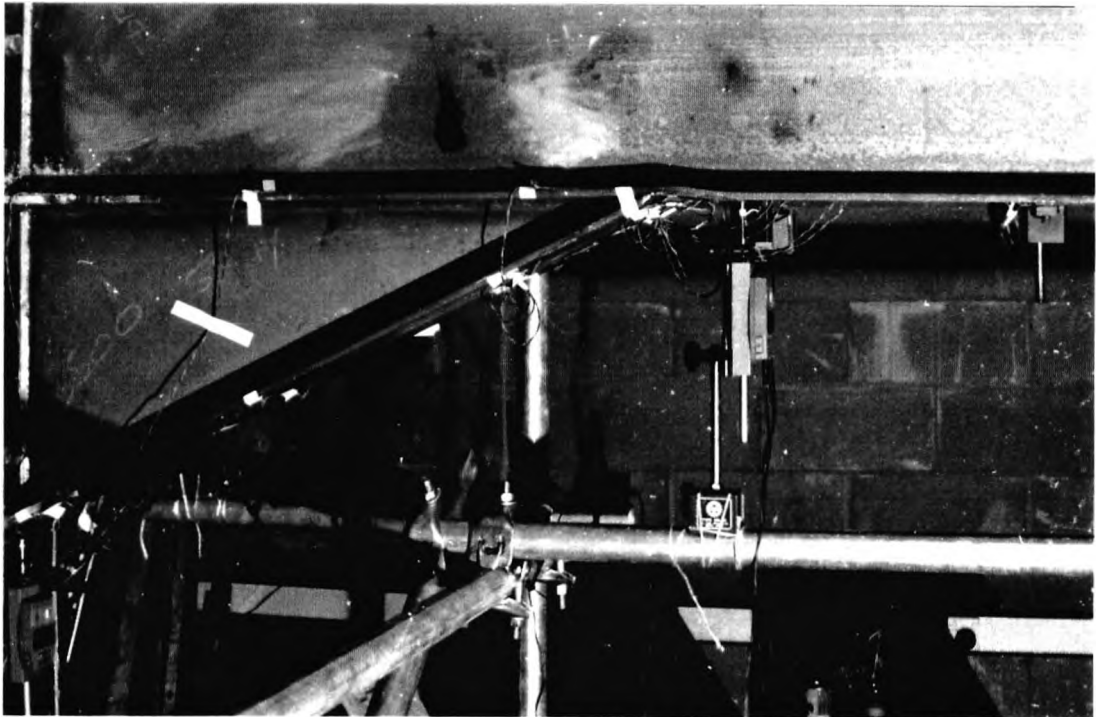
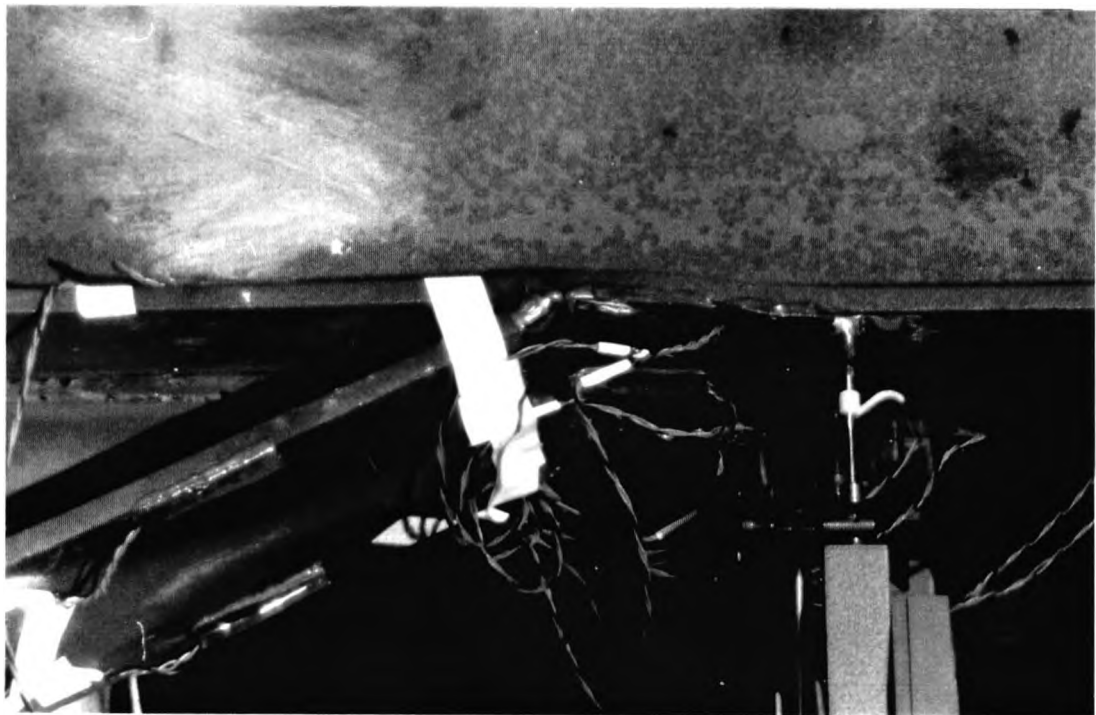


Figure 4.23 Sub-Assembly Test - A Comparison of the Relative Lateral Displacements Between the Tension and Compression Flanges at Selected end Slopes



(a)



(b)

Figure 4.24 Sub-Assembly Ultimate Load Test 1 - Local Flange Buckle in Beam B2



Figure 4.25 Sub-Assembly Ultimate Load Test 2 - Cracking in the Slab Above Beams B1 and B3

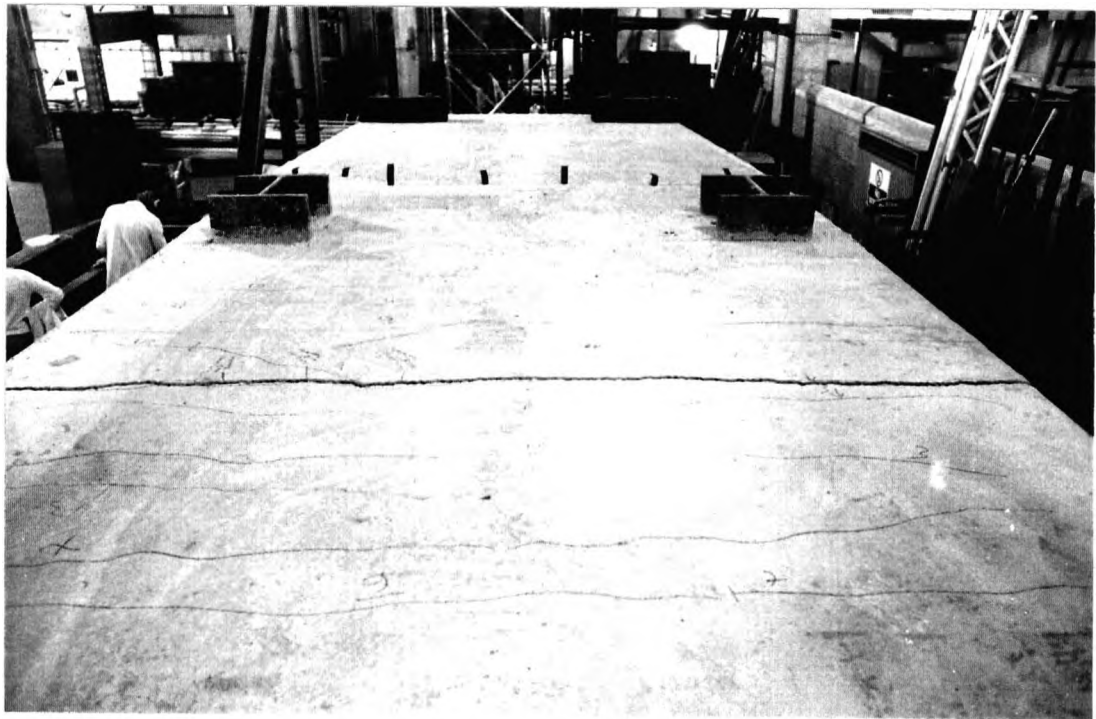


Figure 4.26 Sub-Assembly Ultimate Load Test 2 - Cracking in the Slab Above Beams B2 and B4

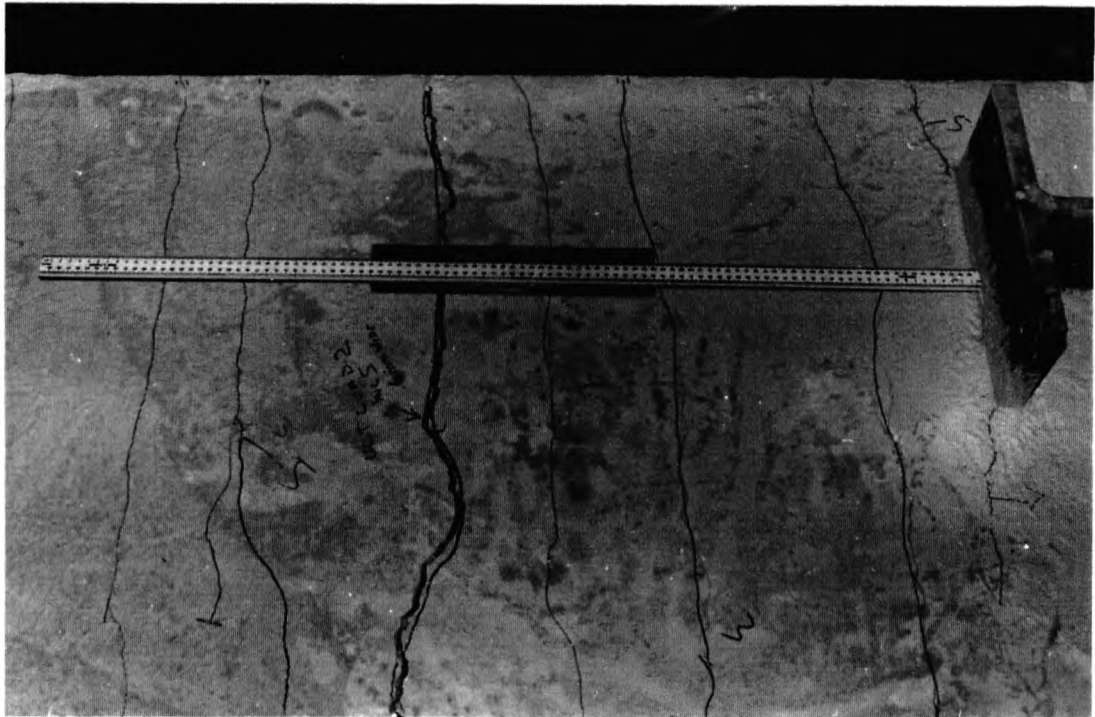


Figure 4.27 Sub-Assembly Ultimate Load Test 2 - Cracking in the Slab Above the Haunch Toe of Beam B1



Figure 4.28 Sub-Assembly Ultimate Load Test 2 - Local Buckling of Beam B2 and Shearing of Knee Brace Connections

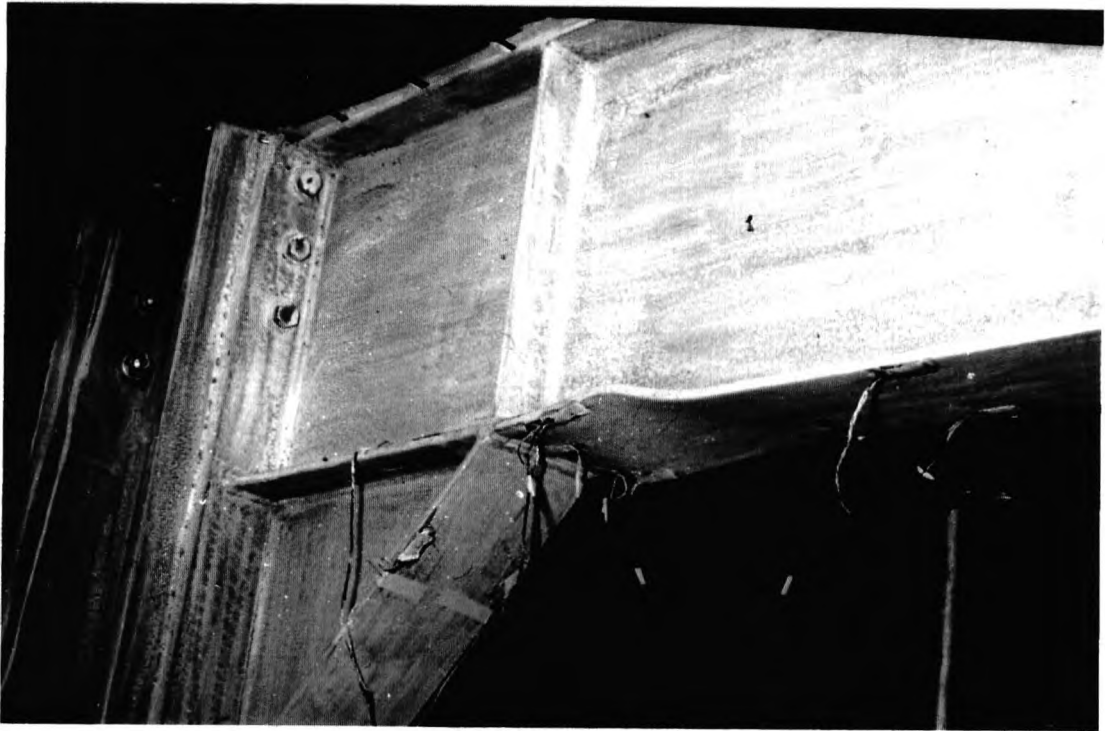


Figure 4.29 Sub-Assembly Ultimate Load Test 2 - Local Buckling Beyond the Haunch Toe of Beam B3



Figure 4.30 Sub-Assembly Ultimate Load Test 2 - Local Buckling Beyond the Haunch Toe of Beam B4



Figure 4.31 Sub-Assembly Ultimate Load Test 2 - Local Web and Flange Buckling of Beam B1



Figure 4.32 Sub-Assembly Ultimate Load Test 2 - Local Web and Flange Buckling of Beam B3

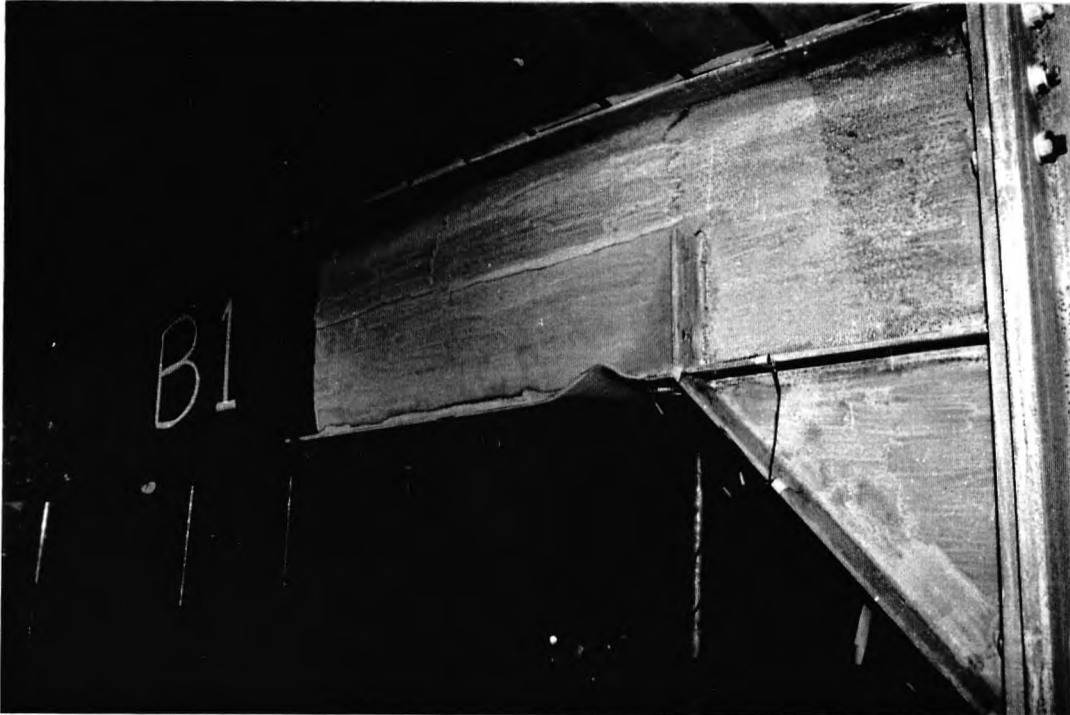


Figure 4.33 Sub-Assembly Ultimate Load Test 3 - Local Buckling of Beam B1

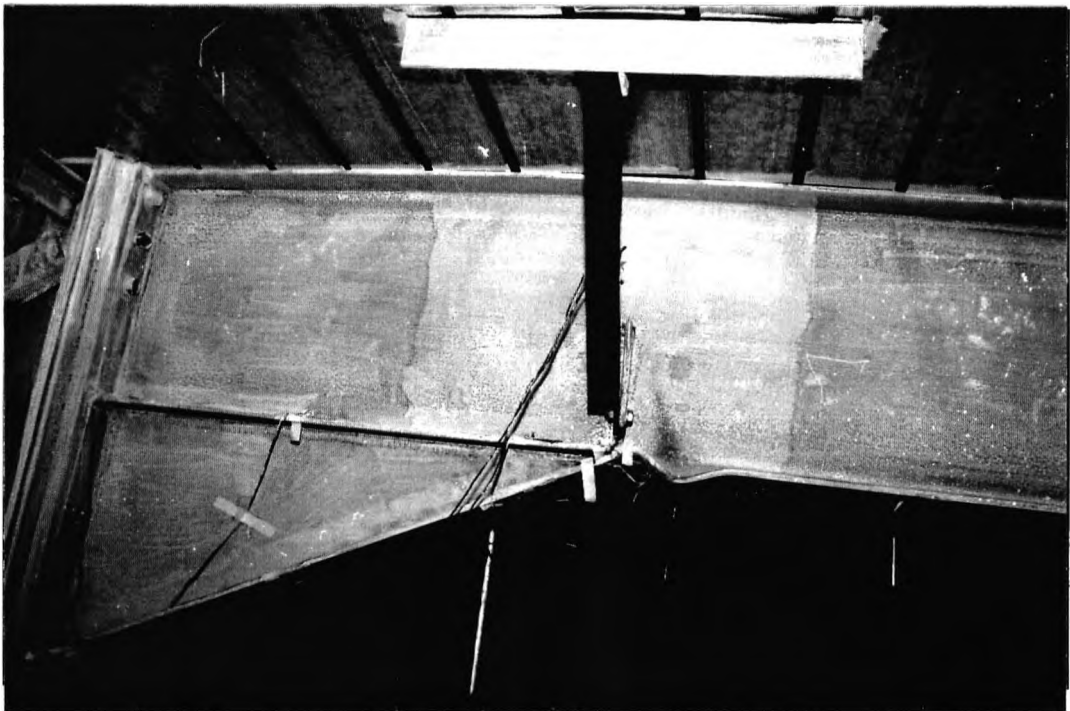


Figure 4.34 Sub-Assembly Ultimate Load Test 3 - Local Buckling of Beam B2 and Shearing of the Knee Brace Connections

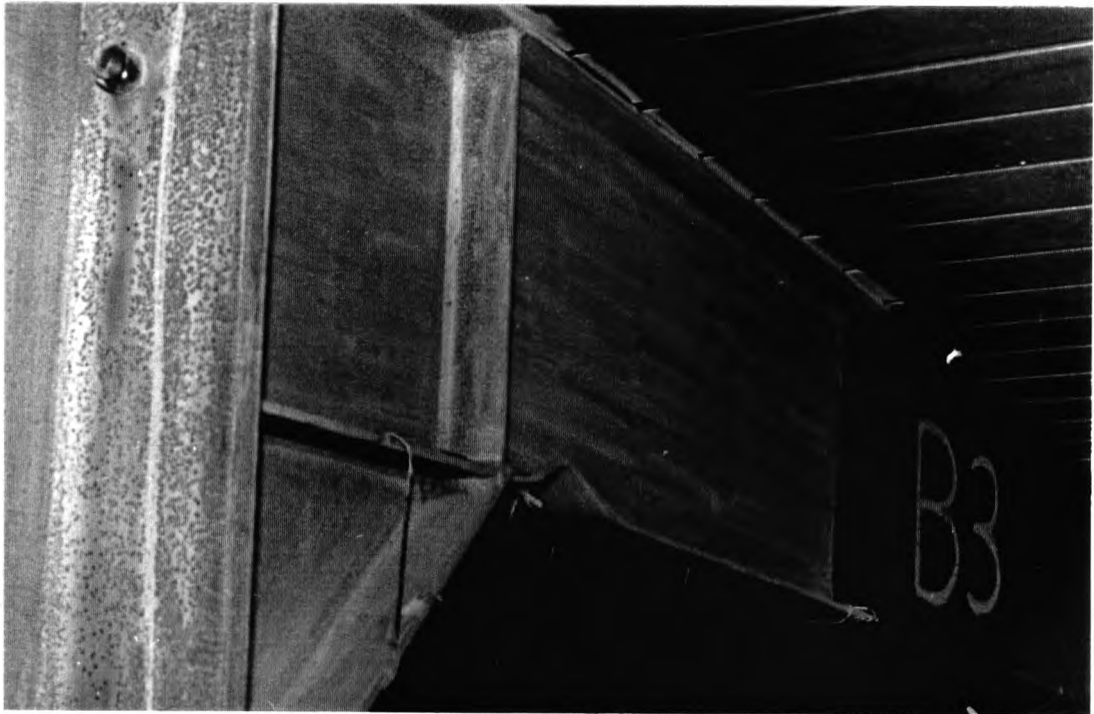


Figure 4.35 Sub-Assembly Ultimate Load Test 3 - Buckling of Beam B3



Figure 4.36 Sub-Assembly Ultimate Load Test 3 - Buckling of Beam B4

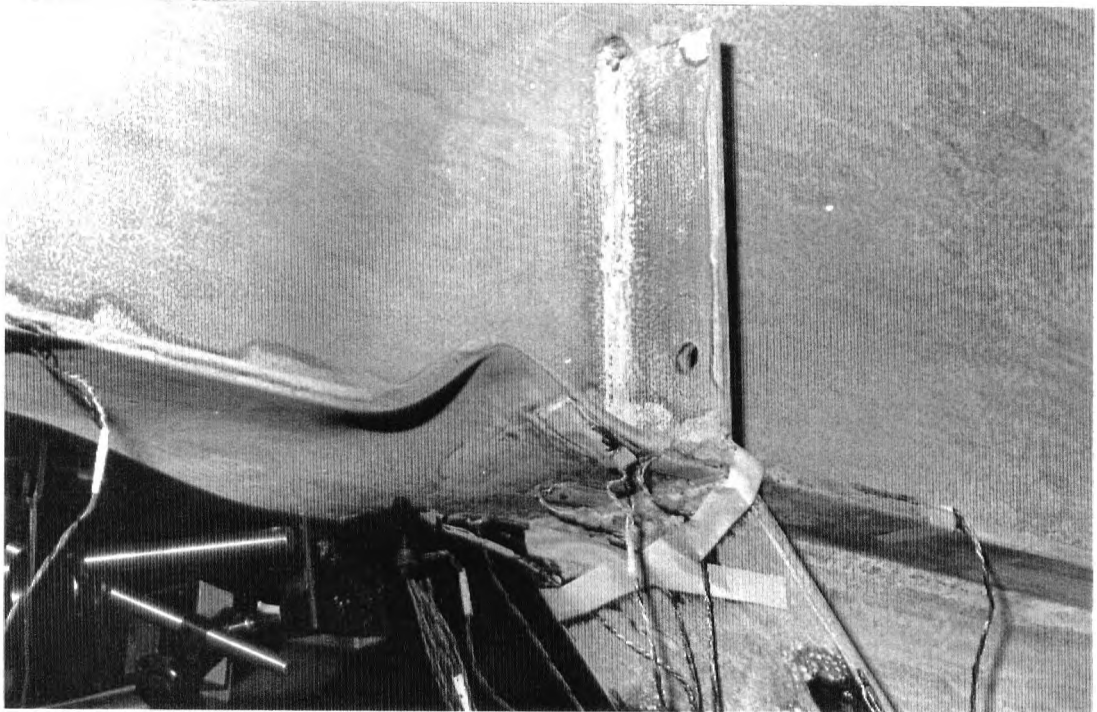


Figure 4.37 Sub-Assembly Ultimate Load Test 3 - Detail of Local Buckling of Beam B1

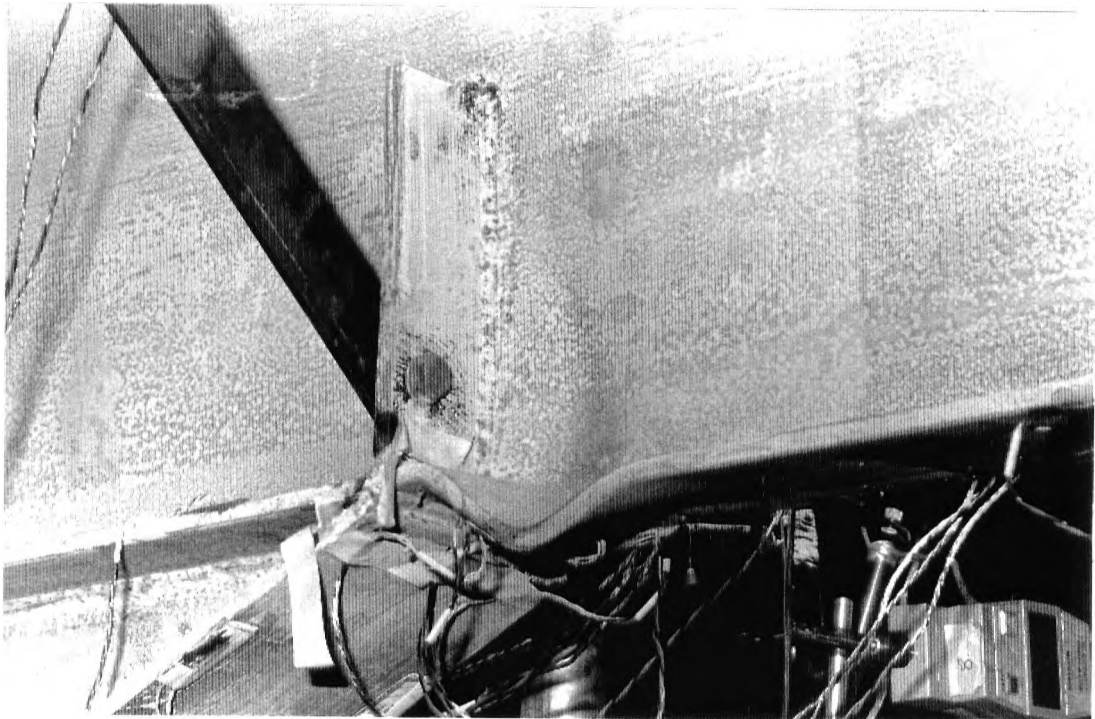


Figure 4.38 Sub-Assembly Ultimate Load Test 3 - Detail of Local Buckling of Beam B2



Figure 4.39 Sub-Assembly Test Ultimate Load
Test 3 - Lateral Distortional Buckling
of Beam B2

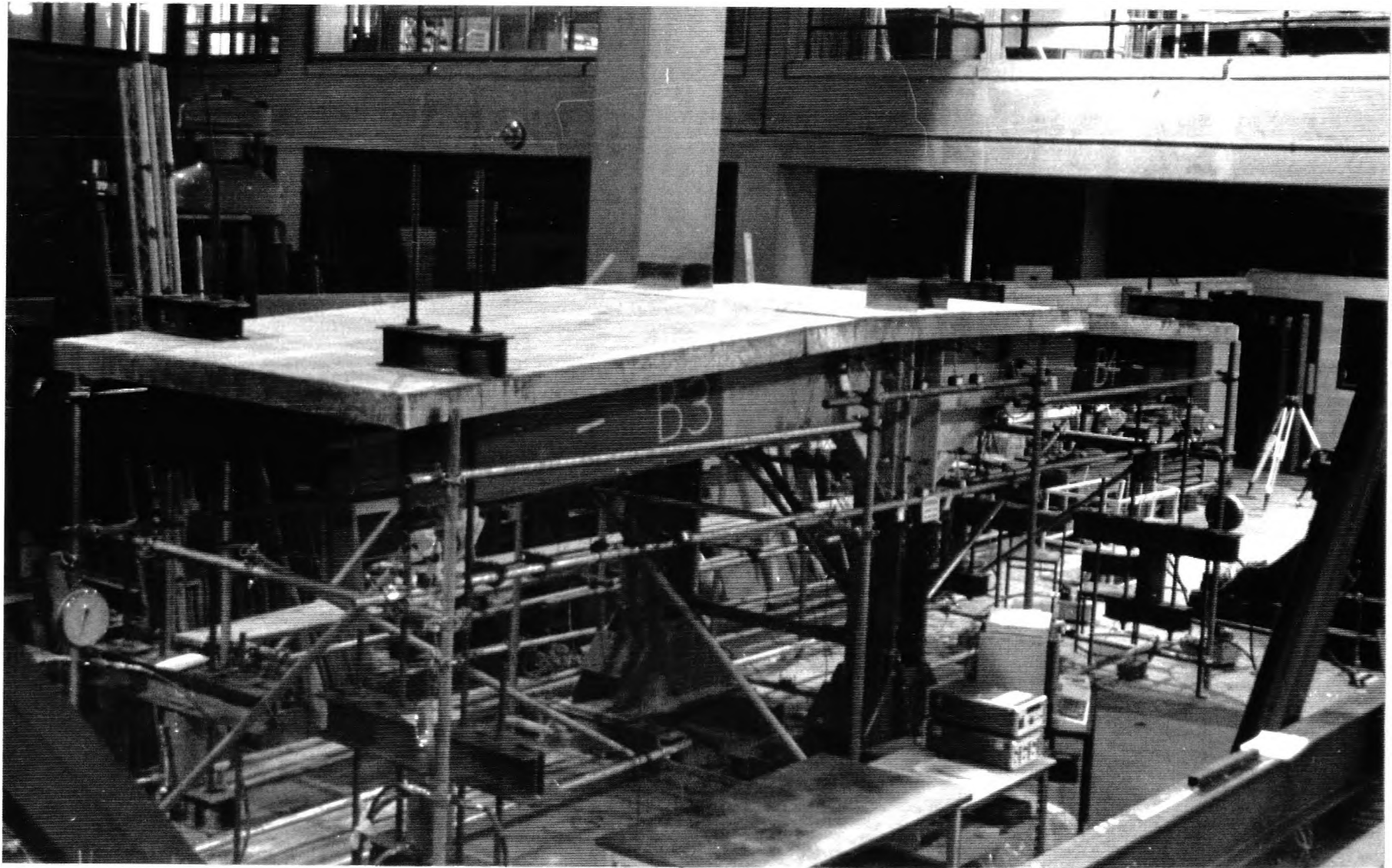


Figure 4.40 Sub-Assembly Ultimate Load Test 3 - Final Deformation of Test Structure

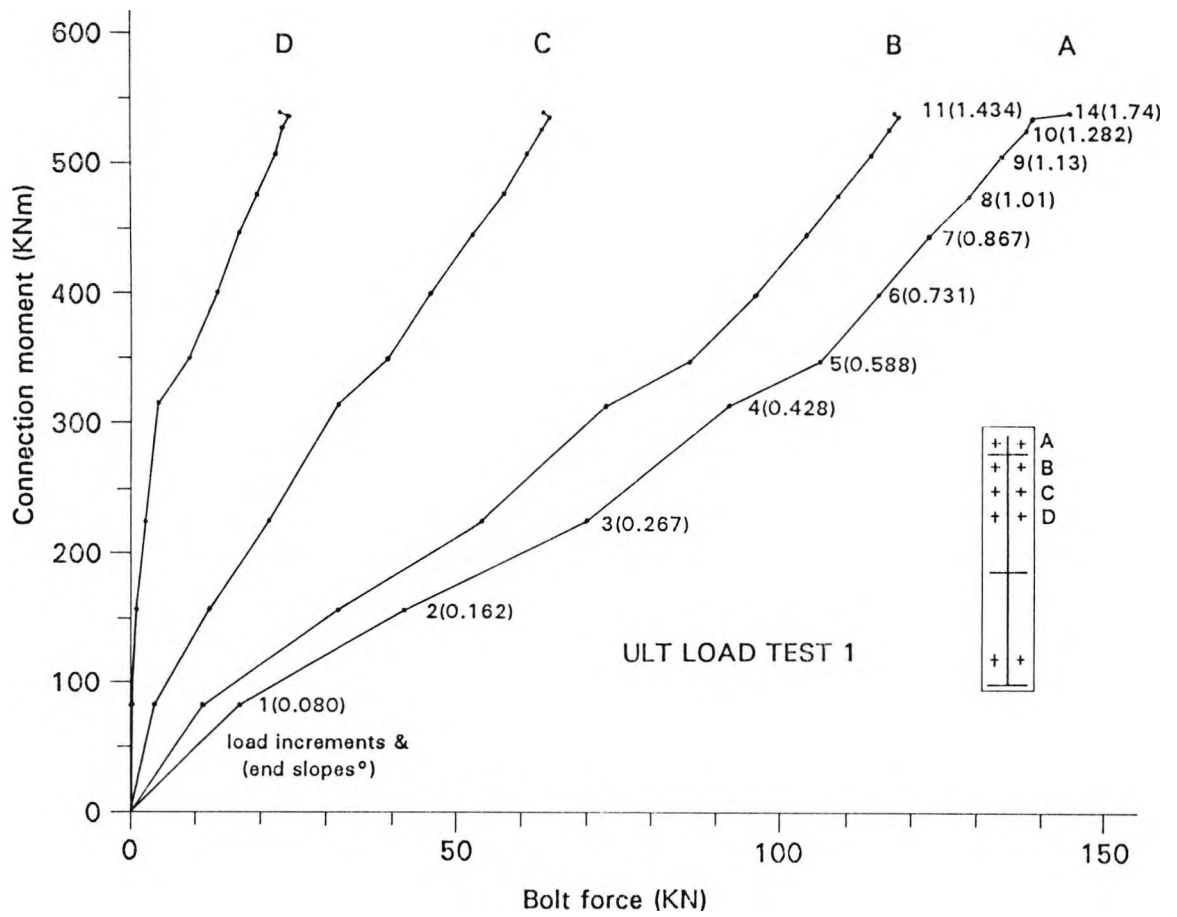


Figure 4.41 Sub-Assembly Ultimate Load Test 1 - Haunch Connection Bolt Force Growth in Beam B1

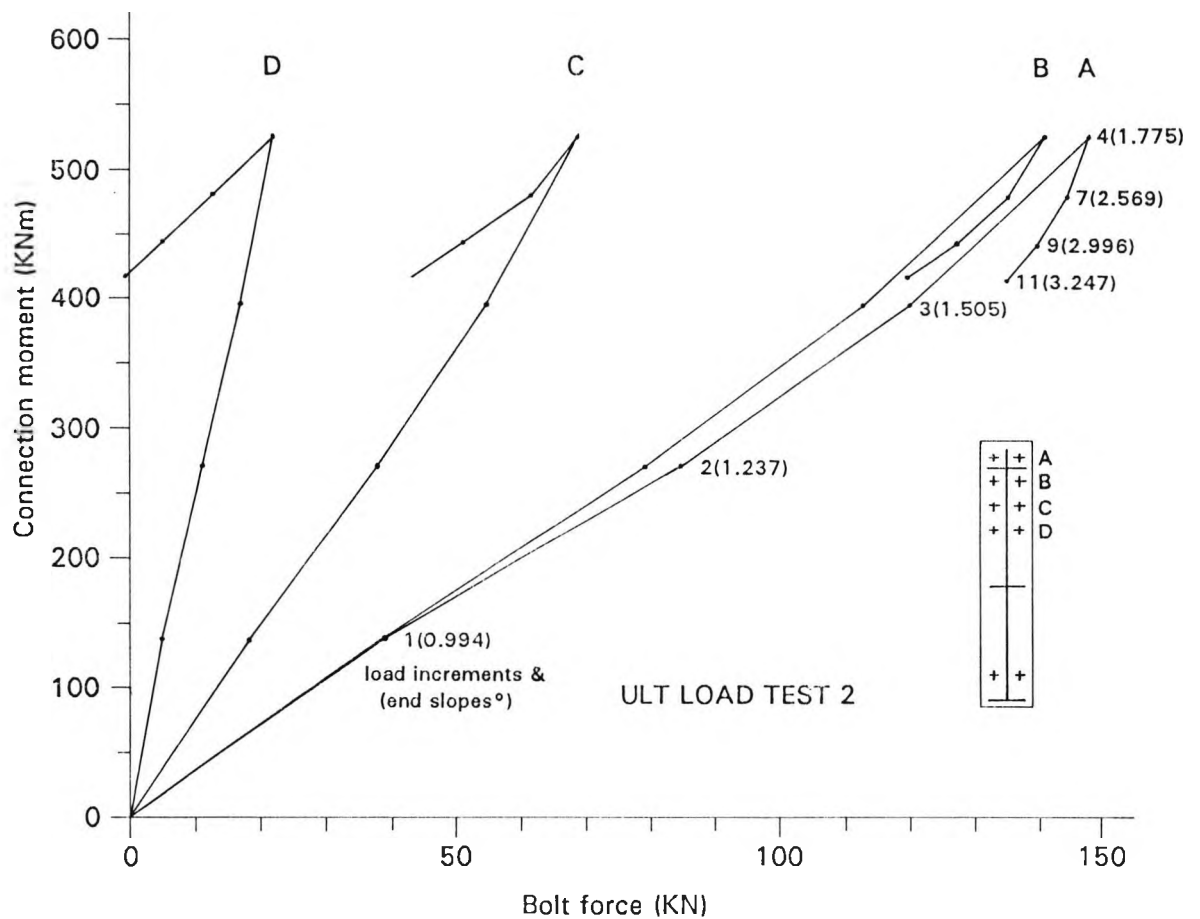


Figure 4.42 Sub-Assembly Ultimate Load Test 2 - Haunch Connection Bolt Force Growth in Beam B1

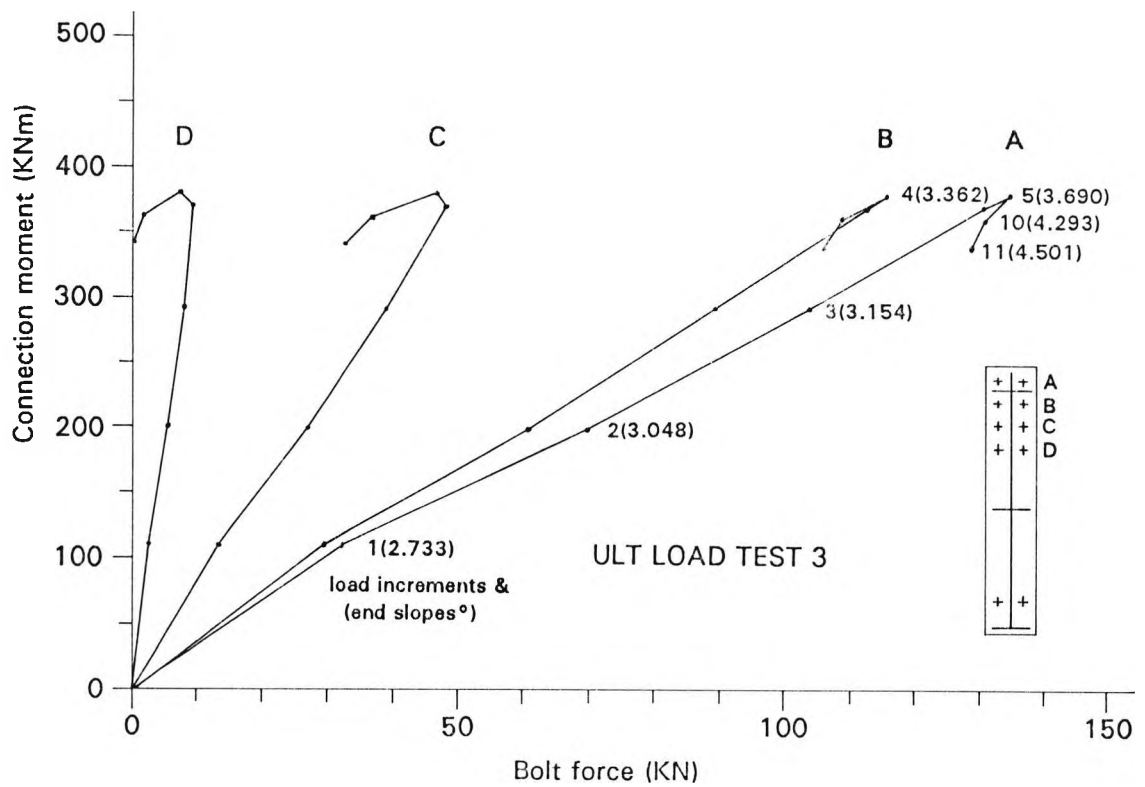


Figure 4.43 Sub-Assembly Ultimate Load Test 3 - Haunch Connection Bolt Force Growth in Beam B1

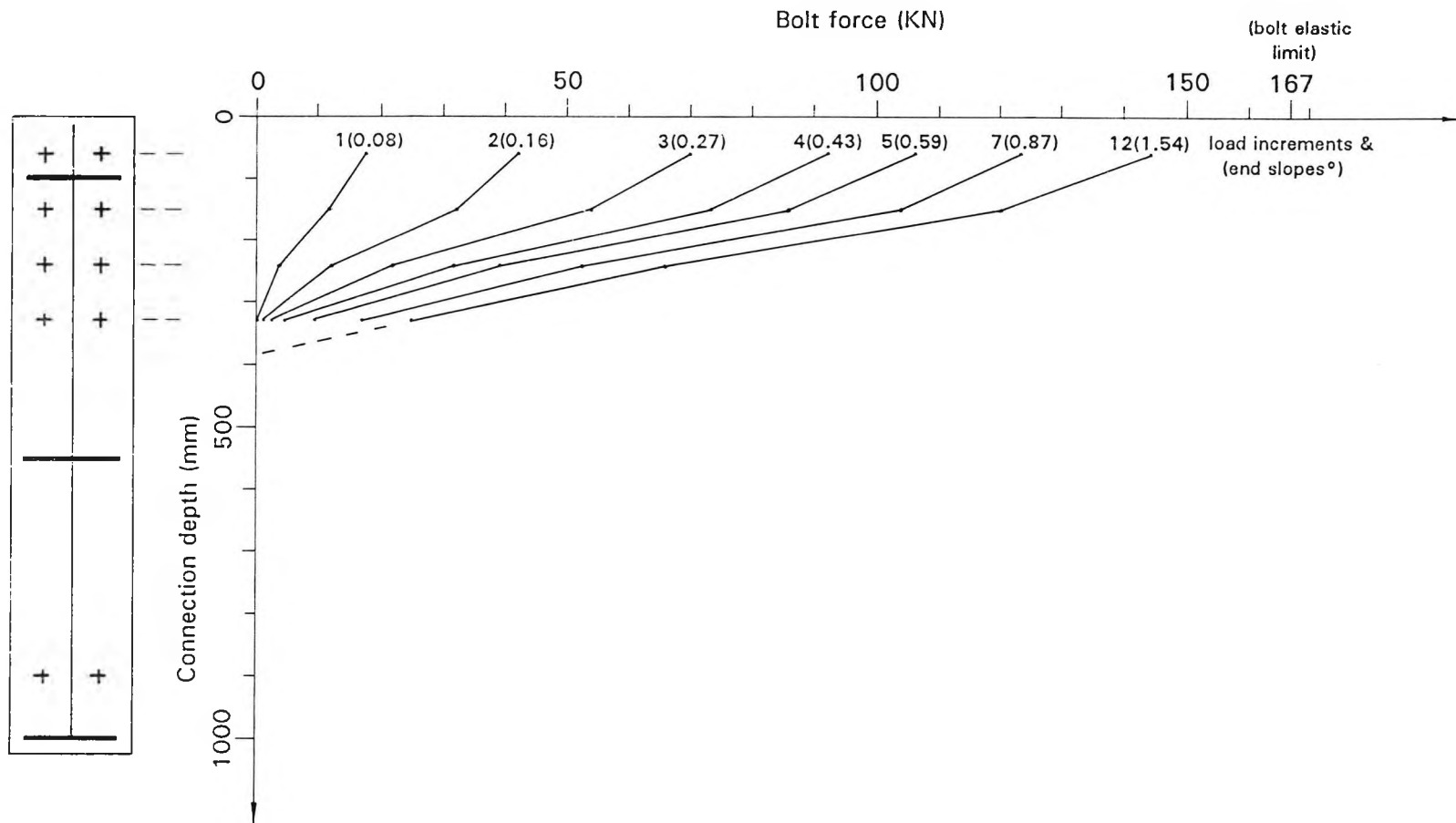


Figure 4.44 Sub-Assembly Ultimate Load Test 1 - Haunch Connection Bolt Force Profiles

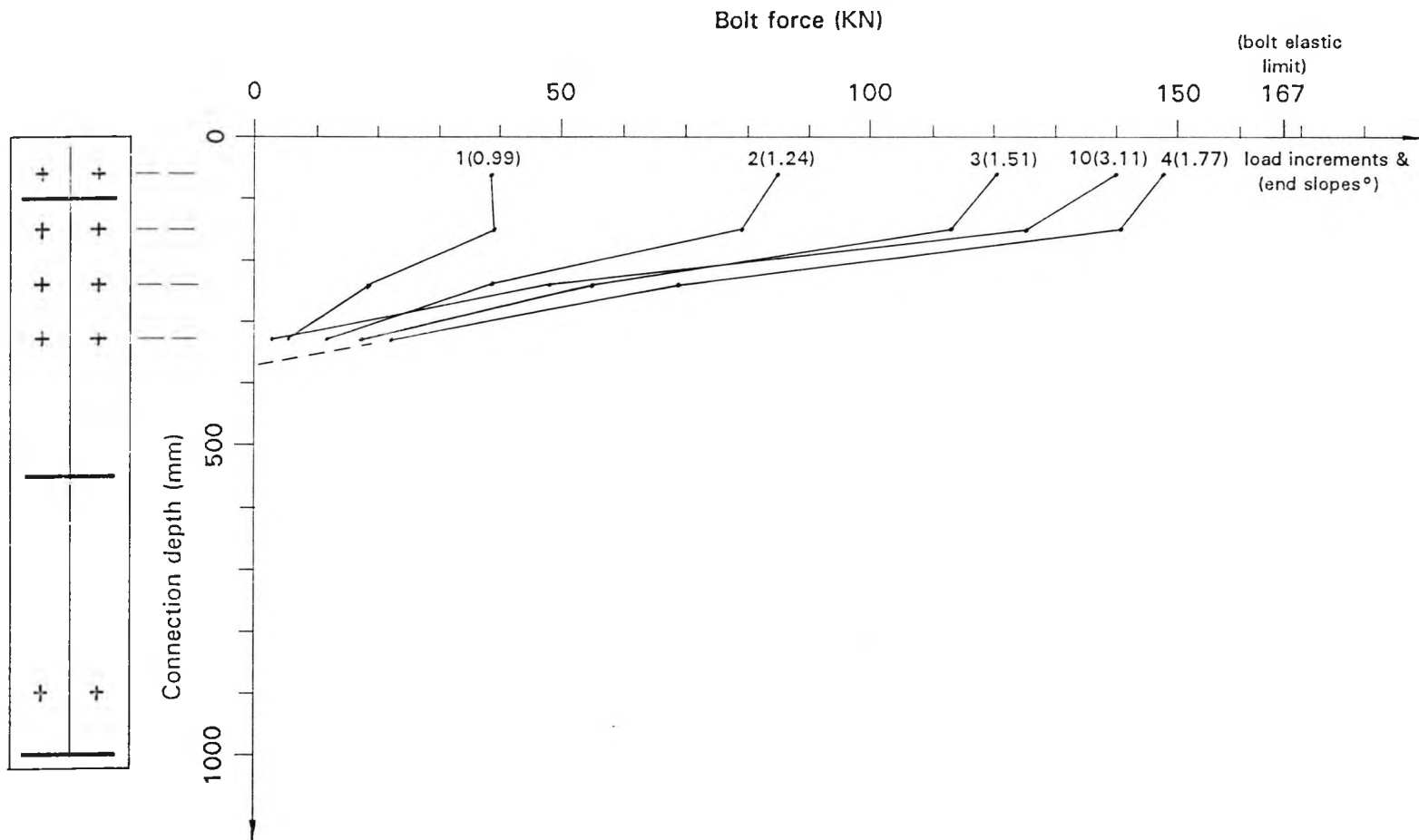


Figure 4.45 Sub-Assembly Ultimate Load Test 2 - Haunch Connection Bolt Force Profiles

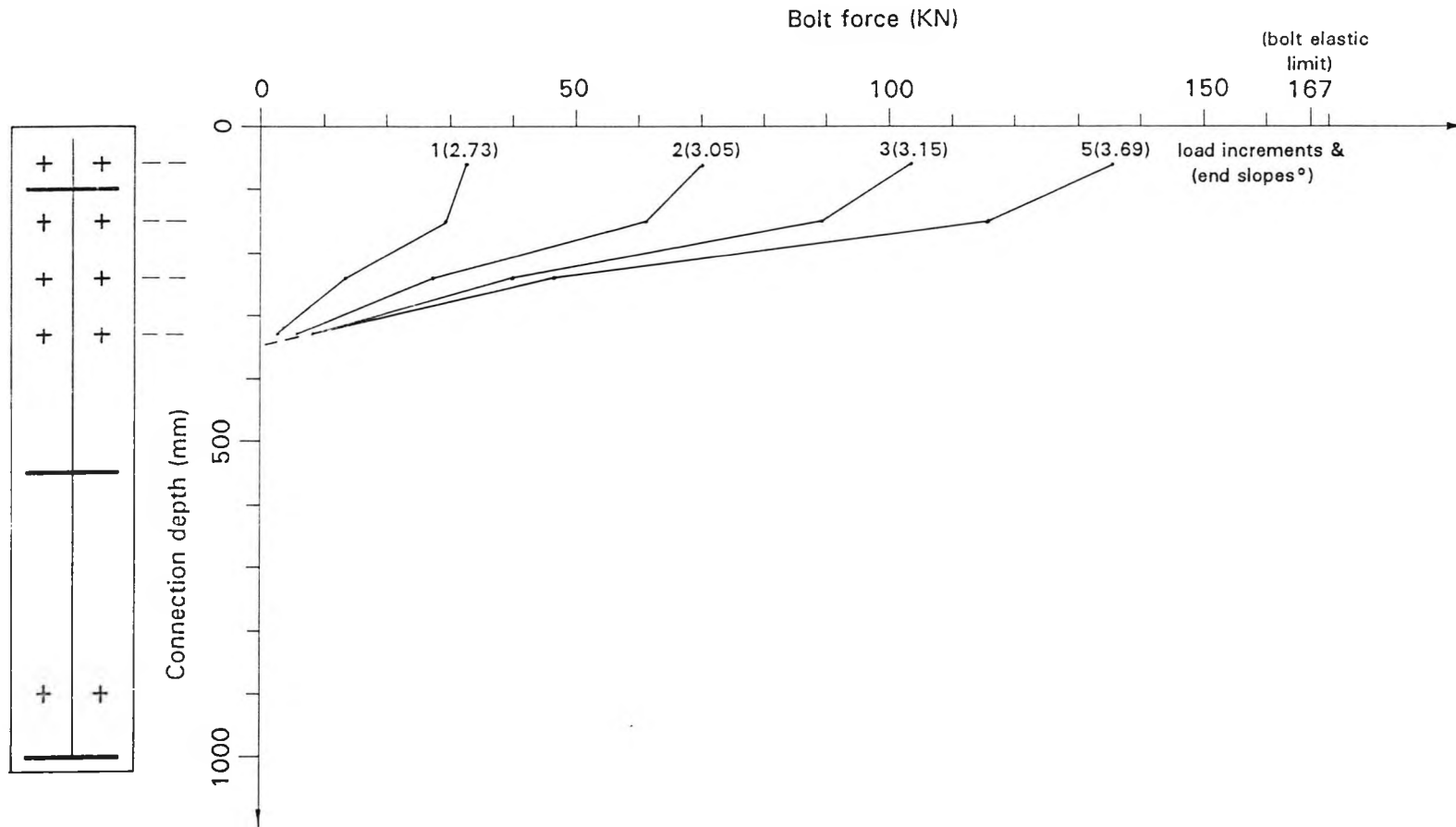


Figure 4.46 Sub-Assembly Ultimate Load Test 3 - Haunch Connection Bolt Force Profiles

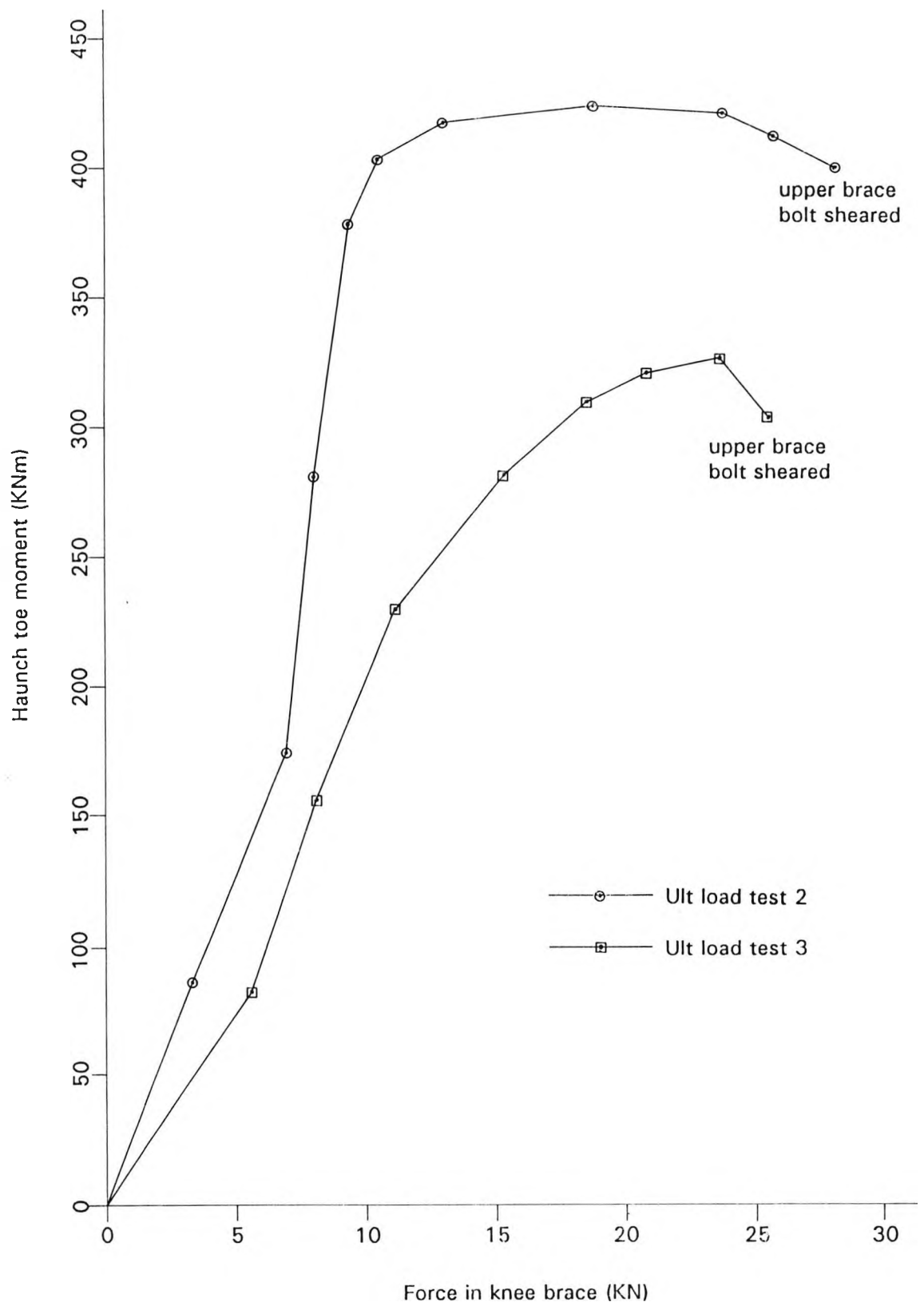


Figure 4.47 Sub-Assembly Load Tests 1 and 2 - Growth in Knee Brace Force with Haunch Toe Moment for Beam B2

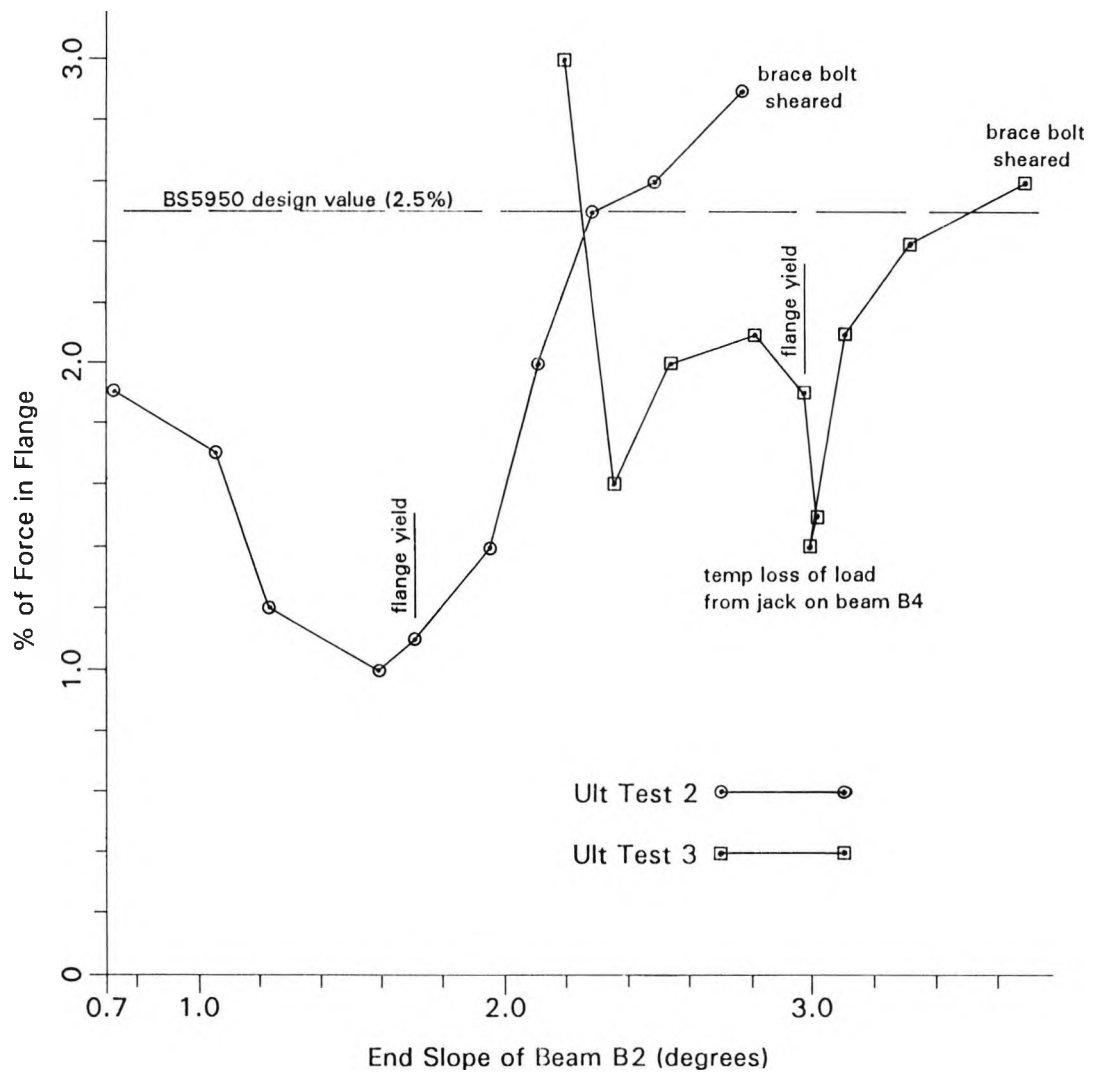


Figure 4.48 Sub-Assembly Ultimate Load Tests 1 and 2 - Horizontal Component of Knee Brace Force Expressed as a Percentage of the Haunch Toe Compression Flange Force in Beam B2, against the Beam End Slope

APPENDIX 4A

MEASUREMENT OF AXIAL FORCE FROM STRAIN GAUGE READINGS IN KNEE BRACE

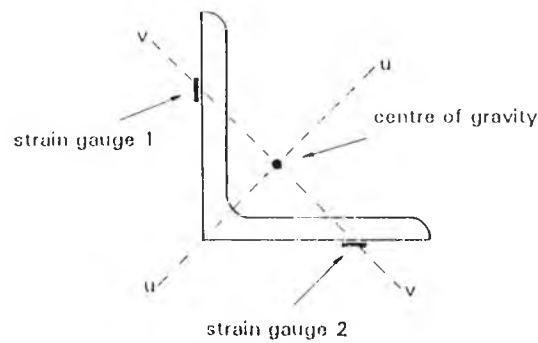


Diagram 4A.1 Sub-Assembly Test - Strain Gauge Arrangement in Knee Brace

Referring to the above diagram, any applied moment can be resolved into two components, consisting of M_u about the u-u axis, and M_v about the v-v axis. With strain gauges positioned on the v-v axis, the strain measured due to M_v will be zero and the contributions of strain due to M_u will be ϵ_u and $-\epsilon_u$ for gauges 1 and 2 respectively. Clearly, by halving the aggregate value of the two gauges, the strains due to M_u cancel out and the axial force can be directly calculated.

CHAPTER 5

COMPARISON OF THE SUB-ASSEMBLY TEST RESULTS WITH THEORY

5.1 ELASTIC STIFFNESS

The Sub-Assembly Test beam stiffnesses were predicted with the use of a computer finite element program, as described later in Chapter 8. The analysis took account of the haunch, and three cases were considered, namely; the steel beam alone (case A), the steel beam plus reinforcing mesh (case B) and the steel beam, mesh and concrete (case C). Case C was calculated by representing the concrete as an equivalent area of steel using a modular ratio of 10, as detailed in Chapter 8. These cases have all been superimposed on the test moment/rotation responses in Figures 4.18 to 4.21.

Referring to figures 4.18 to 4.20, it can be seen that the full composite stiffness was achieved initially in nearly all beams up to a loading of 20% of the maximum ultimate load. The stiffness then declined as the concrete cracked so that, at yield in the beam, the deformation could have been predicted almost exactly by case A. It is to be noted that there is little difference in the stiffness of case A and case B because the area of the mesh was relatively small. The off-loading stiffness was also modelled best by case A until well beyond the maximum loads, when severe deformation had adversely affected the behaviour.

An analysis of the strain gauge readings enabled the positions of the neutral axis to be determined for the beams throughout the tests, and a typical plot is illustrated for beam B1 in Figure 5.1. It is seen that even at working loads the neutral axis at the haunch toe approaches that for the steel beam alone. It then climbs progressively as it moves along the beam to the less stressed region, where it is suggested that the fully composite position would be reached. The figure also shows that as the value of the haunch toe moment increases, so the neutral axis continues to drop throughout the beam towards the non-composite position.

This test evidence serves to underline the commonly held belief that, for design, the concrete strength and stiffness should be neglected in hogging regions. This has been recently re-affirmed by Johnson and Fan {37} who found from some similar tests on cantilevered bridge beams that ‘the elastic behaviour of lightly-reinforced composite cantilevers follows predictions in which the tensile strength of the concrete is neglected, even at loads below service load’.

5.2 MAXIMUM STRENGTHS

The plastic moment strengths for all beams have been calculated for the cases A and B, defined earlier, using the material test results and the measured section profiles. These are presented in Table 5.1. The values have also been compared with the design values to the British Code {11}, ie, with $p_y = 355 \text{ N/mm}^2$.

Beam	M_{\max} (kNm) (test)	$M_{p(A)}$ (kNm) (predicted)	$M_{p(B)}$ (kNm) (predicted)	$\frac{M_{\max}}{M_{p(A)}}$	$\frac{M_{\max}}{M_{p(\text{design})}}$
B1	463	454	480	1.02	1.17
B2	425	446	472	0.95	1.15
B3	464	442	468	1.05	1.14
B4	489	455	481	1.07	1.18

Table 5.1 Sub-Assembly Test - Maximum Haunch Toe Moments Compared with Predicted Plastic Strengths

These values have also been superimposed on the moment/rotation plots in Figures 4.18 to 4.21. The design value has been calculated using a yield strength of 355 N/mm^2 and this results in a plastic moment of resistance of 387 kNm . The test yield stresses, on average, were some 19% higher and this is why all the beams achieved their design values. The contribution of the mesh reinforcement is seen to increase the bare steel section value by some 6%, but when this is neglected, and it usually is because of its lack of ductility {14}, only beam B2 is seen to fail to reach its predicted plastic moment of resistance. This was owing to premature local and lateral distortional buckling brought about by the omission of web stiffening at the haunch toe, and is discussed later - see paragraph 5.4.

5.3 LATERAL DISTORTIONAL BUCKLING

Lateral distortional buckling deformation was evident in all beams to varying degrees, as the lateral profiles of the bottom flanges (Figure 4.23) show, but the mere existence of this does not imply a severe loss of capacity, as the moment/rotation curves show. However, it is instructive to compare the test behaviour with theoretical predictions of buckling load and this is done first with the method developed in Chapter 3.

The 'critical buckling length' (L_{cr}) derived by this method is given by:

$$L_{cr} = 3.74 I_y^{0.25} \left(\frac{D}{t_w} \right)^{0.75} \quad (5.1)$$

which equals 4023mm for the test specimens. This can be compared with the actual buckling lengths that were apparent when the end slope was approximately 3° (52×10^{-3} rads), as shown in Table 5.2.

Beam	Buckling Length (mm)	$\frac{\text{B.Length}}{L_{cr}}$
B1	2300	0.57
B2	2700	0.67
B3	2500	0.62
B4	2200	0.55

Table 5.2 Sub-Assembly Test - Theoretical and Test Values of Lateral Distortional Buckling Length

The test values are much shorter than L_{cr} because the theoretical method was developed for a uniform I-section of equal flanges subject to a uniform moment. In the test the moment was triangular and the presence of the haunch and web stiffening reduced the buckling length because of the extra energy required to induce buckling. The average buckling length was 60% of the critical buckling length and the test value for B2 was the longest. This was owing to the lower torsional

resistance of beam B2, due to the omission of the web stiffening. The predicted buckling moment can, however, take account of the moment shape in the formula for the equivalent slenderness, λ_{LT} , as explained in Chapter 3, such that:

$$\lambda_{LT} = n_t \cdot u \cdot v_t \cdot c \cdot \lambda \quad (5.2)$$

where v_t is given by:

$$v_t = \frac{1}{\left[1 + \frac{1}{40} \left(\frac{\lambda}{x} \right) + \frac{1}{16} \left(\frac{L}{D} \right)^3 \frac{I_w \cdot L}{I_y} \right]^{0.5}} \quad (5.3)$$

Although L_{cr} (4023mm) is actually longer than the test cantilever length (4000mm), it is still appropriate to use L_{cr} in the formula for v_t in order to obtain a maximum value of $(v_t \cdot \lambda)$. Hence, assuming a uniform section, v_t is calculated to be 0.67. The calculation of the slenderness correction factor ' n_t ' for moment shape is given in Appendix G of reference {11}, where the values of the applied moments are compared with their resistances at the quarter points. For plastic design it is practical, although conservative, to assume that the entire haunch is loaded to its full capacity. Hence for beams B1 and B3, $n_t = 0.69$ and for beams B2 and B4, $n_t = 0.743$. The modification factor for haunch length 'c' was calculated to be 1.03 for B1 and B2, and 1.04 for B2 and B4, hence $\lambda_{LT} = 52.9$ for the former and $\lambda_{LT} = 57.5$ for the latter.

Using Table 11 in reference {11} to calculate the bending strength, ie, that which incorporates the Perry-Robertson imperfection allowances, the value of the buckling moment, M_b , can be determined. This was found for beam B1, using the average measured yield stress, to be 339kNm. This is actually lower than M_p , therefore the assumption in the calculation of ' n_t ' that the haunch was fully stressed is incorrect. Thus it can be seen that some iteration is necessary for this calculation and this was carried out and the following values obtained.

Beam	M_{\max} (kNm) (test)	M_b
B1	463	357
B2	425	342
B3	464	354
B4	489	346

Table 5.3 Sub-Assembly Test - Predicted Buckling Moment Values Using Method of Chapter 3

It can be seen that this buckling theory, when applied to the hogging region of a haunched beam, is very conservative both in terms of the buckling length and the buckling moment. It is interesting to calculate a modified buckling moment, referred to here as M_b^* , based on the actual buckling lengths, and these values are presented in Table 5.4.

Beam	Test Buckling Length(m)	n_t	u	v_t	c	λ	λ_{LT}	M_b^*	$\frac{M_{\max}}{M_b^*}$
B1	2300	0.872	0.859	0.920	1.04	74.0	53.0	343	1.35
B2	2700	0.880	0.859	0.876	1.04	86.8	59.8	309	1.38
B3	2500	0.852	0.859	0.900	1.04	80.4	55.0	329	1.41
B4	2200	0.933	0.859	0.931	1.06	70.7	55.9	330	1.48

Table 5.4 Sub-Assembly Test - Modified Values of the Predicted Buckling Moments Using Actual Test Buckling Lengths

The values of M_b^* are actually lower than the previously calculated corresponding values of M_b because, although the quantity $(v_t \cdot \lambda)$ decreases with the reduction of the buckling length (which it does in this case because $L < L_{cr}$), the moment shape is more onerous and the increase in the value of n_t has more than counterbalanced this effect. Hence in this type of situation it can be concluded that M_b is relatively insensitive to the exact buckling length.

Clearly for a haunched beam, from the above comparison, the method as proposed is very conservative because the values of v_t are too high. In the test, three of the beams reached M_p (Table 5.1) and according to the British Code {11}, a value of slenderness (λ_{LT}) of less than or equal to 30 is necessary to attain M_p , and so this

must have been achieved. Therefore, for the method to be accurate, the values of v_t would need to be multiplied by the factors shown in Table 5.5.

Beam	B1	B2	B3	B4
Factor	0.57	0.50	0.55	0.54

Table 5.5 Sub-Assembly Test - Modification Factors for v_t Necessary to Ensure that $\lambda_{LT} = 30$ for the Test Beams

Also, to predict a realistic buckling length, Table 5.2 shows that the value of L_{cr} , as calculated from formula (5.1), would need to be multiplied by a factor of 0.6. However, for non-linear design, it is often not the maximum achievable moment that is of interest but rather a design moment at which a sufficient rotation can be assumed - see later, paragraph 5.4. For this reason, and because of an absence of other test data, it is suggested that, when using this method for the design of haunched beams of the type tested, v_t should be multiplied by 0.75.

However, this would almost certainly lead to a knee brace being required at the haunch toe, but since this test and the subsequent Main Beam Test (- see later Chapter 6) demonstrated the effectiveness of full depth web stiffening, there is some justification, when using these haunch/beam details, for assuming that the haunch toe is restrained and that the unmodified lateral distortional buckling check should be made only from the haunch toe onwards.

It is important to calibrate this method with others, including that published by Roik {36}, which has also been reported in {37}, and which has been adopted in the European Code {15}. The method also calculates the buckling resistant moment for hogging regions where the top flange is continuously restrained and it is discussed in Chapter 3. A simplified form of this, for non-composite symmetric steel sections of at least 'compact' classification, exists whereby the top flange is assumed to be laterally and torsionally rigid. This is given in the form of a slenderness ratio thus:

$$\bar{\lambda}_{LT} = \left[1 + \frac{t_w \cdot h_s}{4b_f \cdot T_f} \right] \left[24 \left\{ \frac{(1-\nu_a^2) \pi p_y}{E \cdot C_4} \right\}^2 \left\{ \frac{h_s}{t_w} \right\}^3 \left\{ \frac{T_f}{b_f} \right\} \right]^{0.25} \quad (5.4)$$

The terms are defined in Chapter 3 and $\bar{\lambda}_{LT}$ is used to determine a value of χ_{LT} which takes account of imperfections and residual stresses.

χ_{LT} is defined for both non-composite and composite beams in EC3 {12}. It is used in the calculation of the buckling moment which is defined in this thesis as M_{d1} to avoid confusion. The buckling moment is then given by:

$$M_{d1} = \chi_{LT} \cdot M_p \quad (5.5)$$

The method does not incorporate a numerical integration to allow for discontinuous moment diagrams, so in the following comparison a linear bending moment has been assumed with M_p at one end and zero at the other. To enable a direct comparison with the previous method, the values of M_b (see Table 5.3) have been recalculated using the same assumption, ie, that 'n_t' = 0.77. These are then referred to as $M_{b(0.77)}$ and are based on an effective length of 4023mm, as before. The values of M_{d1} and $M_{b(0.77)}$ are given later in Table 5.6.

A further comparison can be made with the method of Weston, Nethercot and Crisfield {6}, also described in Chapter 3, which was proposed as a result of a parametric computer study into the hogging region buckling of composite bridge girders. It was also presented in the form of a slenderness parameter ' β ' to be used in conjunction with the British code for the design of bridges {33} such that:

$$\beta = 1.28 \left[\left[\frac{L}{r_y} \right]^{1/2} \cdot \left[\frac{d}{t_w} \right]^{1/8} \right] - 29 \quad (5.6)$$

Again, the terms are defined in Chapter 3 and the equation was used to find a 'basic limiting stress' σ_{li} such that the bending resistance, defined here as M_{d2} , is given by:

$$M_{d2} = Z_p \cdot \sigma_{li} / \gamma_m \cdot \gamma_{f3} \quad (5.7)$$

where γ_m and γ_{f3} are safety factors.

The method assumes a fixed-ended beam bending moment over the full span 'L', so, for a realistic comparison, the test loaded-cantilever-length needs to be multiplied by 4 to determine 'L' in equation (5.6). The predicted bending resistance, M_{d2} , for each of the beams in the Sub-Assembly Test is given in Table 5.6, alongside the other predictions.

Beam	M_{\max} (test)	M_b	$M_{b(0.77)}$	M_{d1}	M_{d2}
B1	463	363	314	352	408
B2	425	348	310	355	411
B3	464	360	310	356	406
B4	489	348	315	358	415

Table 5.6 Sub-Assembly Test - Comparison of Various Theoretical Buckling Moment Resistances in kNm

The model factors for the above are presented in Table 5.7.

Beam	$\frac{M_{\max}}{M_b}$	$\frac{M_{\max}}{M_{b(0.77)}}$	$\frac{M_{\max}}{M_{d1}}$	$\frac{M_{\max}}{M_{d2}}$
B1	1.3	1.47	1.32	1.13
B2	1.24	1.37	1.20	1.03
B3	1.31	1.50	1.30	1.14
B4	1.41	1.55	1.37	1.18

Table 5.7 Sub-Assembly Test - Model Factors for the Various Theoretical Buckling Moment Resistances

It can be seen that the method of Weston et al gives the closest predictions but since the additional torsional stiffness provided by the cutting is not included in any of the analyses, and since the model factor for beam B2 is so close to 1.0 for this method, it has to be questioned whether it is actually conservative for the rolled sections typically used in buildings.

The method proposed in this thesis, without the modifications suggested earlier, is the most conservative of the three and a comparison of $M_{b(0.77)}$ and M_{d1}

shows the Eurocode method to predict larger buckling resistances than it does by the order of 14%. This is logical because the latter method is a more sophisticated method incorporating more energy resisting terms than the proposed method. The use of the 'correct' bending moment diagram (M_b) rather than a linear diagram ($M_{b(0.77)}$) is shown to increase the predictions by the order of 14% and if a similar improvement were assumed for M_{d1} , the average value for beams B1, B3 and B4 would become 1.17, compared with a similar value for the proposed method of 1.34.

5.4 MOMENT/ROTATION CHARACTERISTICS AND HAUNCH TOE STIFFENING

When plastic behaviour is sought, it is necessary to obtain sufficient rotation at the hinge positions to facilitate plastic collapse. The degree of rotation and the percentage of redistribution of moments required are dependent on several factors including the loading type and both the elastic and plastic section properties. In the Sub-Assembly Test, all the beams were close to achieving, or actually achieved, M_p , as shown earlier in Table 5.1. They also reached their design values according to the British Code {11}.

The non-linear behaviour of the beams is compared in Figure 5.2, which shows the moment/rotation characteristics with the 'elastic' component removed. The behaviour of beam B2 in the figure has been plotted between points 1 & 2, 5 & 7 and 8 & 9, but has been extrapolated between points 2 & 5, 3 & 4 and 6 & 10 to show the more realistic effect of providing a knee brace. The elastic component is defined as the rotational movement determined from the unloading stiffness at the end of the Working Load Test, and this amounted to between 0.8° and 1° at the maximum moments. It corresponds to the performance at about 50% of the ultimate load when cracking is not too severe and when yield in the beam has yet to occur.

It is clear that, since the same section was used for each beam, the difference between the responses was mainly due to the different haunch and haunch stiffening details. The negative stiffness experienced in all beams during the latter test stages was due to a combination of local and lateral distortional buckling. Local

buckling generally appeared first and this would imply that at its onset, the rotational stiffness about the vertical axis at the point of buckling was reduced and that lateral distortional buckling was then precipitated. The evidence from the tests, however, is not entirely conclusive on this point. From observations during the test and a study of the growth in the lateral displacements (Figure 4.22), some form of local buckling was present in beams B1, B2 and B4 before a rapid increase in lateral deflections occurred, but for beam B3, despite the presence of local buckling, lateral deflections did not grow at all. This was also observed in the subsequent Main Beam Test (see Chapter 6). The proportions of the cross-section were such that the beams were classified as Class 1 to the British Code {11} (Class 2 using measured properties) and local buckling did not occur, except in Beam B2, until virtually the full plastic state. Therefore, since the cross-section was at this state, lateral distortional buckling may have been precipitated by that alone, whether or not local buckling was present, and this is a philosophy put forward in {37}.

The author would suggest that the important consideration is the degree to which the y-y stiffness of the web and bottom flange has deteriorated as a result of either yielding, which, of course, is followed by strain hardening, or local buckling, and, to what extent this 'end condition' influences the likelihood of lateral distortional buckling anyway. In other words, a torsionally stiff beam with a rapidly declining moment will not be influenced as much by a deteriorating end condition as a relatively torsionally flexible beam, subject to a constant moment. Therefore, it is suggested that lateral distortional buckling does not necessarily follow local buckling, and indeed may occur first, but it depends on the conditions. However, all the research and tests, so far, indicate that the two may be treated separately, ie, that the section classification can be used to limit local buckling and that the lateral distortional buckling may be limited by the methods discussed.

The poor performance of beam B2, shown in Figure 5.2, was due to the high concentrated stress in the web and flange at the haunch toe, caused by the lack of web stiffening. The early lateral movement of the bottom flange caused a large minor axis bending effect on it which led to a premature local buckle on the compression side. This further weakened the beam, which resulted in M_p not being reached. The subsequent addition of the knee brace restored the performance but it

is likely that the initial deformation of the beam restricted its true potential. It should be noted on the evidence of the test, that when a knee brace is provided, a horizontal design force of 3% should be used and the brace bolts should not be less than M16's.

Figure 5.2 also clearly confirms the superior performance of beams B3 and B4, which is undoubtedly due to the torsional restraint and the restriction of the web buckling, provided by the full-depth stiffeners. The relatively rapid drop in strength of beams B1 (and B2) suggests that half-depth stiffeners are inadequate alone and this is further confirmed when the strength of the beams is compared at the same degree of rotation that the subsequent Main Beam Test reached its maximum load, namely 3° - see Table 5.8 below.

Beam	B1	B2 ⁽¹⁾	B3	B4
M/M _p	0.85	0.87	0.96	0.95
M/M _{p(design)} ⁽²⁾	1.0	1.0	1.1	1.1

- (1) values for B2 have been extrapolated
 (2) M_{p(design)} is in accordance with Reference {14}.

Table 5.8 Sub-Assembly Test - Comparison of Haunch Toe Beam Strengths at a Rotation of 3°

The table confirms the marginal loss of strength in beams B3 and B4 at this rotation but does show that the design M_p to the British Code is still achieved.

The degree of rotation necessary for plastic collapse in composite beams has been considered by Kemp {40} and he has introduced the concept of available and required rotation, ie, r_a and r_r, such that:

$$r_a / \gamma_{mr} \geq r_r \quad \text{where } \gamma_{mr} \text{ is a partial safety factor.}$$

The available rotation capacity is then defined as:

$$r_a = (\theta_p + \theta_c) / \theta_e$$

where, at the particular design moment to be achieved,

- θ_e = the rotation assuming uncracked section properties
- θ_c = the rotation assuming cracked section properties, minus θ_e
- θ_p = the total inelastic rotation, minus $(\theta_c + \theta_e)$

If the design moment to be achieved is assumed to be the M_p of the steel beam alone, (calculated from measured properties) then the following results for the test can be obtained, as shown below in Table 5.9, but excluding beam B2 which never attained M_p .

Beam	θ_e°	θ_c / θ_e	θ_p / θ_e	r_a
B1	0.38	1.95	2.79	4.74
B3	0.35	2.03	4.91	6.94
B4	0.36	1.94	5.28	7.22

Table 5.9 Sub-Assembly Test - Available Haunch Toe Rotations

Kemp suggested that the contribution to the value of r_a due to concrete cracking, ie, θ_c/θ_e , would be between 0.7 to 1.5, and the test values in reference {37} confirmed this. However, Table 5.9 shows the values for the author's test are about 2. The value of r_a depends on the precise design moment chosen but the superior performance of beams B3 and B4 is reflected in their higher values. Kemp proposed that to facilitate the 40% redistribution of moments permitted for Class 1 sections in the Codes, {14}, {15}, a required rotation of 3 should be sought, but to allow for uncertainties, γ_{mr} should be put equal to 2. Therefore, a value of r_r equal to 6 would be necessary and the values of r_a for beams B3 and B4, ie, with the full depth stiffeners, both meet this criterion, whereas that of beam B1, with the half-depth stiffeners, does not.

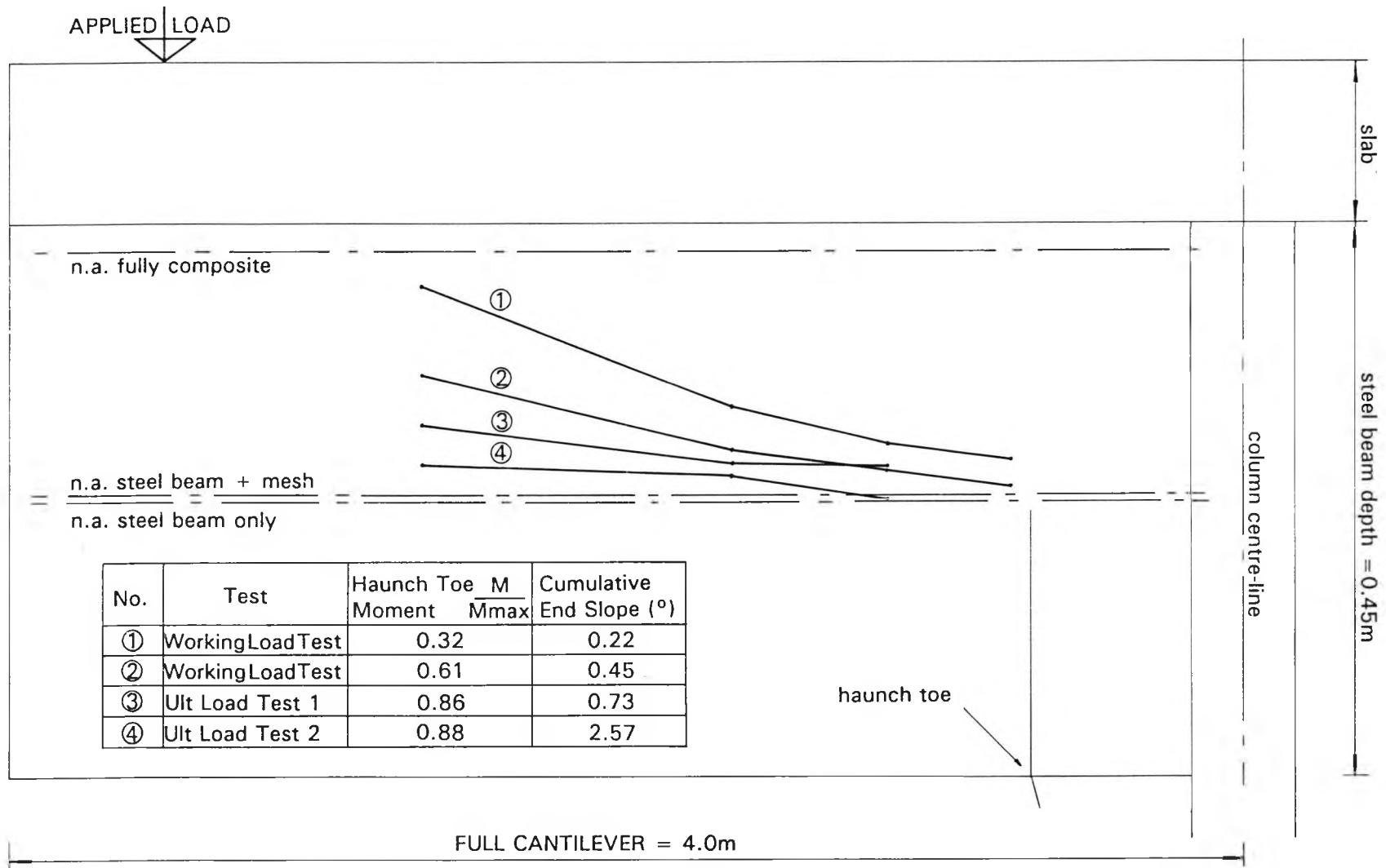


Figure 5.1 Sub-Assembly Test - Progressive Lowering of the Neutral Axis on Beam B1 with Beam Deformation

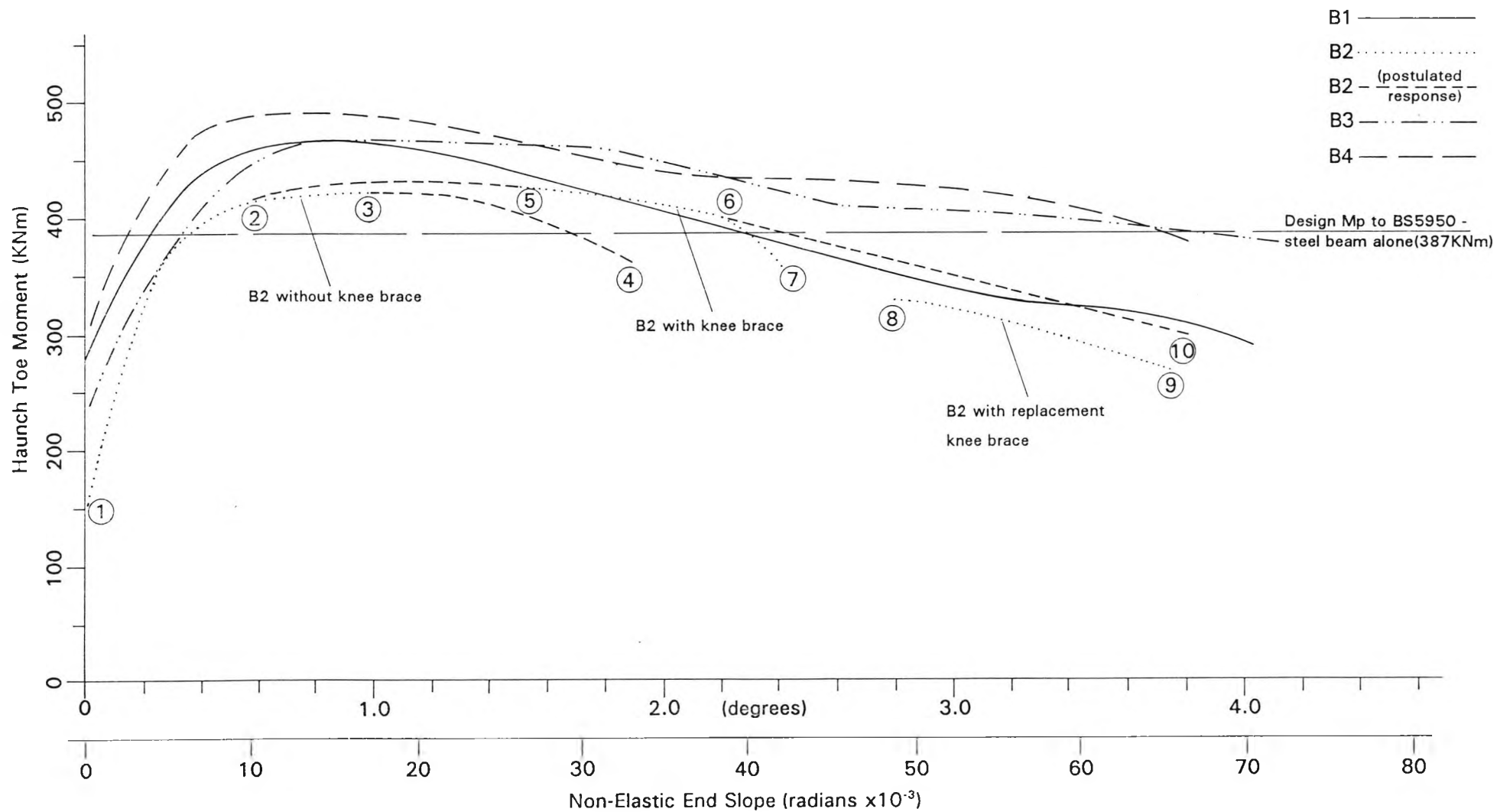


Figure 5.2 Sub-Assembly Test - Comparison of Non-Linear Moment/Rotation Behaviour

CHAPTER 6

EXPERIMENTAL WORK: THE MAIN BEAM TEST

6.1 INTRODUCTION

The purpose of the main beam test was to model a haunched composite beam within a braced single span multi-storey frame. Of particular interest was the likely redistribution of moments around the frame during the formation of plastic hinges in the beam. The load at collapse could then be compared with that obtained from simple plastic theory and hence the proposed design method could be calibrated.

6.2 DESIGN CONSIDERATIONS

6.2.1 The General Test Arrangement

To meet these objectives a test was devised consisting of two columns, each of one storey height in length, with a haunched beam spanning between, and connected at the mid-height of the columns. This sub-frame, shown in Figure 6.1(a), could then model the behaviour of the typical braced multi-storey frame shown in Figure 6.1(b). The mid-heights of the columns were assumed to be the points of contraflexure.

The available laboratory space determined the span of the structure which was set at 13.5m. The test frame was then based on a seven storey structure of this span, with frames at 6.0m centres and with secondary beams at 3.37m - see Figure 6.1(c). The storey height was chosen to be 4.7m and, although slightly higher than normal, this enabled smaller reaction jacking forces to be applied. It was not essential to model a precise storey height because the distribution of moments in a frame is dependent on the relative strength and stiffness of the columns to the beams, and there will be many such combinations occurring in practice. Even within the same multi-storey building, the column size in a given bay will not be subject to the

same axial load as the column rises, so a change in size, and hence stiffness, is likely in the upper storeys.

Owing to the constraints of space, budget and time, it was not possible to construct the ideal arrangement of two parallel frames with a floor spanning between. A compromise arrangement of one frame with cantilevered beams was devised which was stabilised from transverse side-sway by the provision of stub columns positioned under the end pairs of cantilevered beams, and assisted by end bracing. A narrow width of floor was then supported on the short cantilever beams - see Figure 6.2. The torsional restraint offered to the main beam in a real structure - by the complete floor to the adjacent frames - could not be modelled by this arrangement, but this was counterbalanced by the effect of the loading system and also by the presence of the stub columns, which tended to stabilize the structure. The end bracing consisted of scaffolding, and this was carefully installed so as not to increase the stiffness of the structure other than in the plane intended.

6.2.2 Design of the Frame

Design calculations were carried out, as they would have been in practice, to determine the frame sizes, and are presented as the design example in Appendix 9A. They have been carried out in accordance with the relevant British Codes of Practice, references {11} and {24}, but follow a method outlined in reference {3}, devised by this author and Dr R M Lawson. A plastic collapse mechanism was assumed in the main beam at ultimate loads, while the columns were designed to remain elastic under this loading. The beam was designed to act compositely in the sagging region, but non-compositely in the hogging regions, and no special reinforcement was provided over the haunches.

Serviceability calculations included checks on deflections and mid-span stresses, but no checks on stress at the potential hinge positions at the haunches were carried out as it is not required by the codes. The elastic global moments were calculated in the beam by assuming a constant second moment of area, based on the mid-span composite cross-section. The beam end moments were then reduced by 10% to allow for cracking in the hogging regions. The span moments were also

correspondingly increased for the design of the beam, but the column design moments were not reduced.

The frame was also checked at the ultimate state under construction loading but a rigorous analysis of moments during all the phases of construction was not done because it was not considered necessary. A conservative method was adopted, whereby beams inducing the most onerous conditions in a given column length were assumed to be fully loaded at the plastic collapse state, whereas beams relieving those moments were treated as loaded with dead load only, and were also assumed to have non-composite properties. The axial loads were not calculated but a certain percentage of the column capacity, based on detailed calculations of a similar frame, was assumed to resist these.

It is to be noted that the load reduction permitted in the loading code {24} according to the number of floors loaded should not apply to the calculation of moments in a column, but only the axial loads. This is because the column moments in a fixed frame clearly do not depend, in the same way as axial loads, on the total number of floors loaded.

The selected beam and column sections which satisfied the design criteria were a 406 x 178 UB x 74kg/m at grade 50 for the beam and a 305 x 305 UC x 158kg/m at grade 50 for the column. The span/total floor depth ratio was 25, which lay within the range 24 to 28, anticipated in reference {9} to offer an economic solution, satisfying both ultimate and serviceability conditions. This relatively shallow beam was the heaviest in its serial range and was chosen because of its high strength to depth ratio, and its potential for sustained rotation at plastic hinges without premature element buckling. With a more rigorous design, it might have been possible to have chosen a lighter section for the column, but this would not necessarily have been more economic because high stressing of the web and flange around the connection might have necessitated increased stiffening.

Analysis of the selected sub-frame (Chapter 8) showed that some 20% of the elastic end moments would be redistributed to the mid-span at collapse, and the test was intended to provide an opportunity to verify such a theory.

6.2.3 Haunch Design

A haunch length of 615mm was chosen as being appropriate for the main beam section, ie, 4.6% of the span. This enabled a cutting of the same section to be used, with a cutting angle of approximately 45° and a haunch depth equal to twice the beam depth. The haunches were designed to remain elastic at the column face under a moment calculated by assuming a haunch toe moment of $1.1M_p$ (beam). This factor was suggested in Chapter 2 and was employed to limit plastification extending into the haunch, to prevent lateral buckling of the haunch and to prevent the undesirable failure of the connection area, prior to the collapse of the beam. The depth of the haunch was determined by the need to provide a sufficient lever arm for the bolts, and so produce the required connection strength.

6.2.4 Main Beam Stiffening and Lateral Stability

Full depth web stiffeners, of a thickness similar to the beam flanges (10mm), were provided at the haunch toes to prevent premature web buckling at these hinge positions. They also served to assist in the torsional rigidity of the haunch by providing a direct load path from the top flange through to the cutting flange. As in the Sub-Assembly Test, they were supplied in grade 43 steel. Knee braces were also initially designed for the hinge positions in accordance with the Code {11}, but, because of the satisfactory performance of the beams in the Sub-Assembly Test with full depth web stiffeners, it was decided to omit the braces.

The lateral stability was checked in both the construction and in-service conditions. For the construction condition, no restraint was assumed to be offered by the decking, because it spanned in the direction of the main beam, and was weak in the transverse direction. Full lateral and torsional restraint was assumed to the top flange in the in-service condition, ie, provided by the shear connection to the slab, and checks were carried out using the method developed in Chapter 3. No additional bracing, however, was found to be necessary for either condition.

6.2.5 Haunch End Connections

As before, the end connections were designed by assuming $1.1M_p$ at the haunch toe hinge. An arrangement consisting of 8 tension bolts and 4 shear bolts was devised, using M24's, grade 8.8. The design method for the connection and end plate was similar to that for the Sub-Assembly Test, and based on reference {9}. The design capacity of the connections was calculated to be 814kNm. A 25mm thick end plate in grade 50 steel would have sufficed, but a 30mm thick plate was supplied in grade 43 steel. Full strength butt welds were again provided between the cutting flange and the end plate.

6.2.6 Column Stiffening

Tension stiffeners were provided adjacent to the main beam flange to ensure an efficient yield line failure pattern in the column flange. They were not required to strengthen the column web, nor were compression stiffeners required for bearing or buckling of the web, but the latter were included for the following reasons:

- (i) to provide continuity for the load path through the cutting flange, so as to enhance the torsional restraint offered to the haunch toe hinge position and
- (ii) to ensure full bearing support to the cutting flange so as to maximise the lever arm to the tension bolts, and thus improve the connection efficiency.

6.2.7 Floor Slab

With a primary and secondary beam arrangement it was appropriate to span the decking between the secondary beams, and hence the decking ran parallel to the main beam. The width of the floor slab was determined using the latest guidance on effective widths for composite slabs which existed at the time, ie, reference {11} - in its draft state. This recommended an effective width in the sagging region equal to one quarter of the length of the sagging region. For a 'continuous' span of 13.5m, this was calculated to be $0.7 \times 13.5/4 = 2.36\text{m}$, which was rounded up to 2.4m. A slab depth of 130mm with re-entrant type decking was again used, ie, as in the Sub-

Assembly Test. A decking thickness of 1.2mm resulted from the calculations, although a 0.9mm thick deck was subsequently delivered and fixed. This would have had a marginal effect on the dead load deflection between the secondary beams but not on the overall deflections. To achieve a typical 1½ hours fire resistance for this type of structure, an A193 reinforcing mesh was necessary in the slab. As before, a lightweight 30N/mm² concrete mix was chosen, which reflected current practise. For the test a 25N/mm² mix was subsequently ordered because of the tendency for ready mixed concrete to be well over strength.

6.2.8 Secondary Beams

The secondary beams were designed as if they were simply supported over a 6.0m span, although in the test they were actually short cantilevers positioned each side of the main beam. A 254 x 146 UB x 31kg/m, grade 50, section was found to be most suitable according to the design criteria. The end connections were detailed for the actual cantilever moments.

6.2.9 Shear Connector Layout and Longitudinal Shear Reinforcement

The same type of shear connectors were used in this test as for the Sub-Assembly Test, ie, 19mm diameter x 100mm long headed stud connectors. The connection layout was based on the plastic moment diagram at the collapse condition of the beam. Composite behaviour was only assumed in the sagging region, but a nominal spacing (390mm) of connectors was provided in the hogging region in accordance with code requirements. Four connectors were also provided for each cantilever secondary beam and end beam, at 300mm spacing.

A check was made on the ability of the slab to transfer the longitudinal shear from the shear connectors out to the full width of the slab and it was found to be inadequate. Transverse reinforcement was then designed to be placed in the sagging region, ie, T16's @ 390 ctrs. The full end anchorage was subsequently not provided, but the fact that the shear transfer contribution of the decking was neglected in the analysis more than counterbalanced this.

6.2.10 Reactant Frames

These were positioned at each end of the structure to resist the horizontal jacking force from the main column heads (Figure 6.1(a)). The general arrangement of these frames is shown in Figure 6.3. Each frame consisted of a horizontal 'I' section beam laid on its side and loaded in the centre by the column jack. This cross-head beam was supported at each end by a triangular frame bolted to the strong floor. Each reactant frame was designed to resist twice the anticipated collapse reaction from the column heads, ie, 400kN. Members and connections were detailed to facilitate easy fabrication, erection and demolition, with all bolts loaded principally in shear.

6.2.11 Column Base Supports

Each main column was designed to rest on a 100mm diameter steel bar to provide a 'roller' support condition, as shown in Figure 6.4. Under the roller were two spacer plates sandwiching a load cell, and beneath this lay the base plate to the 'channel restraint frame'. The Channel Restraint Frame was simply a large heavy base-plate, stiffened by channel sections to receive and withstand the jacking force applied to the foot of the column. This frame was bolted to the strong floor by two 50mm diameter bolts. The design also provided for additional channels to be bolted to it so as to enable the column to be rigidly held in position during the casting of the floor, etc.

6.3 CONSTRUCTION

Construction commenced with the fabrication of the elements of the reactant frames, which were then erected and bolted to the strong floor. The column base channel restraint frames were also fabricated in house and bolted to the strong floor. This was followed by the attachment of the jacks to the reactant frame cross-head beams, which would eventually apply the reactions to the column heads.

The steel elements comprising the test specimen were all fabricated externally, and erection commenced with the main columns. These were mounted on temporary packs at the correct height and the end beams and stub columns were added. This end frame was braced together by scaffolding, which was used because it was easy to erect and dismantle. The scaffolding was carefully fitted so as not to introduce undesired stiffness in the longitudinal direction. With these two end frames erected and temporarily restrained, the main beam was then laid on the floor. At this point most of the electrical resistance strain gauges were fixed to it, followed by the bolting on of the secondary beams. This beam structure was then raised and bolted to the columns, after which the remaining gauges were attached to the structure.

The test frame was then shrouded by a scaffold frame which served three purposes. Firstly, temporary supports were provided to prop up the ends of the intermediate secondary beams and these were attached to the scaffold frame. These props prevented the main beam from being subject to any out-of-balance torsional effects when constructing the floor. Secondly, it provided a safety 'curtain' for operatives working on the structure, and thirdly, when not being used for temporary support, it was used during the tests as an independent framework for the attachment of the displacement gauges.

The next operation was to construct the floor, which was done exactly as for the Sub-Assembly Test, except that this time the decking ran parallel to the main beam and transverse reinforcement had to be fixed. The decking layout was such that there was a seam joint over the centre-line of the main beam, so a staggered pattern of shear connectors was adopted. Sockets were again provided to allow the loading frame pull-down rods to pass through the floor.

It was considered important to provide the 'correct' end conditions during curing of the floor concrete so as to induce the appropriate moment distribution at the serviceability stages. This meant that the columns had to be on their roller supports, with the appropriate end reactions provided by the reactant jacks, and with no other temporary support in the span. During casting, however, the structure had also to remain stable.

This was achieved by first lifting one of the end frames so as to mount the column on its roller, and by packing up the stub columns to suit. The main column load cell was also inserted at this stage. The column base retaining channels (Figure 6.4), were then firmly fixed against the column faces, before the other end frame was similarly lifted and positioned. At this point the dead weight condition was established by releasing the channels and pumping the reactant jacks up to a value of 4.3kN each. This represented the calculated 'pin-ended' condition and measurements of strain and central deflection were taken. The plumb bobs to the main columns (see later - para 6.5.5), were also set up at this stage and the datums established on the horizontal graded staffs. No attempt was made to jack the columns vertically for fear of overjacking, as it was considered better to have the appropriate reactions, and hence moments and stresses, rather than physically vertical columns. The restraining channels were then again firmly fixed and the temporary span supports connected, so that the floor was ready for casting - see Figures 6.5, 6.6 and 6.7.

The concreting operation procedure was the same as for the Sub-Assembly Test, whereby the concrete was discharged from a skip manoeuvred by the overhead crane. For practical reasons the spreading and tamping had to be done by standing on the floor itself, which is normal commercial practice - see Figure 6.8. After casting, the temporary supports and restraining channels were released, thus allowing the frame to deflect. The calculated column reactions for this state were 20kN and it was found, as might be expected, that the frame had virtually already adopted these values of its own volition. A check on the plumb bob position also confirmed this to be the appropriate reaction and so strain gauge and deflection readings were taken. The increase in central deflection due to the weight of the concrete was found to be 15mm (span/900). After 7 days curing, the temporary supports and restraining channels were repositioned to facilitate the installation of the remaining instrumentation and the loading systems. The final as-built frame dimensions are given in Figure 6.9.

6.4 **LOADING ASSEMBLY**

The schematic arrangement of the loading systems is shown in Figure 6.10 and three independent systems were employed, one for the span and one each for the main columns. The span system consisted of three loading frames positioned at the quarter span points, or rather, as near to these as could be achieved by using the strong floor fixing points. The outer loading frames were similar to those used in the Sub-Assembly Test but the central frame had to be designed differently, to avoid interference with the secondary beams - see Figure 6.11. Each loading frame incorporated a 50 tonne jack with a stroke of 330mm, and all three span jacks were connected to the same hydraulic system operated by two hand pumps. As before, when the jacks were pressured the structure was pulled to the strong floor, but the design of the loading frames again specifically enabled the loading travel to be locked off at anytime to allow for resetting, etc.

Each column system consisted of a jack to the head and, on the opposite face, a jack to the foot, both hydraulically linked to a single hand pump. Equal and opposite reactant loads could then be applied, as shown in the schematic arrangement. The column jacks were rated at 30 tonnes with a stroke of 50mm.

The incremental loading procedure involved pressuring the span jacks first to induce a pre-determined deflection at the centre of the span. The column jacks were then loaded to return the columns to their datums.

6.5 **INSTRUMENTATION**

The instrumentation was comprehensive and included the use of electrical resistance strain gauges, vibrating wire strain gauges, potentiometric displacement transducers (LPDT's), load cells, a dumpy level, plumb bobs and graded staffs.

6.5.1 **The Equipment Specification**

The electrical resistance gauges were again 6mm long Techni-measure gauges, type FLA-6-11, and were fed into the Intercole Spectra data logging system,

as used in the Sub-Assembly Test. Three SAKAE long-travel transducers, models 30HLP200 and 50LP300 with 200mm and 300mm travel respectively, were used and read to the nearest mm. Ten SAKAE medium-travel transducers were employed, of model S30HLP100 with 100mm travel, which read to an accuracy of ± 0.5 mm. A further ten SAKAE transducers, model S8FLP10A, which read to 0.01mm, were used where accuracy and sensitivity was required, but their travel was limited to about 12mm. The above transducers were also fed into the logging system, but in some instances it was necessary to have a visual display directly in mm, and, for this, direct digital readout transducers made by MITUTOYO, model ID-1050E, were used. These had 50mm travel and were sensitive to the nearest 0.01mm.

The vibrating wire strain gauges were of a type developed by the Transport and Road Research Laboratory for the measurement of strains on the surfaces of metal or concrete structural members. They were marketed by Gage Technique and the model used was T/S/R with a gauge length of 139mm, and with an overall range capability of 3000 microstrain. The gauge outputs were fed into a Gage Technique multi-channel data logger, model GT 1179. The load cells were Techni-Measure model CLF-100 and rated at 100 tonnes. They also had their own digital readout monitors, reading to the nearest 0.1 tonne.

6.5.2 Measurement of Strains in the Steel Members

Fifty-three electrical resistance strain gauges were positioned around the specimen and numbered 1-37 and 50-69, as shown in Figure 6.12. Gauges 9 and 10, 32 and 33 were reserved for knee braces, which were subsequently not fitted. Most of the gauges were positioned to confirm the bending moments but Nos 13, 14, 36 and 37 were placed in the web at the mid-height of the stub columns to confirm the axial loads. Most of the gauges were fitted prior to the erection of the structure, but for practical reasons it was not possible to erect the test frame with gauges connected, and even if it had been, it is to be doubted whether reliable information could have been gained about the bare frame steel stresses. It is for these reasons that the datum for these strain gauges was the erected state just prior to casting the slab.

6.5.3 Measurement of Displacements

The large displacements in the span were measured using two systems. Firstly, the long-travel transducers, marked M1 - M3, were positioned close to the three loading points, as shown in Figure 6.13. These were backed up by medium-travel digital readout transducers, marked M4 - M8, which had greater sensitivity. The latter were also used to give visual confirmation of the steadiness of the settlement at each load increment. Gauges marked M6 and M7 were deployed at the ends of the central secondary beams to detect any severe rotation of the slab. During the latter stages of the tests it was envisaged that all these gauges would need to be removed to prevent them being damaged, so a second system of measurement was used. This involved clamping three graded staffs to the main beam, near the loading points, and taking readings using a dumpy level. The readings were then compared with an initial datum to calculate the deflections.

Four medium-travel transducers, marked 81, 82, 91 and 92, shown in the figure, were positioned just beyond the haunches in order to determine the slope at these points. The rotation of the haunch connections and the columns was calculated from the readings of eight small-travel transducers, backed up by four of medium-travel, marked 83, 84, 86 - 89, 93, 94, 96 - 99. Also, two small-travel transducers, marked 85 and 95, were used to detect any slip between the main beam and the columns.

6.5.4 Measurement of Strains in the Concrete Slab

Initially, 20 vibrating wire strain gauges, marked 1 - 20, were fixed to the slab using plastic padding in a layout on half of the slab - see Figures 6.14 and 6.15. The gauges were positioned in four rows of five gauges at the estimated point of contraflexure, the mid-span, near the column and at an intermediate point. They were individually adjusted to give an initial reading of 13000 Hz and were reset between tests.

After carrying out Working Load Test 2, it was clear that some gauges were being unduly influenced by their proximity to the loading frames, so gauges 16, 17, 19 and 20, were removed and a new row labelled 21-25 established.

The strain, ϵ , from two successive readings, T_1 and T_2 , was determined from the relationship:

$$\epsilon = \left[\frac{10^{11}}{T_1^2} - \frac{10^{11}}{T_2^2} \right] \times 3.025$$

where ' ϵ ' has units of micro-strain

6.5.5 Measurement of Column Verticality

To ensure that the top and bottom of each column had been jacked back to its initial degree of verticality, a simple method was employed which had successfully been used on other tests {38}. This involved hanging a plumb bob from a fixed offset at the head of a column, such that the plumb line crossed a graded staff which was fixed to the base of the column. An initial datum line was marked on the staff so that at every load increment the column could be jacked so that the line returned to the datum mark, as shown in Figures 6.13 and 6.16. This was done for each main column and the method was advantageous because it was independent of any longitudinal movement of the test frame along the laboratory floor. It also did not rely on the column being initially vertical but allowed for construction tolerances.

6.5.6 Measurement of Vertical Loads

The vertical reactions under the main columns were measured using the 100 tonne load cells, but the vertical loads in the stub columns were calculated using strain gauges, as outlined in paragraph 6.5.2. An 'ideal' arrangement would have been to support all the columns on load cells, but with the main columns on rollers, it was considered too dangerous because of the potential for longitudinal movement.

6.5.7 Measurement of the Spread of Plasticity

Following the attempt at this made on the Sub-Assembly Test, a mixture of lime and water was tried. It was applied to the haunches and the mid-span areas, but proved to be only partially successful. The 'paint' lost its adhesion at points of high compression and on the compressive side of local buckles, causing it to flake off, but it did not give any visible indication in areas of excessive tensile strain.

6.6 MATERIAL PROPERTIES

Material property tests were carried out on the main beam, concrete, mesh, shear reinforcement and decking. Coupons were machined from sections cut out from the low stressed areas of the beam, at the points of contraflexure. The results of the coupon tests are given in Table 6.1.

Location	Test Number	Yield Stress (N/mm ²)		Ultimate Tensile Stress (N/mm ²)		Elongation (%)	
			Average		Average		Average
Flange	1	368.3	366.9	507.9	506.4	33.3	31.9
	2	365.5		504.8		30.5	
Web	1	404.6	401.6	534.1	533.8	33.8	31.8
	2	398.5		533.5		29.8	

Table 6.1 Main Beam Test - Main Steel Beam Material Properties

The crushing and tensile strengths of the concrete slab were measured using 100mm cubes and 150mm x 305mm long cylinders respectively. The samples were cured by immersion in water and the average result of 3 samples each is presented in Table 6.2.

Age (days)	fcu (N/mm ²)	Tensile Strength (N/mm ²)
7	22.5	
28	34.6	2.5
64	42.5	2.9
113	40.8	
127	47.8	

Table 6.2 Main Beam Test - Concrete Slab Material Properties

Two samples of the mesh reinforcement were tested and the average results are presented in Table 6.3.

Cross-sectional area (mm ²)	Yield Stress (N/mm ²)	Ultimate Tensile Stress (N/mm ²)	Elongation (%)
36.6	425	620	17

Table 6.3 Main Beam Test - Mesh Reinforcement Properties (Type A193)

Two samples of the longitudinal shear reinforcement were also tested and the average results are shown in Table 6.4.

Cross-sectional area (mm ²)	Yield Stress (N/mm ²)	Ultimate Tensile Stress (N/mm ²)	Elongation (%)
196	542	630	23.7

Table 6.4 Main Beam Test - Shear Reinforcement Properties (T16's)

Three samples of the galvanised steel decking were tested and the average results are presented in Table 6.5.

Thickness (mm)	Yield Stress (N/mm ²)	Ultimate Tensile Stress (N/mm ²)	Elongation % (over $4.8 \sqrt{\text{area}}$)
0.865	245	370	38.1

Table 6.5 Main Beam Test - Decking Material Properties

6.7 THE MAIN BEAM TEST RESULTS

Five main loading cases were carried out and are referred to consecutively as Bedding-In, Working Load 1, Working Load 2, Ultimate Load 1 and Ultimate Load 2. A dynamic test was also carried out prior to these.

6.7.1 The Dynamic Test

This test was carried out 57 days after casting the floor slab to determine the frame natural frequency and damping characteristics. This involved exciting the frame by a single impulse at the centre of the span and recording the response. This was done by the author standing up on tip-toe and dropping down onto his heel, ie, a 'heel drop' test. The response was then measured by a displacement transducer located in the centre of the span and connected to an ultra-violet oscillograph (SE model 6012). This plotted the displacement against time and a typical dynamic trace is shown in Figure 6.17. The magnitude of the impulse and hence the maximum amplitude is not important in the calculation of the natural frequency, which is shown in Appendix 6A to be 6.3 Hz, with a damping coefficient equal to 0.023.

6.7.2 Bedding-In Test

The Bedding-In Test was carried out 62 days after casting, with initial horizontal column reactions of 24.1 kN. This represented a slight increase on the value after casting the slab and was due to the weight of the span jacks and loading frames. During the test, the span jacks were loaded in increments which registered 3mm on the mid-span long-travel transducer. At each increment the columns were jacked back to the original datum and this process necessarily caused a slight recovery in the central deflection, which was not further adjusted. Increments, therefore, were not precise, but that was not important.

As this test was conducted to bed-in the elements, only two increments were applied. Unloading was gradual but continuous and the horizontal column reactions reduced accordingly, without the necessity to open the pressure release

valves. The structure returned virtually to its initial state but with a mid-span deflection set of 0.37mm.

An analysis of the results, however, showed that the horizontal column reactions were much higher than the theory suggested. The ratio of the average reaction to the average span jack load was predicted from the computer analysis (Chapter 8) to be 0.82 but the results suggested a value as high as 1.2, some 1.5 times greater - see Figure 6.18. Although subsequent tests proved this to be an initial frictional effect, it was cautiously decided at the time to change the jacking procedure for the following test.

6.7.3 Working Load Test 1

This was carried out 64 days after casting and, for the reason described above, the column jack valves were closed and the jacks were not pumped whilst loading the test. Thus the columns were allowed to drift off the datum and induce whatever reaction they desired against the sealed jack pressure. The test was therefore carried out to see what order of magnitude the reactions would take in comparison with the theory at higher loading, but within the elastic range.

The test frame was loaded in 7 central deflection increments of 5mm to a maximum recorded value of 34.2mm. The maximum span load per jack (3 jacks) was 92.9 kN, ie, 32% of the final ultimate load. The average ratio of the column jack reaction to the span jack load was 0.66, which was of the right order for the test (Figure 6.18). The columns deflected a maximum of 9mm away from the datum and against the jack pressure, which rose to a load of 92.9kN.

Slight diagonal cracking in the concrete slab was observed from the inner column flanges out to the edge of the slab at each end of the structure, when the span load per jack reached 80 kN. These cracks represented the end shearing of the block of concrete restrained by each column from the main part of the slab and this was also observed by the author at tests on a stub girder frame {38}. These cracks were subsequently to open up considerably in the following tests (para 6.7.6). Two

parallel transverse cracks were also recorded above each haunch toe at approximately 500mm spacing, and these opened up to an estimated 0.2mm.

The response of the frame throughout was almost linear, as the plot of span jack load against central deflection, Figure 6.19, shows. On release of the span loading, a permanent central set of 3.25mm was recorded, but the column jacks were then pumped to return the columns back to the datum, and this reduced to 2mm. Since no untoward effect occurred, and the column jack forces were as anticipated, it was decided to repeat this test but to adopt the original jacking procedure, ie, to return the columns to the datum at each increment.

6.7.4 Working Load 2

After replacing and resetting some faulty vibrating wire strain gauges, Working Load Test 2 was carried out 72 days after casting the floor. Central deflection increments were mostly 5mm, up to a maximum recorded deflection of 37.2mm. This was achieved with a span load of 120.3 kN per jack, ie, 42% of the final maximum ultimate load.

The ratio of the average column to span jack load was close to 0.82, ie, that predicted by the analysis by assuming a constant composite stiffness throughout the beam (Figure 6.18). The response of the frame was again virtually linear, as can be seen by the plot of the span load versus central deflection in Figure 6.20. This is also demonstrated by Figures 6.21 and 6.22 which show the moment-rotation curves at the haunch toe positions. The 'rotation' is defined as the difference in slope between a position just beyond the haunch toe and that at the connection, ie, the integration of the whole haunch rotation.

After the maximum load was applied, the specimen was unloaded gradually, but when the columns veered off the datum by more than 5mm, an adjustment was made. It proved to be virtually impossible to release the column and span jacks so as to ensure that the column remained exactly on the datum during unloading, and indeed, it was not absolutely necessary. The permanent set in the centre of the span after unloading was recorded as 1.7mm.

The position of the point of contraflexure was confirmed by readings from the vibrating wire strain gauges to be about 2.3m from the supports, which compares reasonably well with the computer predicted value of 2.01m quoted in Chapter 8. Typical longitudinal strain profiles for the concrete slab are shown in Figure 6.23, but the values in the hogging region are high, owing to cracking of the concrete. On inspection of the slab it was found that a crack passed directly under the hogging region gauges, so these values will be exaggerated. The concrete strain at the centre of the span at the maximum load, ie, 42% of final maximum load, was measured as $536\mu\epsilon$, which compares with a yield value of $2600\mu\epsilon$. The latter figure was calculated using the normal weight concrete stress-strain curve given in reference {41}, Figure 2.1, and modified by replacing the modulus with the expression $\rho^2 \times 10^{-6} \sqrt{(f_{cu}/\gamma_m)}$ given in reference {42}, where ρ is the density in kg/m^3 .

During the latter stages of the test, short central longitudinal cracks appeared in the concrete directly over the haunches, as shown in Figures 6.24(a) and 6.23(b). From observation this was not due to longitudinal shear failure but to transverse hogging of the slab across the haunch region. This is explained because the effective width of the slab above the haunch is confined to a short distance each side of the steel beam (see later Ult. Test 2) and the degree of longitudinal bending, and hence curvature, is not transferred to the longitudinal edges of the slab. This results in a transverse reverse curvature, but, in this case, the effect is exacerbated by the presence of a stiff haunch which forms a 'hard spot'. It is, of course, not just a characteristic of the test arrangement but would also occur in a real situation.

It was also noted during the test that about 75% of the span jack loading went to ground via the main columns and the remainder down the stub columns. This difference was linear and simply due to the relative stiffness of the respective load paths. This is illustrated in Figure 6.25 and means that the shear in the test at the haunch is slightly below what it would be in practice. However, the moments would have been essentially the same, and therefore, it is not considered to have had a significant effect on the behaviour.

6.7.5 Ultimate Load Test 1

Before the test was carried out, it was clear that some of the vibrating wire strain gauges were being unduly influenced by their proximity to the loading frames. A modified arrangement was therefore devised with a new transverse row near the centre of the span - see Figure 6.14. The test then began 112 days after casting and deflection increments of 5mm or 10mm were applied, up to a maximum recorded central deflection of 185.3mm, ie, span/73. At this point the span load per jack was 259.2kN, ie, 90% of the final maximum ultimate load.

The test response was initially linear and followed the stiffness demonstrated in Working Load Test 2, up to a central deflection of 40.6mm. The corresponding span jack load was 128.4kN, ie, 45% of the final ultimate maximum. At 50.7mm, the yield strain was recorded in the bottom flange at mid-span and followed shortly after by yield in the bottom flange at the haunch toes, at a deflection of 55.7mm. As the load was further increased, the stiffness reduced and more transverse cracks appeared in the slab around the haunch toes. At 132mm deflection and with 84% of the final maximum load, there became evidence of local buckling in the compression flanges at the haunch toes, similar to that observed in the Sub-Assembly Tests. Small buckling waves appeared just beyond the haunch toes, with a wavelength of about 125mm and an amplitude of approximately 1.5mm. These local buckles continued to grow in length and magnitude until at the final increment the wave lengths were about 140mm, with amplitudes of 3.25mm and 1.75mm, for haunches B5 and B6 respectively. This was accompanied by spalling of the white 'paint', which indicated the extent of the compression yielding - see Figure 6.26. The unloading stiffness was the same as the initial elastic stiffness and a permanent set of 107mm was recorded at mid-span.

The moment-rotation response at the haunch toes initially followed that of Working Load Test 2, but after the onset of yielding at moments of about 540kNm, the rotational stiffness reduced, as shown in Figures 6.21, 6.22 and 6.27. Above 600kNm, the rate of decrease was rapid and final haunch toe moments of 766kNm and 743kNm were recorded for B5 and B6 respectively. The response of the haunch toes was virtually identical but the behaviour of the mid-span position was different.

Non-linearity of the behaviour of this position appeared, from the moment-deflection graph (Figure 6.27), to begin at the slightly higher moment of 600kNm, although the strain gauge readings indicated surprisingly that yield occurred first in the mid-span. It is clear, however, that moments were being redistributed from the haunches to the mid-span after yielding at the haunch toes occurred. This is seen in Figure 6.28 which shows a definite change in the slope of the span load-moment curves at a jack load of 200kN, ie, 70% of the final maximum ultimate load. A decrease in the haunch toe moments is observed, while a corresponding increase in the mid-span moments occurs. The final value of the mid-span moment, before unloading, during this test was 1003kN. At this value the strain in the upper surface of the concrete was approximately $1927\mu\epsilon$, which is still below the yield value of $2600\mu\epsilon$, quoted earlier. The strain in the under-side of the tension flange at that location measured $20033\mu\epsilon$, which suggests, from the coupon result, that the material was just into the strain-hardening region. The growth in the bending moments is also illustrated in Figure 6.29 which shows the bending moment diagrams.

During the test the ratio of the span jack load to horizontal column reaction continued as before (Figure 6.30), but when the structure became non-linear, this ratio showed a gradual decrease. This is to be expected because of the redistribution of moments. The proportion of span load being supported by the main columns also continued as before at 75%, but with a slight increase towards the end of the test - see Figure 6.25. This was no doubt due to the further weakening of the load paths to the stub columns caused by cracking of the slab.

6.7.6 Ultimate Load Test 2

This test was carried out 126 days after casting, with mid-span deflection increments of between 10mm and 30mm. The maximum span load of 286.1kN per jack was reached at a central deflection of 340.7mm (span/40). The test was, however, continued until the deflection was 401.7mm (span/34) with little decline in the load - see Figure 6.20. The initial response followed the elastic loading path of the previous test up to its maximum load, before resuming the non-linear behaviour. The results indicated that the specimen could have sustained much more deformation without unduly weakening, but the test was terminated soon after the maximum load

had been reached because the behaviour beyond this point was not of prime interest. The unloading stiffness was again similar to the elastic stiffness and a cumulative mid-span deflection of 300.7mm was recorded.

Throughout the test the transverse cracking in the hogging regions of the slab continued to spread and this is shown in Figures 6.31(a) and 6.31(b). The cracks are seen to diminish in spacing from the column to the points of contraflexure, as the curvature of the slab decreases. The points of contraflexure were measured by tape to be 2.1m from the columns, ie, span/64. The diagonal cracking from the columns to the end edges of the slab, mentioned earlier, was seen to open to about 15mm - see Figure 6.32. The transverse hogging curvature over the haunches, as described in Section 6.7.4, was very pronounced and the concentration of bending can also be seen clearly on a typical contour map of the concrete strains, shown in Figure 6.33. This is a computer plot drawn using the gauge sample points and from a series of cross-sections taken along the gauge rows, shown in Figure 6.34, it can be seen how the effective width dramatically reduces from the full width at mid span to much less near the support. It should, of course, be remembered that the slab in the hogging region was not designed to be effective and contained no shear reinforcement. Had it done so, the effective width might have been improved. In a multi-bay frame with a continuous slab there would not need to be the same shear transfer, so the effective width would increase. The change in the strain profiles near the haunch and at mid-span are compared for different load stages in Figure 6.35. This shows that the full width is effective at mid-span for both low and high loadings, but near the haunch, even for low loadings, there is a noticeable drop off, and this increases rapidly as the ultimate load is approached.

The moment-rotation response of the hinge positions was initially linear up to about the previous maximum moments, after which the non-linearity resumed (Figures 6.21, 6.22 and 6.27). The hinges at the haunch toes again behaved almost identically and exhibited a long plastic plateau of moment strength of about 820kNm. A slight decline in strength was noted after a rotation of 3.2° (56×10^{-3} radians) and when the test was terminated, the rotation of these hinges had reached 3.8° (66×10^{-3} radians), with a loss of strength of some 10%. The central hinge again behaved differently and exhibited a steady increase in moment with deformation of the

structure until a capacity of 1160kNm was reached, after which the structure was unloaded. The moments were again being redistributed from the haunch toes to the mid-span, as is shown by the load-moment plots in Figure 6.36. The transfer is clearly seen by the change in the slope of the curves from about 250kN span jack load (the previous maximum), whereby the mid-span moment again increases while that of the haunch toes decreases. The maximum load-carrying capacity of the specimen was therefore achieved when the increase in the central hinge moment could not compensate for the decline in the strength of the haunch toe hinges.

The reduction in strength at the haunch toes was undoubtedly due to the severity of the local flange and web buckling in the compression zones, which got progressively worse as the test proceeded, and is shown in Figures 6.37(a) and 6.37(b). The buckled shape consisted of one side of the flange buckling either upwards or downwards and the other side buckling the opposite way. The web then buckled in a direction in sympathy with this, as one would expect.

The amplitude of the flange buckling varied between 15mm and 20mm. There was little evidence of lateral distortional buckling, as Figures 6.38(a) and 6.38(b) show, and the local deformation was largely confined to 1 x beam depth beyond the haunch toes.

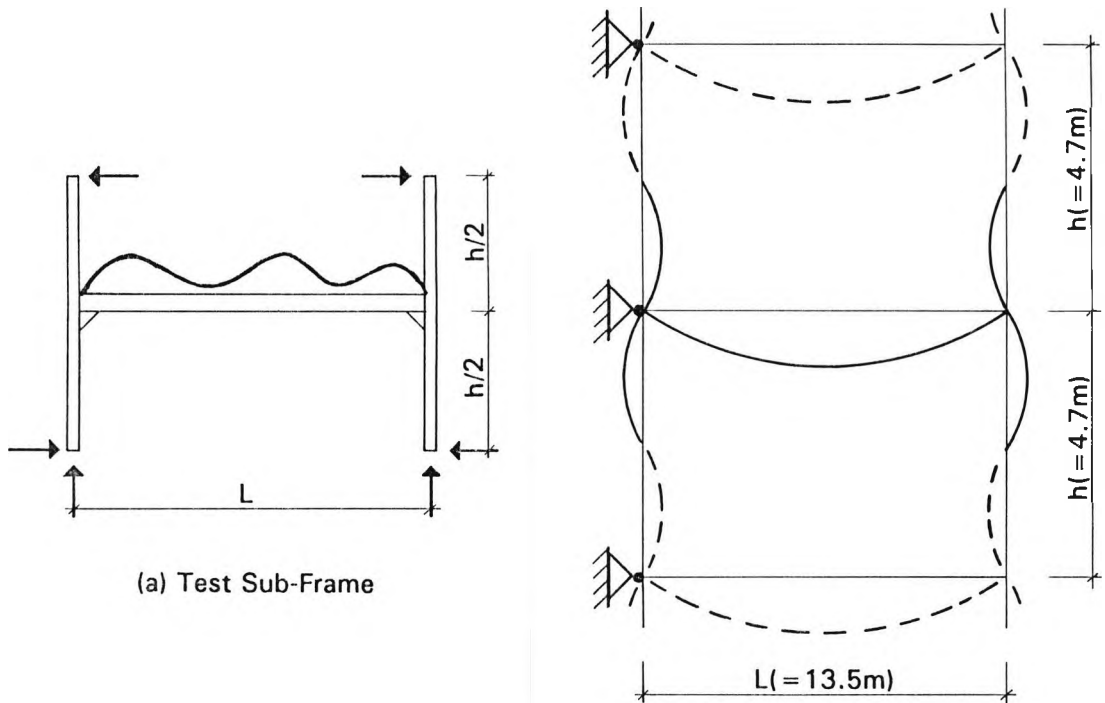
The steady increase in moment at the central hinge position was partly due to the redistribution of moments and also to the reserve of material strength. The extreme tensile strain in the bottom flange at maximum load was about $26,000\mu\epsilon$, which, from the coupon tests, indicates that the stress was at the yield value. The accompanying value of extreme fibre concrete strain was about $2,200\mu\epsilon$, which is actually below the predicted yield value of $2600\mu\epsilon$ and there was no evidence of concrete crushing. There was therefore evidence to suggest, particularly from the slope of the moment-deflection plot (Figure 6.27), that there was still available capacity in this hinge.

The proportion of span load supported by the main columns was initially 77%, but after the previous test maximum load was reached, this increased to 85% (Figure 6.25). This was due to further concrete cracking affecting the load paths to

the stub columns. The ratio of the column jack load to span jack load, Figure 6.39, again followed the elastic value of 0.82, but as the haunch toe hinge moments stabilised, so did the column reactions. Hence this ratio dropped and at the end of the test it was 0.7.

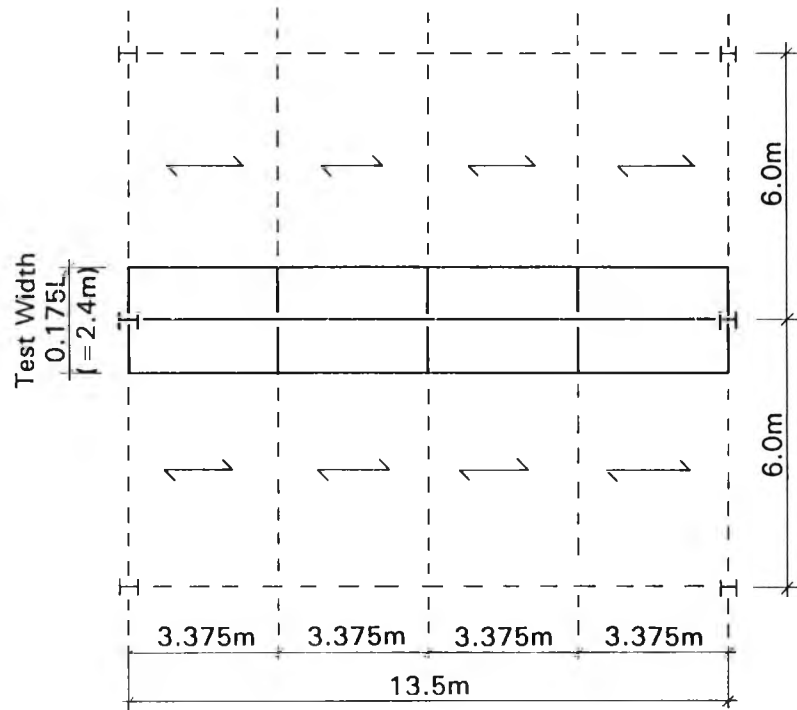
From simple equilibrium calculations, the connections were subject to maximum moments of about 960kNm. This is well above the design strength of 814kNm, but, as discussed later in Chapter 7, the decking made a significant contribution to the hogging region strength because it was rigidly fixed to the main beam and the end beams. However, it is reasonable to assume that much of force in the decking transferred directly to the end beams and not to the bolts, so it is not suggested that the bolt group was under-designed. This is confirmed by the fact that there was no evidence of shear deformation in the columns at the connection height and there was no sign of deformation of the connections themselves. The separation of the beam end plates from the columns was only 1mm at the maximum load and the vertical slippage was less than 1mm.

After the loading frames, etc, had been removed from the specimen, the final deformed shape of the structure could be seen clearly and is shown in Figure 6.40.



(a) Test Sub-Frame

(b) Deflected Shape of Multi-Storey Frame Being Modelled



(c) Floor Arrangement Being Modelled

Figure 6.1 Main Beam Test - Multi-Storey Frame Arrangement Modelled by the Test

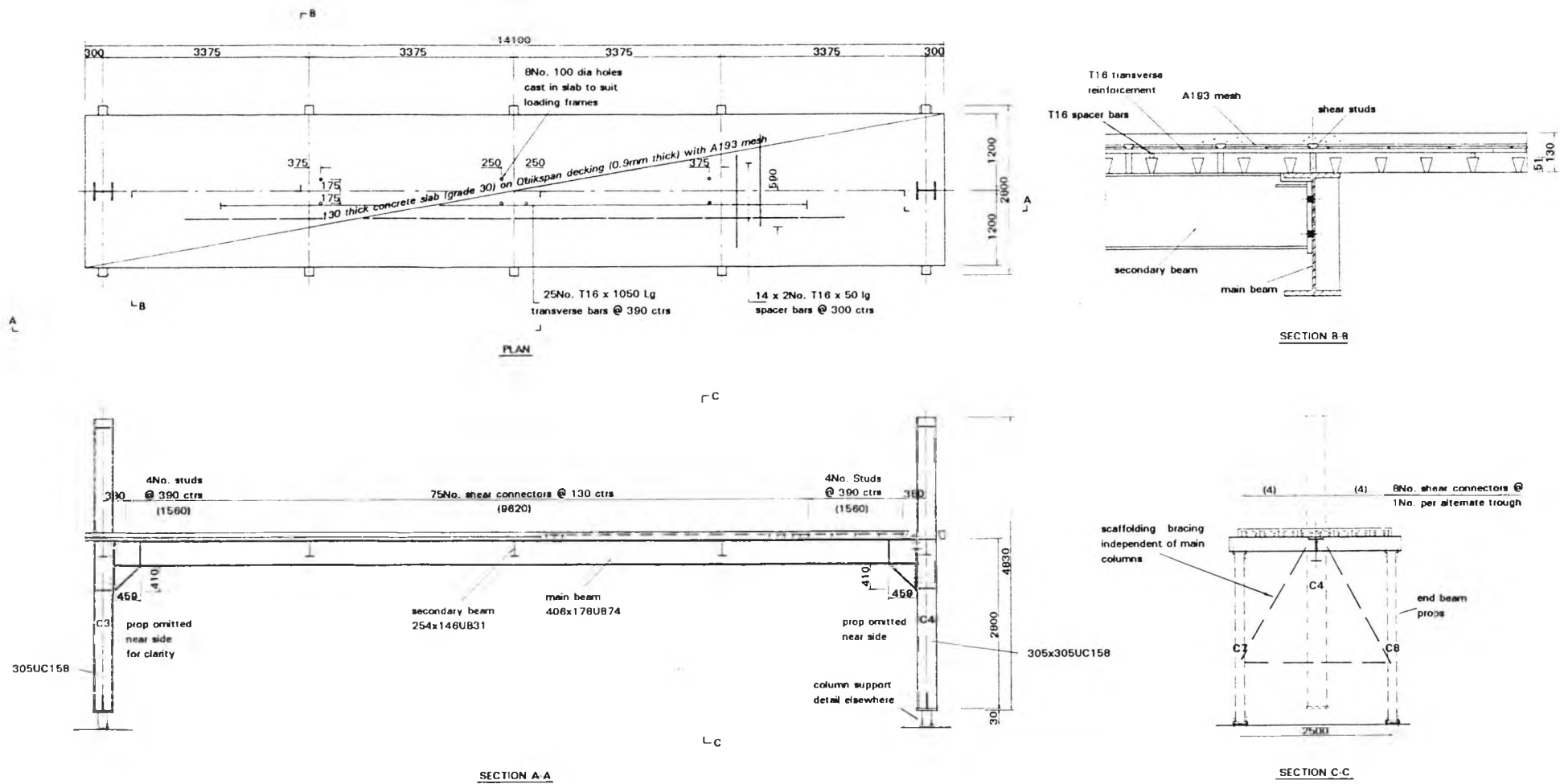


Figure 6.2 Main Beam Test - Specimen General Arrangement

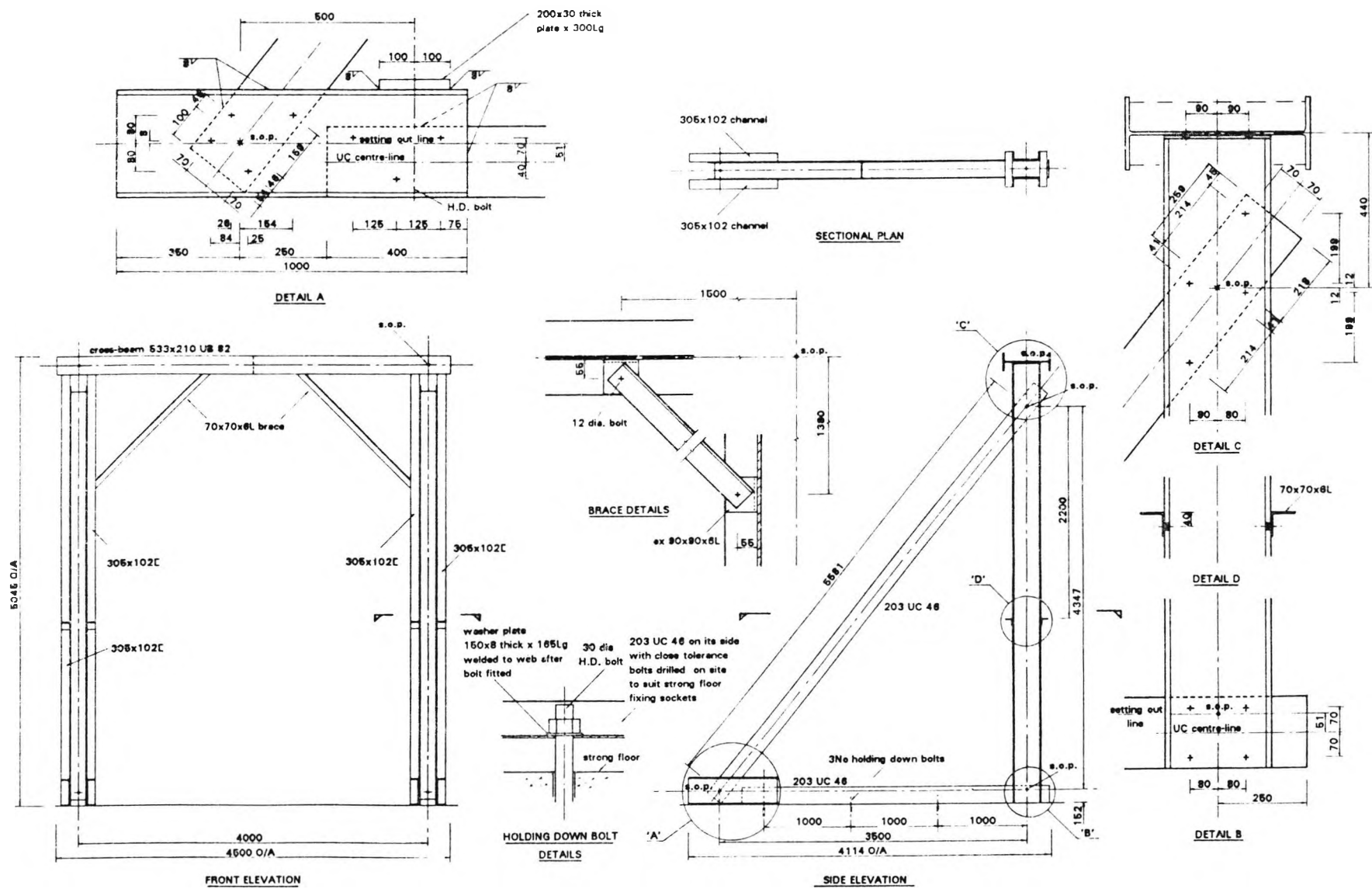


Figure 6.3 Main Beam Test - Reactant Frame General Arrangement

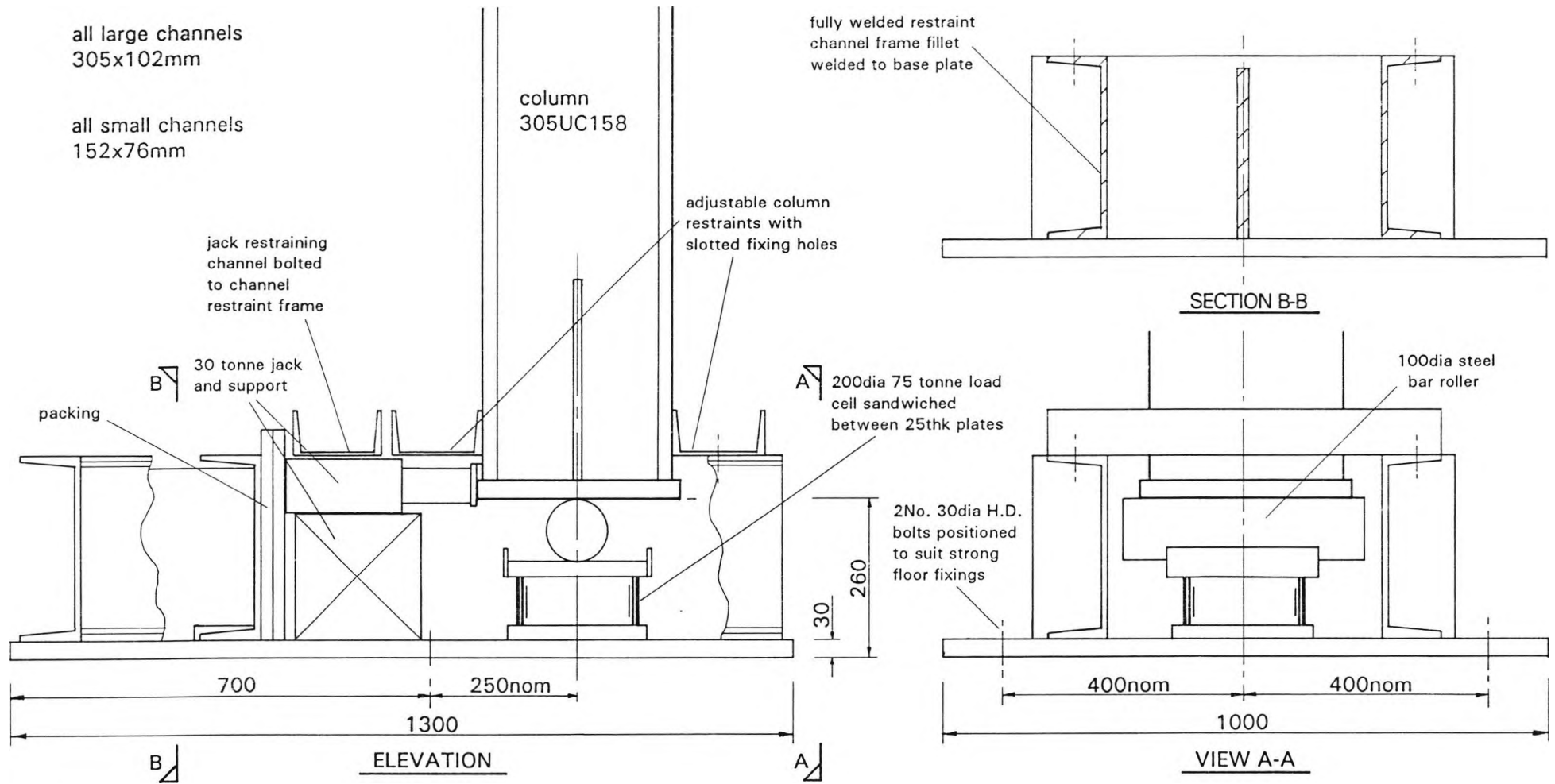
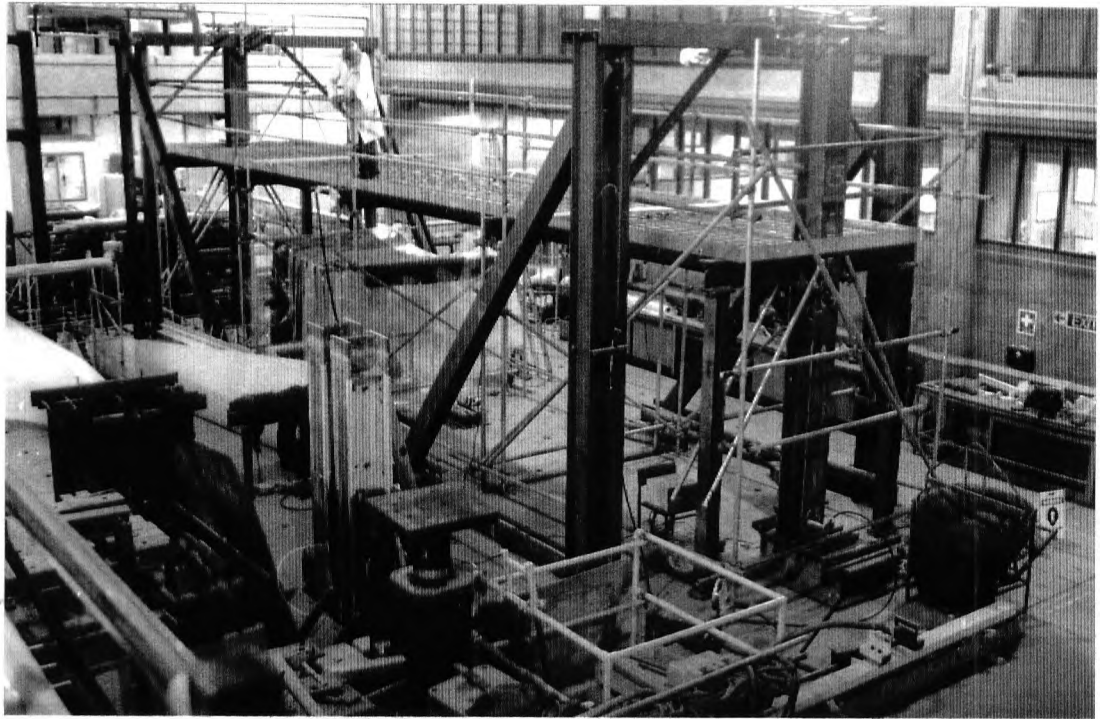
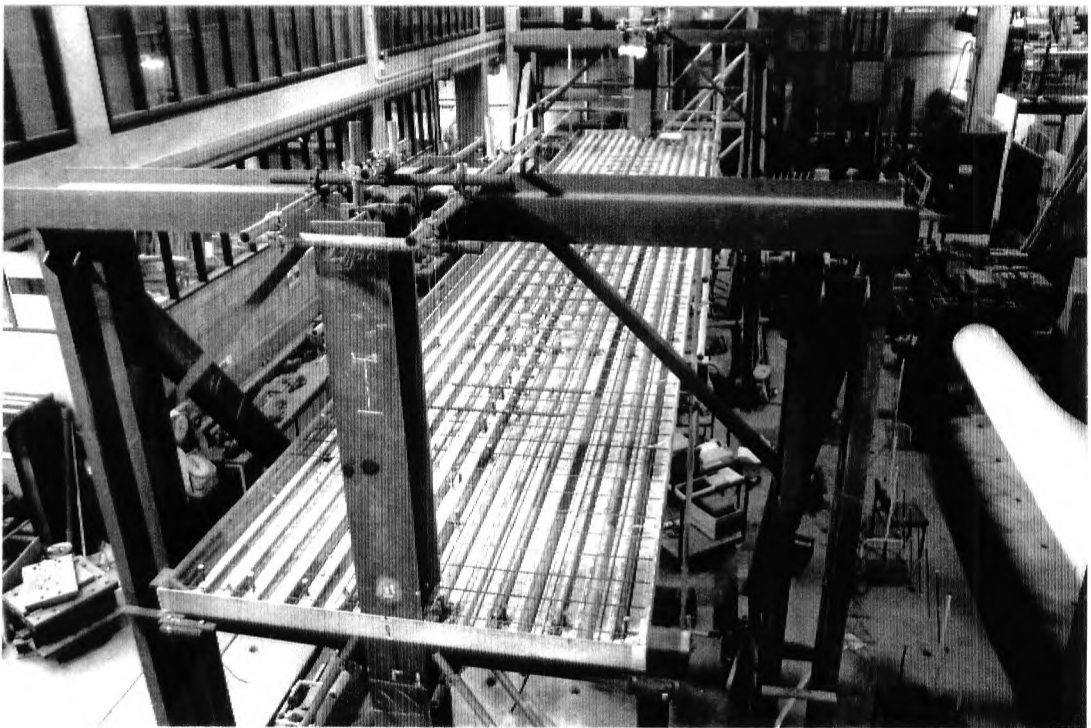


Figure 6.4 Main Beam Test - Column Base Support Assembly



(a)



(b)

Figure 6.5 Main Beam Test - Structure Prior to Casting Floor

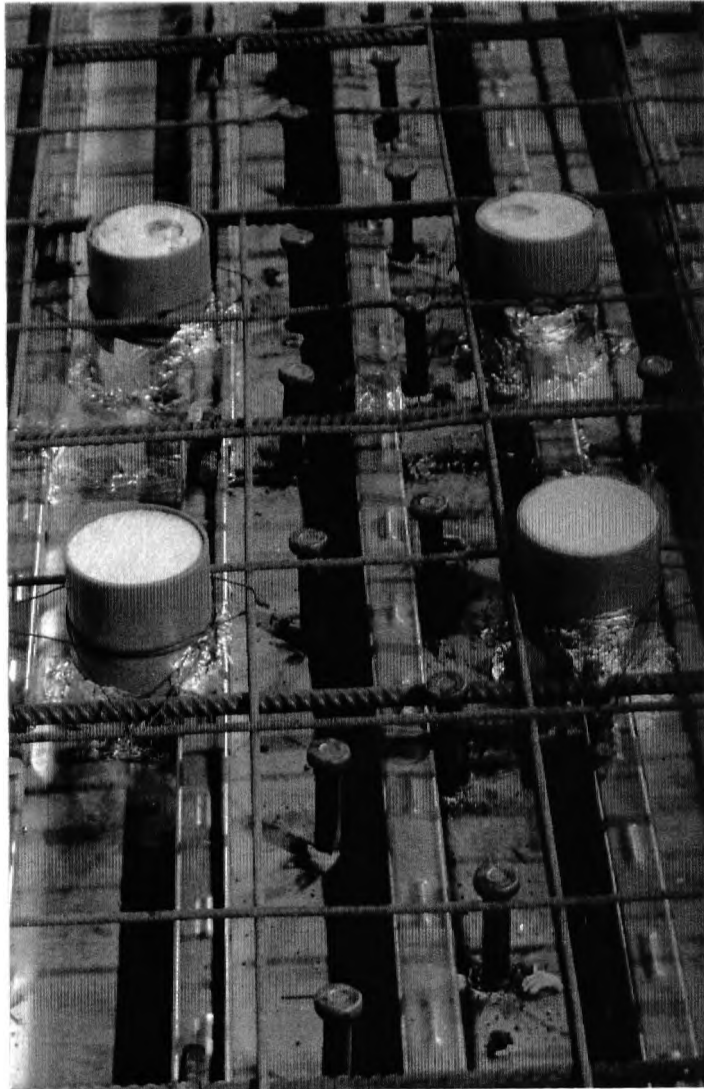


Figure 6.6 Main Beam Test - Pockets for Loading Frame Pull Down Rods

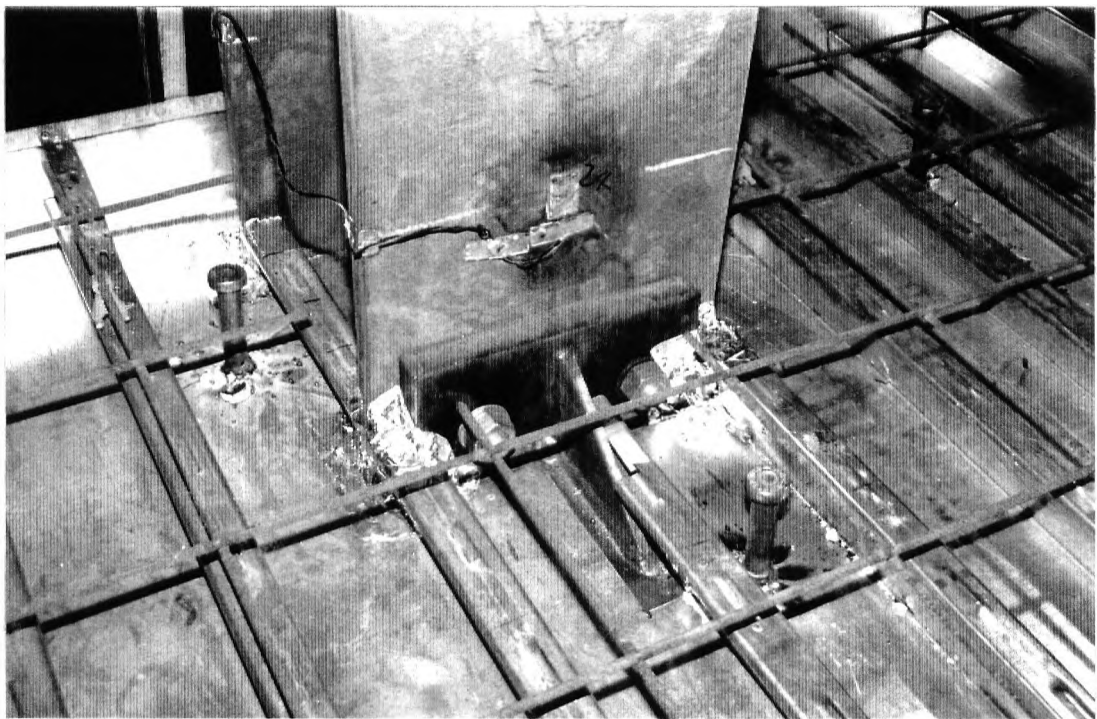
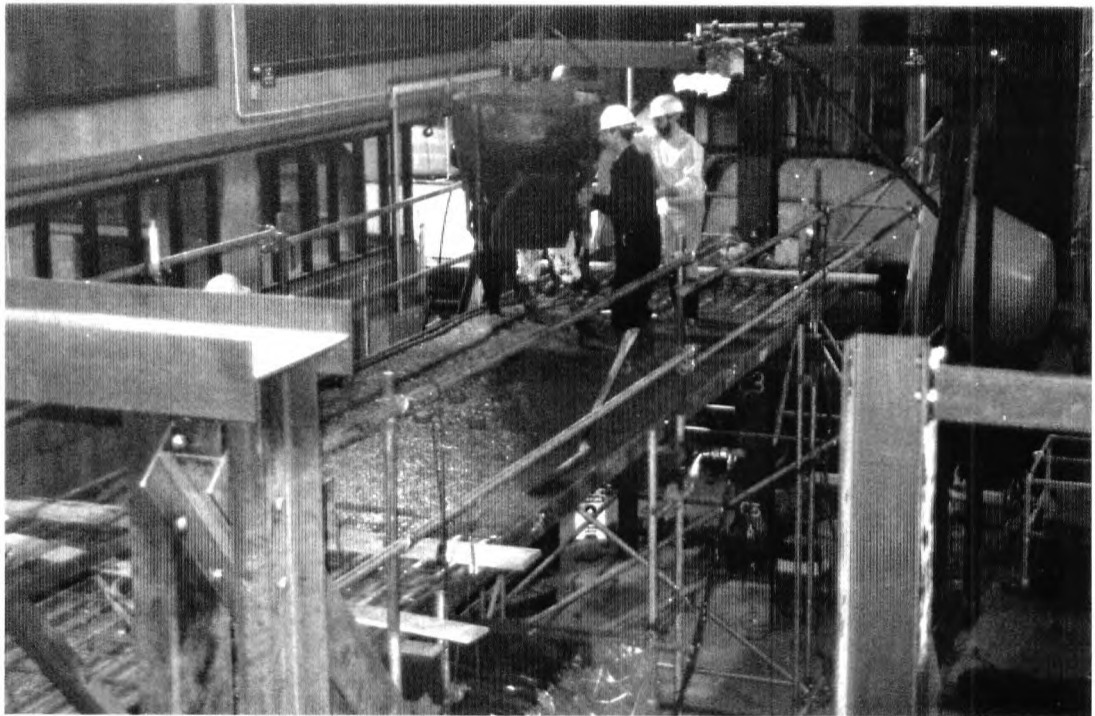
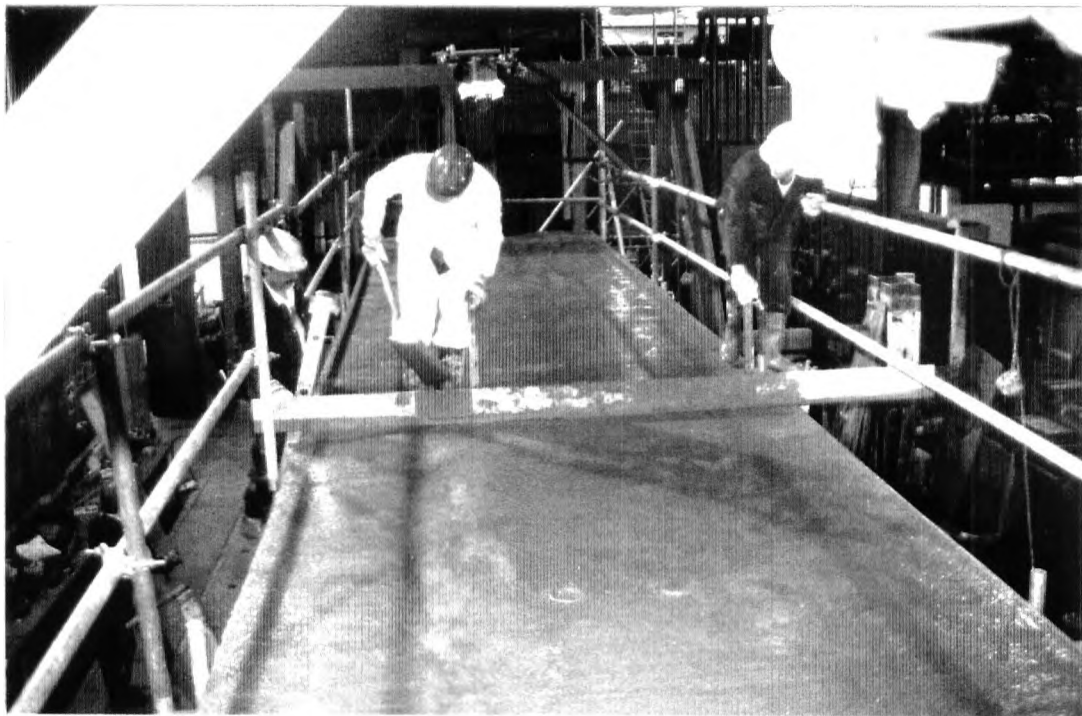


Figure 6.7 Main Beam Test - Floor Detail Around a Column

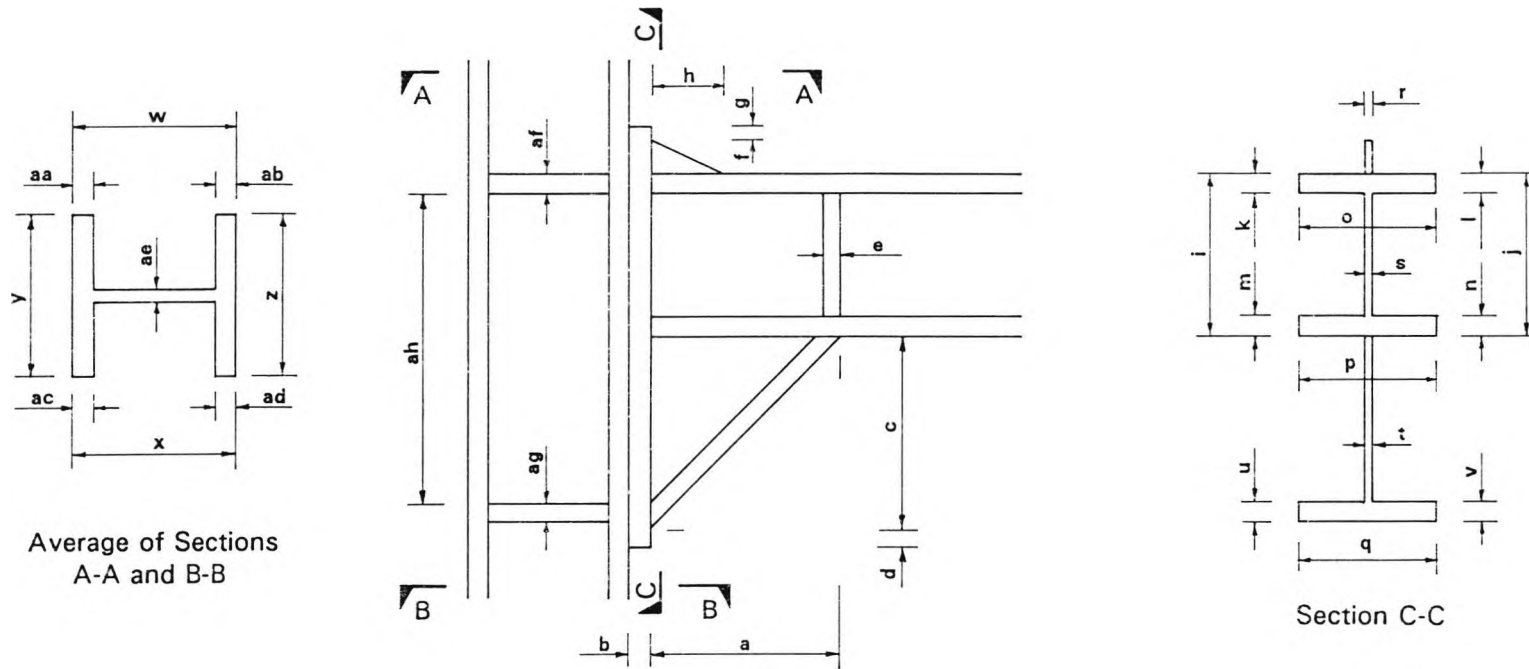


(a)



(b)

Figure 6.8 Main Beam Test - Casting the Slab



Haunch/Column Details B5/C3 and B6/C4

Dimension	a	b	c	d	e	f	g	h	i	j	k	l	m	n	o	p	q
B5	422	30	410	20	15.1	105	19	147	417.7	416.6	14.84	15.84	16.61	15.16	180.1	180.0	187.8
B6	428	30	407	25	15.7	100	19	155	416.8	417.3	16.06	14.91	14.97	16.66	180.3	179.9	188.0
Dimension	r	s	t	u	v	w	x	y	z	aa	ab	ac	ad	ae	af	ag	ah
B5/C3	10.1	9.4	10.44	16.42	15.75	331.9	335.2	312.0	312.6	23.05	24.38	25.58	25.34	15.65	9.65	9.65	795
B6/C4	10.0	9.9	10.2	15.95	15.93	330.8	334.8	311.7	312.1	23.45	24.47	25.65	25.09	15.65	9.64	9.65	794

Figure 6.9 Main Beam Test - The As-Built Dimensions

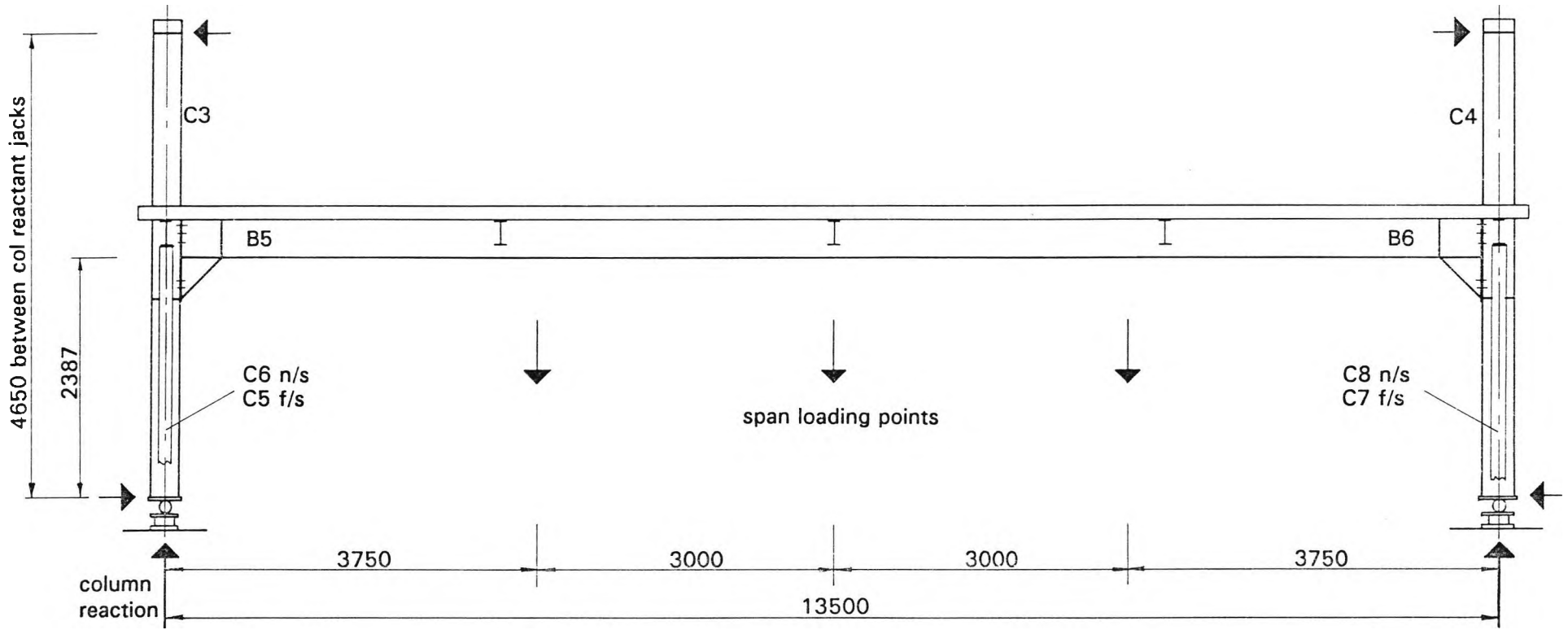


Figure 6.10 Main Beam Test - Arrangement of the Loading Systems

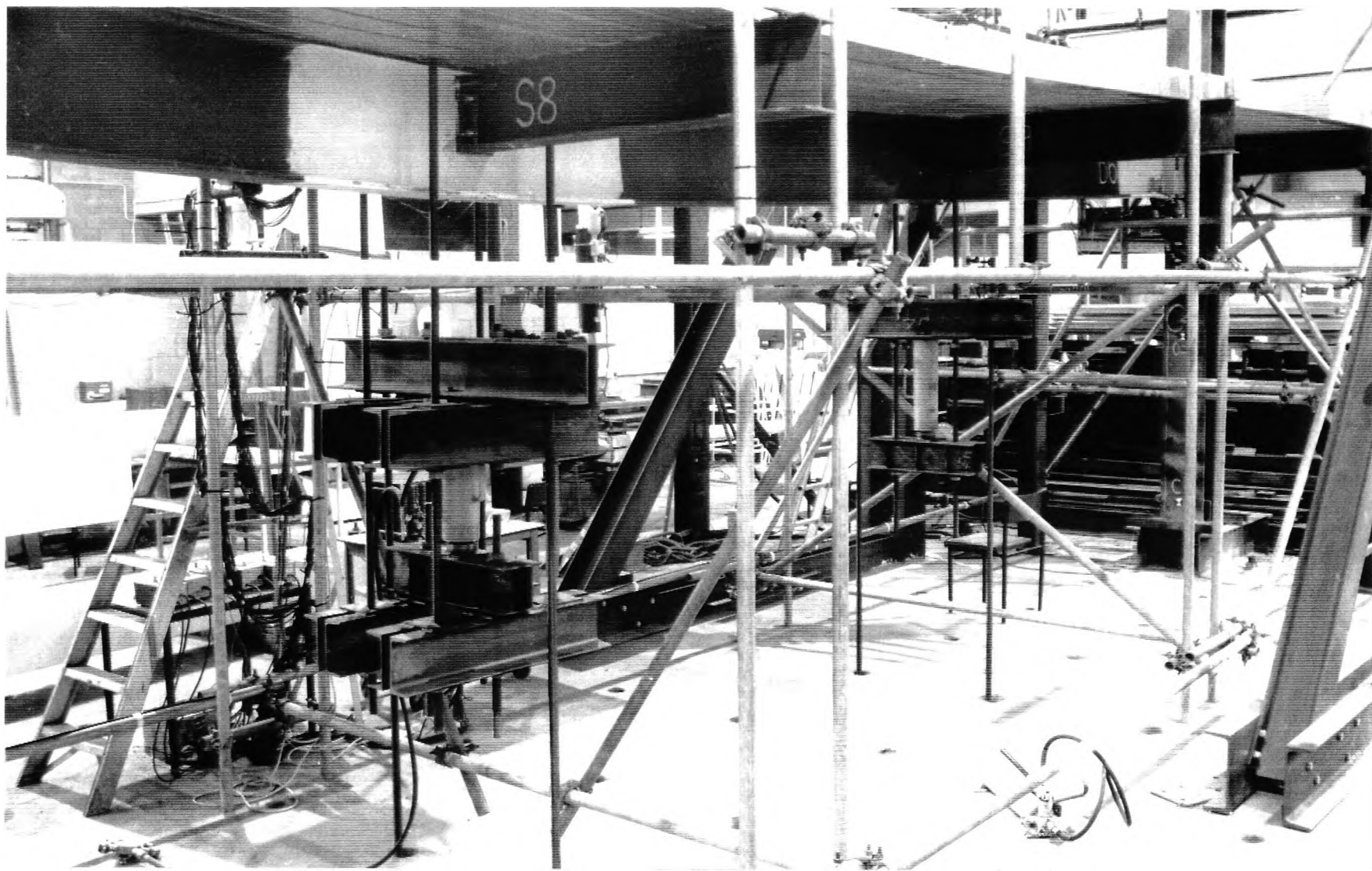


Figure 6.11 Main Beam Test - The Central Loading Frame and an Outer Loading Frame

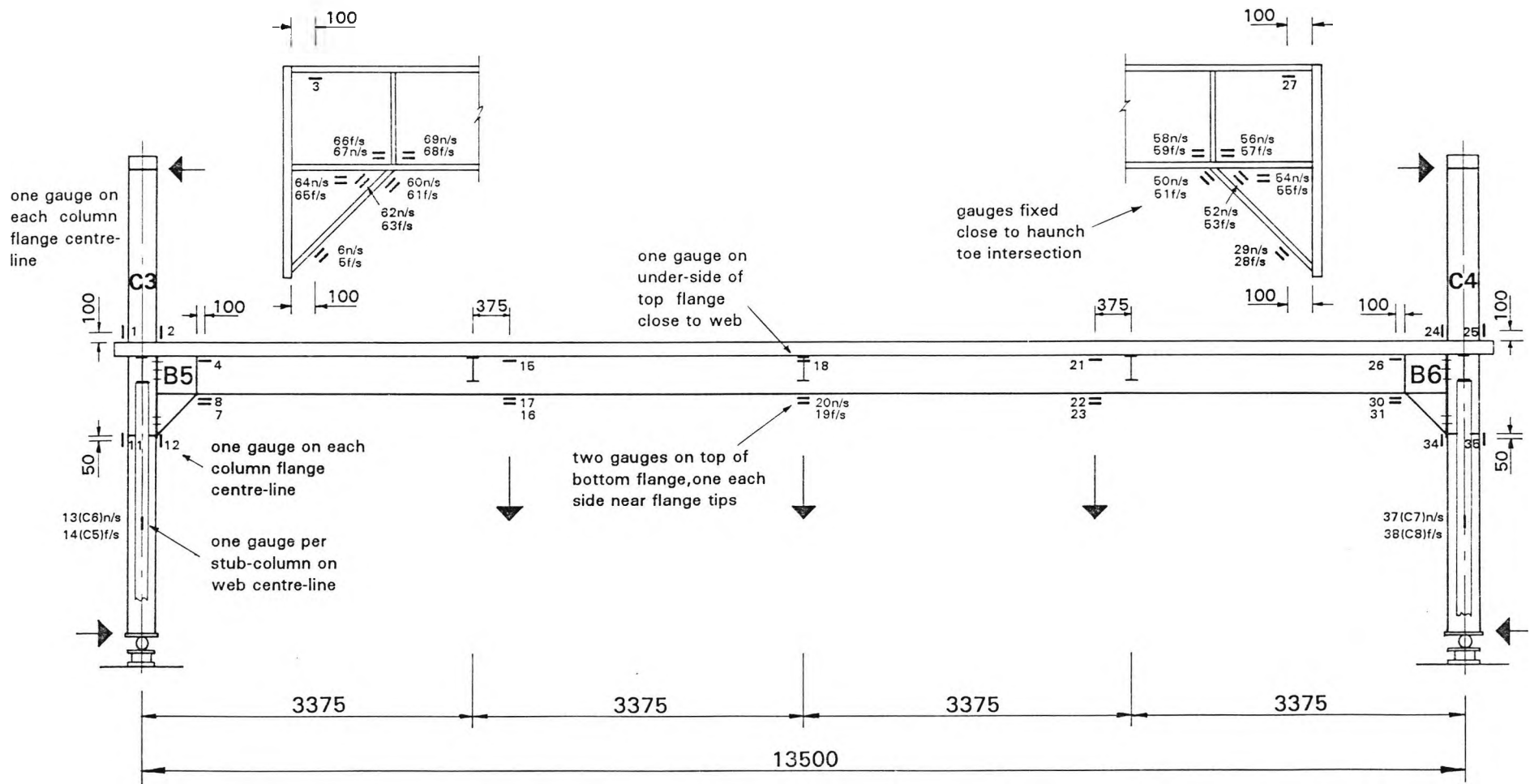


Figure 6.12 Main Beam Test - Electrical Resistance Strain Gauge Layout

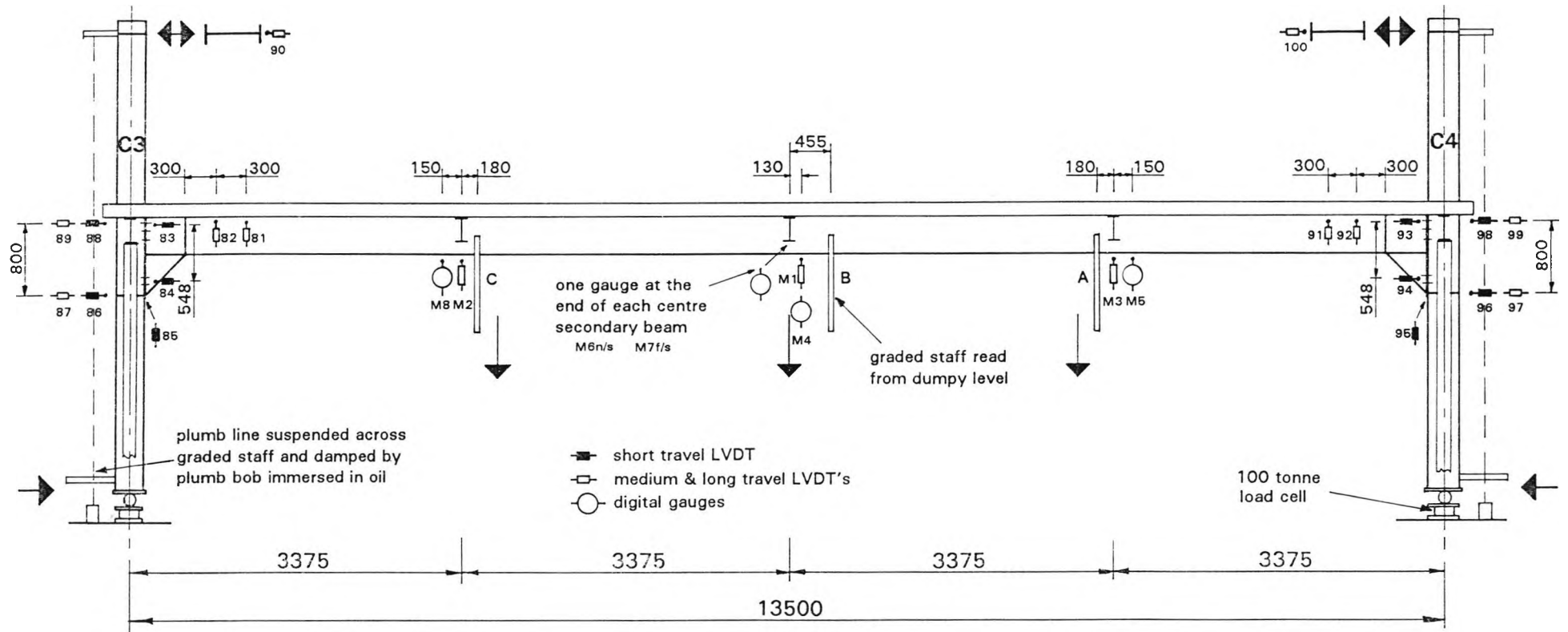


Figure 6.13 Main Beam Test - Frame Displacement and Column Verticality Measurement Arrangements

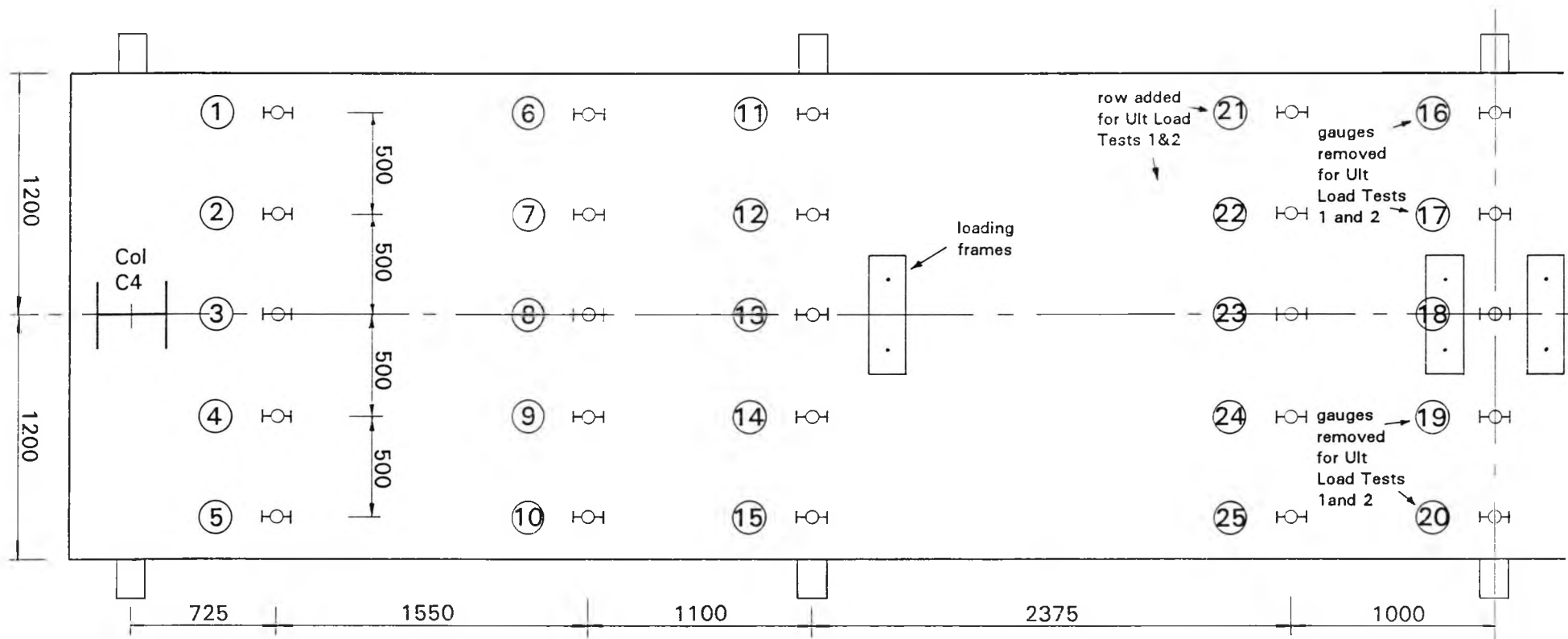


Figure 6.14 Main Beam Test - Vibrating Wire Strain Gauge Layout

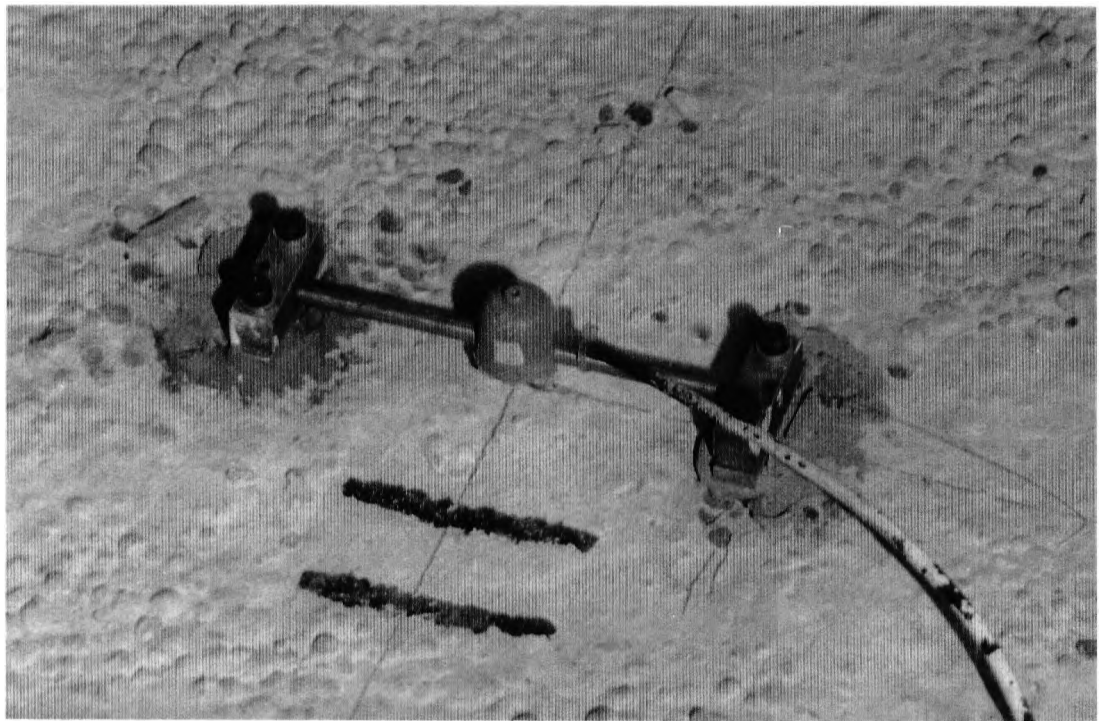


Figure 6.15 Main Beam Test - Vibrating Wire Strain Gauge

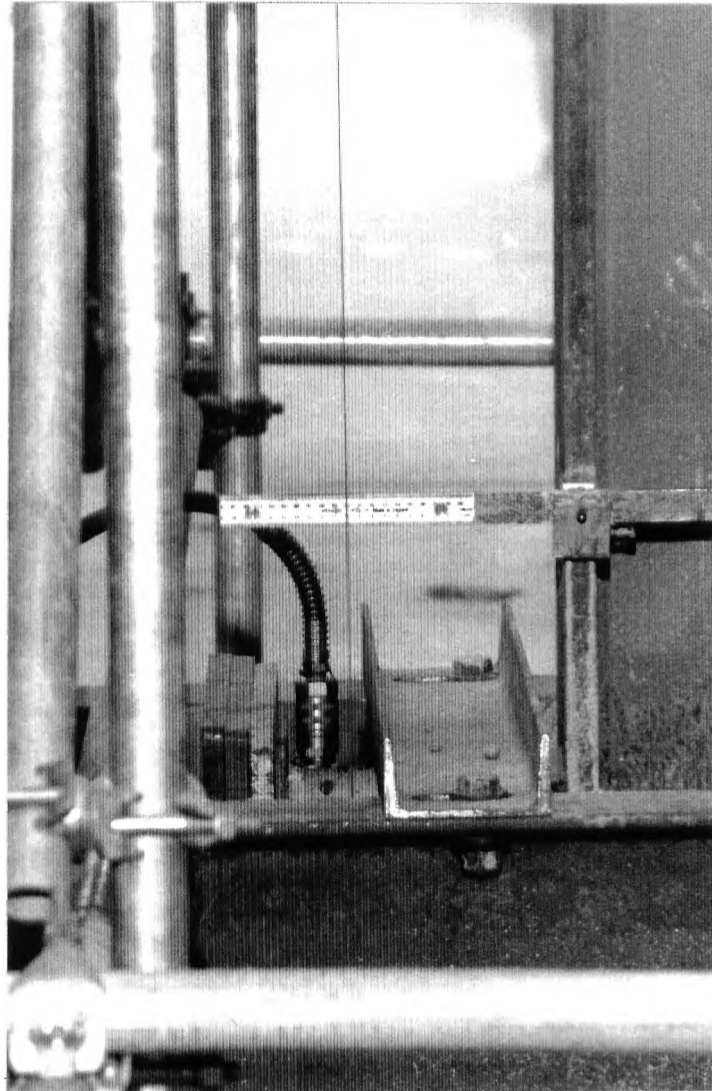


Figure 6.16 Main Beam Test - Graded Staff Arrangement for Column Verticality Check

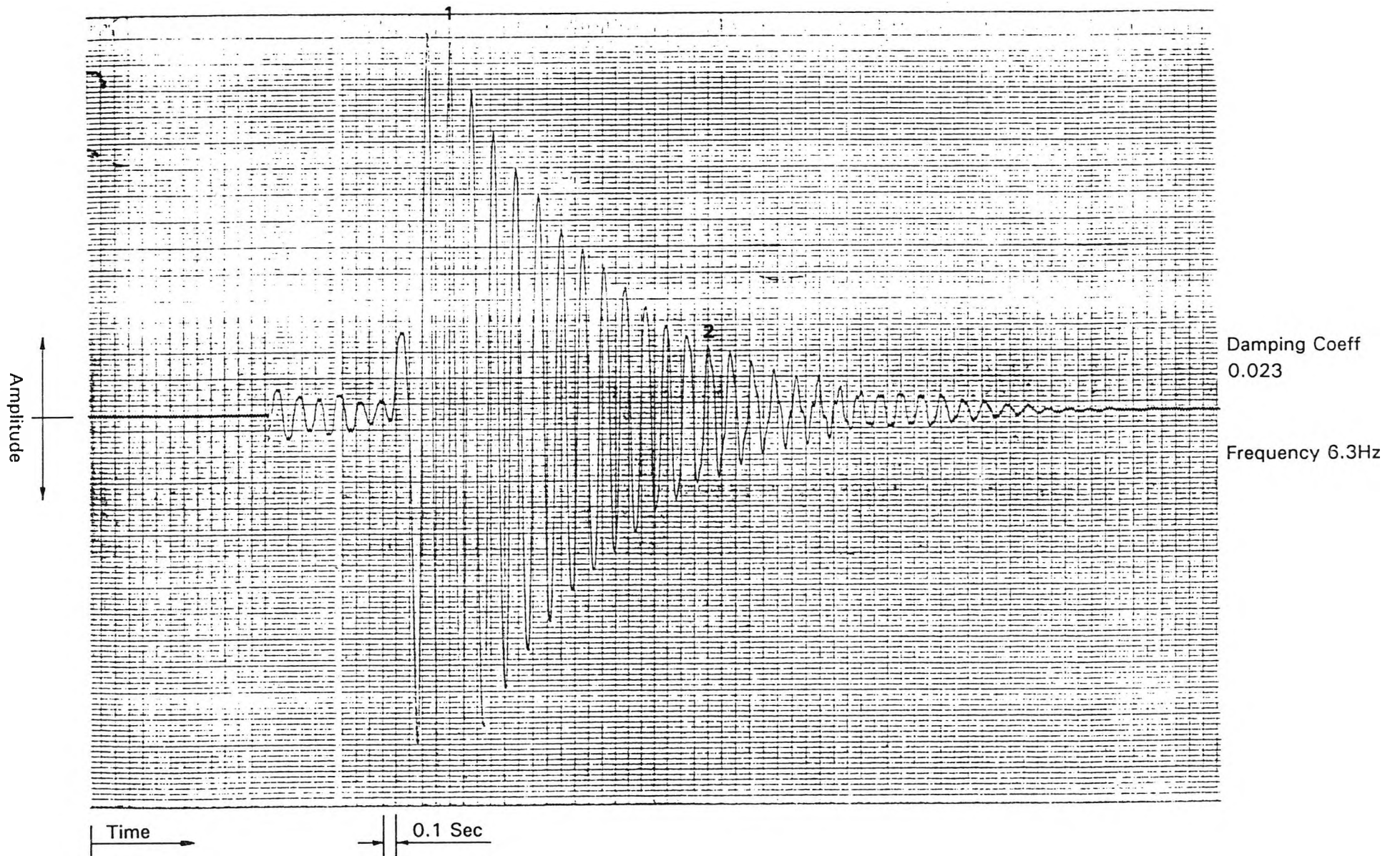


Figure 6.17 Main Beam Test - Dynamic " Heel Drop " Test Plot

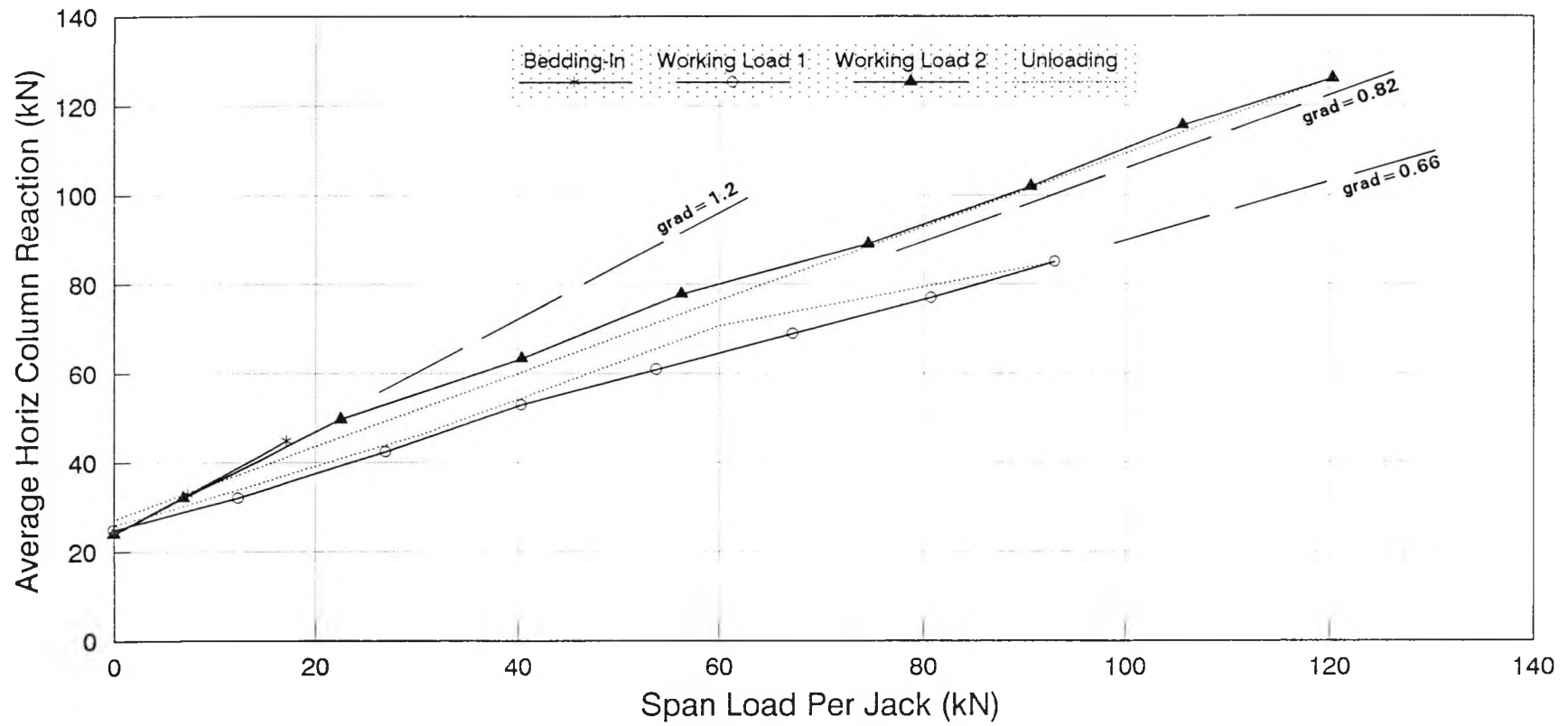


Figure 6.18 Main Beam Test - Growth of Horizontal Column Reactions with Span Loading

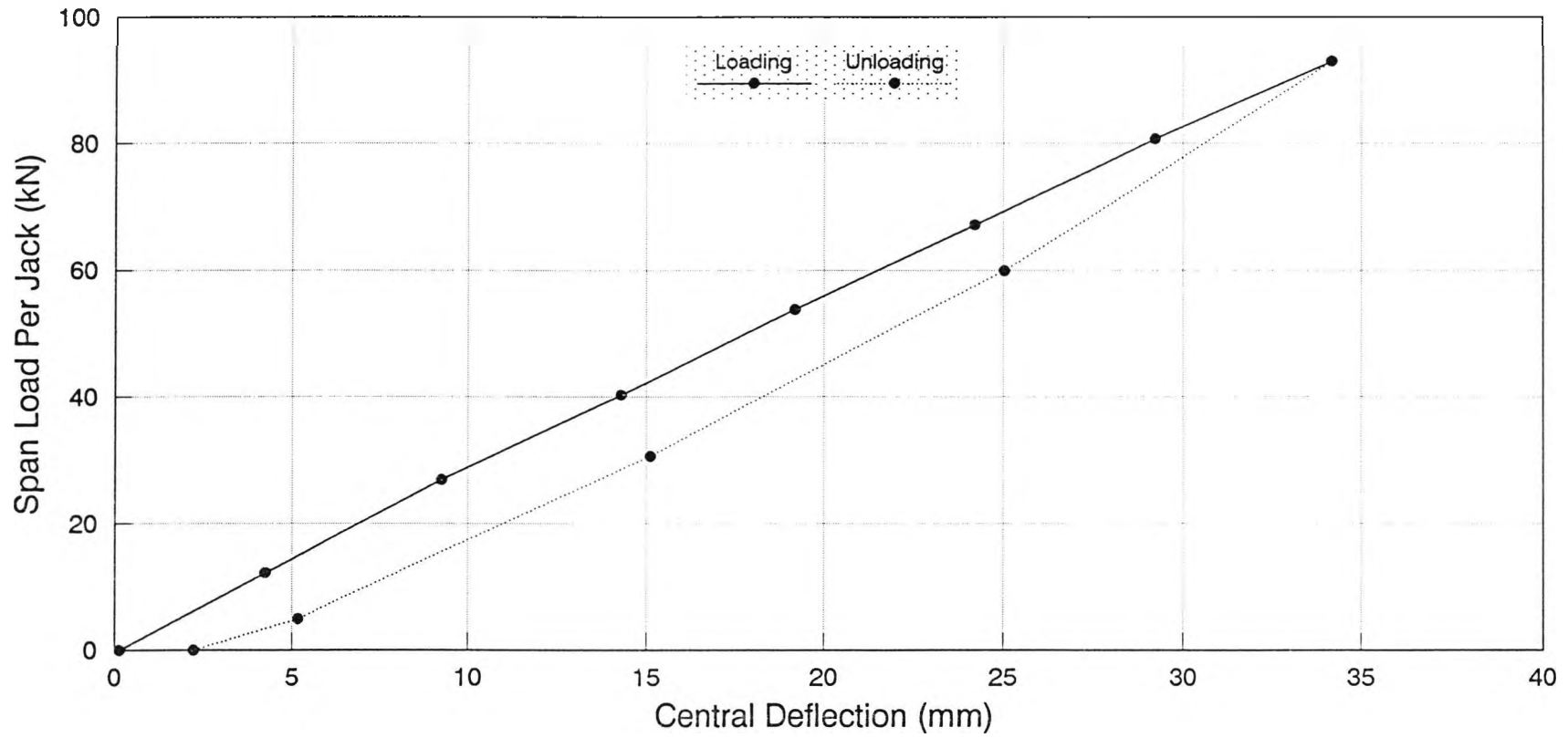


Figure 6.19 Main Beam Working Load Test 1 - Span Load versus Central Deflection

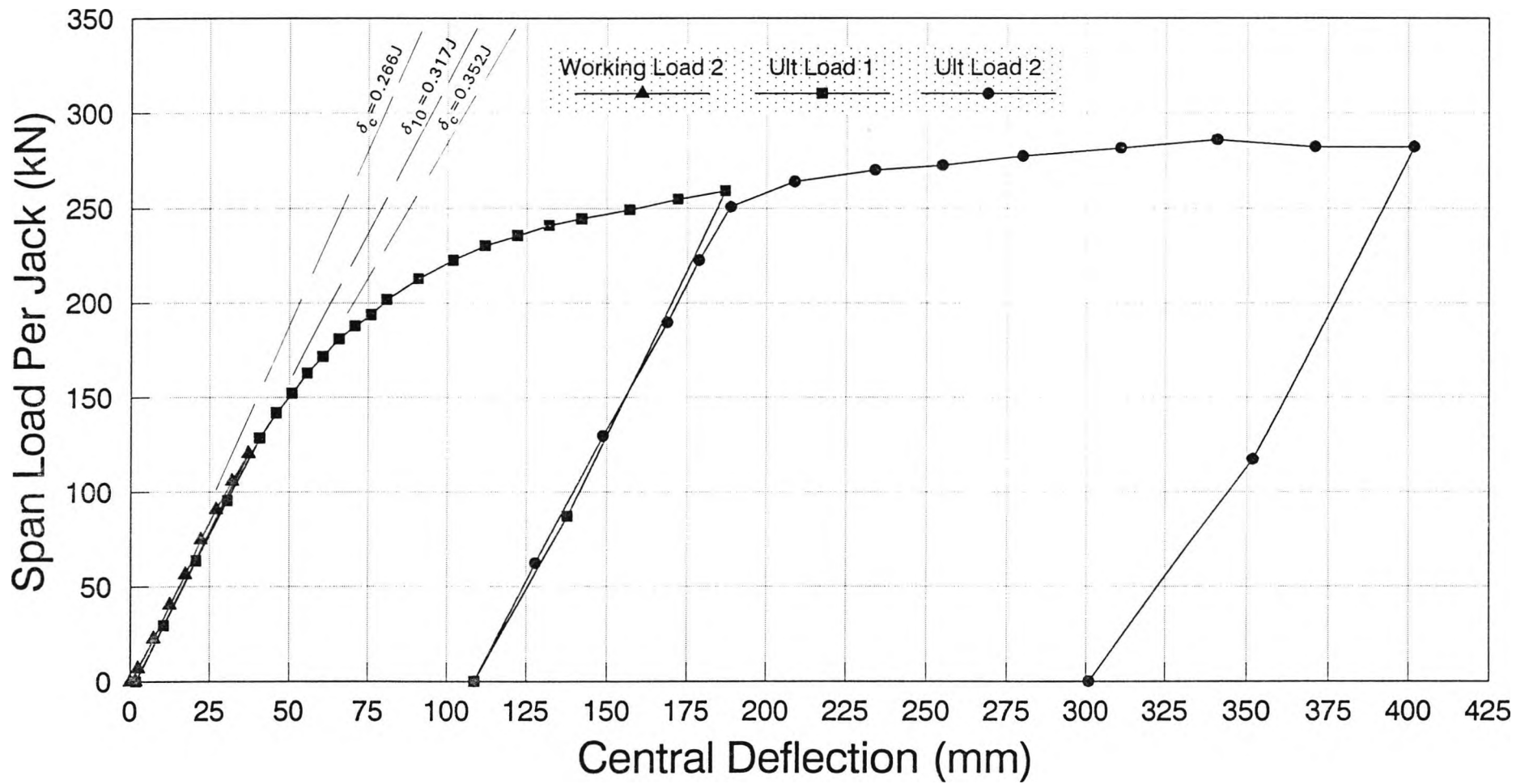


Figure 6.20 Main Beam Test - Span Load versus Central Deflection

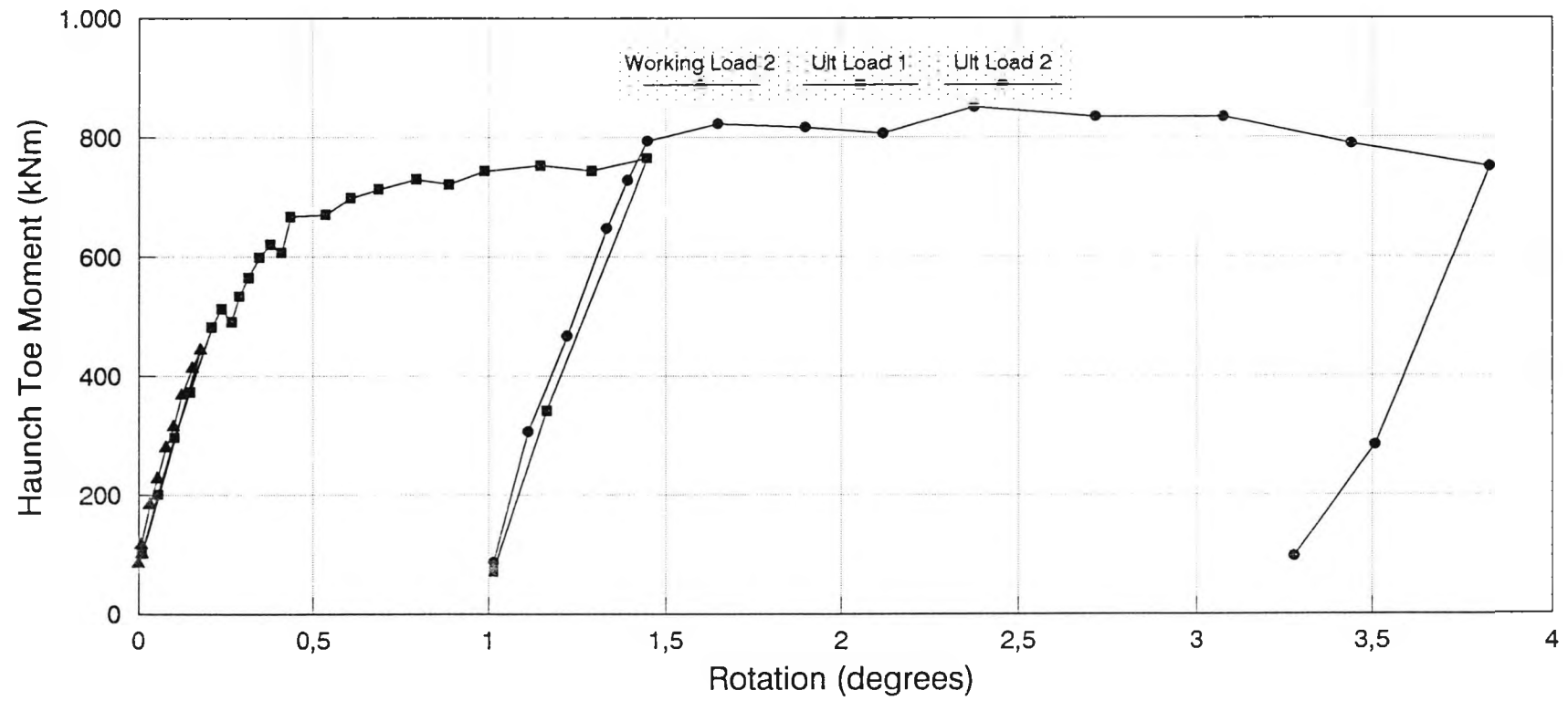


Figure 6.21 Main Beam Test - Haunch Toe B5 Moment/Rotation Characteristics

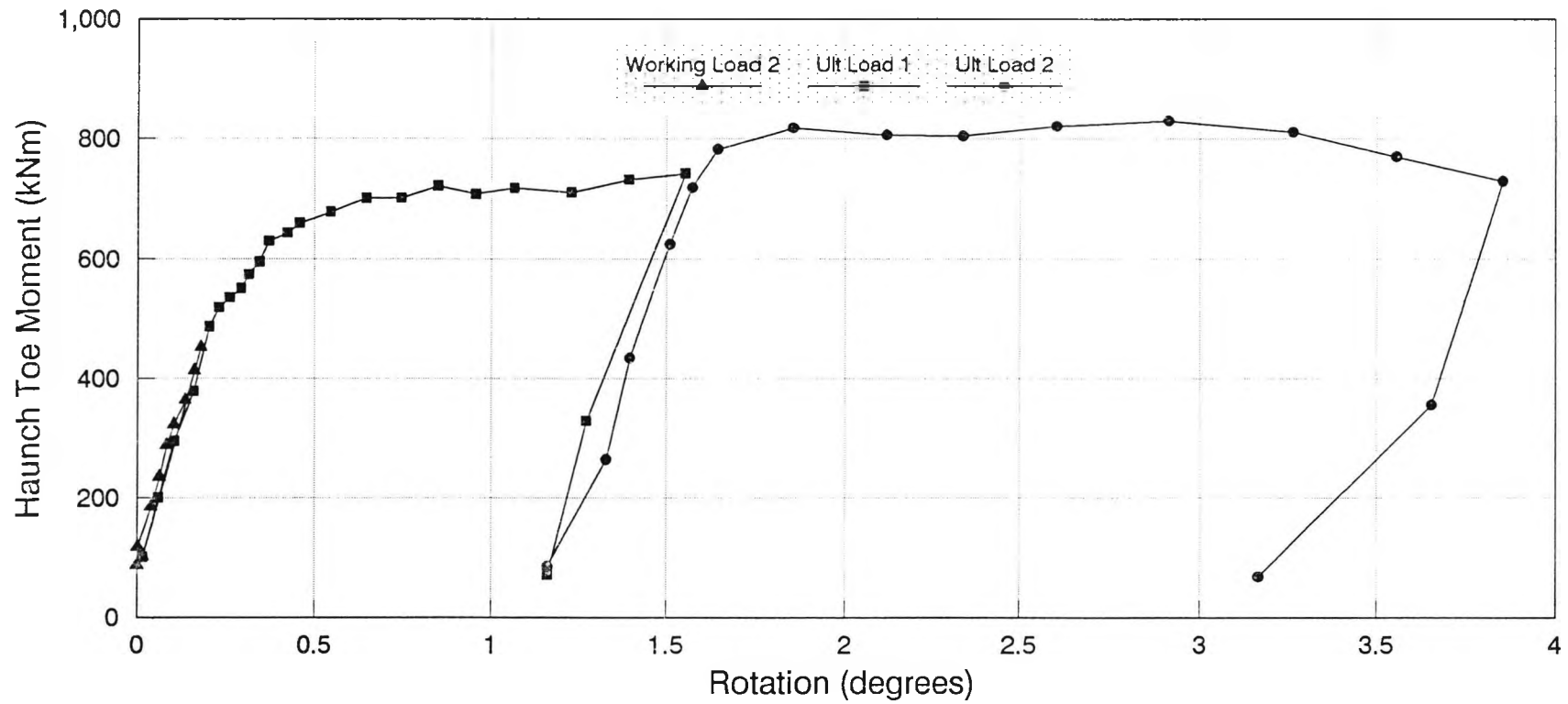


Figure 6.22 Main Beam Test - Haunch Toe B6 Moment/Rotation Characteristics

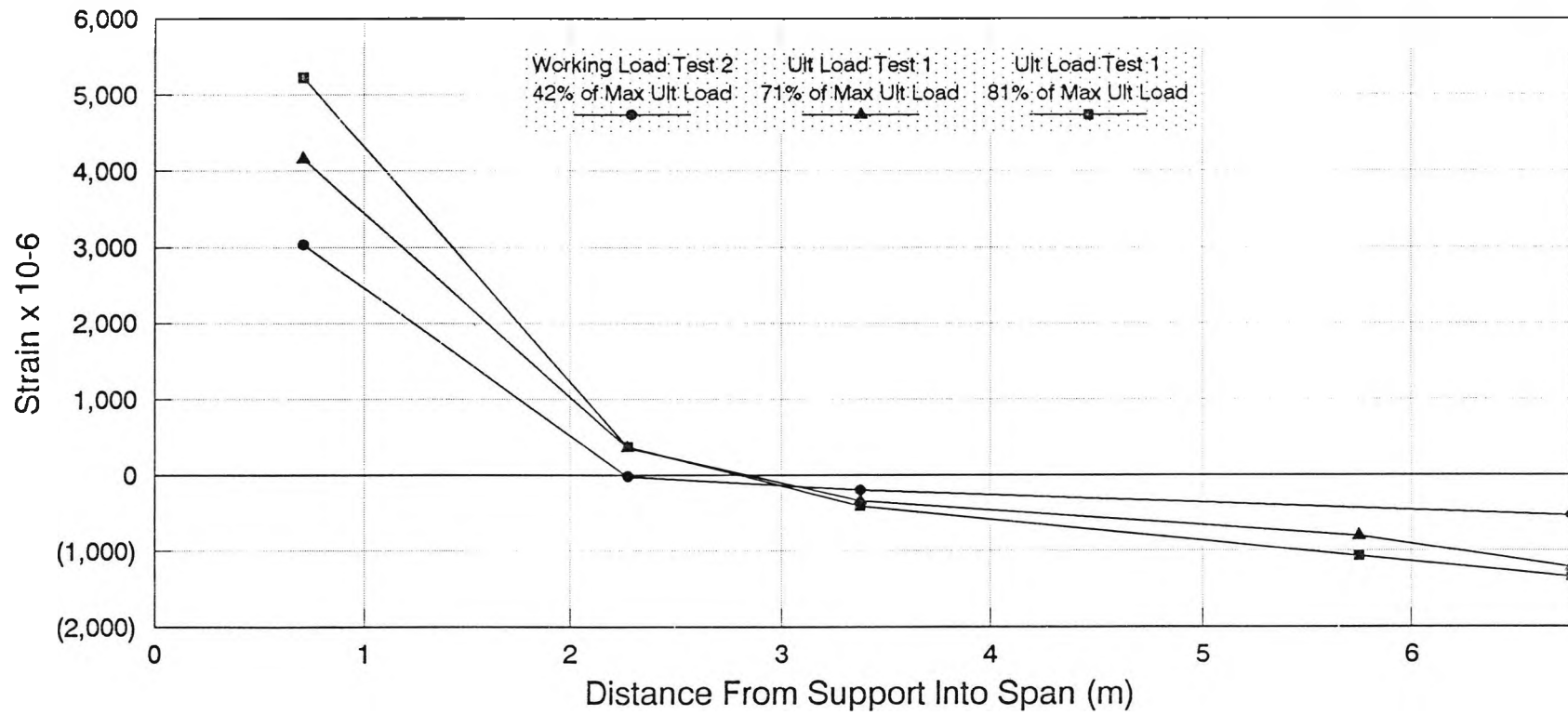
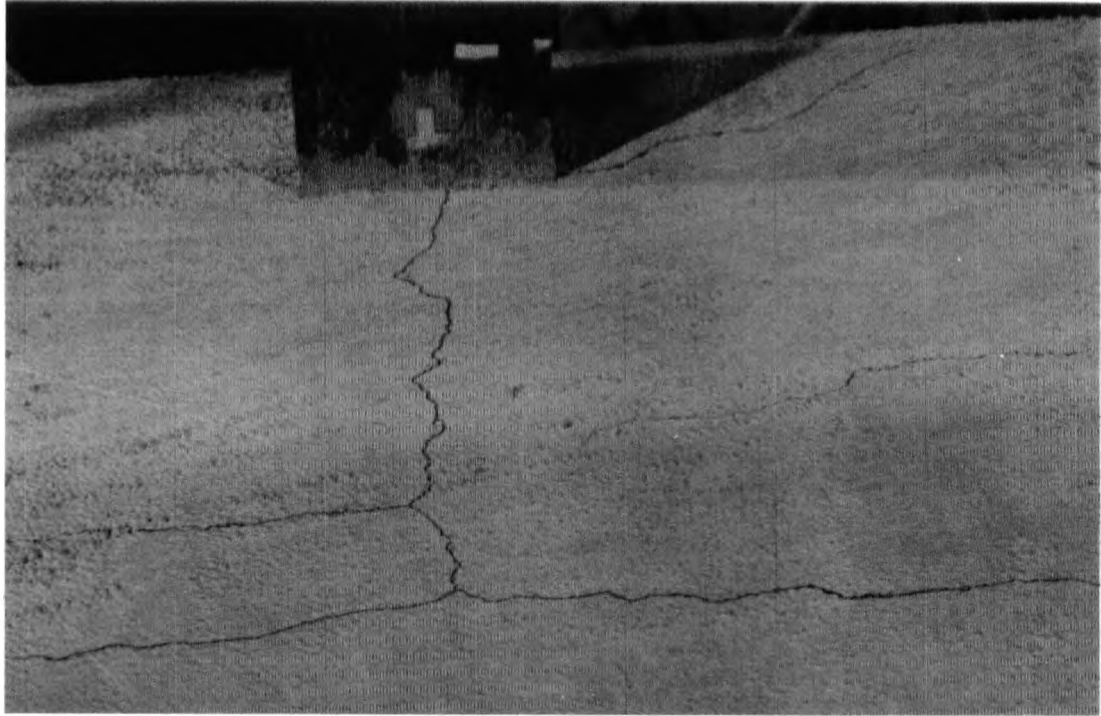
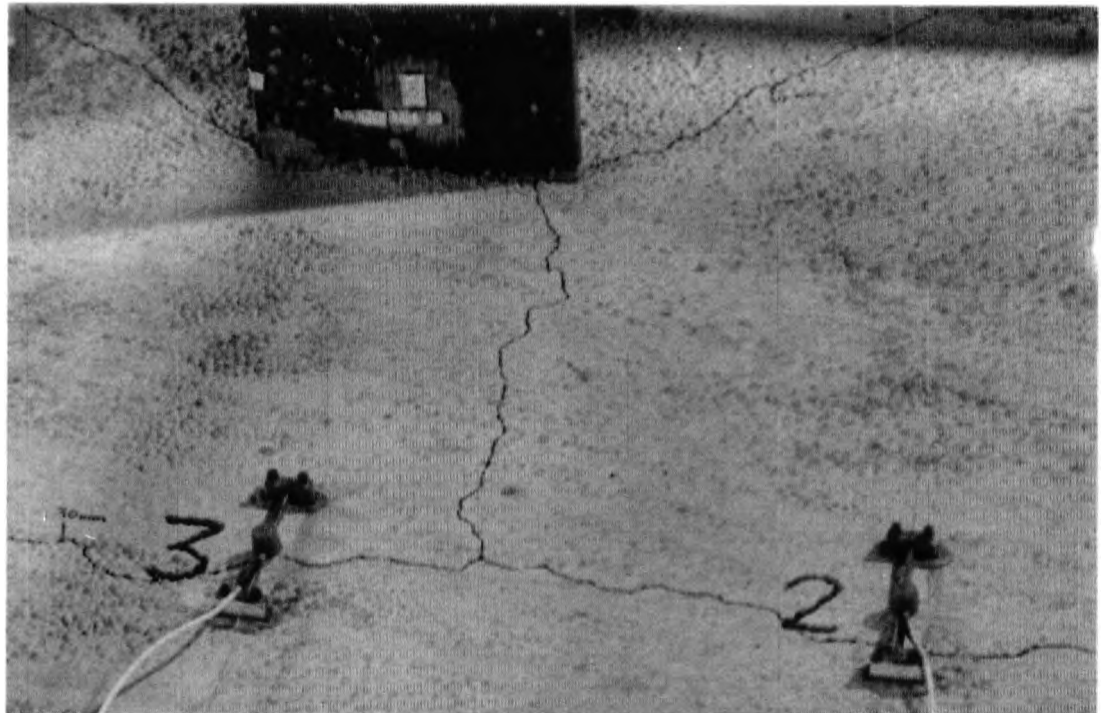


Figure 6.23 Main Beam Test - Typical Longitudinal Concrete Strain Profiles for Half of the Span



(a) Above Haunch B5



(b) Above Haunch B6

Figure 6.24 Main Beam Working Load Test 2 - Cracking in the Slab Above the Haunches

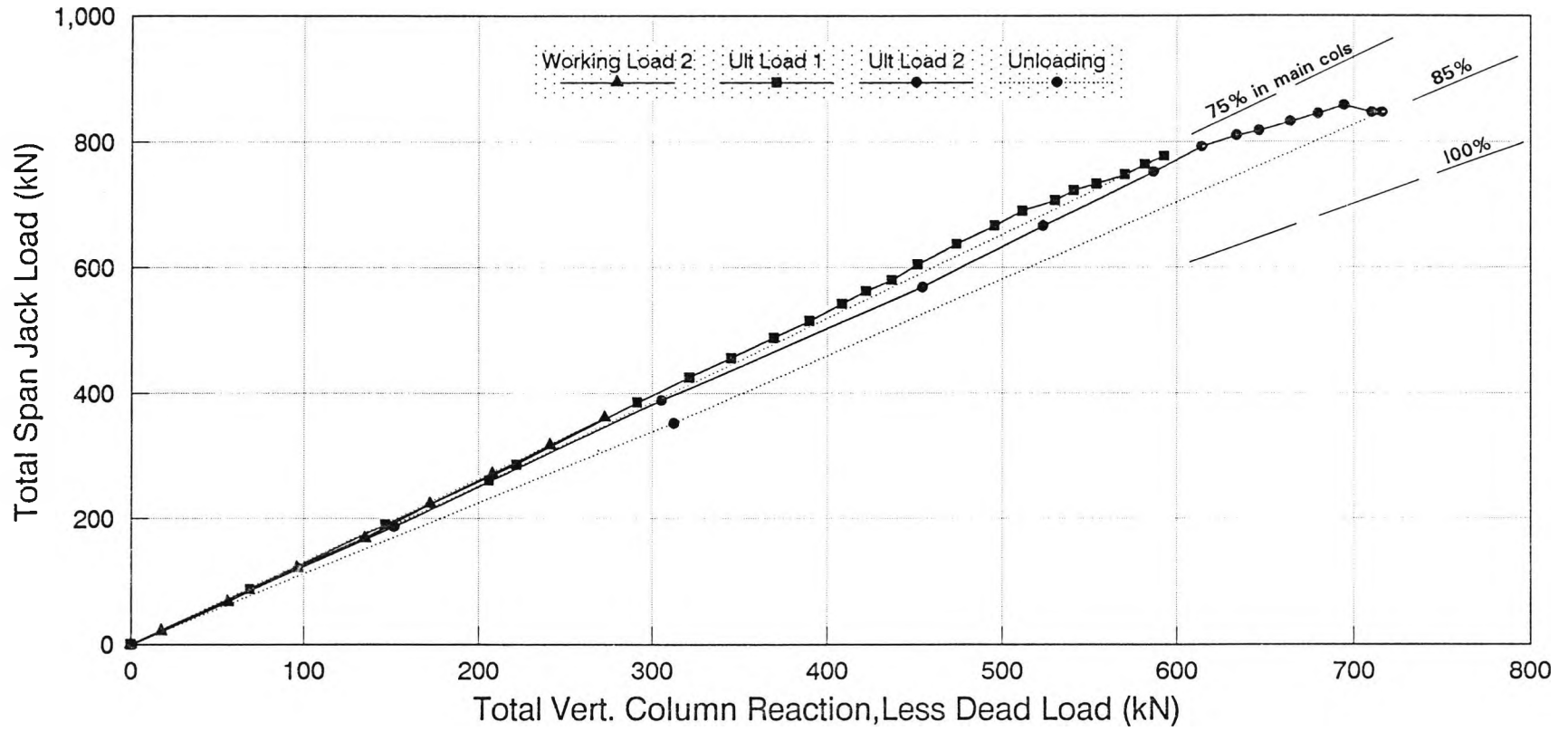
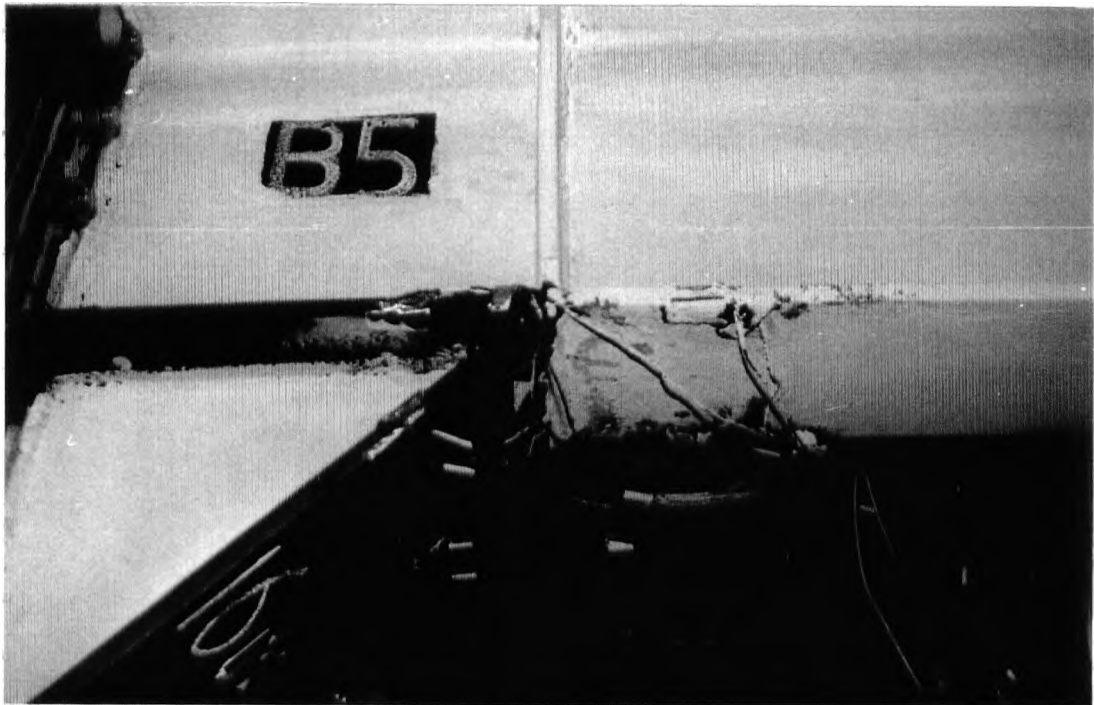


Figure 6.25 Main Beam Test - Degree of Span Load Supported by the Main Columns



(a) Haunch B5



(b) Haunch B6

Figure 6.26 Main Beam Ultimate Load Test 1 - Buckling and Yielding Adjacent to the Haunch Toes

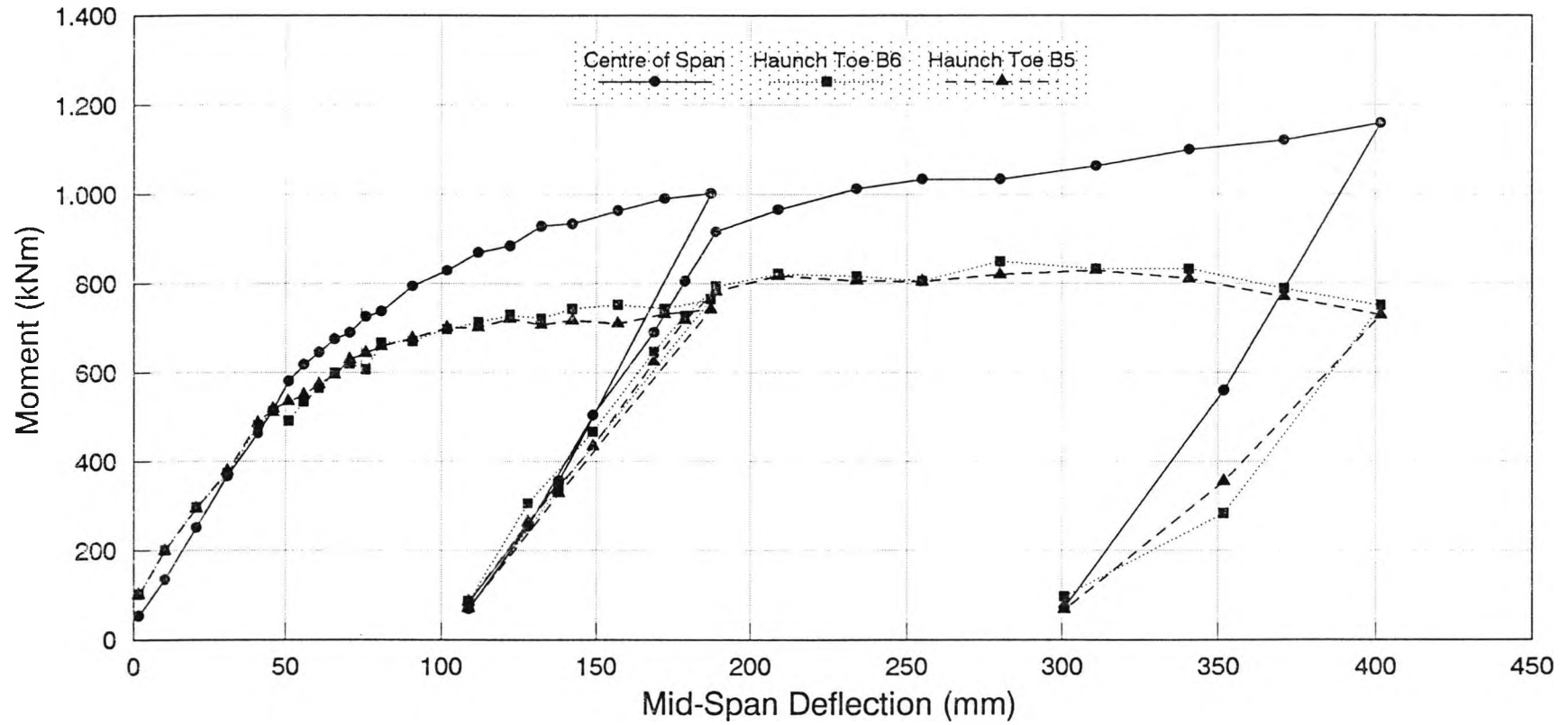


Figure 6.27 Main Beam Ultimate Load Tests 1&2 - Hinge Moments versus Mid-Span Deflection

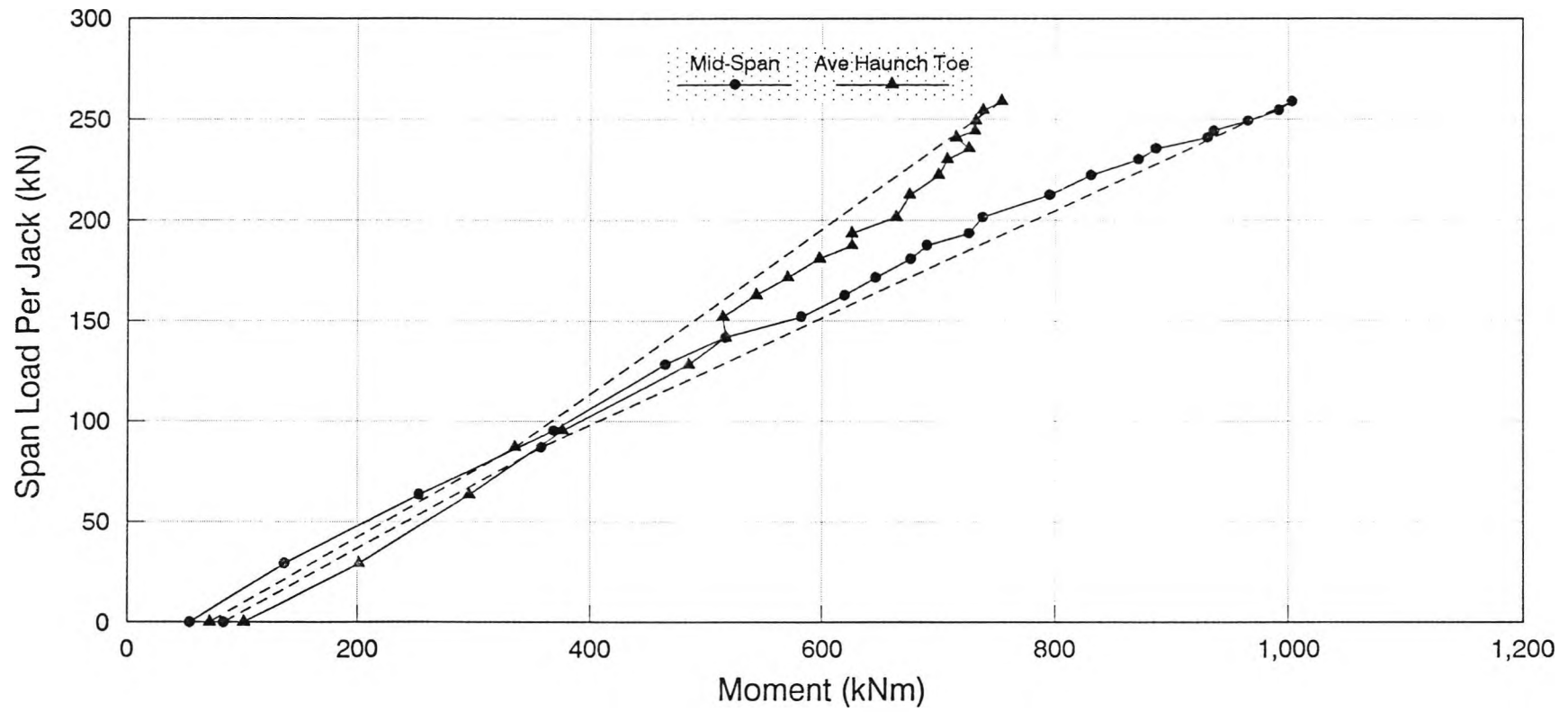


Figure 6.28 Main Beam Ultimate Load Test 1 - Growth of Moments at the Hinge Positions with Span Loading

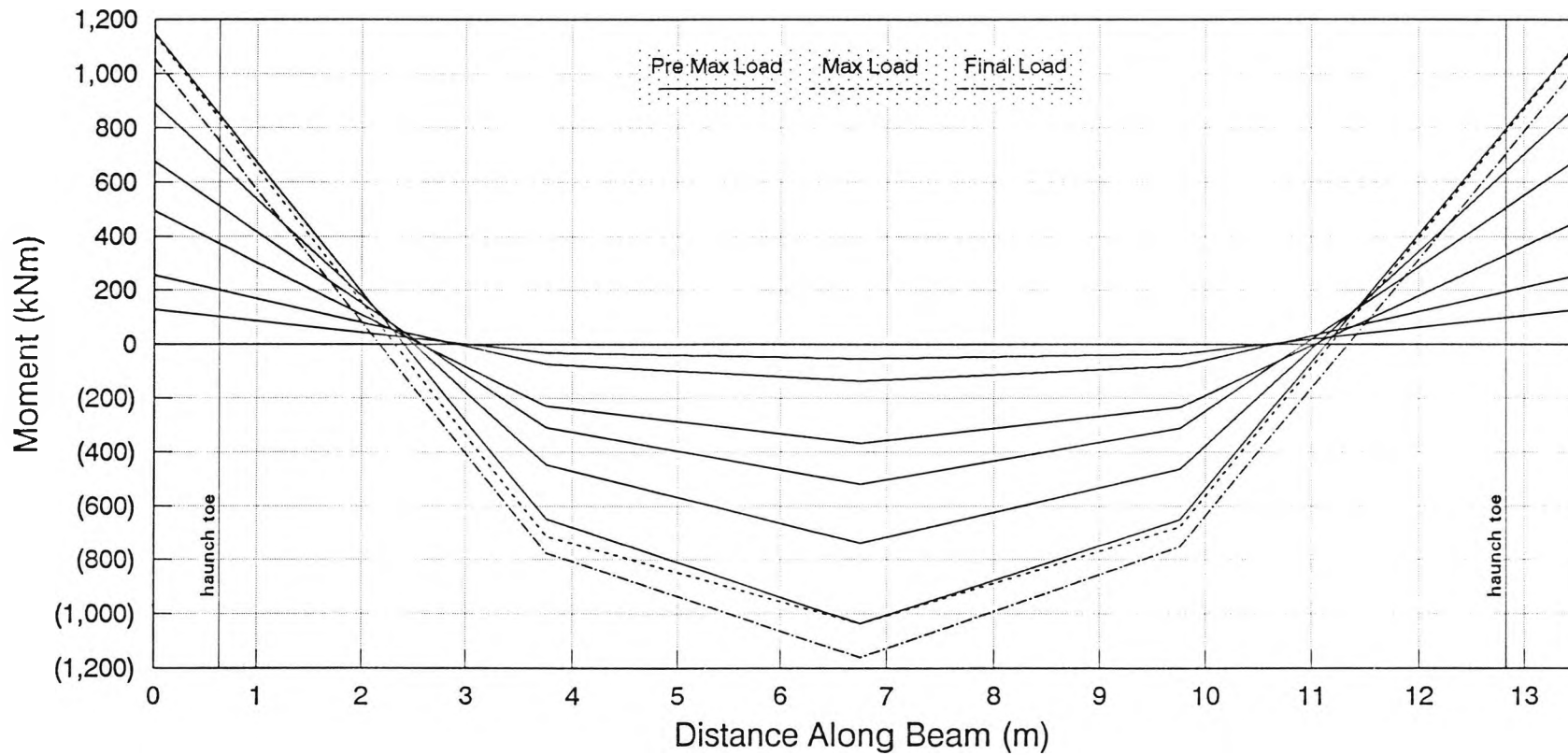


Figure 6.29 Main Beam Ultimate Load Tests 1&2 - Typical Bending Moment Profiles

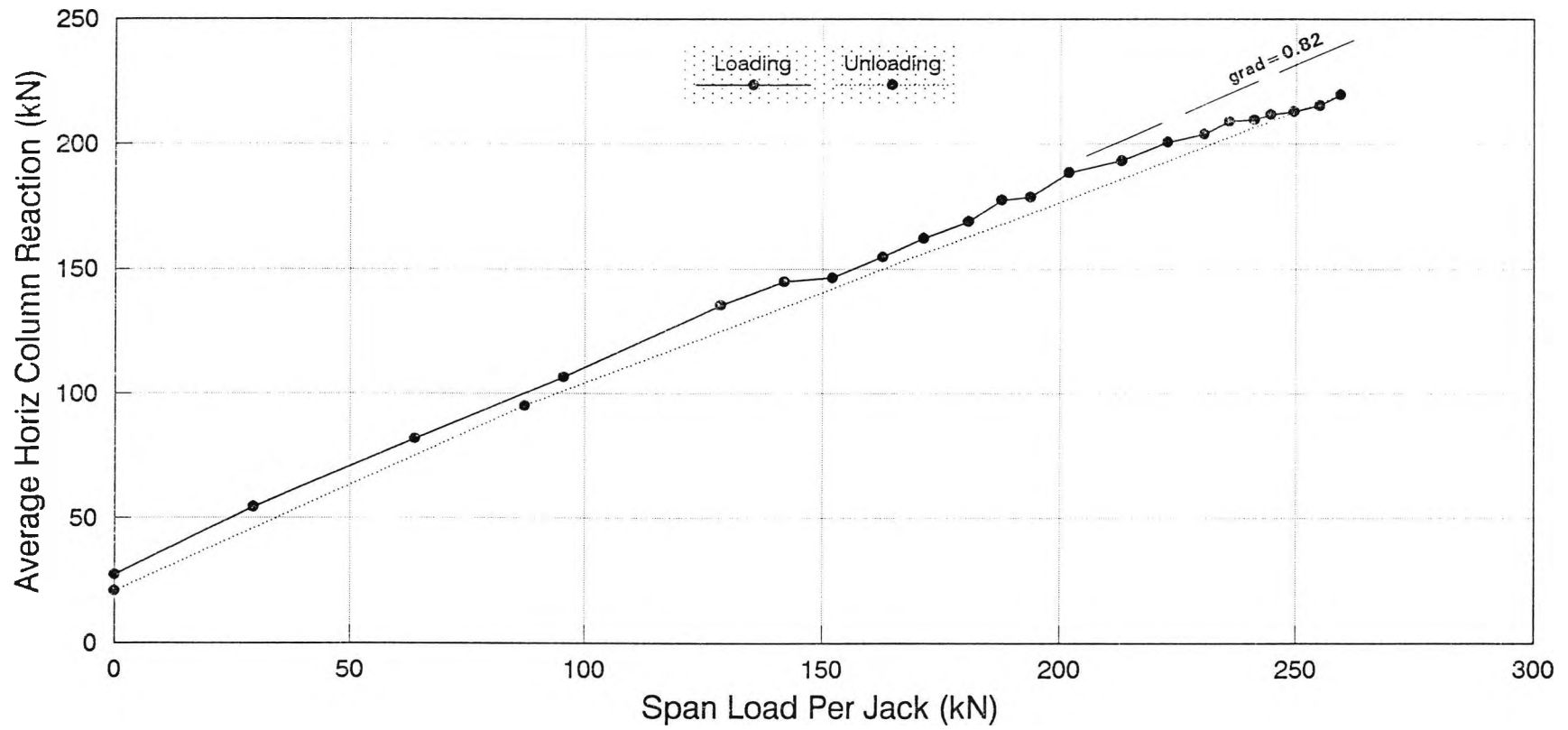
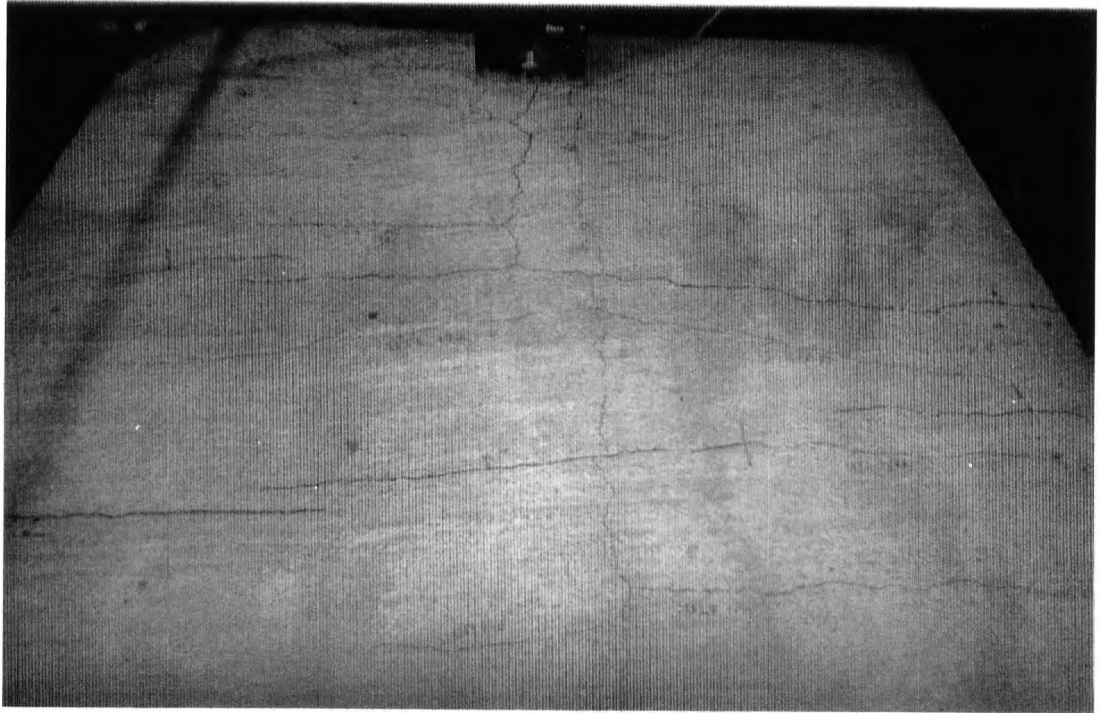
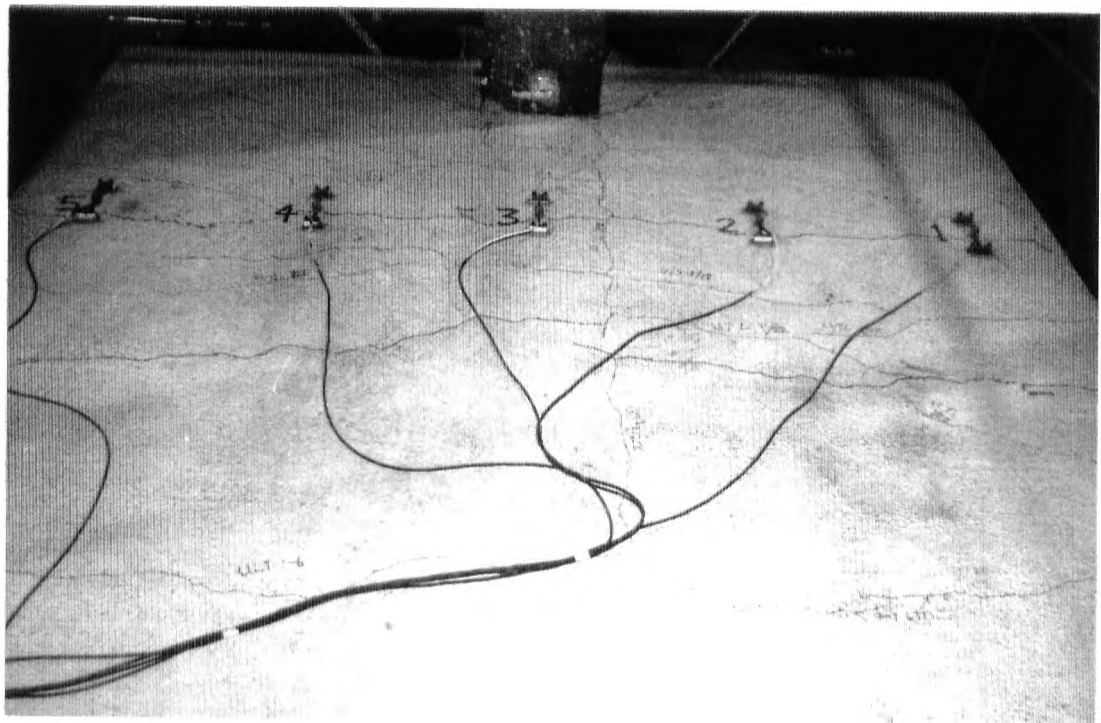


Figure 6.30 Main Beam Ultimate Load Test 1 - Growth of Horizontal Column Reactions with Span Loading



(a) Above Haunch B5



(b) Above Haunch B6

Figure 6.31 Main Beam Ultimate Load Test 2 - Cracking in the Slab



Figure 6.32 Main Beam Ultimate Load Test 2 - Diagonal Cracking in the Slab Close to Column C4

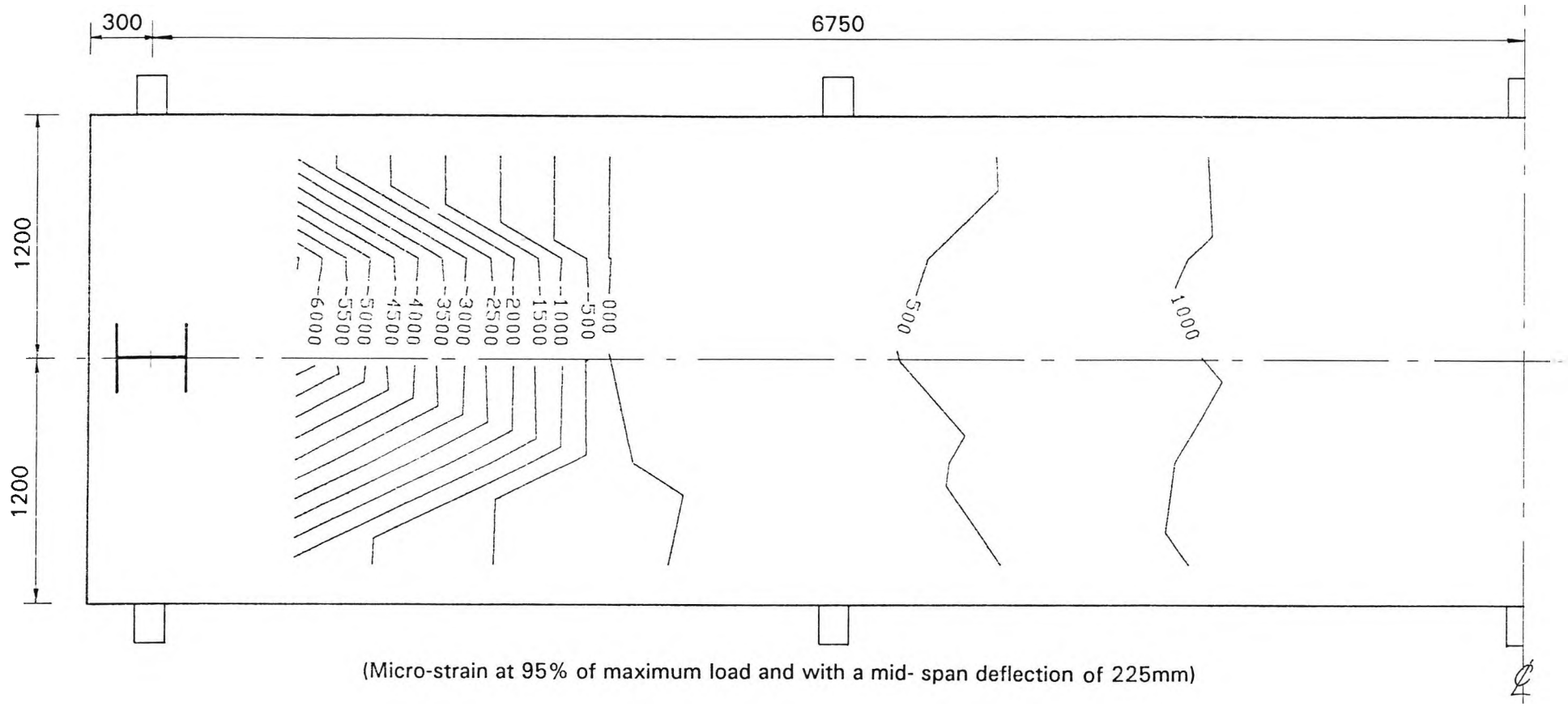
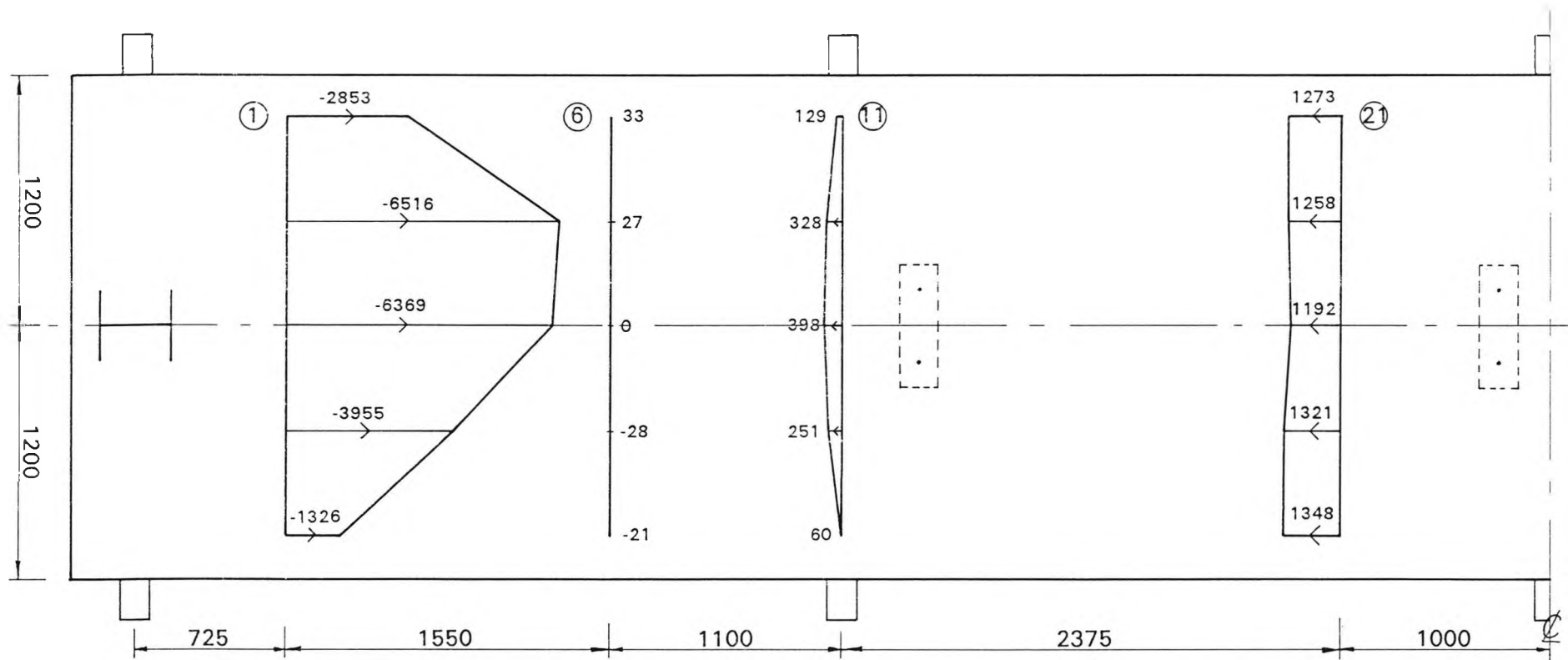


Figure 6.33 Main Beam Ultimate Load Test 2 - Concrete Longitudinal Strain Contours on Half of the Span



(Micro-strain at 95% of maximum load and with a mid-span deflection of 225mm)

Figure 6.34 Main Beam Ultimate Load Test 2 - Transverse Profiles of Longitudinal Concrete Strain

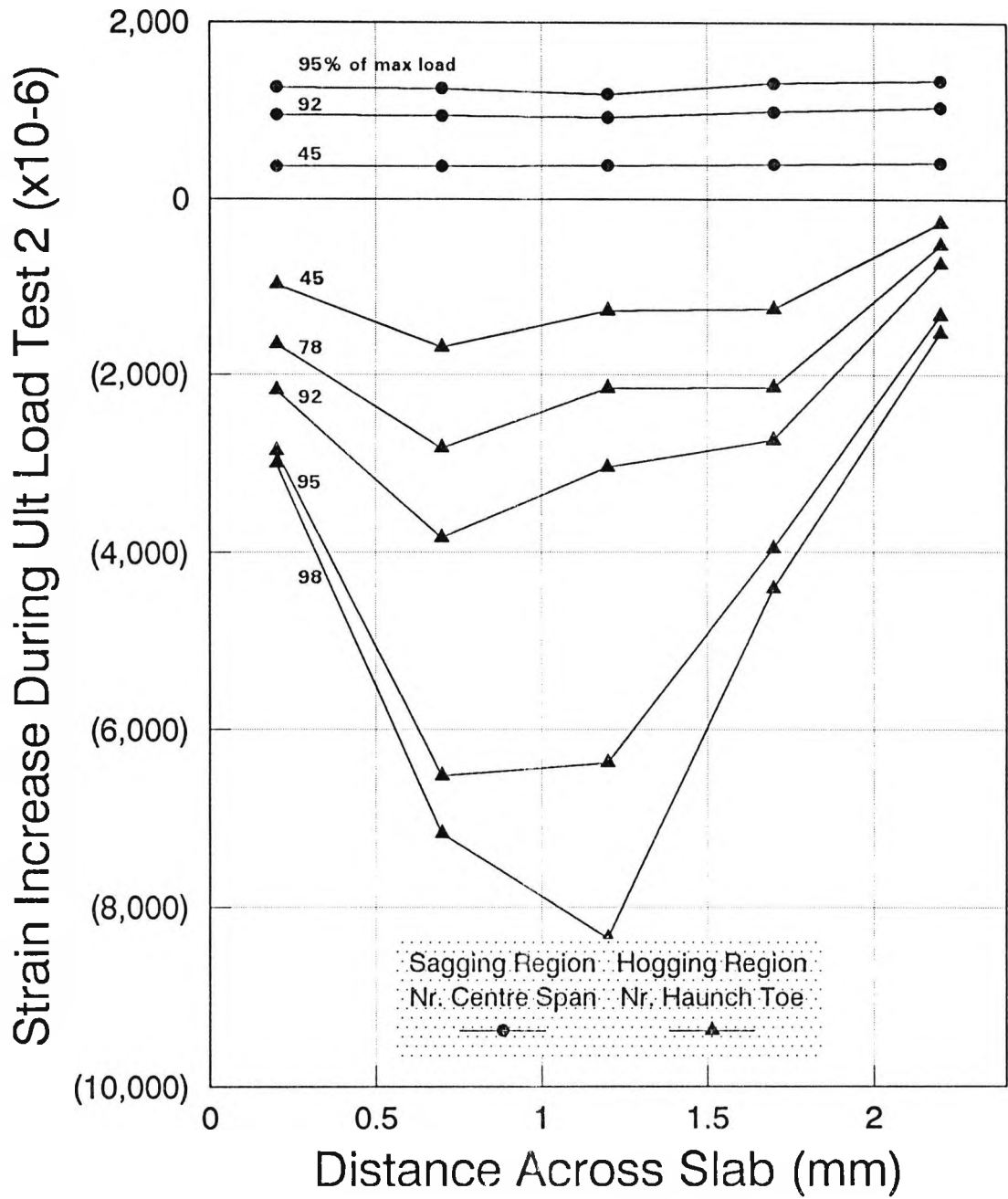


Figure 6.35 Main Beam Ultimate Load Test 2 - Transverse Concrete Strain Profiles

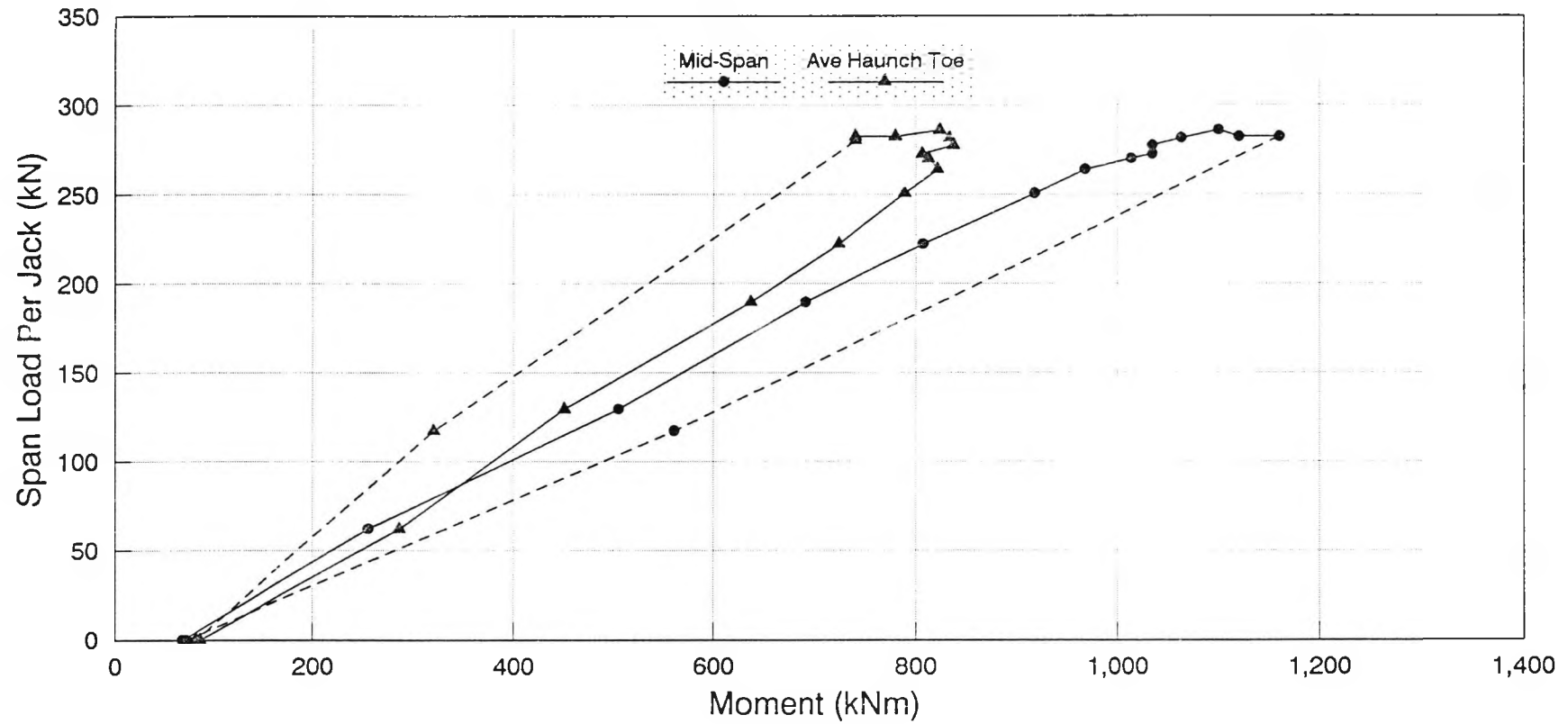
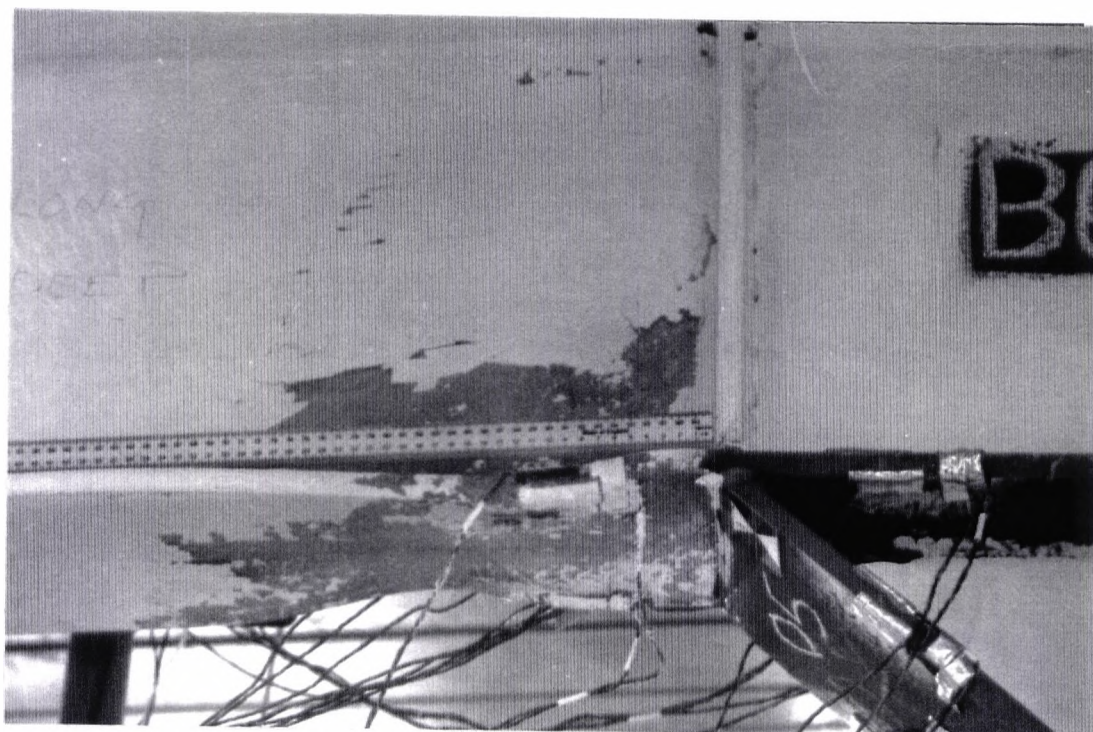


Figure 6.36 Main Beam Ultimate Load Test 2 - Growth of Moments at the Hinge Positions with Span Loading

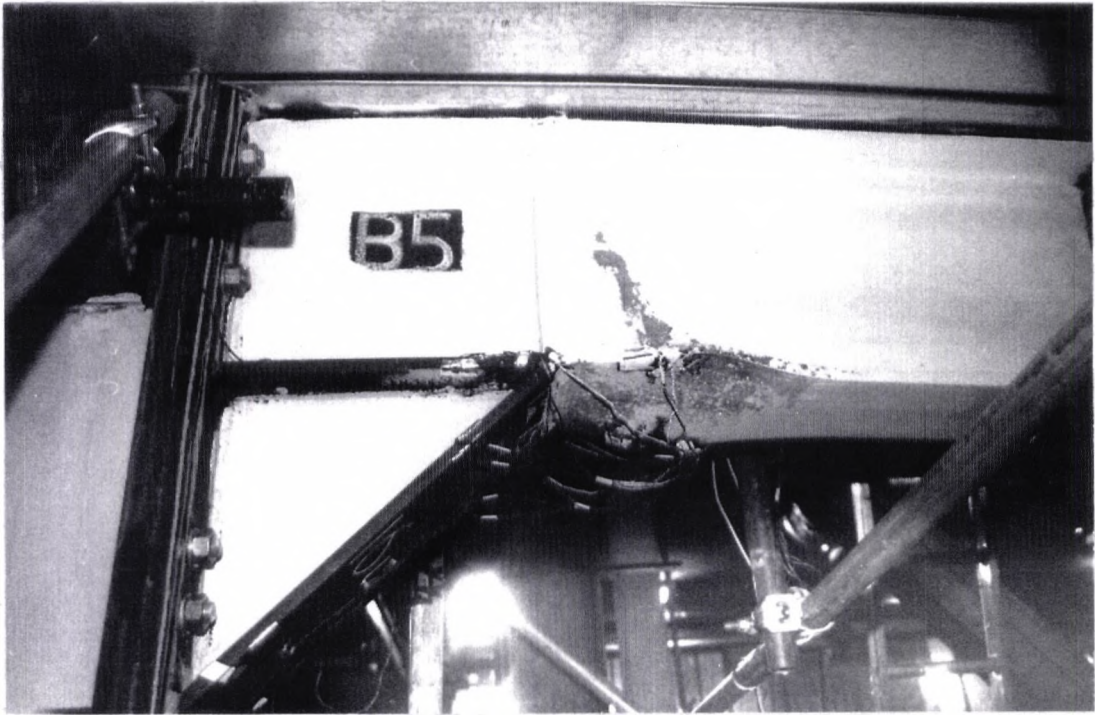


(a) Haunch B5

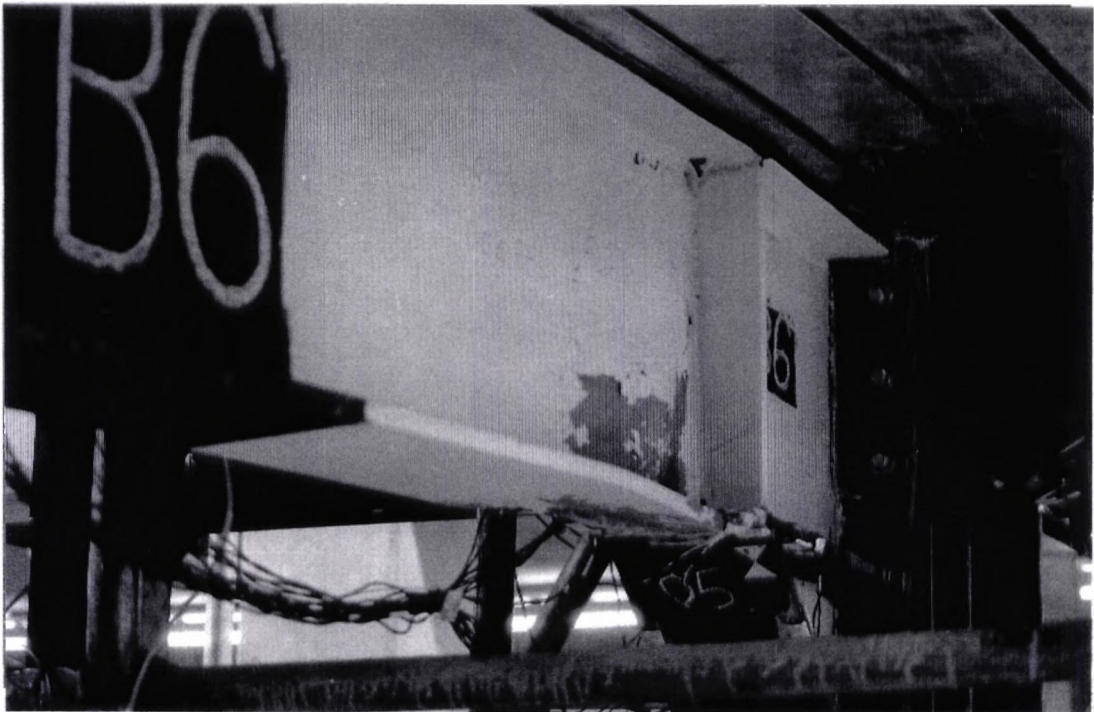


(b) Haunch B6

Figure 6.37 Main Beam Ultimate Load Test 2 - Buckling and Yielding Adjacent to the Haunch Toes



(a) Haunch B5



(b) Haunch B6

Figure 6.38 Main Beam Ultimate Load Test 2 - Beam Deformation Near the Haunches

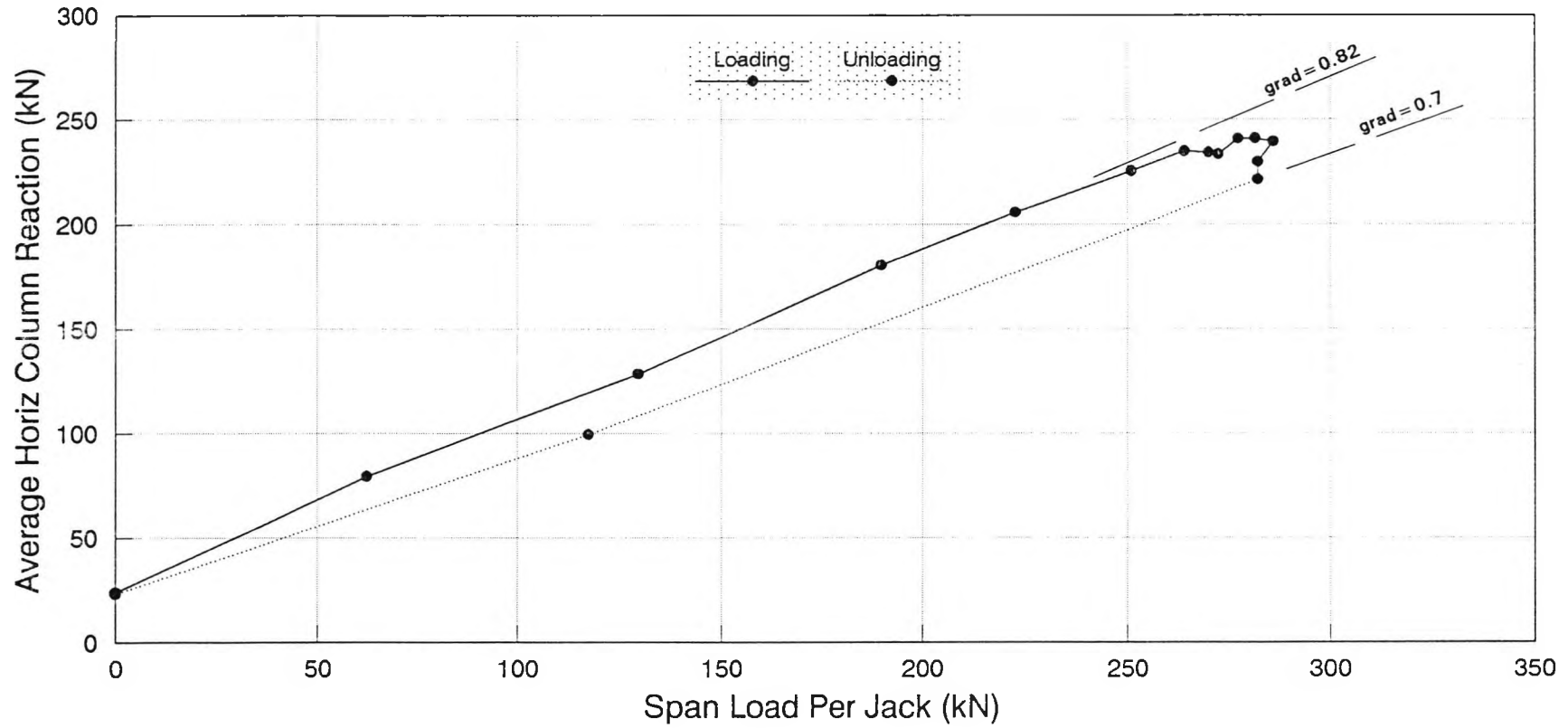


Figure 6.39 Main Beam Ultimate Load Test 2 - Growth of Horizontal Column Reactions with Span Loading

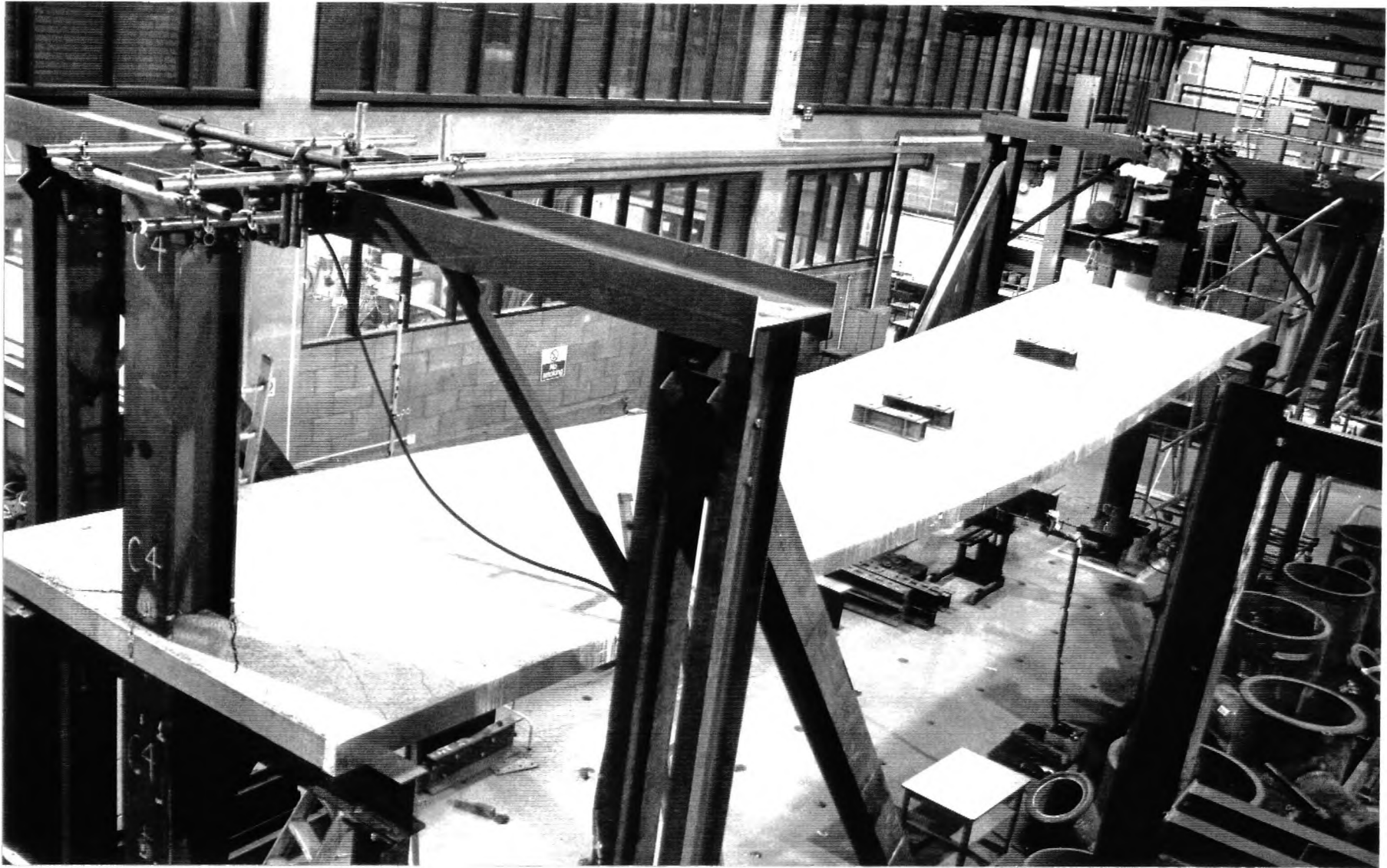


Figure 6.40 Main Beam Ultimate Load Test 2 - Final Deformation of Test Structure

APPENDIX 6A

ANALYSES OF MAIN BEAM DYNAMIC TEST

6A.1 Natural Frequency

Referring to Figure 6.17 the number of cycles between points 1 and 2 is 12. The time interval between these points is 1.9 seconds, hence the frequency

$$= \frac{12}{1.9} = \underline{6.3 \text{ Hz}}$$

For low damping, which is typical in steel structures, this is equivalent to the natural frequency {43}.

6A.2 Logarithmic Decrement

Let the ratio of the displacement magnitudes between successive peaks = x_r/x_{r+1} . Then the 'logarithmic decrement' is defined as

$$\delta = \left(\frac{x_r}{x_{r+1}} \right)$$

For displacement peaks x_r and x_{r+p} with n cycles between,

$$n \delta = \ell_n \left(\frac{x_r}{x_{r+p}} \right)$$

For the test, referring again to the figure, $x_r = 124$ units at point 1 and $x_{r+p} = 22.5$ units at point 2, and $n = 12$. Therefore

$$12 \delta = \ell_n \left(\frac{124}{22.5} \right) = 1.707$$

$$\underline{\underline{\delta = 0.142}}$$

6A.3 Damping Ratio

The damping ratio, γ , is a quantity which is intended to give an indication of the degree of damping relative to critical damping, ie., that which is severe enough to prevent any oscillation. It can be expressed in terms of the logarithmic decrement, such that

$$\delta = 2\pi\gamma (1 - \gamma^2)^{-1/2}$$

For small γ , such as in building structures, $\delta = 2\pi\gamma$. Hence for the test,

$$\underline{\underline{\gamma = 0.023}}$$

CHAPTER 7

THE COMPARISON OF THE MAIN BEAM TEST RESULTS WITH THEORY

7.1 DYNAMIC BEHAVIOUR

The dynamic test response of the main beam test (Figure 6.17) followed a classical harmonic decaying behaviour and the measured natural frequency, calculated in Appendix 6A, can be compared with the theoretical prediction. It is shown in Chapter 2 that the natural frequency, f , of a pin-ended 'H' frame can be calculated by the formula:

$$f = f_o \sqrt{\frac{(3\phi_c + 1)}{(0.6\phi_c + 1)}}$$

where f_o = natural frequency of a similar beam with simply-supported ends

and ϕ = $\frac{I_c L}{I_B h}$ and is defined in Chapter 2

f_o can be evaluated {26} from the following self-weight deflection formula quoted in Chapter 2

$$f_o = \frac{18}{\sqrt{y}} (H_z)$$

where y = maximum short term deflection due to the self-weight in mm

The total self-weight of the structure within the beam span was 100 kN. Therefore the self-weight deflection is given by:

$$y = \frac{5WL^3}{384EI}$$

Using the short-term second moment of area, calculated in the Appendix 7A,

$$y = \frac{5 \times 100 \times 13.5^3 \times 10^9}{384 \times 205 \times 83807 \times 10^4} = 18.6 \text{ mm,}$$

hence $f_o = \frac{18}{\sqrt{18.6}} = 4.17 \text{ Hz,}$

but $\phi_c = \frac{38700 \times 13.5}{83807 \times 2.35} = 2.65$

and therefore $f = 4.17 \sqrt{\frac{(3 \times 2.65 + 1)}{(0.6 \times 2.65 + 1)}}$

$$\underline{f = 7.74 \text{ Hz}}$$

This compares reasonably well with the test value of 6.3 Hz, but the difference might be due to a number of factors, including the neglect of the mass of the columns and reactant frames, which would have moved in sympathy, and, therefore, would have absorbed some energy. Also, the column end conditions were not strictly 'pins' because, although restrained by the jacks, at the bases they were also supported on rollers, which would have reduced the stiffness of the frame. Both these effects would have served to lower the natural frequency.

The damping ratio for the test can also be compared with suggested values for floors given in reference {26}. These values are quoted as follows:

$\gamma = 0.015$ is a lower limit for an unfurnished floor of composite deck construction

$\gamma = 0.03$ is for normal, open plan, well-furnished floors

$\gamma = 0.045$ is for a floor with partitions which effectively interrupt all relevant modes of vibration.

It is seen that the test value of 0.023 agrees well with these values as it lies between the first two cases.

7.2 ELASTIC BEHAVIOUR

The main beam test elastic behaviour was predicted with the use of computer analysis, whereby the frame was modelled by beam elements, as described in Chapter 8. Two cases were considered, one with a constant beam stiffness (Case 1), and one where the contribution of the concrete was neglected over the hogging region (Case 2). The exact length of the hogging region was determined by iteration to be 15% of the span, and this agrees reasonably well with the value from the test concrete strain profiles (Figure 6.21), where it is shown to be about 17% in the elastic stages.

For design, it was proposed in Chapter 2, that to allow for the effect of cracking in the hogging region, the beam end moments should be reduced by 10% when determining the serviceability limit states (except that of dynamic sensitivity). This can be examined in relation to the 'effective' stiffness that the rule implies by comparing it with the test behaviour, as now follows:

Using the following formula for the maximum beam deflection, δ_c , defined in Chapter 2, where:

$$\delta_c = \delta_o [1 - 0.6 (M_1 + M_2)/M_o],$$

together with the formula for the end moments in a pin-ended 'H' frame, also defined in Chapter 2, where:

$$M_{\text{support}} = \text{FEM} \times \frac{3\phi_c}{(3\phi_c + 1)},$$

a relationship can be found between δ_c and the maximum deflection, δ_{10} , in a beam whose end moments have been reduced by 10%. This can be shown to be:

$$\frac{\delta_c}{\delta_{10}} = \frac{(1-1.2\psi)}{1-1.08\psi}, \text{ where } \psi = \frac{\text{FEM} \times 3\phi_c}{M_o (3\phi_c + 1)}$$

Hence the influence of this rule on the deflection depends on the loading case and the relative member stiffeners.

For the test, $\phi_c = 2.65$ and $\psi = 0.548$,

$$\text{therefore } \frac{\delta_c}{\delta_{10}} = \frac{(1-1.12 \times 0.548)}{1-1.08 \times 0.548} = 0.839, \text{ or } \delta_{10} = 1.19\delta_c$$

ie, the deflections are predicted to increase by 19%. The computer analysis predicted a ratio of the maximum deflection to a span jack load of 0.266 for case 1. Hence, to include cracking according to the above rule, this would become 0.317. This modified stiffness has been superimposed on the load/deflection plot (Figure 6.20) and it is seen to lie between that for cases 1 and 2. Also, as the serviceability load level normally amounts to about 50% of the collapse load, because of partial safety factors, it is shown that this rule predicts the test behaviour extremely well up to this point, and, at least under these conditions, can be recommended.

A plot of the strain gauge readings in the form of beam cross-sectional strain profiles has been made and examples at several positions along the beam, at three different load levels, are illustrated in Figures 7.1. and 7.2. It can be seen that they confirm the observed curvature of the structure. They also confirm that the concrete above the haunch toes in the hogging regions is not effective at working load levels because the position of the neutral axes are close to the centre of the steel

section. At mid-span (Figure 7.2) the position of the neutral axis can be compared with theory and, using the short-term modulus, calculations in Appendix 7A.2 show that this lies 139 mm below the upper surface of the concrete. The test value at 42% of the maximum load agrees well with this and is shown to be 124 mm.

The apparent step in the strains between the steel beam and the concrete slab in the figures is due to two reasons. Firstly, the steel strain is mainly shown as cumulative strain, so there is an initial strain in the steel due to the non-composite dead load stage, whereas, at this point, the concrete strain is zero. Secondly, as the load increases, the efficiency of the shear connection decreases because of the flexibility of the shear connectors, therefore the strain in the concrete will lag behind that of the steel beam.

The ratio of the horizontal column reactions to a span jack load was predicted by the computer analysis to be 0.82 in the elastic state and, apart from the initial frictional effect which occurred in the Bedding-In test, this value was confirmed by the test results (see Figures 6.18, 6.30 and 6.39).

7.3 PLASTIC BEHAVIOUR

The test behaviour followed a very plastic path, which was shown clearly in Figure 6.20. The most important aspect, however, is whether or not the collapse load predicted by the theory was sustained. If it is assumed that the beam failed by simple plastic collapse, that is to say, that discrete hinges were formed at the haunch toes and at the mid-span, then, by using the yield strength values from the material tests, the plastic hinge resistances can be found and the collapse load predicted.

7.3.1 Haunch Toe Strength

The plastic moment of resistance of the bare steel beam section has been calculated in Appendix 7B.2 and was found to be 564kNm. This value would normally apply at haunch toe positions when no composite action is provided for, such as in this case. This value can be compared with the behaviour of the hinges, as shown in Figure 6.27, and it will be seen that a value of about 800kNm was

actually achieved. Clearly, therefore, the decking and the mesh must have been contributing to the strength, since strain hardening alone could not account for the difference. If these components are included over an effective breadth including only those decking sheets directly fixed to the main beam (ie. 1200mm), then the revised strength, which is calculated in Appendix 7B.4, is found to be 709.2kNm. Although this is 25% above the former value, it is still less than the test value, but this smaller difference may be explained by strain hardening of the components. The exact degree of strain at the underside of the haunch toes could not be ascertained during the latter stages of the test, because the onset of local buckling distorted the strain gauge readings and made them difficult to interpret reliably, but, at collapse, yield values were recorded in both the upper flanges.

The decline in the strength of the haunch toes, as explained in Chapter 6, was due to local buckling and not to distortional buckling. Therefore, an assessment of the strength based on consideration of the latter is really inappropriate, but it is interesting to calculate design values for comparison. If restraint is assumed to be provided by the web stiffeners at the haunch toe, and buckling is restricted to the length between the haunch toe and the first secondary beam, then, by using the proposed method outlined in Chapter 3, λ_{LT} is found to be 24.6, and the full M_p (532kNm) at the haunch toe can be achieved. However, if the unrestrained length is taken as the distance from the column to the secondary beam, ie, where no haunch restraint is assumed, then the design strength drops to $0.96M_p$. This represents only a slight decrease, but, if the section was less stocky, the reduction could be much greater. For either case the design strength is conservative.

It could be suggested that, had the decking run transversely to the main beam, the haunch toe strength would have been much less. This would no doubt be true, but, from the experience of the sub-assembly tests, which contained more slender sections, it is likely that M_p would still have been attained.

7.3.2 Mid-Span Composite Strength

An analysis of the capacity of the mid-span section has been undertaken in Appendix 7B.6 and the plastic moment of resistance was found to be 1131.5kNm.

This compares very well with the test values (Figure 6.27), which showed a steady increase throughout the test to 1160kNm, despite the later weakening of the beam as a whole. At the point of maximum load, the mid-span moment was 1100.5kNm.

The position of the plastic neutral axis (p.n.a) is predicted by calculations in Appendix 7B.5 to be 82.9mm above the upper steel flange, but from inspection of the mid-span section strain profile, shown in Figure 7.2, the p.n.a is shown by extrapolation to be about 47mm above the flange. However, this estimate is somewhat imprecise, because strain measurements within the depth of the concrete are really necessary to establish accurately the extent of the concrete compressive stress block, but the figure does show that, as the load increases, and yielding spreads in the beam, so the plastic neutral axis rises.

The degree of strain in the steel beam, as discussed in Chapter 6, was within the yield plateau at the maximum load, but the concrete strain was 20% below its yield value, and this might explain why the p.n.a. was apparently lower than predicted. As stated, this hinge therefore had a further slight reserve of strength, but it can be concluded that the theory does give a reasonable conservative estimate of its capacity.

7.3.3 Frame Strength

The collapse load can now be calculated according to plastic theory. Diagram 7.1, below, shows the equilibrium diagram for one half of the main span, and hinges are assumed exactly at the haunch toe and mid-span positions. The weakest section within the haunch toe areas in the test was not precisely at the haunch toes but within a depth D from them towards the mid-span. However, since design analyses do not normally take this into account, the slight improvement in strength that results from this effect will be ignored here also.

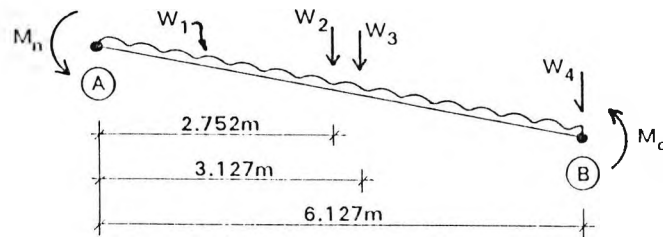


Diagram 7.1 Plastic Collapse Equilibrium Diagram for one Half of the Main Beam Span

- Let
- J = load from one beam jack (kN)
 - W_1 = weight of main beam = 0.73kN/m
 - W_2 = self weight point load from secondary beams = 19.8kN
 - W_3 = jacking load + jacking frame self weight = $(J + 2.5)$ kN
 - W_4 = {jacking load + central jacking frame self weight + secondary beam point load}/2
= $\{J + 5.6 + 19.8\}/2$ kN
 - M_n = haunch toe plastic moment of resistance (kNm)
 - M_c = mid-span plastic moment of resistance (kNm)

Referring to the diagram, by taking moments about point A, the collapse equation becomes:

$$M_n + M_c = \frac{(J + 19.8 + 5.6)}{2} \times 6.127 + (J + 2.5) \times 3.127 + 19.8 \times 2.752 + 0.73 \times 6.127^2/2$$

$$\therefore M_n + M_c = 153.8 + 6.19J$$

If M_n is assumed to be the bare steel beam strength, it is found that $J = 249.1$ kN. This leads to a test model factor for the maximum load of $286.1/249.1 = 1.15$. If, however, M_n includes the contribution from the decking and the mesh, it is found that $J = 272.5$ kN, which leads to a model factor of 1.05.

A design example, presented later in Appendix 9A, was based on the test frame dimensions and assumed a building grid of 13.5m x 6.0m, with the same steel sections. The design calculations show that a total unfactored main beam span load of 637.8kN could be supported, ie., $637.8/(13.5 \times 6.0) = 7.9\text{kN/m}^2$. However the total maximum load supported by the test beam was 837.1kN, ie., 10.3kN/m^2 , which represents a 30% margin over the design value.

The above figures show that where the decking in a frame runs parallel to the main beam and is positively fixed by shear connectors, it can make a significant contribution to the hogging region strength, which would be grossly underestimated by assuming that the bare steel beam section acts alone. It is not recommended that the strength of the mesh be included for design purposes, because, although it did not break in this test, it has done so in others, and its ductility cannot be relied upon. The above results also confirm that the positive moment composite strength can be satisfactorily predicted, which, when the decking strength is included in the negative moment-regions, leads to a reasonable estimate of the frame strength.

Little eventual redistribution of the moments took place at the maximum load because the haunch toe hinges were much stronger than originally anticipated, but the test showed that 3° of rotation was still necessary to support the maximum load.

APPENDIX 7A

MAIN BEAM TEST ELASTIC SECTION PROPERTIES

7A.1 Short-Term Uncracked Composite Stiffness

The composite beam stiffness, I_g , is given in {14} by the equation

$$I_g = I_x + \frac{B_e (D_s - D_p)^3}{12 \alpha_e} + \frac{A B_e (D_s - D_p) (D + D_s + D_p)^2}{4 \{A \alpha_e + B_e (D_s - D_p)\}}$$

where	A	=	area of section
	B_e	=	effective concrete flange breadth
	D	=	depth of steel section
	D_p	=	overall depth of profiled decking
	D_s	=	overall depth of slab
	I_x	=	major axis second moment of area of steel section
	α_e	=	modular ratio of steel to concrete

NB. The effective breadth of the concrete is taken as the value recommended in {14}, calculated as follows:

$$B_e = 0.7 \times \frac{13500}{4} = 2363\text{mm}$$

This is very close to the actual test value of 2400mm.

Therefore, for the test, using the short-term modular ratio for lightweight concrete of 10,

$$I_g = 27300 + \frac{2363 (130 - 51)^3}{12 \times 10 \times 10^4}$$

$$+ \frac{95 \times 10^2 \times 2363 (130 - 51) (413 + 130 + 51)^2}{4 \{95 \times 10^2 \times 10 + 2363 (130 - 51)\} \times 10^4}$$

$$\underline{I_g = 83807 \text{ cm}^4}$$

7A.2 Composite Uncracked Section - Elastic Neutral Axis Position

For an uncracked composite beam, the depth of the neutral axis below the top of the concrete flange, y_g , based on short-term properties, is given in {14} by:

$$y_g = \frac{A \cdot \alpha_e (D + 2D_s) + B_e (D_s - D_p)^2}{2 \{A \cdot \alpha_e + B_e (D_s - D_p)\}}$$

Therefore, for the test,

$$y_g = \frac{95 \times 10^2 \times 10 (413 + 2 \times 130) + 2363 (130 - 51)^2}{2 \{95 \times 10^2 \times 10 + 2400 (130 - 51)\}}$$

$$\underline{y_g = 138.6 \text{ mm}}$$

APPENDIX 7B

MAIN BEAM TEST PLASTIC SECTION PROPERTIES - USING MEASURED DIMENSIONS

7B.1 Bare Steel Section - Plastic Neutral Axis Position

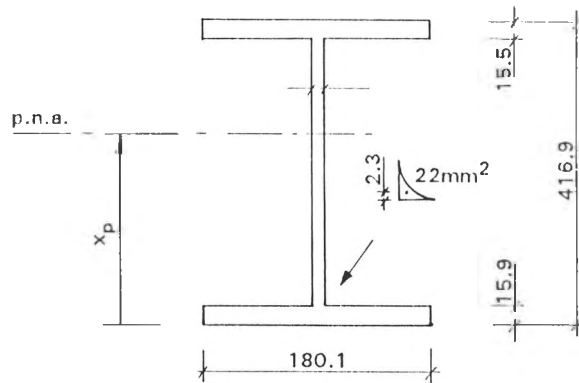


Diagram 7B.1 Main Beam Test - Bare Steel Section

Let x_p = distance from u/side of bottom flange to p.n.a.
 σ_f = yield stress in the flanges
 σ_w = yield stress in the web

By equating forces above and below the p.n.a, but neglecting the fillets:

$$180.1 \times 15.9 \sigma_f + 9.5 (x_p - 15.9) \sigma_w$$

$$= 180.1 \times 15.5 \sigma_f + 9.5 (416.9 - 15.5 - x_p) \sigma_w$$

Hence $x_p = \frac{3964.4 \sigma_w - 72 \sigma_f}{19 \sigma_w}$

But from the materials tests (Chapter 6)

$$\sigma_f = 366.9 \text{N/mm}^2; \sigma_w = 401.6 \text{N/mm}^2$$

$$\therefore \underline{\underline{x_p = 205.2 \text{mm}}}$$

7B.2 Bare Steel Section - Plastic Moment of Resistance

Referring to Diagram 7B.1 and taking moments about the plastic neutral axis:

$$\begin{aligned}M_p &= 180.1 \times 15.9 (205.2 - 15.9/2) \times 366.9 \\&+ 9.5 \frac{(205.2 - 15.9)^2}{2} \times 401.6 \\&+ 9.5 \frac{416.9 - 205.2 - 15.5)^2}{2} \times 401.6 \\&+ 180.1 \times 15.5 (416.9 - 205.2 - 15.5/2) \times 366.9 \\&+ 2 \times 22 (416.9 - 205.2 - 15.5 - 2.3) \times 366.9 \\&+ 2 \times 22 (205.2 - 15.9 - 2.3) \times 366.9 \\&= (207.0 + 68.2 + 73.6 + 209.1 + 3.1 + 3.0) \times 10^6 \text{Nmm}\end{aligned}$$

$$\therefore \underline{M_p = 564.0 \text{kNm}}$$

7B.3 Combined Section (Steel Beam + Decking + Mesh) - Plastic Neutral Axis Position

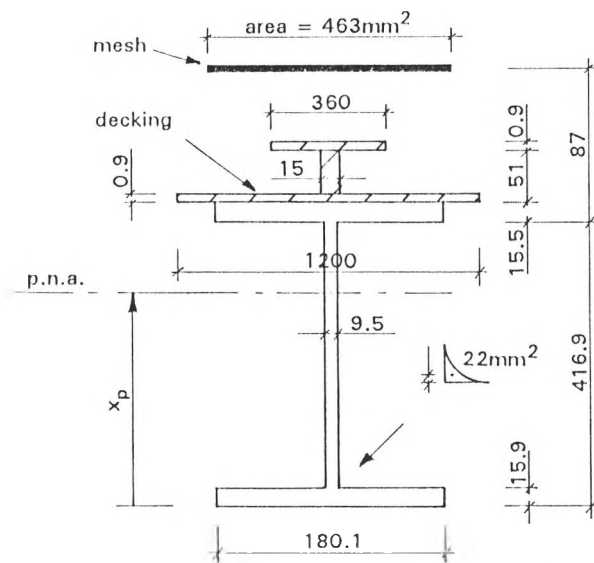


Diagram 7B.2 Main Beam Test - Combined Section (Steel Beam + Decking + Mesh)

Assume that only two decking sheet widths are effective because only two were rigidly connected to the steel beam by shear connectors.

- Let x_p = distance from u/side of bottom flange to p.n.a
 σ_d = yield stress in decking
 σ_m = yield stress in mesh

As before, by equating forces above and below the p.n.a but neglecting the fillets:

$$\begin{aligned}
 & 180.1 \times 15.9 \sigma_f + 9.5 (x_p - 15.9) \sigma_w \\
 & = 180.1 \times 15.5 \sigma_f + 9.5 (416.9 - 15.5 - x_p) \sigma_w \\
 & + 1200 \times 0.9 \sigma_d + 15 \times 51 \sigma_d + 360 \times 0.9 \sigma_d + 436 \sigma_m
 \end{aligned}$$

Hence $x_p = \frac{3964 \sigma_w - 72 \sigma_f + 2169 \sigma_d + 463 \sigma_m}{19 \sigma_w}$

But from the materials tests (Chapter 6)

$$\sigma_f = 366.9\text{N/mm}^2, \sigma_w = 401.6\text{N/mm}^2, \sigma_d = 245\text{N/mm}^2 \text{ and} \\ \sigma_m = 425\text{N/mm}^2$$

$$\therefore \underline{\underline{x_p = 300.6\text{mm}}}$$

7B.4 Combined Section (Steel Beam + Decking + Mesh) - Plastic Moment of Resistance

Referring to Diagram 7B.2 and taking moments about the plastic neutral axis:

$$\begin{aligned}
 M_p &= 180.1 \times 15.9 (300.1 - 15.9/2) \times 366.9 \\
 &+ 9.5 \frac{(300.1 - 15.9)^2}{2} \times 401.6 \\
 &+ 9.5 \frac{416.9 - 300.1 - 15.5)^2}{2} \times 401.6 \\
 &+ 180.1 \times 15.5 (416.9 - 300.1 - 15.5/2) \times 366.9 \\
 &+ 2 \times 22 (416.9 - 300.1 - 15.5 - 2.3) \times 366.9 \\
 &+ 2 \times 22 (300.1 - 15.9 - 2.3) \times 366.9 \\
 &+ 1200 \times 0.9 (0.9/2 + 416.9 - 300.1) \times 245 \\
 &+ 15 \times (51 - 0.9)((51 - 0.9)/2 + 0.9 + 416.9 - 300.1) \times 245 \\
 &+ 360 \times 0.9 (0.9/2 + 51 + 416.9 - 300.1) \times 245 \\
 &+ 463 (87 + 416.9 - 300.1) \times 425 \\
 &= (306.9 + 154.1 + 195.8 + 111.7 + 1.6 + 4.6 + 31.0 + \\
 &26.3 + 13.4 + 40.1) \times 10^6 \text{Nmm}
 \end{aligned}$$

$$\underline{\underline{\therefore M_p = 709.2 \text{kNm}}}$$

7B.5 Composite Section at Mid-Span - Plastic Neutral Axis Position

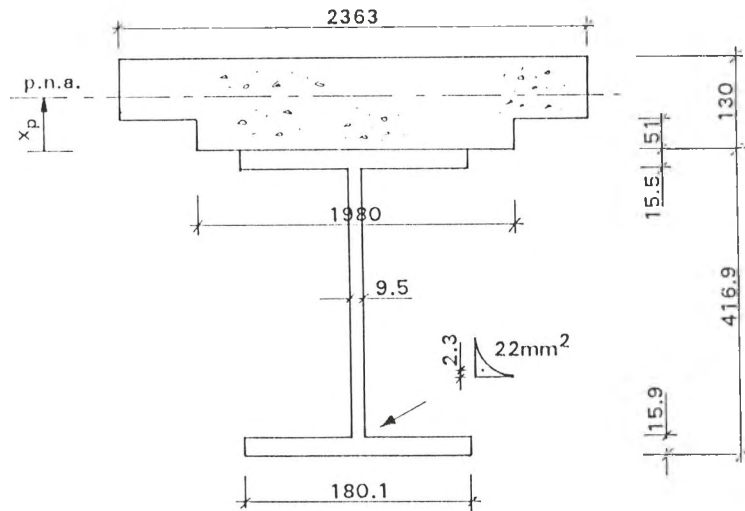


Diagram 7B.3 Main Beam Test - Composite Section at Mid-Span

Let x_p = distance from top of upper steel flange to p.n.a
 f_{cu} = cube strength of concrete

NB. As before, the effective breadth of the concrete is assumed to be the value recommended in {14}, which is very close to the actual value.

By equating forces above and below the p.n.a:

$$180.1 (15.5 + 15.9) \sigma_f + 9.5 (416.9 - 15.5 - 15.9) \sigma_w + 4 \times 22 \sigma_f = 2363 (130 - x_p) \times 0.67 f_{cu}$$

$$\therefore x_p = \frac{205817 f_{cu} - 5743 \sigma_f - 3662 \sigma_w}{1583 f_{cu}}$$

But from the material tests (Chapter 6)

$$\sigma_f = 366.9 \text{ N/mm}^2, \sigma_w = 401.6 \text{ N/mm}^2 \text{ and } f_{cu} = 48 \text{ N/mm}^2$$

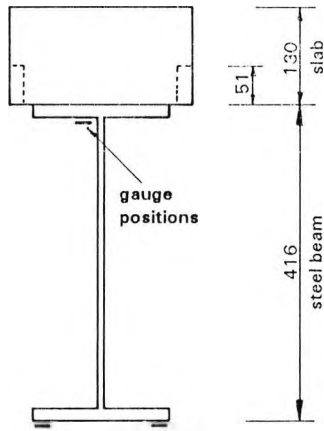
$$\therefore x_p = \underline{\underline{82.9 \text{ mm}}}$$

7B.6 Composite Section at Mid-Span - Plastic Moment of Resistance

Referring to Diagram 7B.3 and taking moments about the top of the upper steel flange.

$$\begin{aligned}M_p (= M_c) &= 2363 (130 - 82.9) ((130 - 82.9)/2 + 82.9) \times 0.67 \times 48 \\&+ \frac{180.1 \times 15.5^2}{2} \times 366.9 \\&+ 9.5 (461.9 - 15.5 - 15.9)((416.9 - 15.5 - 15.9)/2 + 15.5) \\&\quad \times 401.6 \\&+ 180.1 \times 15.9 (416.9 - 15.9/2) \times 366.9 \\&+ 2 \times 22 (416 - 15.9 - 2.3) \times 366.9 \\&+ 2 \times 22 (15.2 - 2.3) \times 366.9 \\&= (381 + 7.9 + 306.2 + 429.7 + 6.4 + 0.3) \times 10^6 \text{Nmm}\end{aligned}$$

$$\therefore \underline{M_c = 1131.5 \text{kNm}}$$

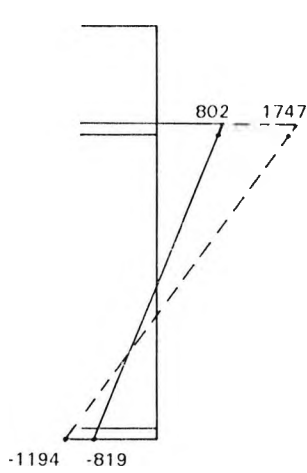


Elastic Composite
Beam Section

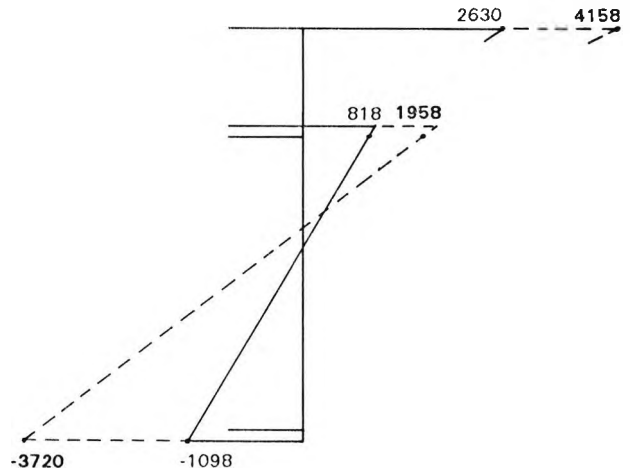
Key

— Cumulative strain $\times 10^{-6}$ at 42% of max load
 - - - " " " " 71% " " "

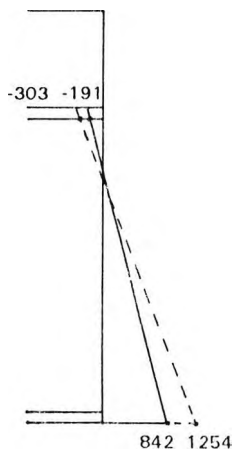
(negative Strain = compression)



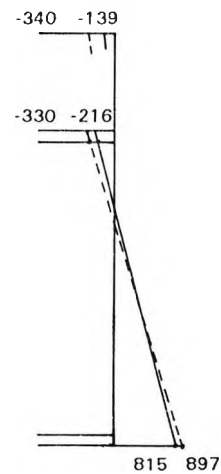
Near Haunch Toe B5
(gauges 4,7&8)



Near Haunch Toe B6
(gauges 26,30&31)



At 1/4 Point Near B5
(gauges 15,16&17)



At 1/4 Point Near B6
(gauges 21,22&23)

Figure 7.1 Typical Cross-Sectional Strain Diagrams for Selected Positions Along the Main Beam

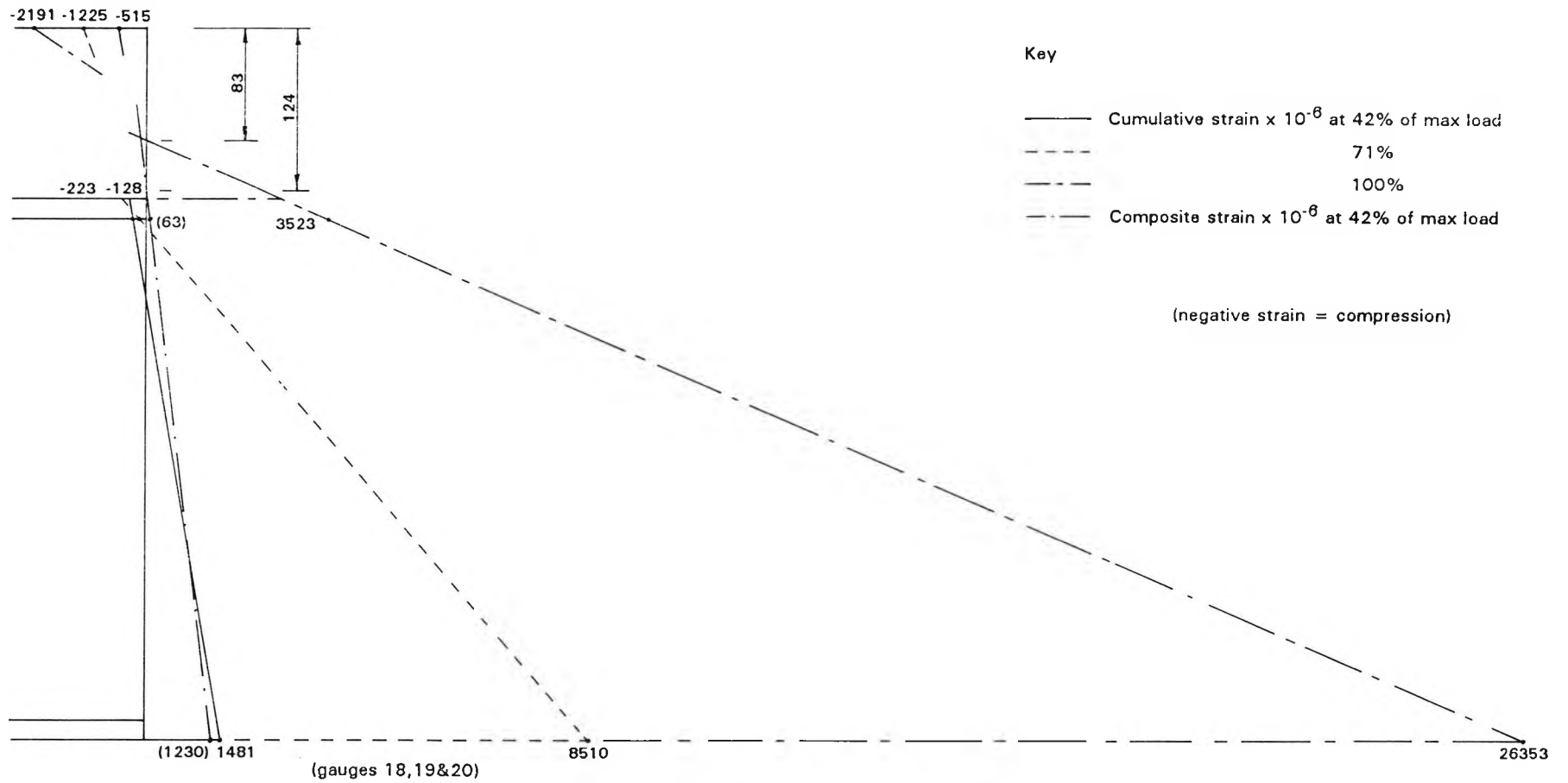


Figure 7.2 The Cross-Sectional Strain Diagram at the Main Beam Mid-Span Position

CHAPTER 8

COMPUTER STUDIES

8.1 INTRODUCTION

A finite element computer study was carried out by Dr Qiao Li under my general guidance. Dr Li was on temporary secondment for work experience at City University from China and had a specialist knowledge of finite element analysis. Both elastic and elasto-plastic studies were undertaken to predict the behaviour of the Sub-Assembly tests and also to provide the basis for possible further studies. Good agreement was achieved in the much more complex elasto-plastic state and this has also been reported elsewhere {44}.

A small parametric study was also undertaken to investigate the stress flow in a haunch under elastic conditions to provide for design guidance of weld and stiffening. A further plane-frame analysis was also carried out to predict the elastic behaviour of the Main Beam test.

8.2 ANALYSIS OF THE SUB-ASSEMBLY TESTS

8.2.1 Elastic Numerical Model and Analyses

The test beams were modelled using a LUSAS finite element package with 'semi-loof' thin shell and bar elements. The shell elements were either triangular or quadrilateral in shape with 6 or 8 nodes respectively. Each node had 3 translational degrees of freedom and an additional degree of freedom was provided at 8 'loof' points located at $1/\sqrt{3}$ x the distance between the mid-side and end nodes.

For these initial elastic studies, which were carried out for the comparison of stiffnesses, each beam was modelled using a finite element mesh similar to that shown in Figure 8.1 but with slight variations due to the different stiffening arrangements etc. Fixed end conditions were assumed at the column interface, line 'A' in the figure, and the centre line of the top steel beam flange was both laterally and rotationally fixed, line 'B' in the figure. No initial imperfections or residual stresses were included.

Three comparisons were made for each beam, namely; the steel beam alone, the steel beam plus reinforcing mesh and, finally, the steel beam, mesh and concrete slab. The former analyses neglected the concrete slab but the latter represented it as an equivalent steel area using a modular ratio of 10, which is recommended in reference {14} for lightweight concrete subject to short term loading. The shear connection of the mesh to the steel beam was modelled by using a series of diagonal and vertical bar elements of large cross-sectional steel area (10^6mm^2) arranged in the form of a Pratt cantilevered truss. This ensured that minimal shear deformation would occur, which was considered reasonable for elastic conditions. No attempt was made to model the progressive cracking of the slab because of the complexity.

Haunch toe moments against beam end slope was plotted for the above cases and the results are shown in figures 4.18 to ^{4.21} in Chapter 4. Good agreement is seen between the computer predictions when the concrete was neglected.

8.2.2 Elasto-Plastic Numerical Model and Analyses

The finite element model for the elasto-plastic analysis was an evolved version of that for the elastic studies and is shown in Figure 8.2. A finer mesh was adopted around the haunch toe area to model more accurately the larger deformation occurring there. An even finer mesh was tried but it produced the same results, thus indicating that the adopted mesh was about right. The geometric non-linearity was initially provided by utilising a 'Total' Lagrangian formation which took account of large displacements but assumed small rotations. The results using this were clearly unrealistic and under-estimated the post-buckling strength by as much as 50%. Subsequently an 'Updated' Lagrangian formation which provided for both large displacements and rotations was used with success and adopted for the non-linear study. It was also found that the special bar elements introduced to provide a shear key to the mesh were causing instabilities in the analysis. As deformation proceeded, convergence of the matrix solution at each displacement increment became difficult until divergence occurred and no solution could be obtained. Since the concrete was being neglected and the mesh contributed little to the overall strength, it was decided to add an area of steel to the top of the top flange in a way which gave the same position for the plastic neutral axis, ie, with an equivalent moment of area. Thus the bar elements were omitted and convergence greatly improved.

The edge conditions were the same as for the elastic case except for one case with beam B2 where a lateral rotational spring stiffness was incorporated at the column end. Residual stresses were again not included but an initial imperfection profile was included this time and took the form of a sine function both longitudinally and vertically, as given in Figure 8.3. The maximum imperfection was assumed at the haunch toe and was based on the fabrication tolerances for I beams given in Table 5 of reference {45}. A value of 3mm was used for most of the analyses but a study with different values was made for beam B2. The quarter wave buckling length L_o , shown in the figure, was based on the actual test deformed shapes. The initial displacement assumed at the column, although not accurate, was not considered critical and to model a zero imperfection at the column a much more complicated continuous function would have been required.

Non-linear material properties were incorporated by approximating the results obtained from the beam coupon tests. 'Model' stress/strain profiles were derived using four straight lines, with different curves being used for the webs and flanges as shown in Figures 8.4 to 8.7.

8.2.3 Elasto-Plastic Results and Discussion

Generally the computer analysis predicted the elastic behaviour and maximum load accurately but the post-buckling strengths were under-estimated in some cases and over estimated in others. This is a reflection of the complexity of the behaviour in this region and is illustrated in Figures 8.8 to 8.11, which show the haunch toe moment versus the beam end slope for each beam. The computer results follow the test results for beam B1 most closely, whilst those for beams B3 and B4 under-estimate the post-buckling strengths by some 12-15%. Interestingly the negative load stiffness in this region agrees well with the tests.

A more detailed study was carried out for beam B2, whose behaviour was least well predicted. Separate cases were considered, including the different haunch toe stiffening arrangements which were used in the tests. Figure 8.9 shows that the maximum strength for this beam in all cases was over estimated by about 10%. This can be explained by reference to Figure 8.14, discussed later, which shows that the lateral deflection at the haunch toe is considerably under-estimated at only a quarter of what it was in the test at this stage. Why this was so was not entirely clear because by changing the magnitude of the initial imperfection, also discussed later, a corresponding significant drop in the maximum strength was not obtained. A change in the column end boundary condition to a spring considerably reduced the post-buckling strength as can be seen in Figure 8.9, but the maximum strength only marginally. In fact from the result of that case it would appear that a fixed end condition was more realistic.

One possible explanation could be the omission of residual stress patterns due to the welding at the haunch toe, which could cause early yielding and hence premature buckling. The assumption then follows, that the presence of the stiffeners negates this effect, since test results in those cases are accurately predicted. Another

explanation might be that in situations without stiffeners the initial imperfection profile is more critical. Suffice it to say that with greater resources the problem could have been examined further but it is considered unlikely that real structures would be fabricated without stiffeners because of the problem of web buckling.

Referring again to Figure 8.9 for beam B2, the analysis confirms the improved performance by the provision of a brace and might have predicted the latter stage more closely had the brace bolt not have sheared off in the test, causing severe permanent deformation. The analysis surprisingly indicates only a minimal improvement in the maximum strength with a brace, and an improvement of less than 10% over the practical post buckling range. This could not be entirely corroborated by the test because the haunch stiffening arrangements were changed during the test, but there was a slight improvement in the strength after the brace had been added. By observations of the deformation during the test the author intuitively believes that without the addition of the brace the growth in lateral deflection would have been much greater, and the post-buckling strength much lower, than was otherwise the case although this is not confirmed by the computer analysis.

The influence of the amplitude of the lateral imperfection is also shown by consideration of beam B2 in Figure 8.12. As mentioned earlier, it can be seen that only the post-buckling behaviour is affected and not the maximum load. The predicted strength in the post-buckling region is also unaffected when the maximum imperfection is set at 3mm or below but when it is increased to 6mm a fall in strength is noted. In general it was found that the best predictions were obtained with the 3mm, ie, the recommended fabrication tolerance.

The deformed shape of the haunch toe buckling was predicted quite accurately by the computer as Figure 8.13 for beam B4 shows. The local buckling in the flange and web can be seen quite clearly and matches that shown in the photographs of the tests in Chapter 4. The growth in the lateral deflection was, however, generally under-estimated and greatly so in the case of B2, as mentioned. Figures 8.14 and 8.15 show a comparison of the computer predictions of lateral displacement with the test results. It is interesting to note that the test results in the figure continue until the beam end slope reached 3° whereas the computer

plots terminate when the beams reached between 4° and 5° end slope, and yet the computer values are smaller. Beam B2 is seen to display a curious behaviour, such that a buckle to one side is predicted, followed by a final buckle in the other direction. This actually occurred in the test but to a lesser extent. This effect is also illustrated in Figure 8.16, which shows typical lateral profiles predicted by the computer. Good agreement is achieved with the test profiles although, as stated, the magnitude is generally under-estimated. The apparent sharp change in the lateral slope from the predicted peak value near the haunch is, of course, exaggerated by the scale and the fact that the profiles do not include the initial imperfection. It should also be noted that the buckle occurs just beyond the haunch toe and that the haunch is laterally very stiff.

8.3 ANALYSIS OF THE MAIN BEAM TEST

8.3.1 Numerical Model

A simple plane frame finite element analysis was carried out on the main beam test to predict the elastic behaviour. The presence of the end stub columns was ignored and, being symmetrical, the frame was then divided into two with the conditions of zero slope and longitudinal displacement on the centre line as shown in Figure 8.17. This part-frame was then divided into 5 beam elements but the haunch was ignored, although the connection was assumed to be rigid. The contribution of the decking was neglected but the mesh reinforcement was included. A modular ratio of 10 was used for the concrete and the voids created by the decking in the concrete were neglected. Two analyses were carried out, one with a constant composite beam stiffness assumed (Case 1) and one where the contribution of the concrete was neglected over the hogging region (Case 2).

8.3.2 Results of the Main Beam Test Analysis

Referring to Figure 8.17, the results sought for each of these analyses included the central deflection, δ_c , and the magnitude of the column horizontal reactions, H, such that they could be expressed as linear functions of the applied span jack loads, J. The results are given below in Table 8.1 and where δ_c is expressed in mm, H and P in kN, and θ in degrees $\times 10^{-3}$.

	Case 1	Case 2
δ_c/J	0.266	0.352
H/J	0.819	0.645

Table 8.1 Computer Studies - Results from the Main Beam Test Analysis

The analysis of Case 2 involved some iteration to determine the length of the hogging region, which was found to be 15% of ^{the} span. The results are compared with the test behaviour in Chapter 7.

8.4 HAUNCH PARAMETRIC STUDY

8.4.1 Introduction

A limited parametric study was undertaken to investigate the elastic stress flow at the haunch toe area in order to make recommendations for the design of welds and web stiffening. The parameters of interest were the depth and length of the haunch cutting. A comparison with related work published by other researchers was also made and the results are shown to be similar.

8.4.2 Numerical Model

The finite element model was based on that used for the elastic analysis of Sub-Assembly Test beam B4 and therefore the cross-section geometry relates to a 457 x 152 UB 52 with full depth stiffeners 10mm thick welded at each side of the haunch toe - see Figure 8.1. The model again assumed that the beam top flange was both torsionally and laterally fixed along its centre line and that the end condition near the column was fixed. The welds joining the cutting web and cutting flange to the beam flange were assumed to be equal in thickness to the elements themselves. The model also neglected the strength of the concrete but included the mesh reinforcement as before.

Four different cutting lengths (L_c) were considered: 1 x main beam depth (1D), 2D, 3D and 4D, with cutting depths varying from 0.4D to 2.5D. Some of the combinations studied would entail the cutting being made from a different section to the main beam but they are included for completeness.

8.4.3 Results of Haunch Parametric Study

The results presented are the values of the forces in the intersecting elements at the haunch toe and the longitudinal shear stress profiles along the beam to cutting web weld. The terms are shown in Diagram 8.1 and defined below:

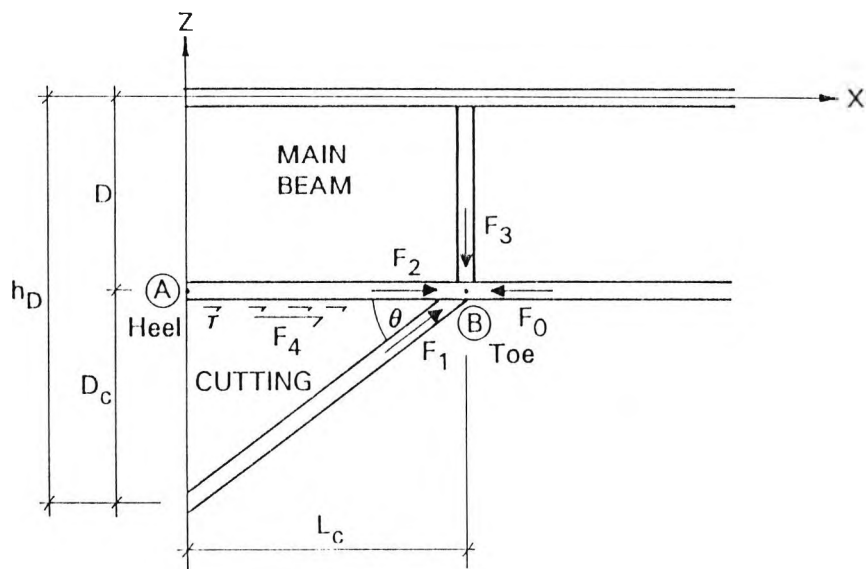


Diagram 8.1 Haunch Forces Determined

h_D	=	haunch depth
D	=	main beam depth (between flange centres)
D_c	=	cutting depth (to flange centre-lines)
L_c	=	cutting length
θ	=	haunch toe angle
$F_o = \sigma A_f$	=	force in beam compression flange just beyond the haunch toe

where σ = average longitudinal stress across the flange width just beyond the haunch toe

A_f = area of main beam flange

F_1 = force in cutting flange adjacent to the haunch toe

F_2 = force in beam flange on the cutting side of the haunch toe

F_3 = force in the stiffeners

$F_4 = \int_0^{L_c} \tau t_{cw} dx$ = total cutting web to beam flange shear

where τ = cutting web to beam flange shear stress

t_{cw} = cutting web thickness

The results are presented in Figures 8.18 to 8.24. The cutting flange force, F_1 , is found to vary between about 55% and 65% of F_o in the practical range considered but it does not have a simple relationship with the haunch trigonometry - see Figure 8.18. F_2 , shown in Figure 8.19 varies between 45% and 75% of F_o but increases with the toe angle as one would expect, but again in no regular way. F_3 , also increases with the toe angle from virtually zero at a 4° toe angle up to 30% of F_o at 50° . It does have a relationship which can be reasonably approximated by a simple trigonometrical function, as discussed later. Figure 8.18 also shows that the value of the total cutting web longitudinal shear force, F_4 , was found to vary most and the highest value of $1.2 F_o$ was obtained for the longest haunch considered ($L_c = 4D$). Values of $F_4/F_o > 1$ are of course possible because this force is not part of the resolution of forces at the haunch toe and it is logical that the longer the integrated length, the higher the force ratio.

Figure 8.20 shows the maximum value of the cutting web weld stress, τ , plotted against the beam flange stress at the haunch toe, σ , and it is seen that for the practical haunch range the value of τ is always under 40% of σ . The profiles of τ along the cutting are illustrated in Figures 8.21 to 8.24 and these show that the value is small at the column end but it then rises to a peak at or near the haunch toe. For shallow toe angles the stress profiles are more even but with steeper angles the stress gradient is seen to increase towards the toe. The negative values occurring in some cases at the column end reflect the drop in the neutral axis with the deeper haunches.

8.4.4 Work by Other Researchers

A similar study was undertaken by Morris and Andrade {46,47} based on the tests by Nakane {48}, and who were concerned with the behaviour of some typical portal frame haunches. That type of haunch is normally much longer and shallower because it applies to roofing members (rafters) and not floor members, which have a different plastic design moment profile. Another difference is that the top (tension) flange is not continuously restrained as it is in a composite floor, but is only restrained at discrete points. At the haunch toe, rafters are normally fully restrained by knee braces and partial depth stiffeners but at other points they may be only laterally restrained.

Morris and Andrade carried out computer studies on some haunched cantilevers using 'semi-loof' finite elements with a tri-linear stress/strain profile and they also included residual stresses. The steel section mainly used for their study was a 356 x 127 UB 33 with a haunch depth of 2D and a haunch length of 5.4D. The cantilever length, ie, the distance to the point load, was a variable in their study but the results referred to later apply to a length of 9.6D, whereas the length in the current study was 8.8D.

They studied the magnitude of the force in the cutting flange at the haunch toe (F_1) and obtained values of between 77% and 91% of the rafter flange force (F_o) in the elastic state which compares with 54% and 67% for the current study. At failure their values dropped to 66% and 84% and they attribute this drop to the influence of residual stresses at working load levels. The difference between our values reflects both the length of the haunch and the inclusion of residual stresses. They also plotted the variation of cutting web to beam flange shear stress and there is agreement with our results, particularly for the longest haunch considered, ie, when $L_c = 4D$.

From their consideration of different cantilever lengths, Morris and Andrade were able to investigate the effect of the proximity of the point of contraflexure on the moment-rotation characteristics. They assumed that M_p occurred at the haunch toe for each case and, by moving the point of contraflexure, the

moment gradient and hence the stress across the haunch, could be varied. They found that when the stress at the haunch heel at collapse was greater than about 0.75 of the heel yield moment, then the haunch toe moment capacity and the moment-rotation capacity reduced because of the presence of residual stresses. This led them to recommend that the haunch should be proportioned so that this figure was not exceeded.

A further relevant comment from their work was that they recommended welding the cutting flange to the beam despite any detrimental effects from the induced weld stresses. They found that without this weld, not only was the moment capacity of the member reduced but, more importantly, the in-plane rotational capacity was impaired and extensive haunch web yielding occurred well below the serviceability load levels.

8.4.5 Design Recommendations from Parametric Study

The following geometric limitations apply:

toe angle θ (or $\tan^{-1} (D_c/L_c)$);	$5.7^\circ \leq \theta \leq 51.3^\circ$
cutting length L_c ;	$D \leq L_c \leq 4D$
haunch depth h_D ;	$1.4 \leq h_D/D \leq 2.5$

- (i) Force in the cutting flange, $F_1 = 0.7 F_o$
- (ii) Force in the haunch web stiffeners, $F_3 = F_o \sqrt{(1 - \cos \theta)/3}$
- (iii) Beam flange to cutting web weld;

assume a linear shear stress distribution across the haunch with a value of τ/σ at the heel given in Table 8.2 up to a value of τ_{\max} given by $\tau_{\max}/\sigma = 0.12 \tan \theta + 0.2$

τ/σ	0	0	0.05	0.05
L_c	D	2D	3D	4D

Table 8.2 Computer Haunch Parametric Study - Design Values of τ/σ at the Haunch Heel for Various Haunch Lengths

These design shear stress values assume an effective weld thickness equal to the web thickness, but the weld actually provided can be sized on a pro-rata basis.

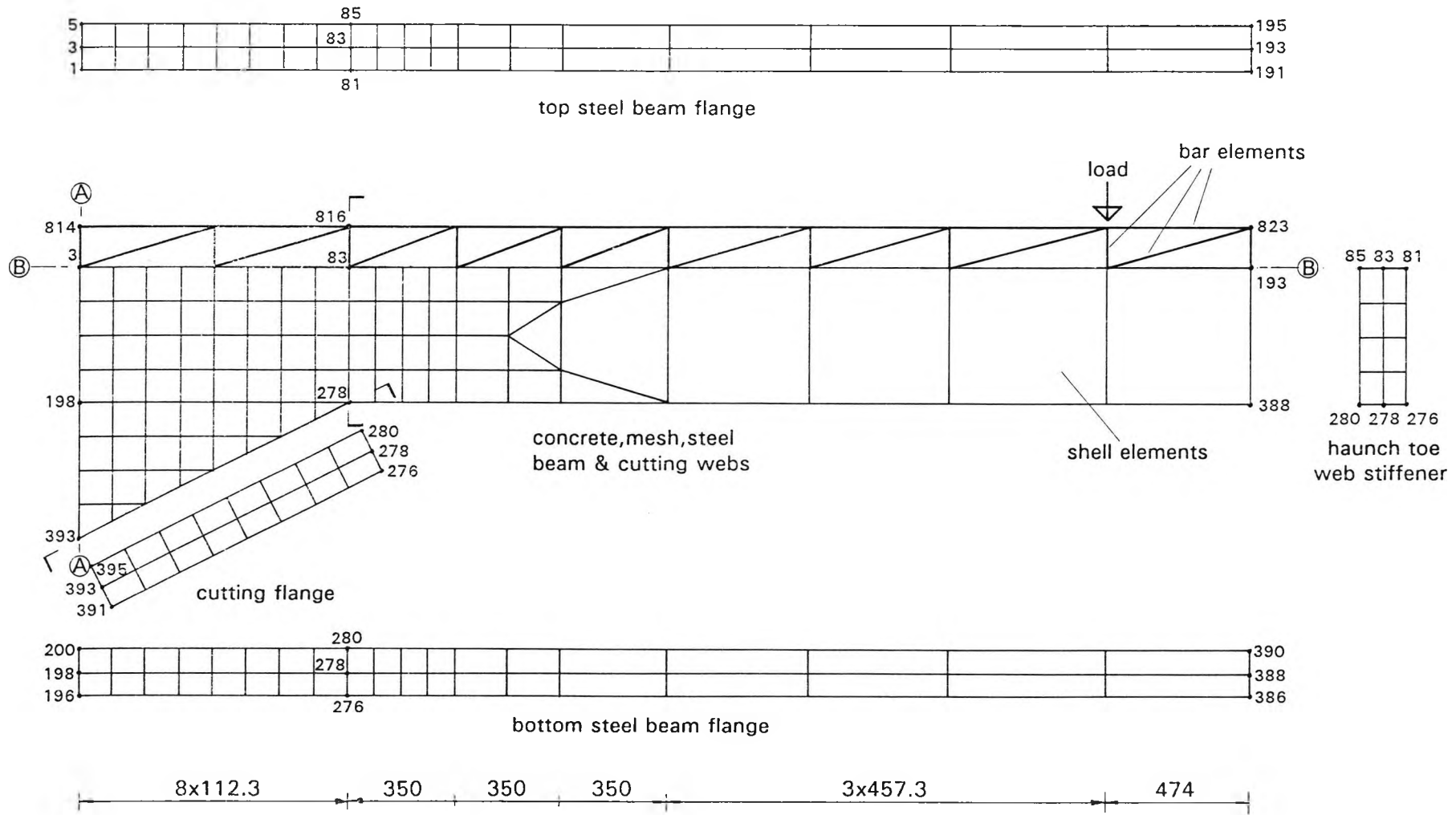


Figure 8.1 Computer Studies - Typical Finite Element Model for Elastic Analysis of the Sub-Assembly Tests

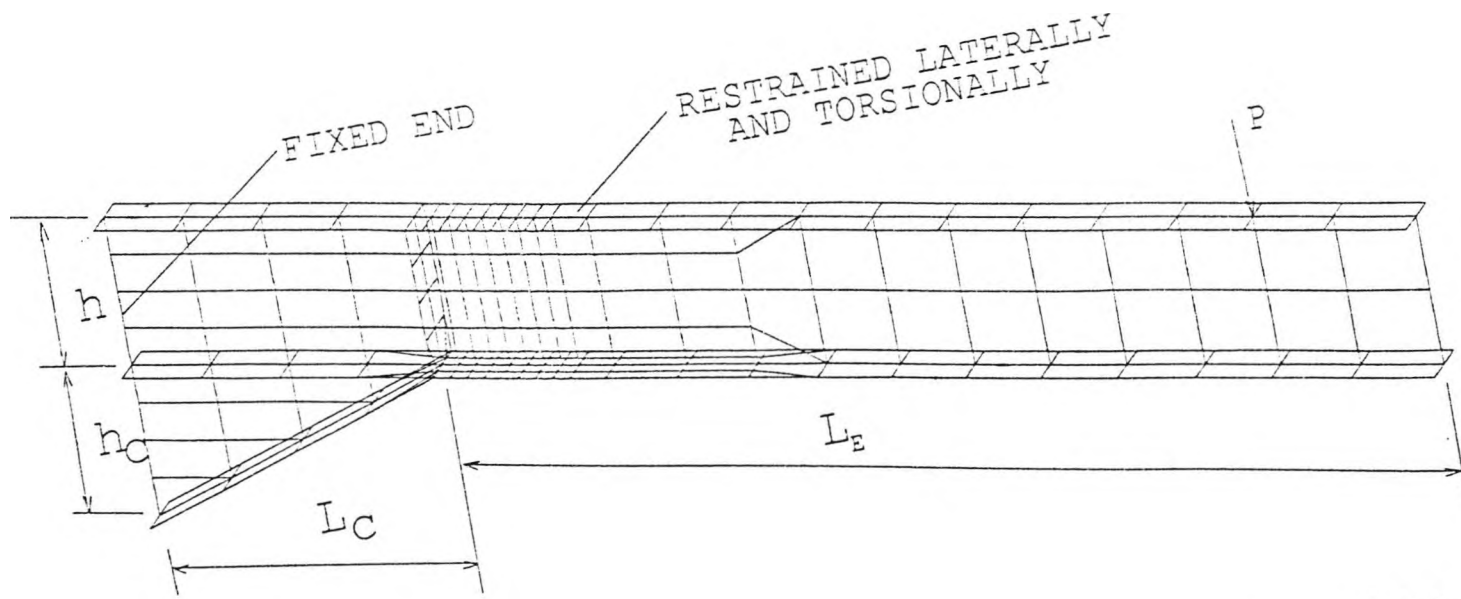
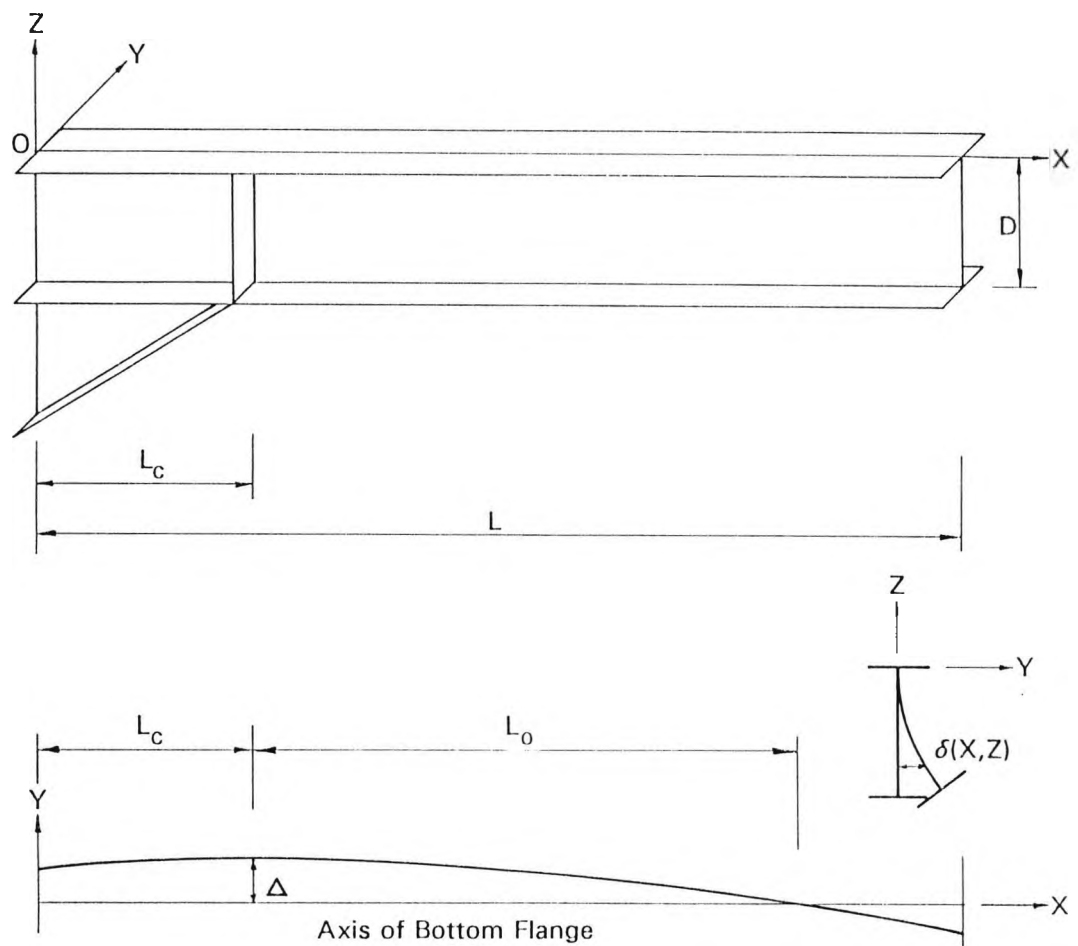


Figure 8.2 Computer Studies - Typical Finite Element Model for Non-Linear Analysis of the Sub-Assembly Tests



The initial imperfection of the web and bottom flange is:

$$\delta(x, z) = \Delta \left[1 - \cos \left| \frac{\pi z}{2 D} \right| \right] \cos \frac{\pi(x - L_c)}{2L_0}$$

- where: Δ is the maximum lateral imperfection of bottom flange.
 L_0 is the quarter wave length of buckling $\approx 0.6 (L - L_c)$ according to the test results.
 L_c is the length of the cutting.

Figure 8.3 Sub-Assembly Tests - Initial Imperfections used in the Non-Linear Analysis

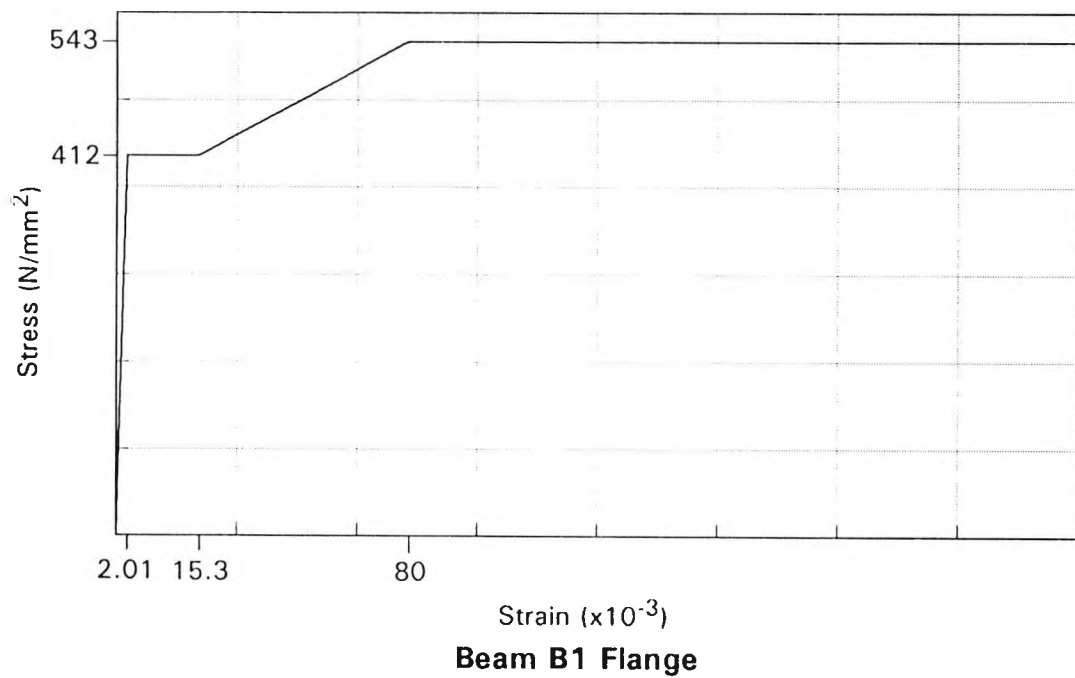
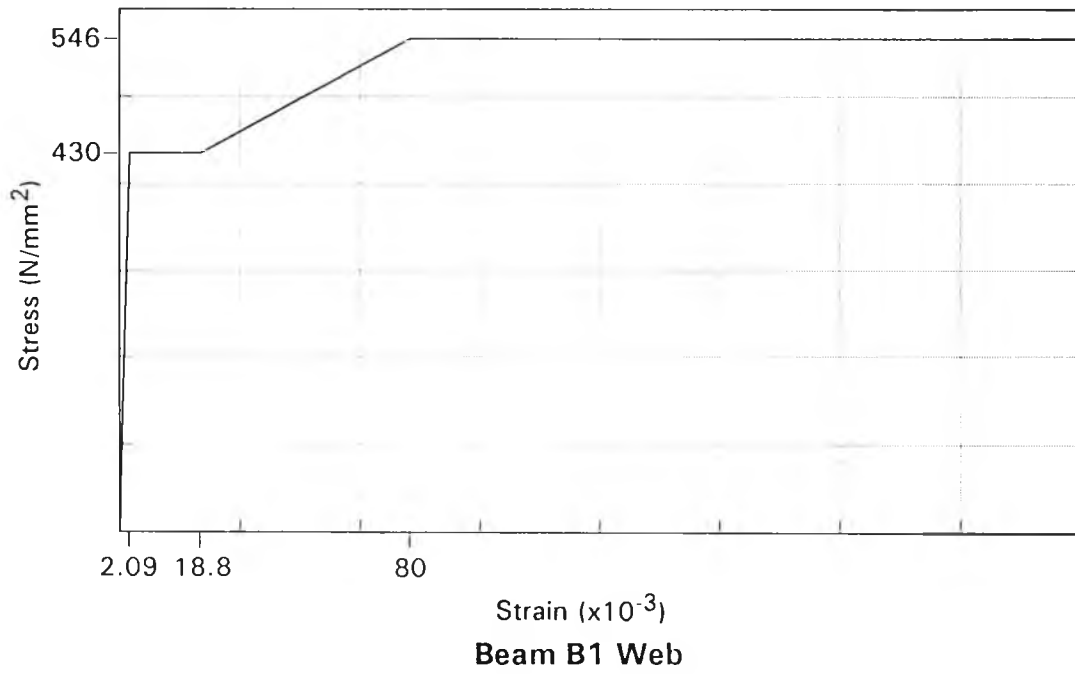


Figure 8.4 Computer Studies - Model Stress/Strain Curves for Sub-Assembly Test Beam B1

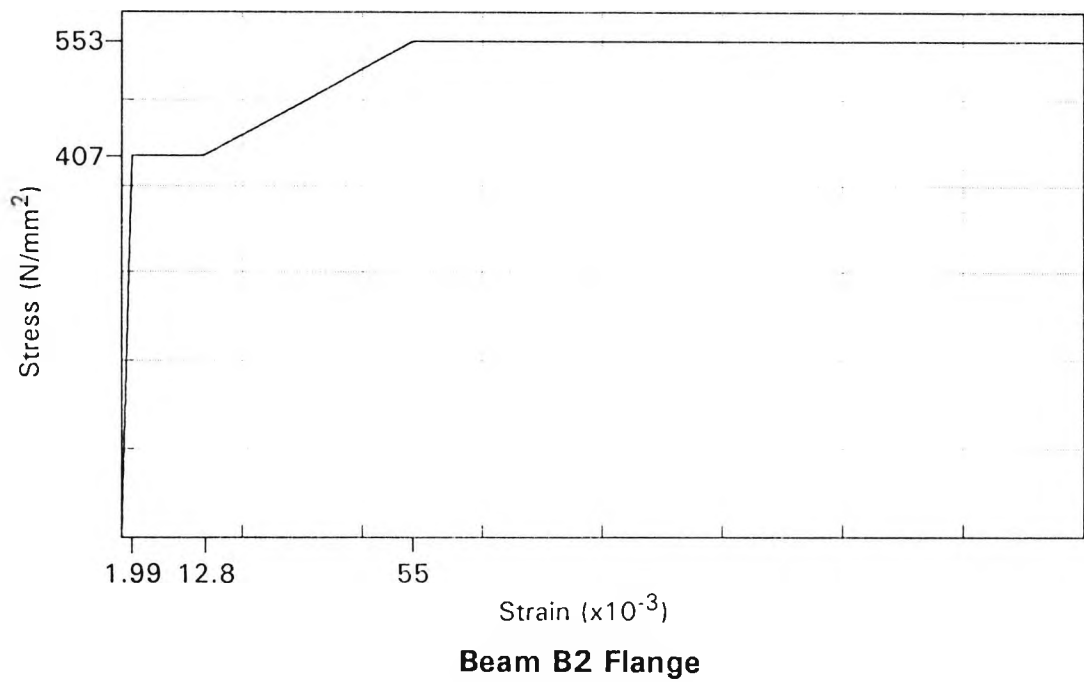
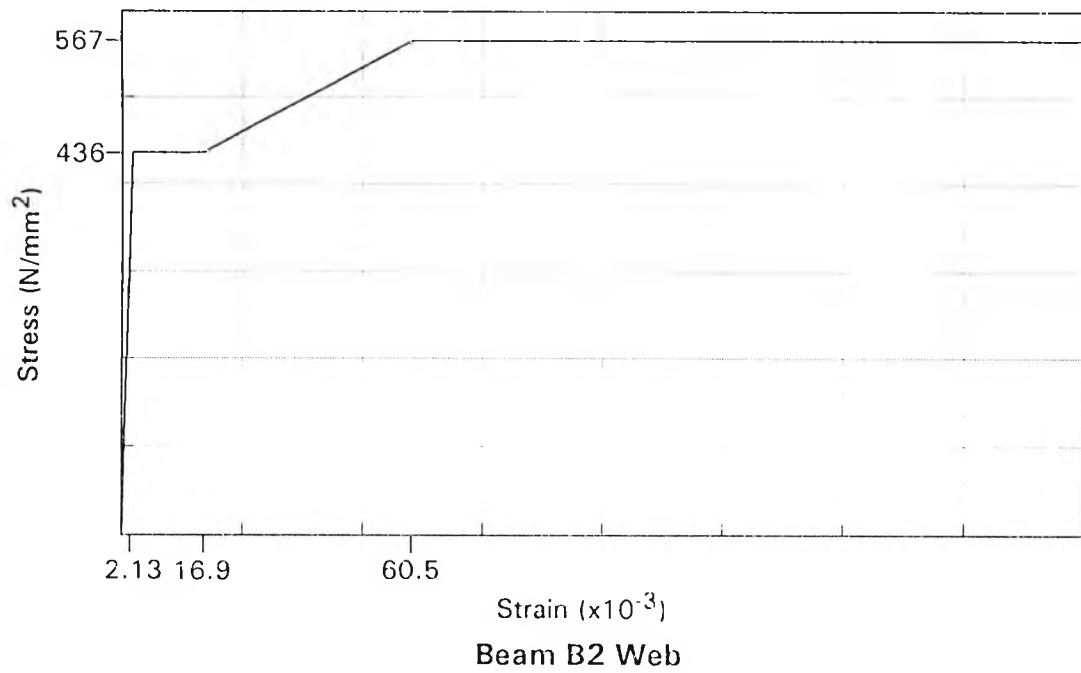


Figure 8.5 Computer Studies - Model Stress/ Strain Curves for Sub-Assembly Test Beam B2

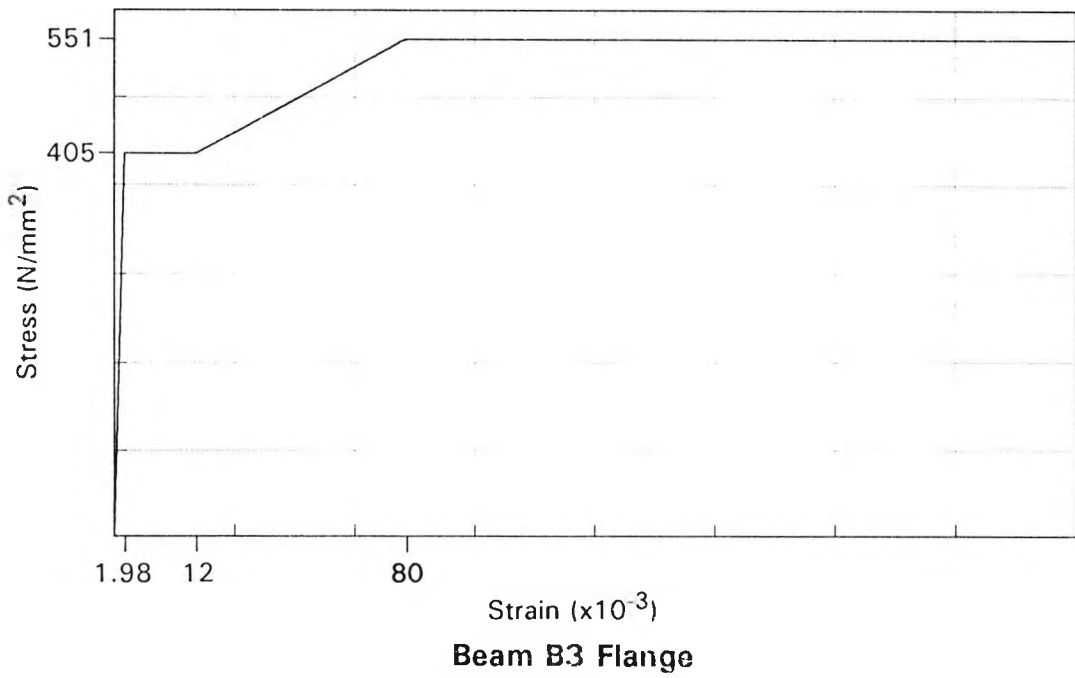
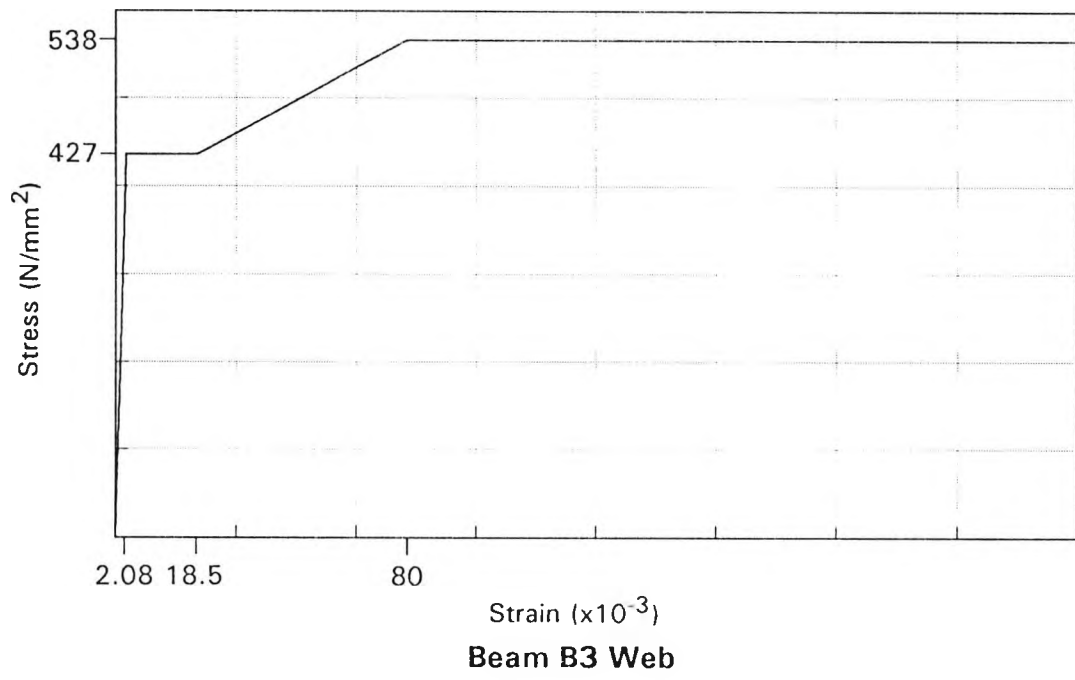


Figure 8.6 Computer Studies - Model Stress/Strain Curves for Sub-Assembly Test Beam B3

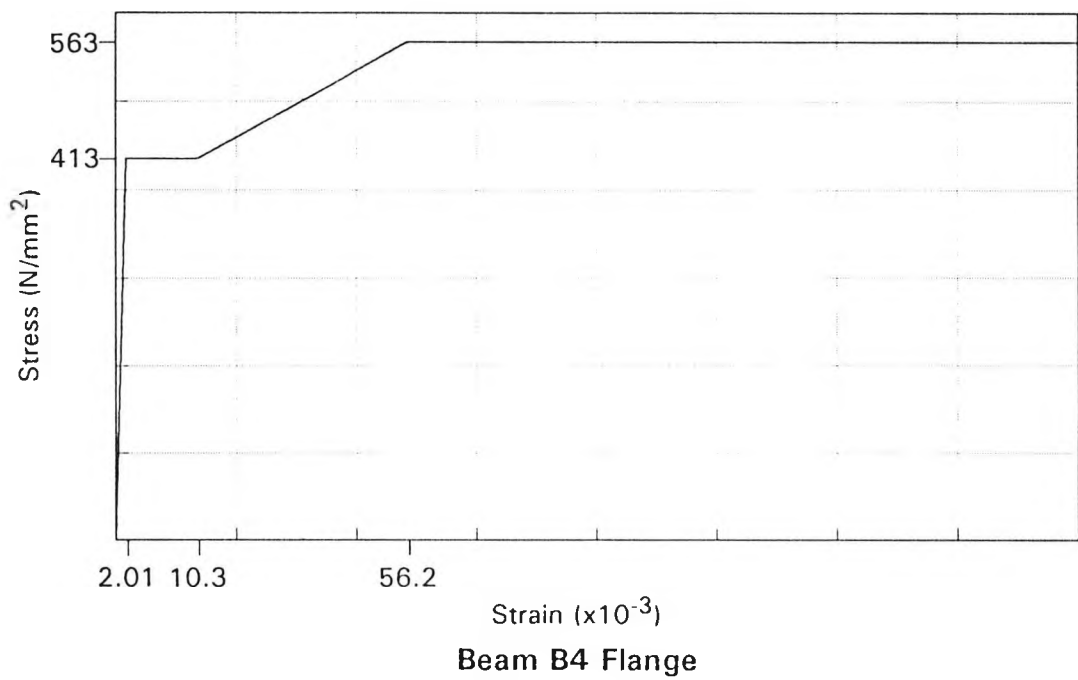
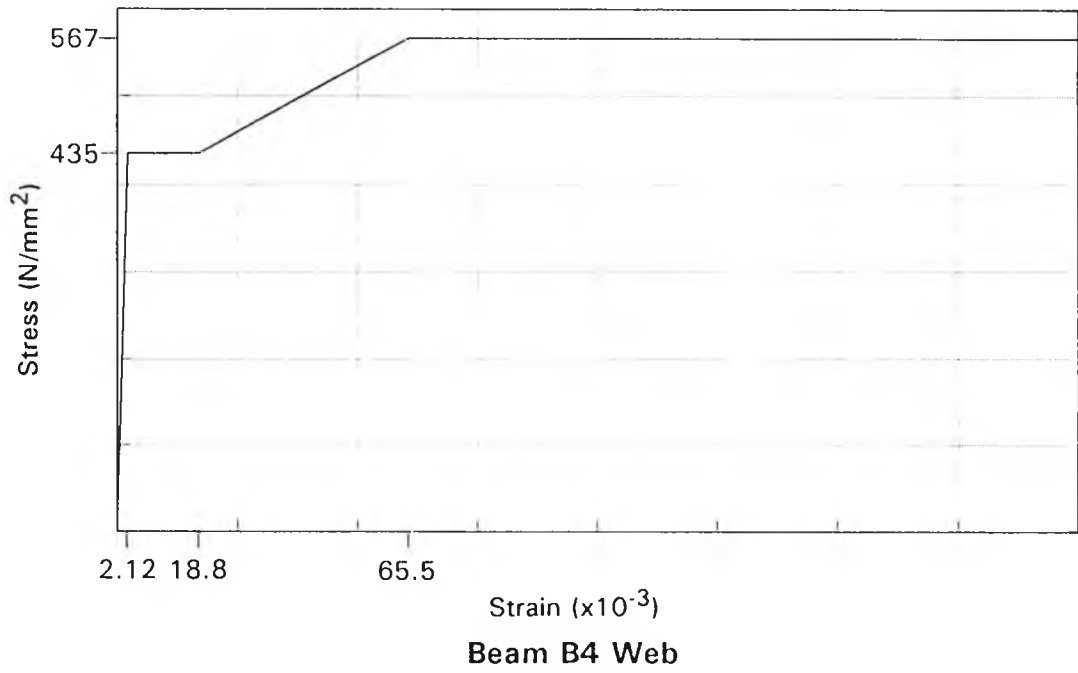


Figure 8.7 Computer Studies - Model Stress/Strain Curves for Sub-Assembly Test Beam B4

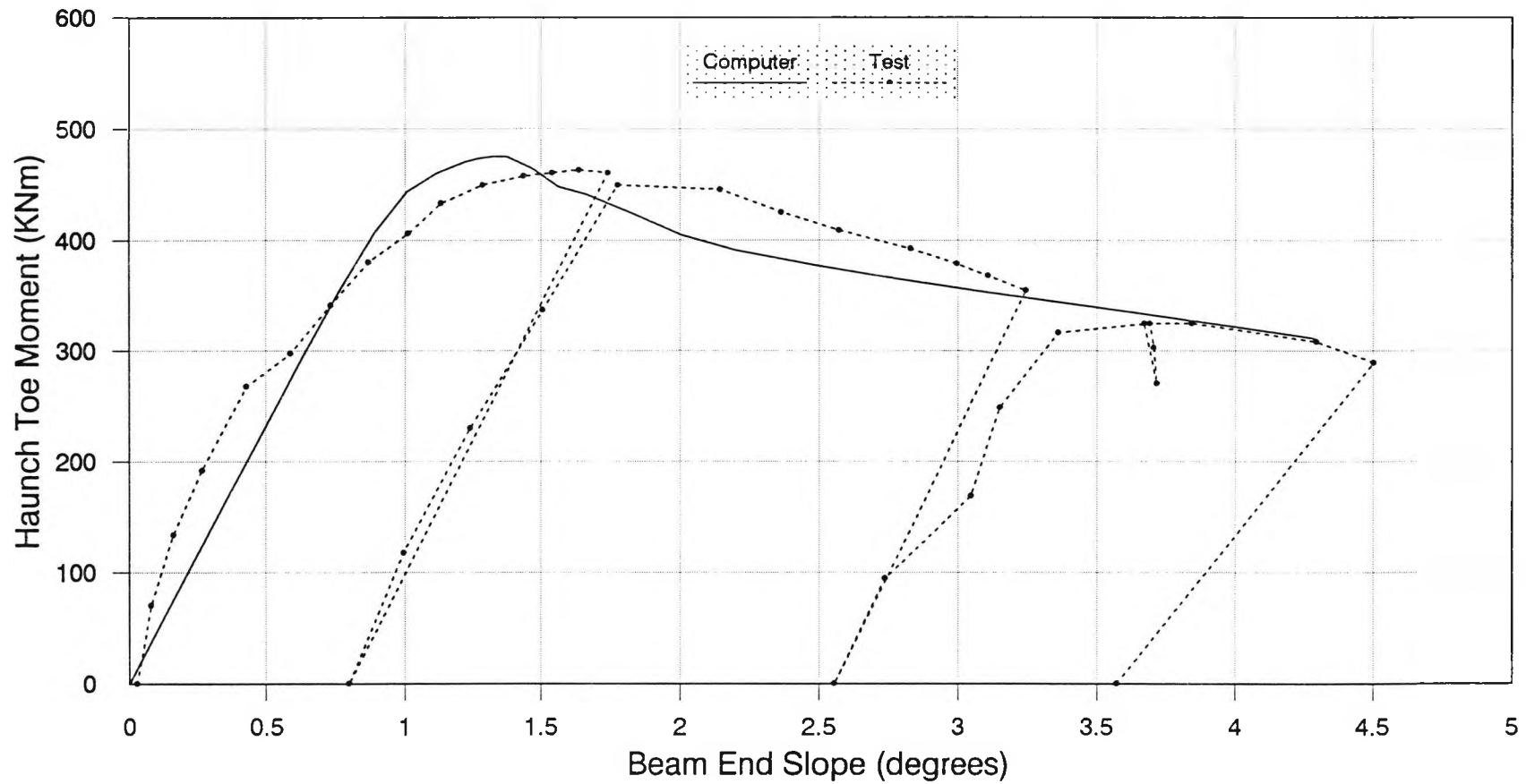


Figure 8.8 Computer Results - Haunch Toe Moment/Rotation Comparison for Sub-Assembly Test Beam B1

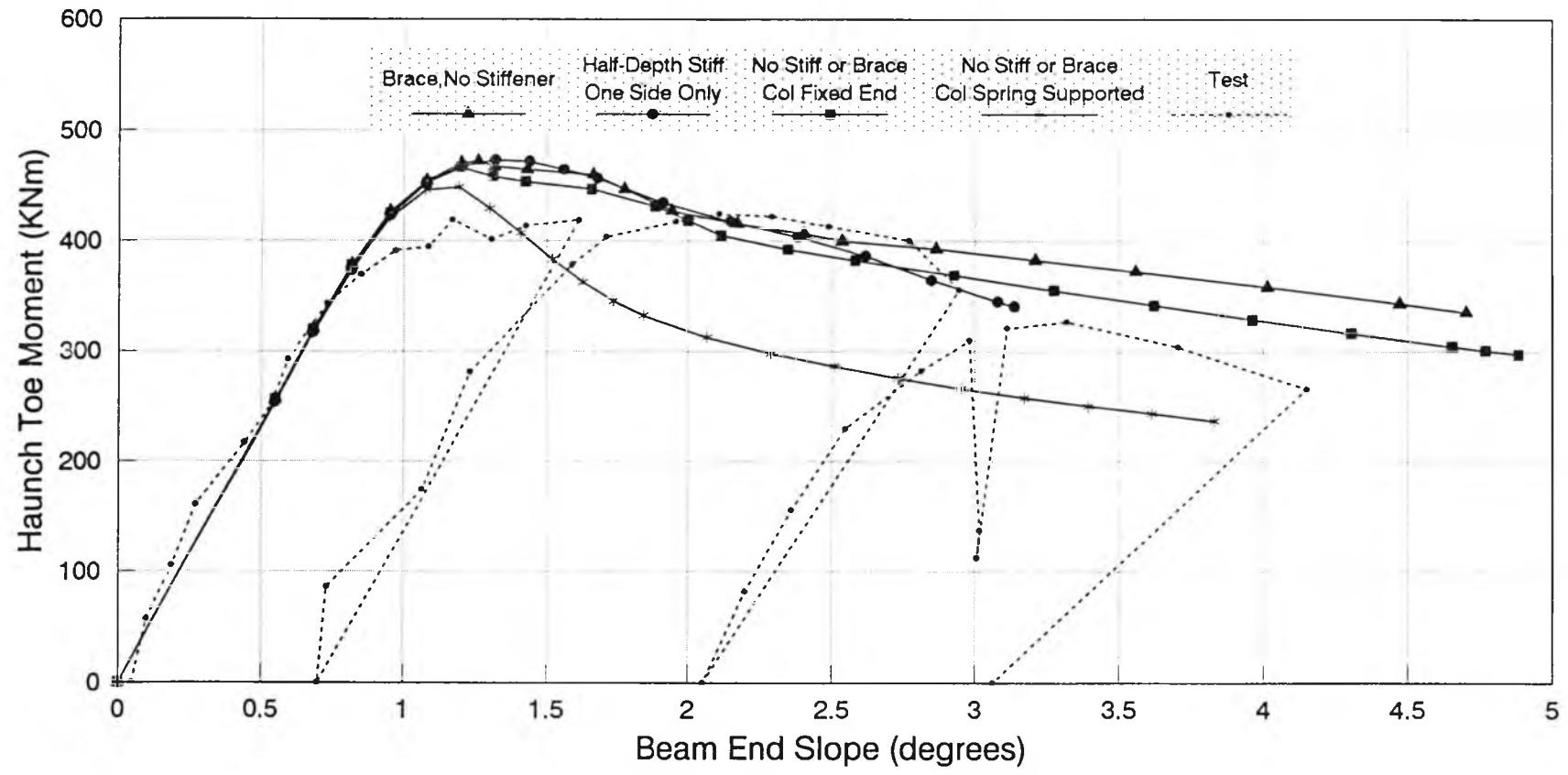


Figure 8.9 Computer Results - Haunch Toe Moment/Rotation Comparisons for Sub-Assembly Test Beam B2

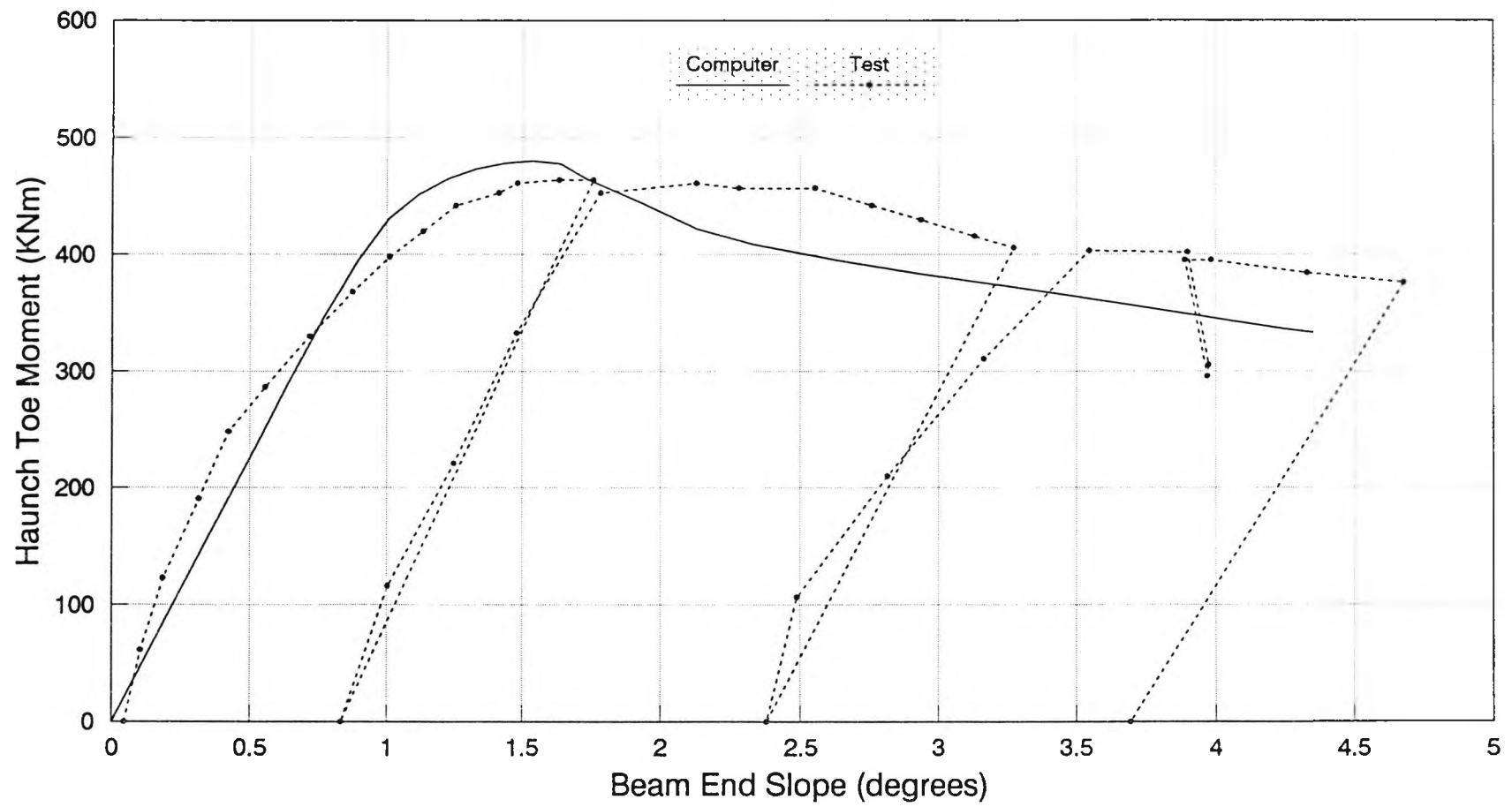


Figure 8.10 Computer Results - Haunch Toe Moment/Rotation Comparison for Sub-Assembly Test Beam B3

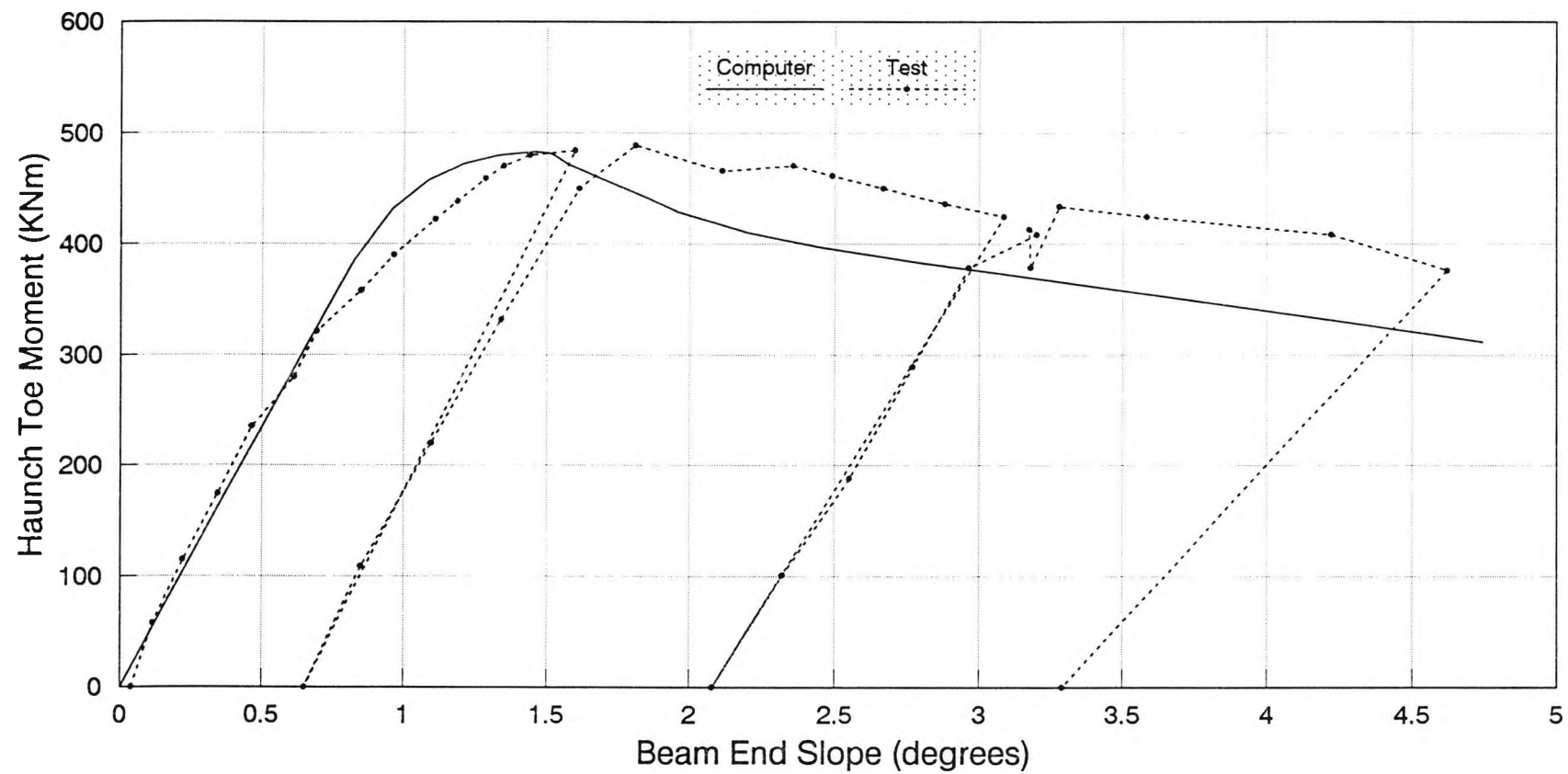


Figure 8.11 Computer Results - Haunch Toe Moment/Rotation Comparison for Sub-Assembly Test Beam B4

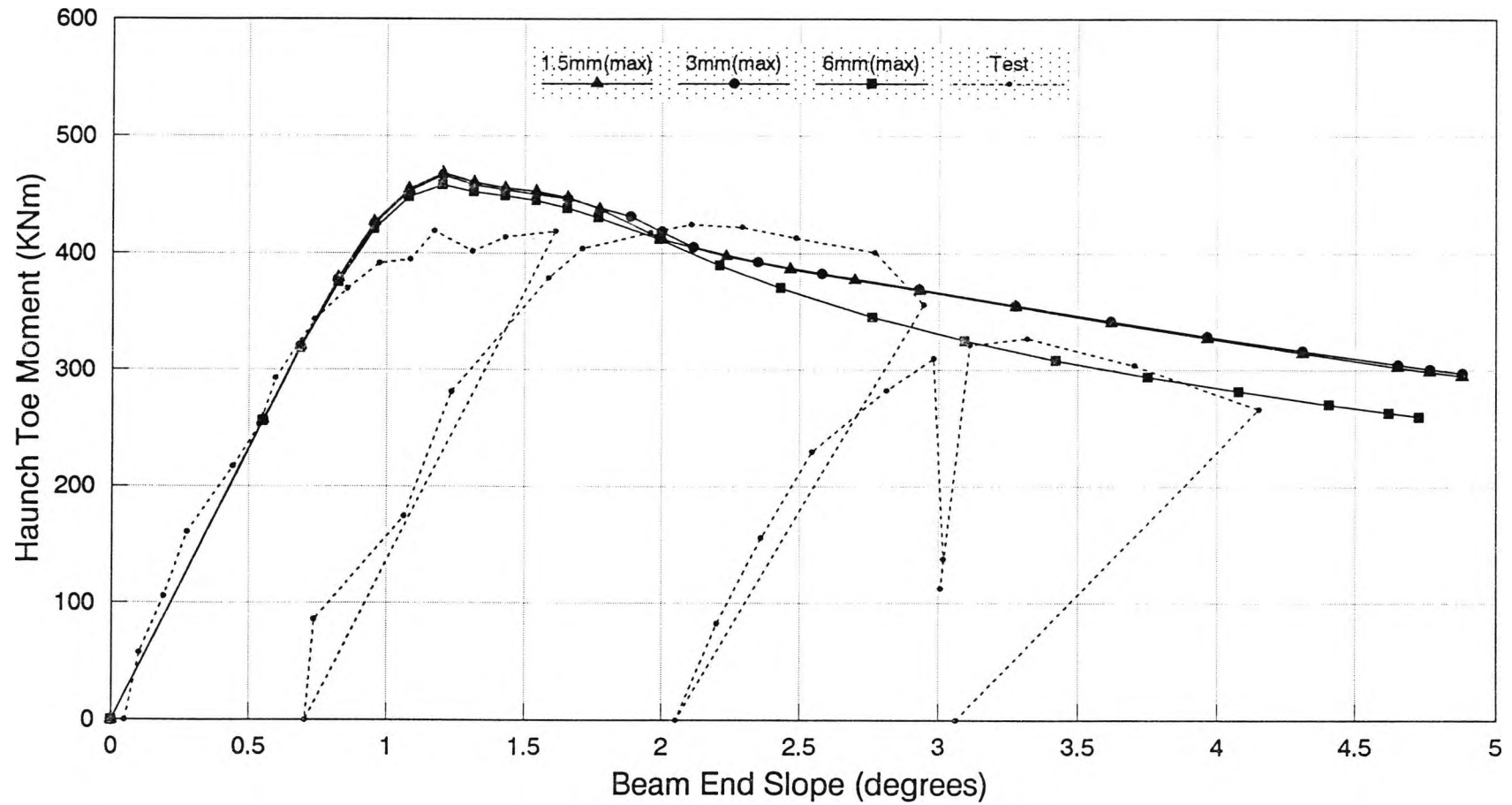


Figure 8.12 Computer Results - The Influence of Maximum Imperfection on the Behaviour of Sub-Assembly Test Beam B2

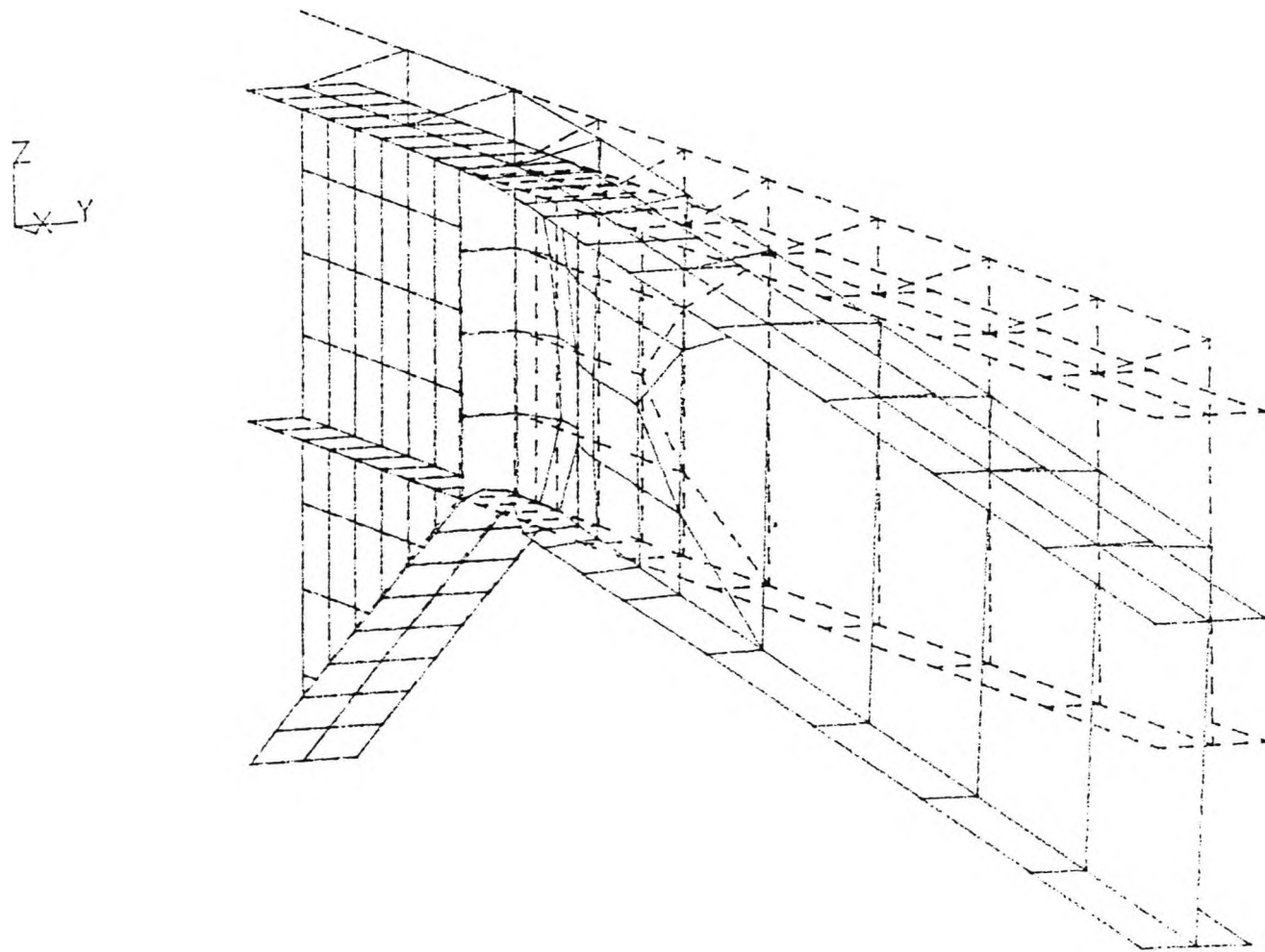


Figure 8.13 Computer Results - The Deformed Shape of Beam B4

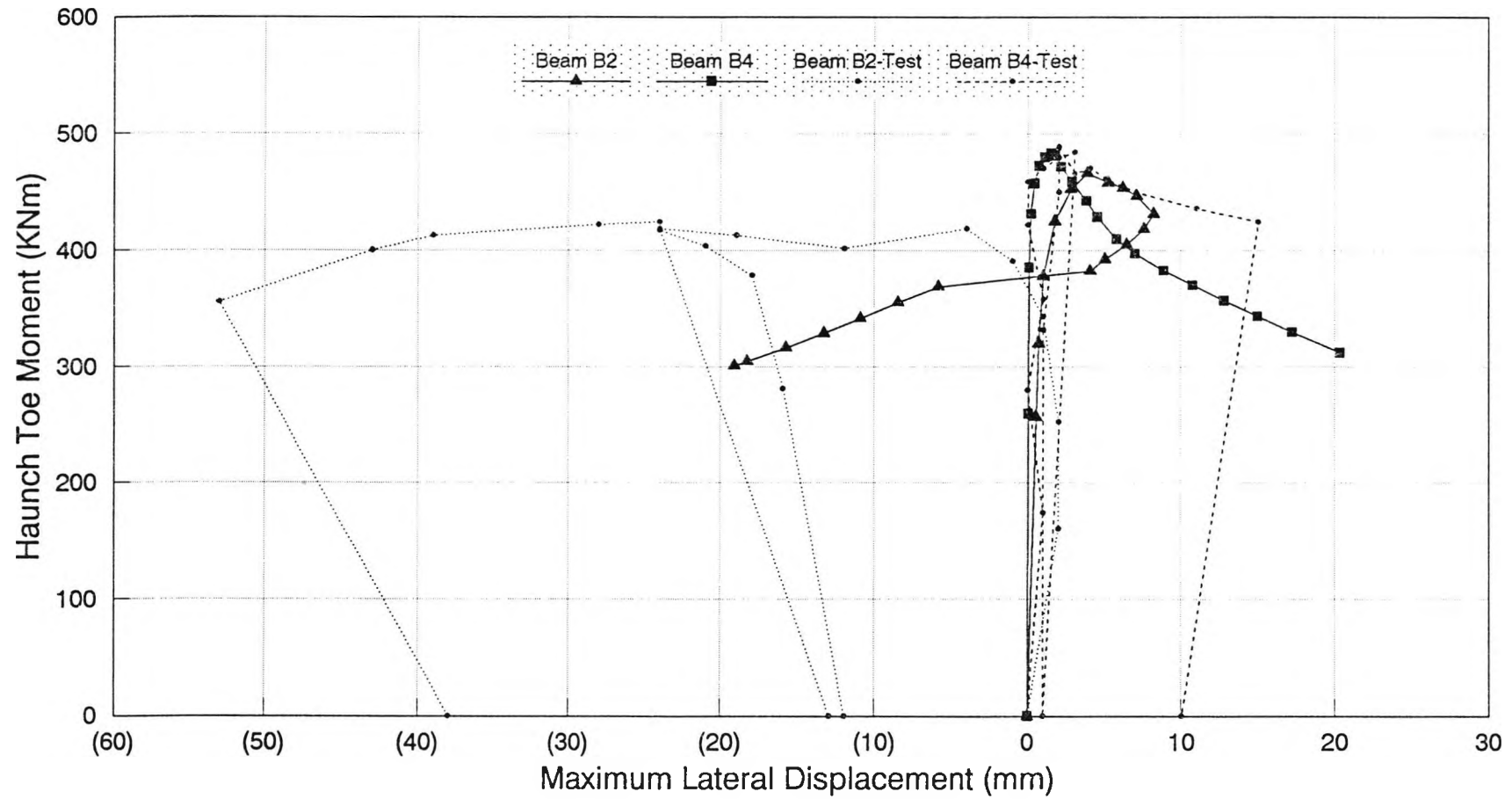


Figure 8.14 Computer Results - Moment/Lateral Displacement Comparisons for Sub-Assembly Test Beams B2 & B4

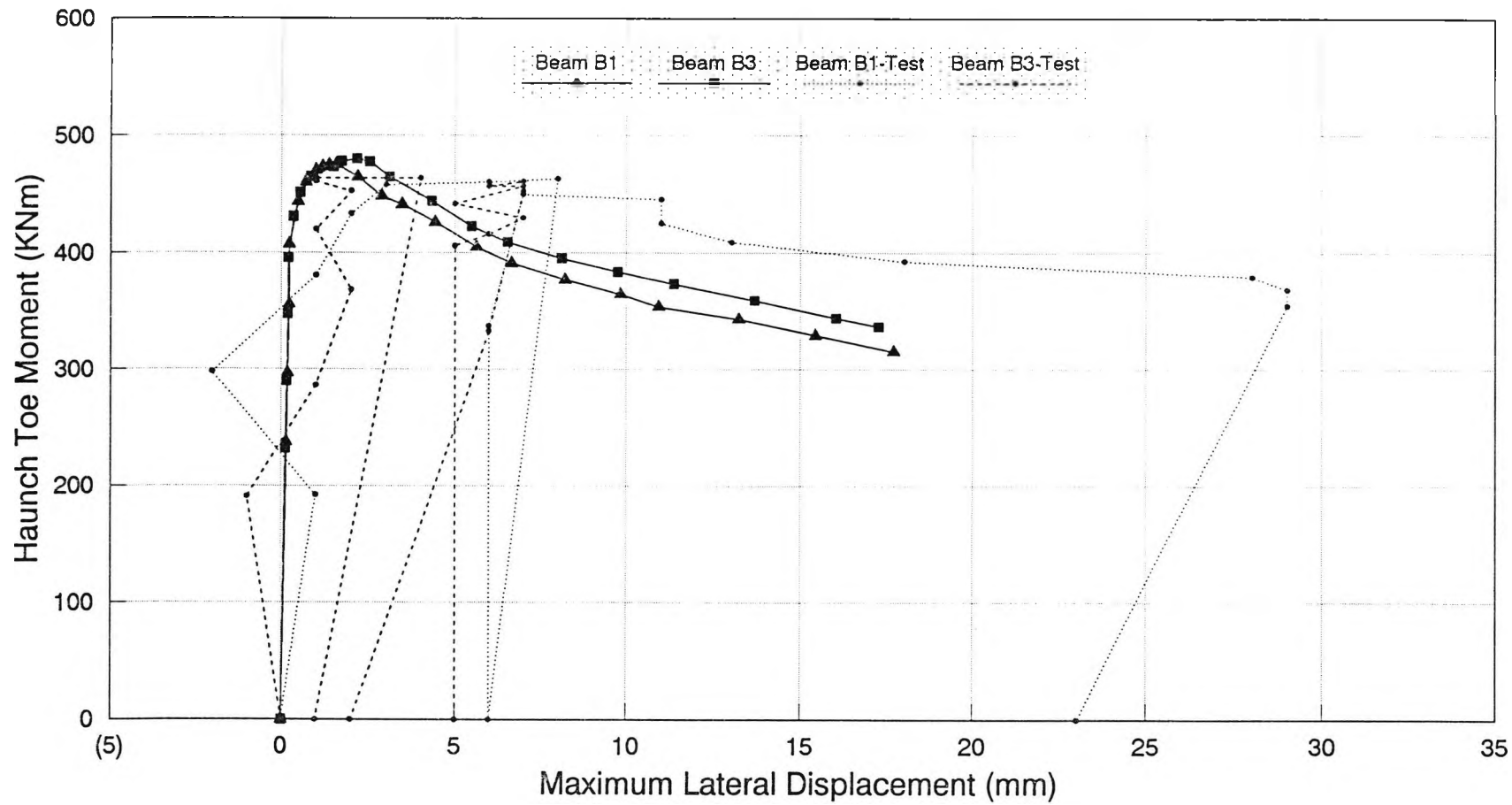


Figure 8.15 Computer Results - Moment/Lateral Displacement Comparisons for Sub-Assembly Test Beams B1 & B3

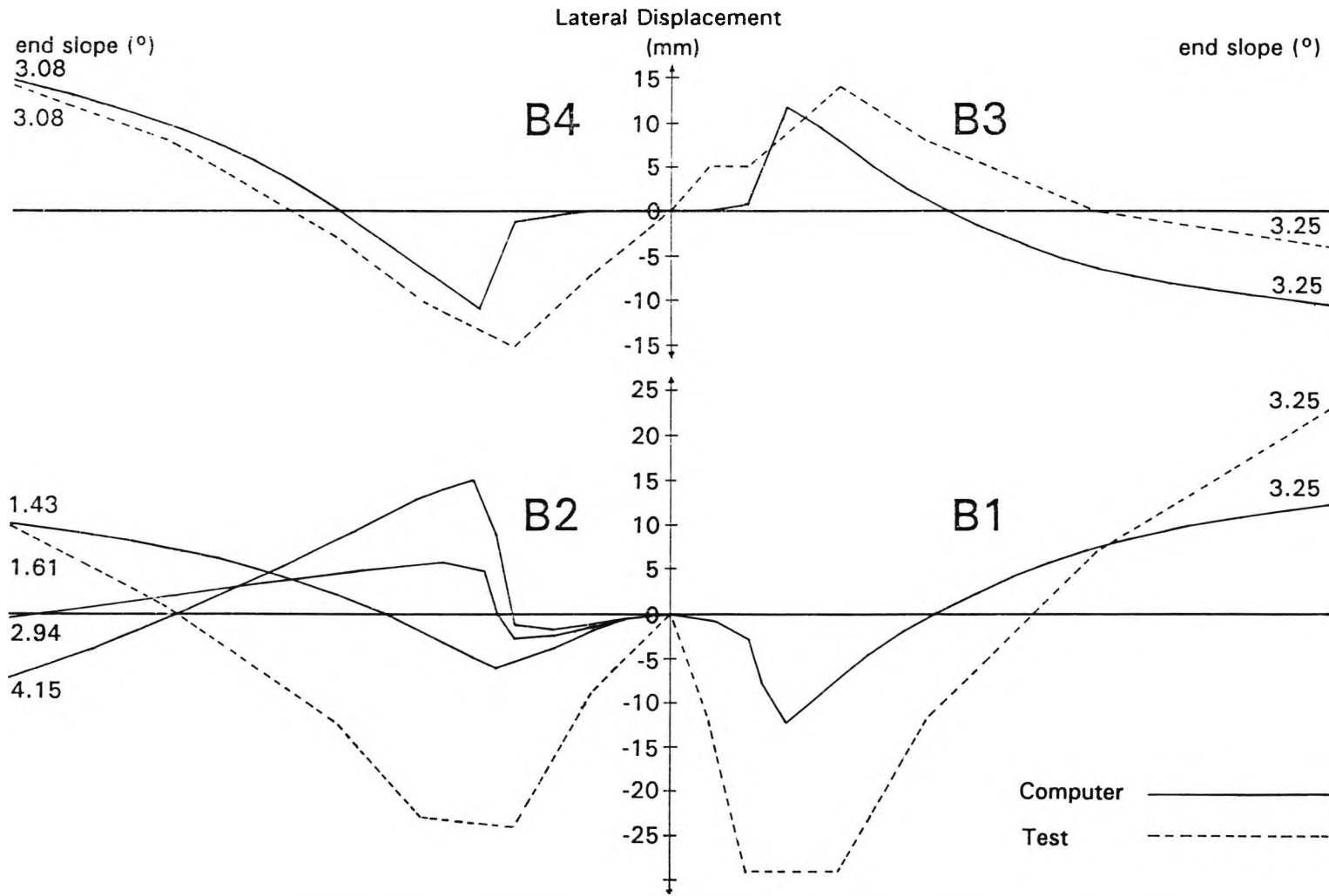


Figure 8.16 Computer Results - Comparison of Lateral Displacement Profiles for the Compression Flanges in the Sub-Assembly Beam Tests

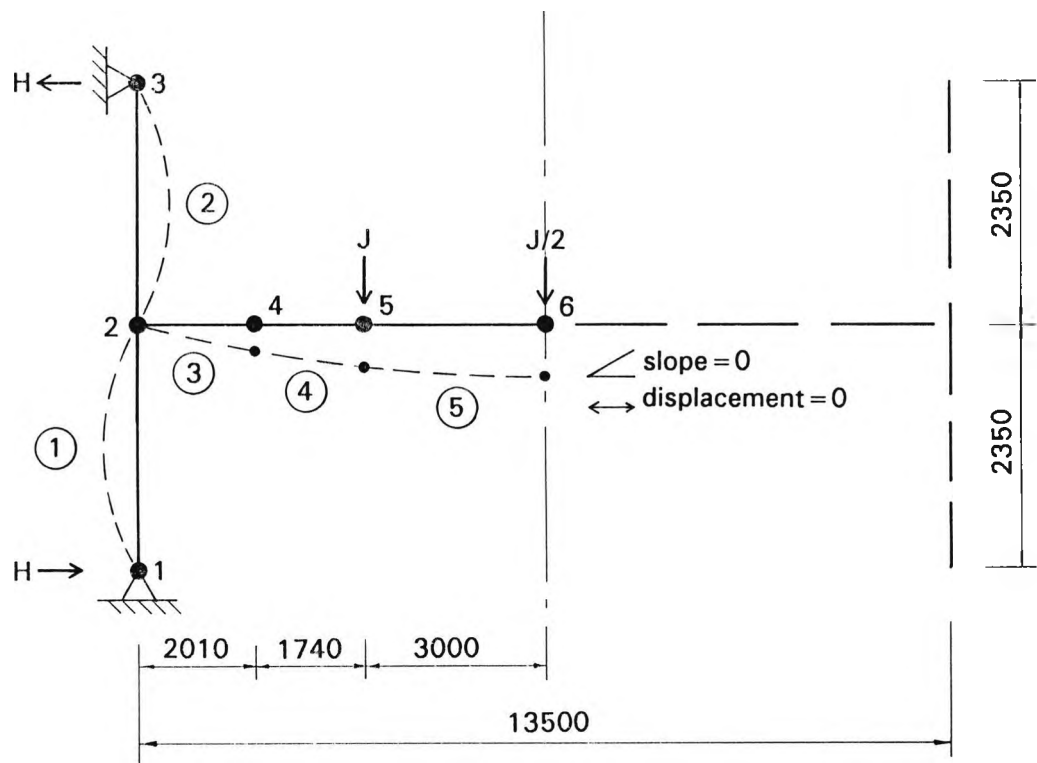


Figure 8.17 Computer Studies - Main Beam Test Finite Element Model

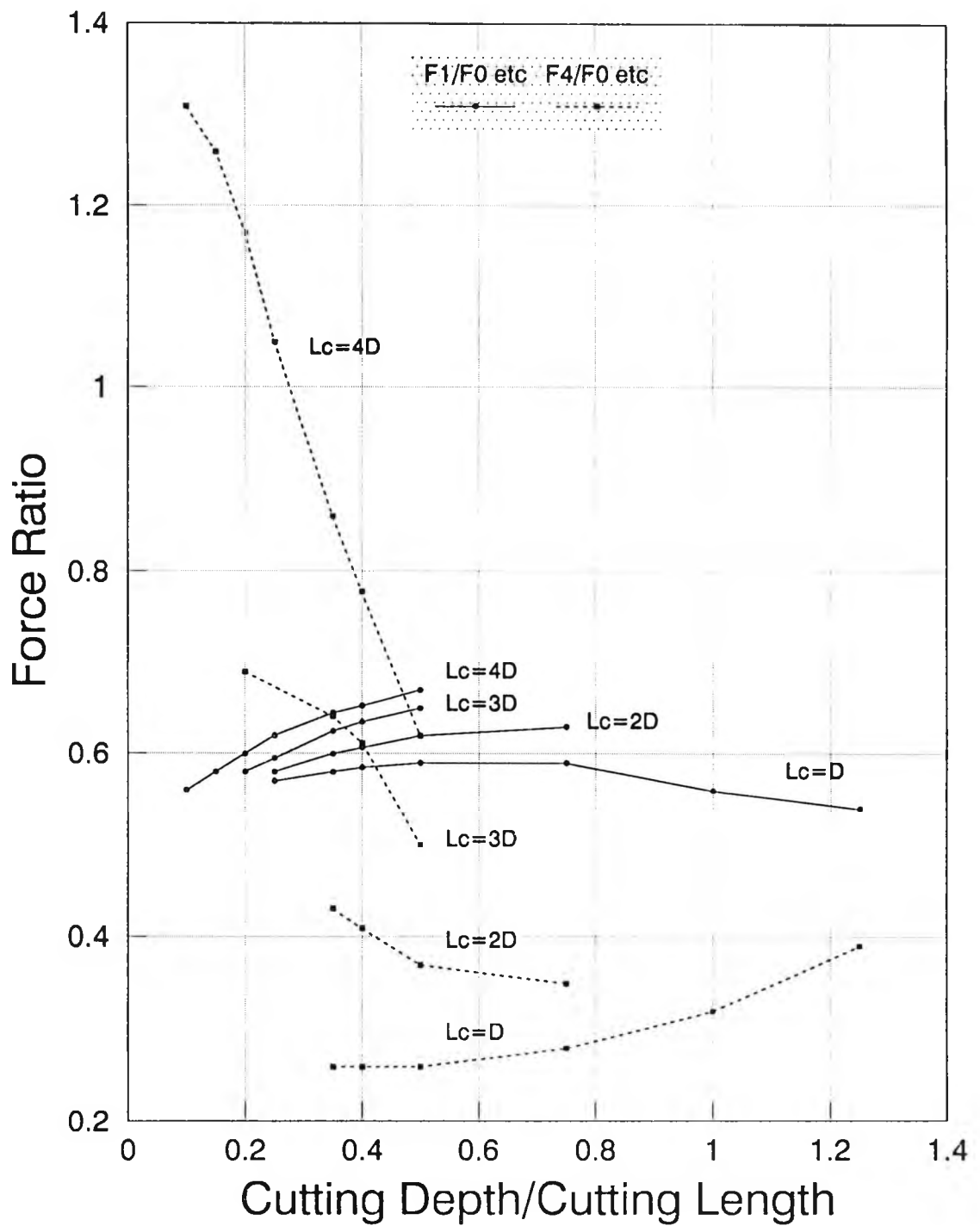


Figure 8.18 Computer Studies - Haunch Toe Force Ratios $F1/F0$ and $F4/F0$ versus the Cutting Depth/Length Ratio

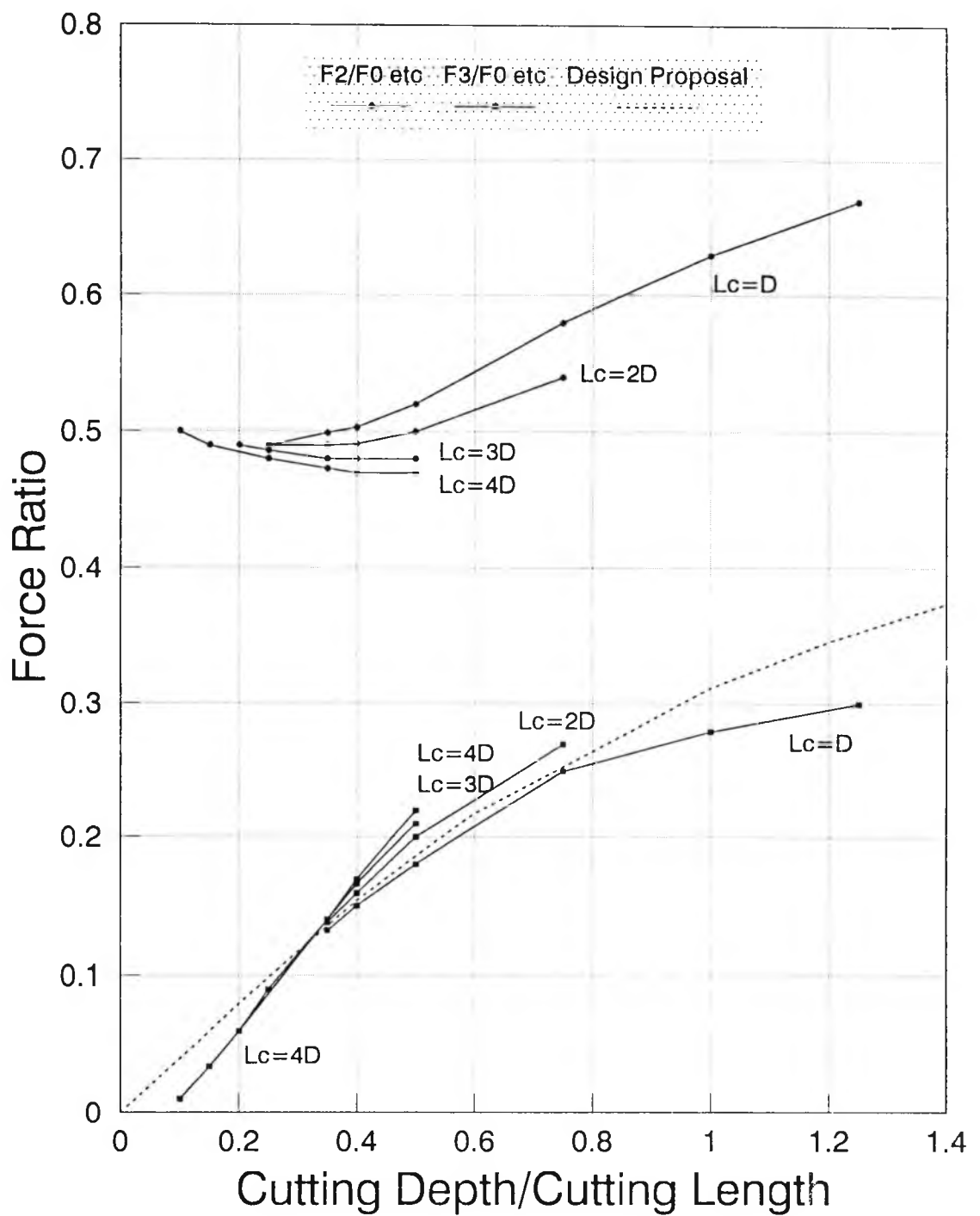


Figure 8.19 Computer Studies - Haunch Toe Force Ratios $F2/F0$ and $F3/F0$ versus the Cutting Depth/Length Ratio

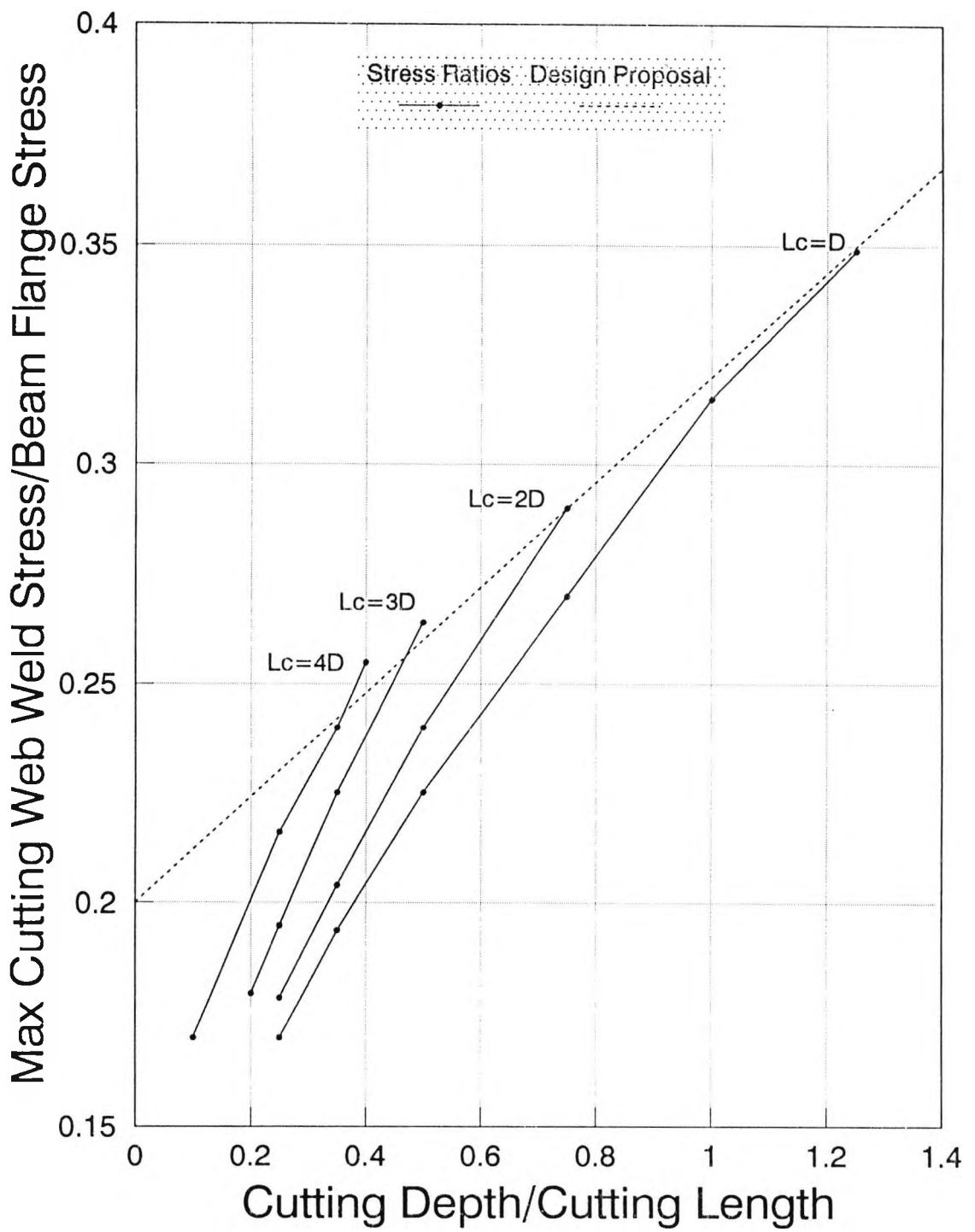


Figure 8.20 Computer Studies - Maximum Cutting Weld Stress Relationship with the Cutting Depth/Length Ratio

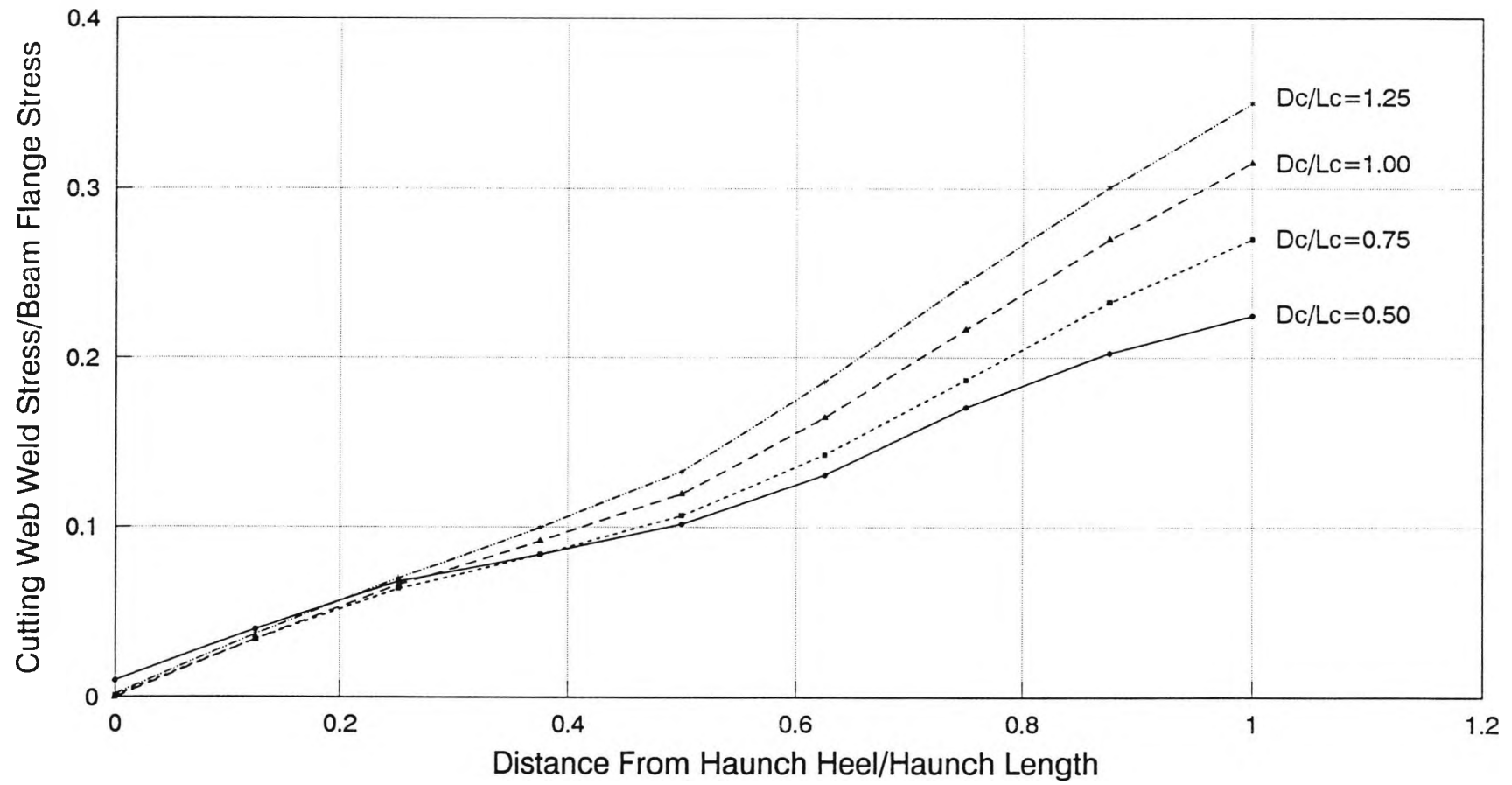


Figure 8.21 Computer Studies - Cutting Web Weld Stress Profile - Case $L_c = D$

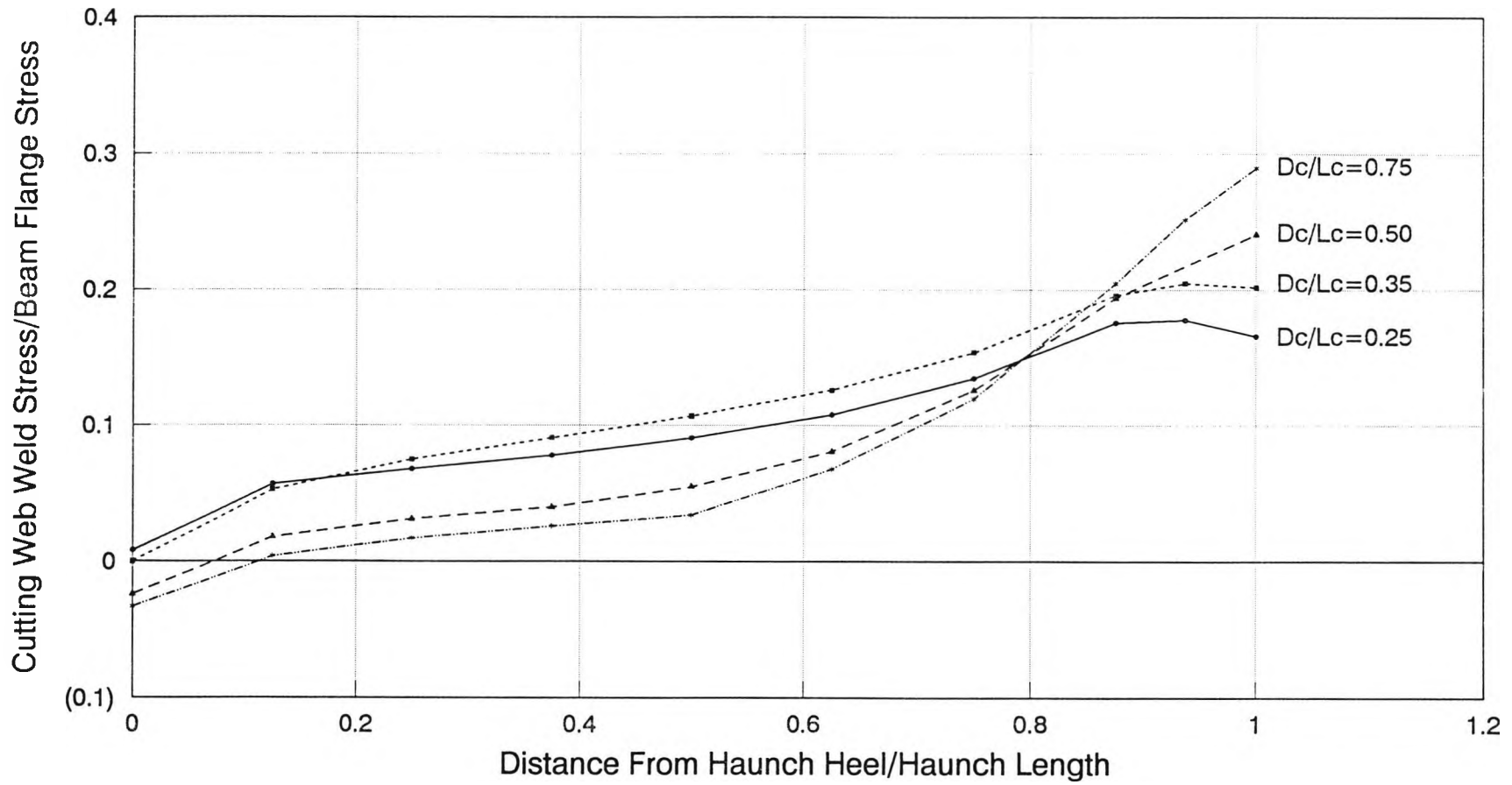


Figure 8.22 Computer Studies - Cutting Web Weld Stress Profile - Case Lc = 2D

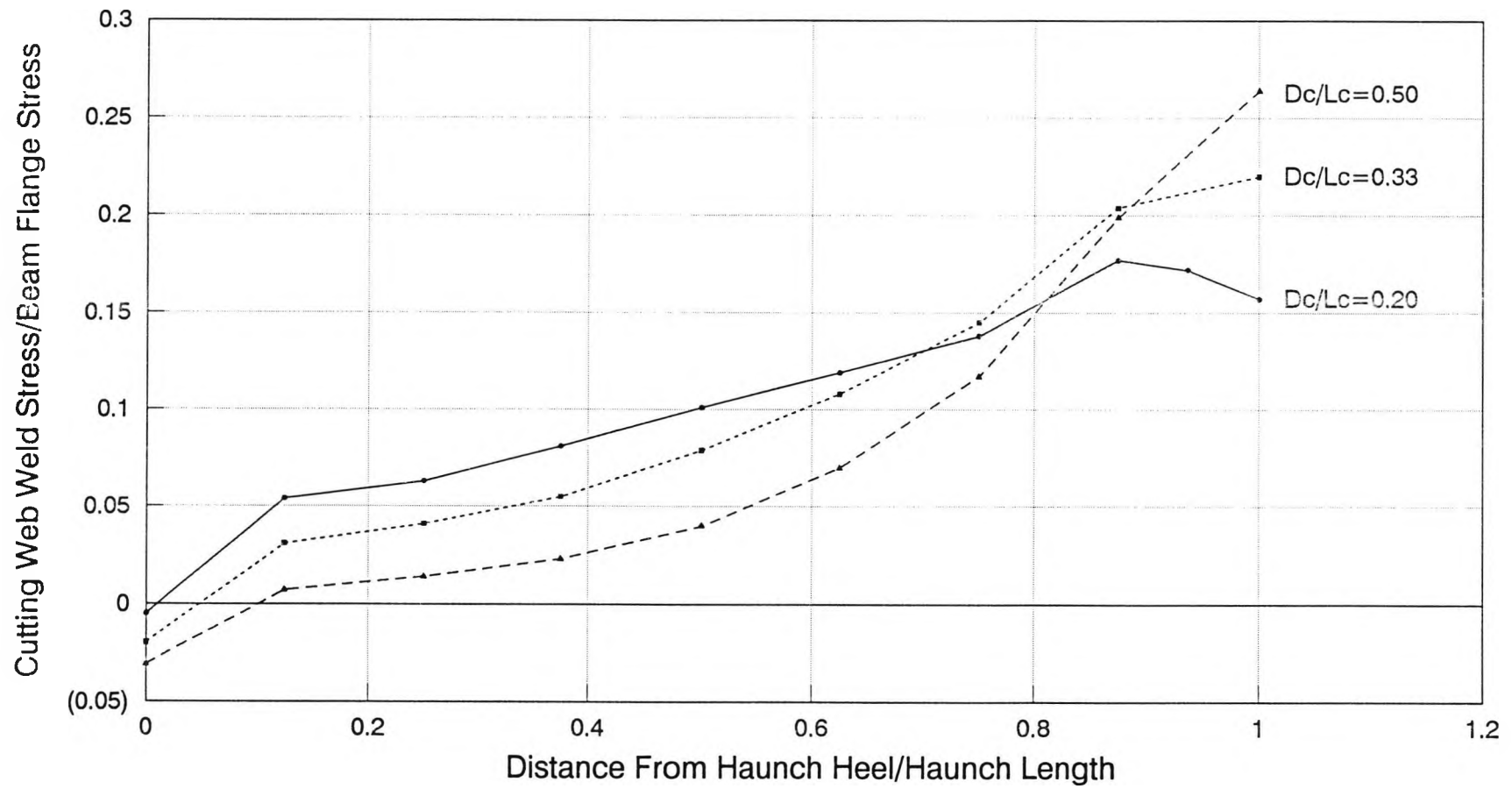


Figure 8.23 Computer Studies - Cutting Web Weld Stress Profile - Case $L_c = 3D$

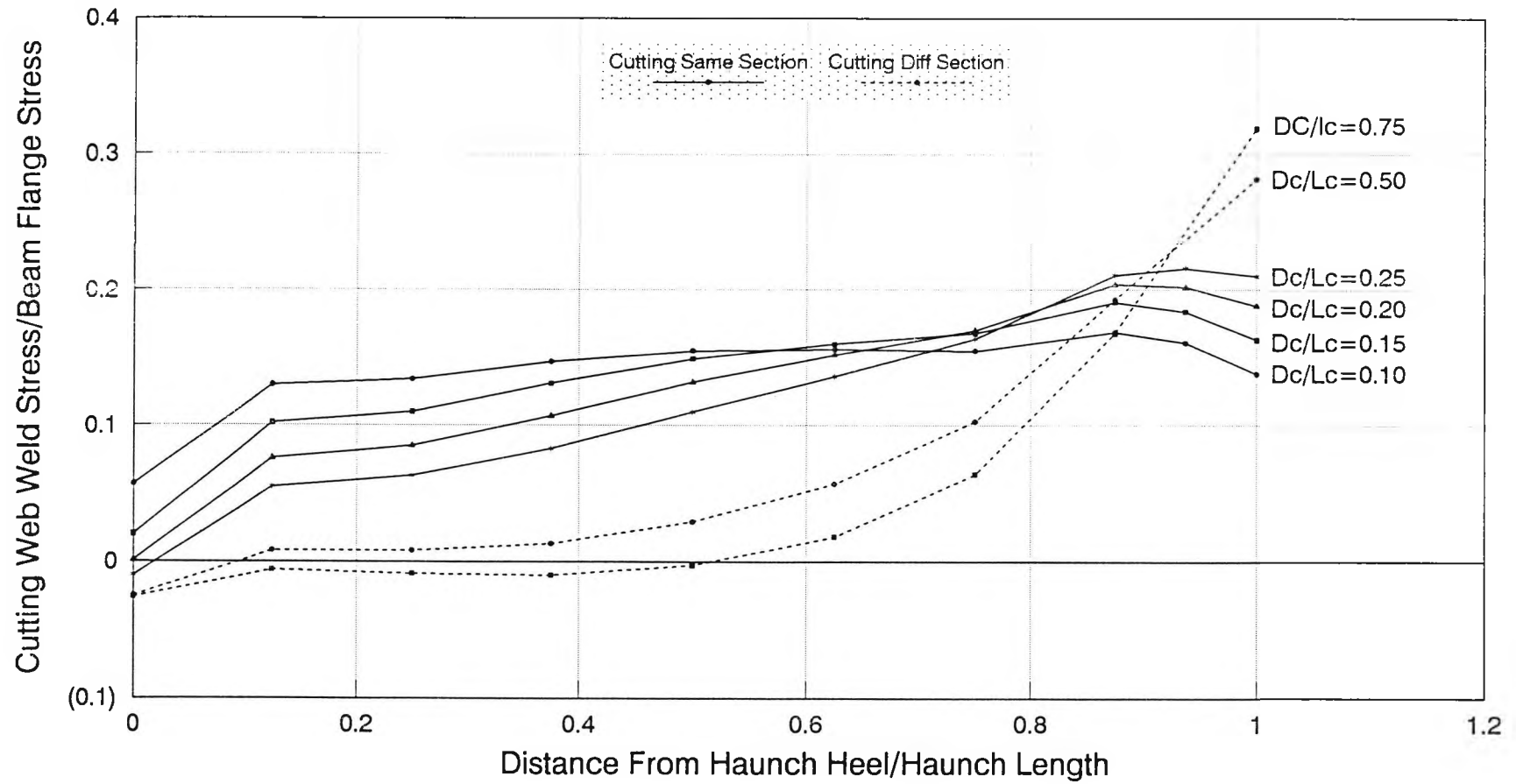


Figure 8.24 Computer Studies - Cutting Web Weld Stress Profile - Case $L_c = 4D$

CHAPTER 9

CONCLUSIONS, RECOMMENDATIONS AND FUTURE WORK

9.1 CONCLUSIONS AND RECOMMENDATIONS

9.1.1 General

The main conclusion from this work is that the system of building incorporating haunched composite steel frames is a viable alternative to other framing systems. It is also concluded that the performance of two full-scale tests has been safely and reasonably accurately predicted by the theory that has been specifically developed. In the light of this, the design method has been applied in detail in a worked example in the Appendix at the end of this Chapter.

9.1.2 Dynamic Behaviour of the Main Beam Test

The calculation of the natural frequency for typical rigid frames was outlined in Chapter 2, and the prediction for the test showed reasonable agreement with the recorded value, although the inertia of the test rig is believed to have influenced the result slightly. The value of the critical damping ratio, however, agrees well with published values for unfurnished composite construction {26}.

9.1.3 Elastic Behaviour of the Tests

The behaviour of the tests showed a gradual decline in stiffness from the initial values, which were comparable to an 'uncracked' hogging region concrete section, to values which were comparable to the stiffness of a 'cracked' hogging region. This result confirms earlier research, and the recommendations, therefore, must continue to be that no account of the stiffness of the concrete should be taken in hogging moment regions (other than for dynamic calculations). The 10% reduction in end moments, proposed in Chapter 2 to allow for the concrete cracking, was shown to give an accurate prediction of the serviceability behaviour, and is recommended.

9.1.4 Section Classification

The section classification of composite beams is normally only relevant for hogging moment regions, because there the compression flange is not restrained by the floor slab, whereas in sagging regions it is restrained. The moment redistribution design method, outlined in Chapter 2, and based on the British Code for the design of composite beams {14}, permits the use of sections of all classifications when considering these factors, but the plastic design method can only be applied to beams with a 'plastic' classification. Both the column and beam sections used in the tests were 'plastic', and so no conclusions can be drawn which would change these methods with regard to this aspect.

9.1.5 Hogging Region Moment Capacity

Both tests confirmed that the tensile strength of the concrete should be neglected in hogging moment regions, and the Sub-Assembly Test showed that, when the decking spans transversely to the beams, it also contributes little to the strength of these regions. However, the main beam test clearly demonstrated that, when the decking is spanning parallel to the beam, it can make a significant contribution to the strength of the section. This is only likely to apply where the decking is positively fixed to the beam with shear connectors down the length of the decking and along its ends. Also, the contribution is unlikely to be so great if end lap joints occur within the hogging region. It may not be prudent to recommend that this effect be included in design because of the restriction of the decking layout and the degree of site supervision that would be required, but on the other hand, since it is likely to occur, it seems logical to include it. Perhaps more consideration could be given to this point.

It is not recommended that the contribution of the mesh be included in design calculations, because, although it did not fracture in the Main Beam Test, it did so in the Sub-Assembly Test, and other researchers have also confirmed that its ductility cannot be relied upon.

9.1.6 Sagging Region Moment Capacity

The Main Beam Test behaviour confirmed that the conventional plastic stress block theory for composite sagging regions gives a good estimate of the strength.

9.1.7 Local and Lateral Buckling

9.1.7.1 Test Behaviour

The tests confirm that, in hogging moment regions when composite beams buckle, they do so in the form of either a local buckle, a lateral distortional buckle, or a combination of the two, but not as a lateral torsional buckle - where the section rotates as a whole. The tests also showed that, when it occurs, particularly with regard to a local buckle, the decline in strength can still be gradual, and the structure can behave plastically. All the test specimens exhibited some form of buckling, but, as explained in the text, the important factor is the characteristics of the moment/rotation curve at the critical sections, ie, in this case, at the haunch toes. The tests also showed that local buckling does not necessarily precipitate lateral buckling, and they suggested that the stockier the section, the less likely it is to do so. Despite the presence of buckling, however, they also showed that with appropriate detailing, as discussed later, satisfactory performance can still be achieved.

9.1.7.2 Comparison of Test Behaviour with Theory

The design method for the treatment of lateral distortional buckling, developed in Chapter 3, has been shown by the tests to be conservative when applied to haunched composite beams. The buckling length was over-estimated by the theory by about 40%, and the maximum capacity by 30%. This was mainly due to the extra lateral stiffness which the cutting and web stiffening provided. From the analysis of the results of the Sub-Assembly Test in Chapter 5, it was found that, for haunched composite beams, the value of the critical buckling length, L_{cr} , calculated from equation 3.35, can be overestimated by 60%. It is ^{therefore} suggested that the value of the

slenderness parameter, v_t , calculated from equation 3.22, should be multiplied by 0.75 to produce realistic design values. However, on the basis of the tests, it is clear that, when a full depth stiffener is provided both sides of the web at the haunch toe, and when the minimum shear connection is maintained over the whole hogging region, the haunch is sufficiently stiff to assume that the haunch toe position is restrained. The possibility of buckling need only then be checked beyond the haunch, in towards the span. This is recommended for design, but only where the haunch cutting lengths are no greater than 2 x beam depth.

9.1.7.3 Comparison of the Proposed Method with Other Methods

The proposed method of design in Chapter 3 was compared with other methods which check for lateral distortional instability. The comparison showed that similar results were obtained when the slenderness, λ , lay between 75 and 125, but, beyond this range, notable differences occurred, although mainly on the conservative side. Exceptions included the EC4 method {15}, which demonstrated a surprising increase in strength with slenderness beyond $\lambda = 125$. It is suggested that this method may not consider the possibility of multiple buckling waves, ie, the harmonics of a particular wavelength. Also, the method of Weston et al {29}, which was really developed for bridges, was shown to be very conservative for values of $\lambda > 125$, and unsafe for values of $\lambda < 100$. This method is therefore not recommended for composite building structures.

9.1.7.4 Influence of Slab Flexibility

The influence of slab flexibility on the buckling behaviour was also considered, and, because of the uncertainty of the effectiveness of the concrete slab in providing torsional restraint to deep steel sections, it is suggested that this restraint be neglected in certain cases. These are determined by the ratio of the beam web bending stiffness to the concrete slab transverse bending stiffness, and a criterion for this has been proposed in Chapter 3. In practice, for internal beams, restraint can be assumed for almost all sections up to 457mm serial size. Beyond that, the heavier sections in each serial size may not pass the criterion, but they can still be designed by assuming lateral restraint only to the top flange.

9.1.8 Moment/Rotation Characteristics

The moment/rotation characteristics of the haunch region were specifically examined by the tests, and also by the computer study outlined in Chapter 8, discussed later. The degree of rotation obtained from the Sub-Assembly Tests was compared in Chapter 5 with theoretical requirements specified by Kemp {40}. It was found that only those beams with full depth stiffeners fitted both sides of the web at the haunch toes passed the criterion. These specimens continued to sustain their design plastic moments of resistance up to a value of 4° (70×10^{-3} rads) rotation, and it is interesting to note that the maximum load was achieved in the Main Beam Test when the haunch toe rotations were of the order of 3° (52×10^{-3} rads). The performance of the test specimen without these stiffeners is considered to be unsatisfactory, and the specimen with half-depth stiffeners, although improved, is also considered to be unsatisfactory.

The effectiveness of a haunch toe knee brace was not conclusively proved by the tests because the brace bolts sheared, and this allowed the beam to deflect laterally, which weakened it. Allowing for this, the test showed that a design force for the brace of $2\frac{1}{2}\%$ of the force in the beam flange is appropriate. Also, as is normal practice, it is recommended that whatever the design forces are in the brace, the brace bolts should be no smaller than M16's. It is also recommended that, whether a knee brace is provided or not, full depth stiffeners should be fitted both sides of the web at the haunch toe, not only to provide a torsional restraint load path at that point, but also to prevent web buckling - caused by the vertical component of the cutting flange force.

9.1.9 Computer Studies

9.1.9.1 Moment/Rotation Characteristics

The determination of the moment/rotation characteristics for the Sub-Assembly Test beams was one of the main purposes of the computer study, so that, with good agreement with the test results, further simulated tests could be carried out. It can be concluded that the use of semi-loof shell elements, with the geometric non-

linearity being provided by utilizing an 'Updated' Lagrangian Formation, is satisfactory for this type of structure, and reasonable agreement was achieved in the study.

The elastic behaviour of the specimens was very well predicted by the model and the maximum strength and post-buckling behaviour was also generally well predicted, but with a slight underestimation of the latter. The moment/rotation characteristics of the case without haunch toe stiffening was not as well predicted, and the maximum strength was overestimated by some 10%. It is suggested that the effect of residual stresses may have affected this specimen much more adversely than the others, and these were not included in the mathematical model. The shape and location of the local buckling, and the lateral distortional buckling mode shapes, were well-predicted, although the magnitude and the growth of the lateral displacements were generally underestimated by the computer program.

Comparative computer studies also showed that the best agreement with the test results was obtained when normal fabrication tolerances were used as the maximum lateral imperfection. From a simulated variation of the beam minor axis end conditions, it was found that the best agreement was achieved by assuming that they were fixed.

9.1.9.2 Element Forces at the Haunch Toe

The computer model was also used to study the forces in the elements intersecting at the haunch toe, and design values are suggested in Chapter 8. The study was based on elastic behaviour without residual stresses, and it is therefore approximate. Only a limited geometric range for the haunch was considered, and this was related to the practical range appropriate for haunched composite beam construction.

One notable conclusion was that the cutting flange force at the haunch toe intersection, within the geometric parameters considered, varied between 54% and 67% of the force in the bottom beam flange, and a value of 70% is recommended for the design of the toe weld.

9.1.10 Beam to Column Connections

The haunched beam end connections in the tests were all extended end plate 'rigid' connections, with a fillet stiffener included above the top flange. From plots of the bolt forces in the Sub-Assembly Test, it was clear that the connections were never loaded beyond their elastic range. The maximum moments in the Main Beam Test were calculated from equilibrium to be well above their design values. However, it is concluded that this was due to the enhancement of the strength of the hogging region by the rigidly-fixed decking, which, in this particular case, ran parallel to the main beam. In other words, it is suggested that the force induced in the decking, whilst increasing the section strength and the connection strength, actually by-passed the bolt group, and so it was not over-loaded. This is also confirmed by the fact that little deformation of the connection elements was observed in this, or the previous, test. It is therefore concluded that the design method outlined in the design guide {9} is reasonable.

9.2 DESIGN EXAMPLE

To illustrate the design method which has been developed, a detailed design example is presented in Appendix 9A. It is set out as it would be in commercial practice and it is based on a seven-storey single-span building which is braced against side-sway. The floor grid consists of a 13.5m main beam span with 6.0m span secondary beams at 3.375m centres. The storey height is assumed to be 4.7m, with a floor zone of 1.2m.

The Main Beam Test was specifically designed to model this frame arrangement, and the section sizes determined from the calculations are those actually used in the test. A direct comparison can therefore be made between the results of these calculations and the performance of the test. The principle conclusion from this is that the test frame supported 30% more load than the design calculations suggest, which represents a generous safety margin.

The frame in the example is designed by using the 'plastic' method, but an example of the 'redistribution' method is given in the published design guide {9}. Both the construction and in-service conditions are considered at the appropriate ultimate and serviceability limit states. A detailed design of the haunch and the end connection is also included.

9.3 FUTURE WORK

9.3.1 Computer Studies

The finite element model has been developed and shown to produce reasonable predictions of the hogging region behaviour of composite beams, and it is suggested that further use should be made of it. In particular, the behaviour of more slender sections could be investigated to ascertain their moment/rotation characteristics. Non-standard sections and haunches made up of fabricated sections could also be examined to investigate their efficiency and susceptibility to buckling. The model could also be used to study the performance of further alternative stiffening details at the haunch toe, such as the use of web stiffeners which are almost full-depth, but do not require welding to the upper steel beam flange. The provision of these would avoid the cost of accurately fabricating the stiffeners to 'fit' each beam, but the loss of torsional rigidity at the haunch toe might be too great.

The model itself could also be improved by incorporating residual stresses, and, possibly, by revising the initial imperfection curve.

9.3.2 Future Testing

Where reasonably accurate computer simulation is possible, it is unlikely to be cost-effective to carry out full-scale testing. The effect of including heavy reinforcement to maximise the hogging region strength is not easily modelled, and could be the subject of future testing. The point of this would be to establish an upper bound to the strength of this region, but yet, to confirm that it would still be sufficiently ductile, and not unduly susceptible to buckling.

Advantages might also be gained in continuous composite construction by providing frames without fully rigid full-strength connections, which are expensive to fabricate. In many cases, it might be more appropriate to use a deeper beam with weaker, or partial-strength, connections. These are simpler connections which are weaker than the beam section, and, as such, the hogging hinge forms in the connection and not in the beam. The tensile forces in the connection could be designed to be resisted by the reinforcement or the bolts, or a combination of the two. The areas of uncertainty would include the serviceability performance and the moment/rotation capability necessary for plastic collapse. Some work has been carried out in this area by recent researchers, but more is needed to develop the idea, including further full-scale frame tests.

APPENDIX 9A

DESIGN EXAMPLE

Index

Design Data	1
Floor Slab Design	3
Secondary Beam Design	4
Main Beam Plastic Design	5
Column Design	12
Main Beam Construction Condition	15
Main Beam Elastic Properties	18
Main Beam Serviceability Conditions	19
Floor Dynamic Sensitivity	25
Main Beam Shear Connection Design	30
Main Beam Lateral Stability Check	33
Main Beam Longitudinal Shear Check	39
Haunch and Haunch Connection Design	42
Column Stiffening Checks	49
Haunch Toe Web Stiffener Design	53



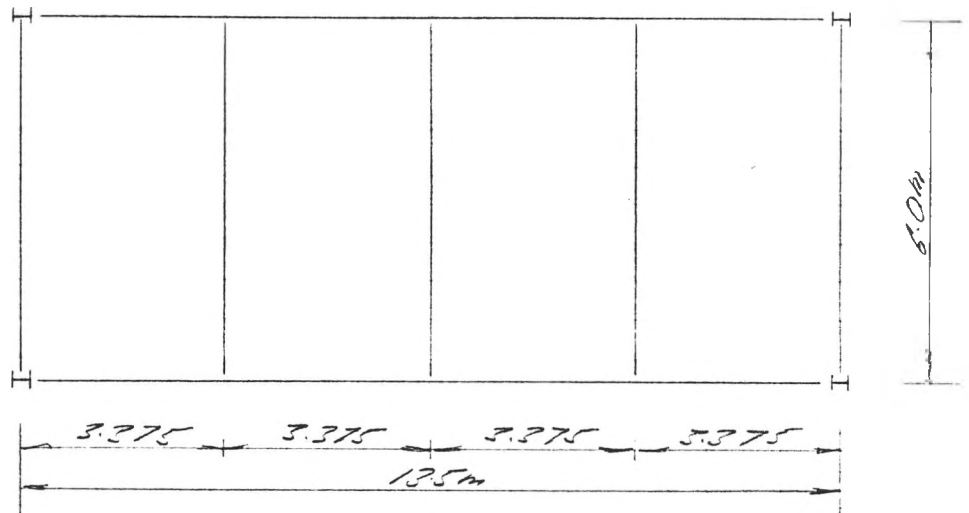
Job No.	Sheet / of	Rev.
Job Title <i>DESIGN EXAMPLE</i>		
Subject <i>Design Data</i>		
Client	Made by <i>J.H.R.</i>	Date
	Checked by	Date

DESIGN OF COMPOSITE HAUNCHED
MAIN BEAM SUB-FRAME

*A 7 storey, single span building
braced against side sway is considered*

Typical floor plan (part)

*Design
Reference
clauses
refer to
BS5950
pt 3.1
unless
otherwise
stated*



Frame Data

*Main beams ~ 13.5m span with rigid
connections to columns
secondary beams ~ 6.0m span ~ simply supported
storey height ~ 4.7m
Fire resistance ~ 1 1/2 hrs
Column bases ~ fixed*

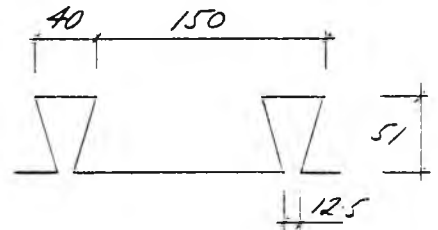


Job No.	Sheet 2 of	Rev.
Job Title	DESIGN EXAMPLE	
Subject	Design Data	
Client	Made by J.W.R.	Date
	Checked by	Date

Deck Data

profile height = 51mm

trough spacing = 150mm



Shear Connector Data

diameter = 19mm

length (as welded) = 95mm

Concrete Data

compressive strength = 30 N/mm²

type ~ lightweight, density = 1800 kg/m³

Slab Data

depth = 130mm

span = 3275mm

Design Loading Data

occupancy ~ 4.0 kN/m²

partitions (imposed) ~ 1.0 kN/m²

ceiling and services ~ 0.5 kN/m²
raised floor ~ 0.2 kN/m² } superimposed dead load = 0.7 kN/m²

construction load (temporary) ~ 0.5 kN/m²



Job No.	Sheet 2 of	Rev.
Job Title	DESIGN EXAMPLE	
Subject	slab Design	
Client	Made by JWR	Date
	Checked by	Date

Design Loading Data (contin)

sheet 4

slab weight = 2.32 kN/m^2

sheet 6

secondary beams (self wt) = 0.3 kN/m

main beams (self wt) = 0.75 kN/m

SLAB DESIGN

ref 'The
fire
resistance
of composite
floors with
steel decking'
by SCI
Table 7

minimum recommended slab thickness for
 $\frac{1}{2}$ hr. fire resistance using dovetail decking
and lightweight concrete is $125 \text{ mm} < 130 \text{ mm}$ $\therefore \text{OK}$

max recommended span = $3.6 \text{ m} > 3.375 \text{ m}$ $\therefore \text{OK}$

recommended fire mesh is A193

from manufacturer's data, assuming a double
span, an adequate gauge thickness is 1.2 mm
with a decking depth = 51 mm ($= D$)

— u —

hence fire resistance condition $38 \leq D \leq 50$
is virtually satisfied.

decking wt from manufacturer's data = 0.18 kN/m^2



Job No.	Sheet 4 of	Rev.
Job Title DESIGN EXAMPLE		
Subject Secondary Beam Design		
Client	Made by J.W.R	Date
	Checked by	Date

slab dead wt ~

$$\text{area of void} = 51 \left(\frac{40-12.5}{2} + 12.5 \right) = 1339 \text{ mm}^2$$

$$\text{area per metre} = \frac{1339 \times 1000}{150} = 8925 \text{ mm}^2/\text{m}$$

$$\begin{aligned} \text{wt. of concrete} &= \left(\frac{130 \times 10^3 - 8925}{10^6} \right) \times 1800 \text{ kg/m}^3 \times \frac{9.81}{10^3} \\ &= 2.12 \text{ kN/m}^2 \end{aligned}$$

$$\text{add decking wt.} = 0.18 \text{ kN/m}^2$$

$$\text{reinforcement} = 0.03 \text{ kN/m}^2$$

$$\underline{\underline{2.33 \text{ kN/m}^2}}$$

SECONDARY BEAM DESIGN

simply supported internal span = 6.0m and @ 3375m ctrs

In-service ultimate condition (composite) ~

Loading:

$$\text{Imposed live ~ occupancy} = 4.0 \text{ kN/m}^2$$

$$\text{~ partitions} = 1.0 \text{ kN/m}^2$$

$$\underline{\underline{5.0 \text{ kN/m}^2}}$$

$$\text{Dead ~ floor slab} = 2.33 \text{ kN/m}^2$$

Super dead ~ ceiling, services

$$\text{\& raised floor} = 0.7 \text{ kN/m}^2$$

$$\underline{\underline{3.03 \text{ kN/m}^2}}$$



Job No.	Sheet 5 of	Rev.
Job Title	DESIGN EXAMPLE	
Subject	Main Beam Plastic Design	
Client	Made by J.W.R	Date
	Checked by	Date

beam self wt, say = 0.3 kN/m

Factored design load per secondary beam
 $= [1.6 \times 5.0 + 1.4(3.03 + 0.3/3.375)] \times 3.375 = \underline{41.7 \text{ kN/m}}$

from a separate computer analysis (- see sheet 6)

Use 254 x 146 UB31 grade 50 with 16 studs

MAIN BEAM DESIGN (internal span)

In-service ultimate condition (composite)

Loading:

Imposed live - occupancy ~	4.0 kN/m ²
~ partitions ~	<u>1.0 kN/m²</u>
	5.0 kN/m ²

but loaded area per beam

$$= 3 \times 3.375 \times 6.0 = 61 \text{ m}^2$$

∴ reduce loading by 6.1% $- \underline{0.3 \text{ kN/m}^2}$
4.7 kN/m²

33 6377



Job No.	Sheet 8 of	Rev.
Job Title <i>DESIGN EXAMPLE</i>		
Subject <i>Main Beam Plastic Design</i>		
Client	Made by <i>JWK</i>	Date
	Checked by	Date

JOB REFERENCE JR1
BEAM REFERENCE

DESIGN CODE	CIUD	SPAN	6.0 m
FLOOR TYPE	HOLDRIB	FLOOR DEPTH	130 mm
DECK DEPTH	51.0 mm	DECK TROUGH CENTRES	152.5 mm
BEAM CENTRES	3.4 m	NUMBER REQUIRED	1
CONCRETE TYPE	LW	MODULAR RATIO	15
CONCRETE GRADE	30 N/mm ²	STEEL GRADE	50
IMPOSED LOAD	5.0 kN/m ²	SLAB WEIGHT (DRY)	2.34 kN/m ²
WEIGHT OF CEILING ETC	0.7 kN/m ²		
UD CONSTRUCTION LOAD	0.5 kN/m ²	POINT CONSTRUCT. LOAD	4.0 kN
SHEAR STUD DIAMETER	19 mm	STUD LENGTH	95 mm

UNPROPPED COMPOSITE DESIGN TO SCI RECOMMENDATIONS, NAT. FREQUENCY LIMIT 5.0 HZ

DESIGN : A CON. SHEAR, B CON. BEND, C CON. LTB, D COMP SHEAR, E COMP BEND
CRITERIA : F STEEL STRESS, G CONCRETE STRESS, H DEFLECTION, I VIBRATION

SERIAL	SIZE	DEFL		DES	UMAX	NO. BS5950 STD	WT BEAM	TOT STD	COST BEAM	COST STD	COST TOTAL	
		CON	IMP									
203x133x	25	30	13	F	0.97	24	N	152	24	0	24	24
203x133x	30	25	11	F	0.82	20	N	162	20	0	20	20
254x102x	22	25	11	F	1.00	20	N	133	20	0	20	20
254x102x	25	21	10	F	0.87	18	N	152	18	0	18	18
254x102x	28	18	9	F	0.76	18	N	170	18	0	18	18
254x146x	31	16	9	F	0.68	18	N	188	18	0	18	18
254x146x	37	13	7	E	0.57	18	N	224	18	0	18	18
254x146x	43	11	7	E	0.51	18	N	261	18	0	18	18
305x102x	25	16	8	F	0.81	16	N	152	16	0	16	16
152x152x	30	41	16	F	0.97	34	N	192	34	0	34	34
152x152x	37	33	13	F	0.80	28	N	224	28	0	28	28
203x203x	46	16	9	E	0.58	18	N	279	18	0	18	18
203x203x	52	14	8	I	0.55	18	N	315	18	0	18	18
203x203x	60	12	7	I	0.53	18	N	364	18	0	18	18
203x203x	71	10	6	I	0.49	18	N	430	18	0	18	18
203x203x	86	8	5	I	0.46	18	Y	521	18	1	18	19
254x254x	73	7	5	I	0.43	18	Y	442	18	0	18	18
254x254x	89	5	4	I	0.40	18	Y	539	18	1	18	19

A, B OR AB AFTER THE SECTION INDICATES TRANSVERSE REINFORCEMENT MUST BE CHECKED

REACTIONS: DEAD LOAD 32.8 kN IMPOSED LOAD 50.6 kN

ASSUMED COSTS:- STEEL BEAMS / TONNE 1 SHEAR STUDS 1
COSTS AND QUANTITIES INCLUDE 1 % FOR FITTINGS ETC.

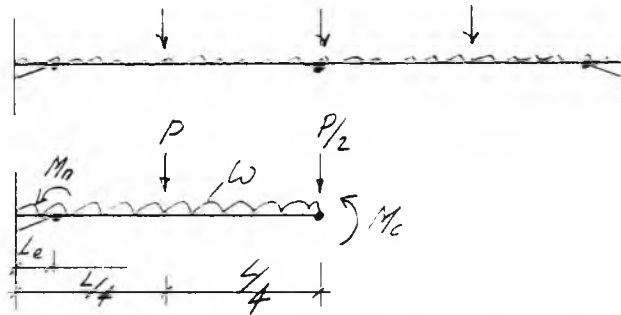
***** For conditions of use refer to first page of output or manual *****



Job No.	Sheet 8 of	Rev.
Job Title	DESIGN EXAMPLE	
Subject	Main Beam Plastic Design	
Client	Made by J.W.R.	Date
	Checked by	Date

plastic design of main beam ~

for a mechanism between the haunch tips ~



M_n = hogging plastic moment of resistance at haunch tip

M_c = sagging plastic moment of resistance at centre

moments about haunch tip ~

$$M_c + M_n = P\left(\frac{L}{4} - L_e\right) + \frac{P}{2}\left(\frac{L}{2} - L_e\right) + w\left(\frac{L}{2} - L_e\right)^2/2$$

$$M_c + M_n = \frac{P}{2}(L - 3L_e) + \frac{w}{2}\left(\frac{L}{2} - L_e\right)^2$$



Job No.	Sheet 9 of	Rev.
Job Title DESIGN EXAMPLE		
Subject Main Beam Plastic Design		
Client	Made by J.W.R.	Date
	Checked by	Date

The collapse factor of safety F where
Loading = $F(1.6W_L + 1.4W_D)$ is given by

$$M_0 + M_n = F \left\{ \frac{P}{2}(L - 3L_0) + \frac{W}{2} \left(\frac{L}{2} - L_0 \right)^2 \right\}$$

Hence to satisfy the ultimate condition, $F \geq 1$

ie
$$\frac{M_0 + M_n}{\left\{ \frac{P}{2}(L - 3L_0) + \frac{W}{2} \left(\frac{L}{2} - L_0 \right)^2 \right\}} \geq 1$$

Trial beam size ~ typically span/total depth
ratio lies between 24 and 28

try 26, hence $\frac{13500}{26} - 130 = D = 389 \text{ mm}$

Try 406 x 178 UB 74 kg/m grade 50

The section is 'plastic' for both hogging and
sagging and hence is suitable for plastic design

Composite sagging moment resistance at centre -
 M_0 (neglecting concrete between voids) ~

Effective flange width B_e

$$= 2b_e = 2L_z/8 = 2 \times 0.7 \times 13500/8 = \underline{2363 \text{ mm}}$$

Resistance of concrete flange

$$R_c = 0.45f_{cu} \cdot B_e (D_s - D_p)$$

$$= 0.45 \times 30 \times 2363 (130 - 51) / 10^3 = \underline{2520 \text{ kN}}$$

B35750
pt 3.1
cl 4.5

cl 4.6

B.2.1



BS5750
pt 3.1
B.2.1

Resistance of overall web depth

$$R_w = R_s - 2R_f$$

but $R_s =$ Resistance of steel beam = $A \cdot p_y$

and $p_y = 255 \text{ N/mm}^2$

$$\text{hence } R_s = \frac{95 \times 10^3 \times 255}{10^3} = \underline{\underline{3373 \text{ kN}}}$$

$R_f =$ Resistance of steel flange = $L \cdot T \cdot p_y$

$$\therefore R_f = \frac{179.7 \times 160 \times 355}{10^3} = \underline{\underline{1021 \text{ kN}}}$$

$$\text{hence } R_w = 3373 - 2 \times 1021 = \underline{\underline{1321 \text{ kN}}}$$

BS5750
pt 2.1
B.2.2

For full shear connection, since $R_c > R_w$
case 2 applies. Since $R_s > R_c$ case (a) applies

Hence,

$$M_o = R_s \frac{D}{2} + \frac{R_c (D_s + D_p)}{2} - \frac{(R_s - R_c)^2}{R_f} \cdot \frac{T}{4}$$

$$= \frac{3373 \times 412.8}{2 \times 10^3} + \frac{2520(130+51)}{2 \times 10^3} - \frac{(3373-2520)^2}{1021 \times 10^3} \cdot \frac{16.0}{4}$$

$$\therefore M_o = \underline{\underline{721 \text{ kNm}}}$$

Negative moment section resistance at haunch tip

For no reinforcement over haunch, $M_n = M_s$
but check for effect of shear -

sheet 7

Shear force F_v at support reaction = 368 kN



Job No.	Sheet 11 of	Rev.
Job Title	DESIGN EXAMPLE	
Subject	Main Beam Plastic Design	
Client	Made by J.W.R.	Date
	Checked by	Date

RS5750
pt 1
cl 9.2.3

No reduction is made in the moment resistance
if $F_v < 0.8P_v$

where $P_v = 0.6p_y$ $F_v = \frac{0.8 \times 355 \times 9.7 \times 12.8}{10^3} = 853 \text{ kN}$

$0.8P_v = 0.8 \times 853 = 512 \text{ kN} > 368 \text{ kN}$

$\therefore \underline{M_n = M_s = 532 \text{ kNm}}$

Haunch length, $L_e \sim$

Try a haunch length = 5% span or a 45° cutting

5% span $\sim 0.05 \times 13500 = 675 \text{ mm}$

45° cutting $\sim 110 + \frac{330}{\text{span}} \times 2 \text{ column} + 30 \text{ end plate} = 605 \text{ mm}$

but put $L_e = 615 \text{ mm}$

Hence check ultimate condition \sim

$\frac{921 + 532}{\left\{ \frac{240.7}{2} (135 - 3 \times 0.615) + 1.05 \left(\frac{135 - 0.615}{2} \right)^2 \right\}} = 1.007 > 1$

sheets
727

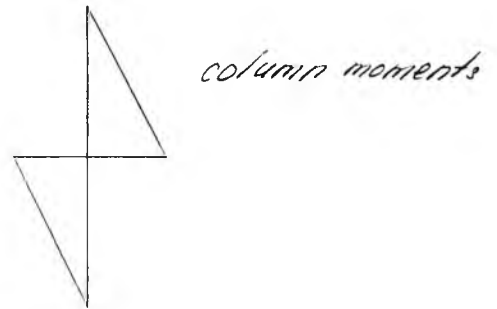
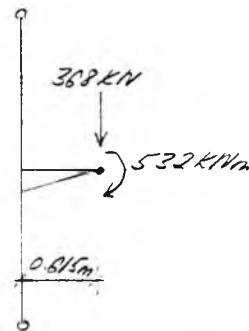
$\therefore \underline{\underline{\text{Ultimate condition satisfied}}}$



Job No.	Sheet 12 of	Rev.
Job Title DESIGN EXAMPLE		
Subject Column Design		
Client	Made by J.V.R.	Date
	Checked by	Date

COLUMN DESIGN

Preliminary sizing ~ use reduced subframe
and neglect relieving effect of other floors



$$\text{max col moment} = \frac{388 \times 0.615 + 532}{2} = 379 \text{ kNm}$$

assume 50% of col capacity resists axial loads

$$\therefore \text{PMR req'd} = \frac{379}{0.5} = 757 \text{ kNm}$$

could use 305UC137, but for improved flange
thickness to avoid column stiffening

try 305 x 305 UC 158

Column design moments ~

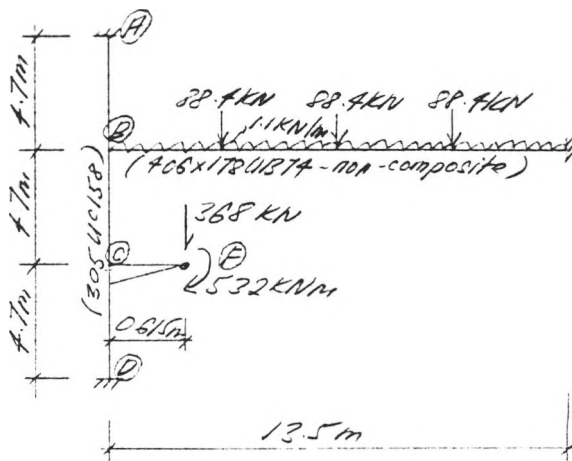
For simplicity and to be conservative, assume
full loading on beams producing the most onerous
column moments - using composite beam properties
and assume only dead + superdead loads on
relieving beams - using non-composite properties.



Job No.	Sheet 13 of	Rev.
Job Title DESIGN EXAMPLE		
Subject Column Design		
Client	Made by J.W.K.	Date
	Checked by	Date

Hence loading diagram using appropriate sub-frame
is ~

BS5950
pt 1
Fig 11



where dead + super-dead load
from secondary beams
(shd 7) = 28.7 kN

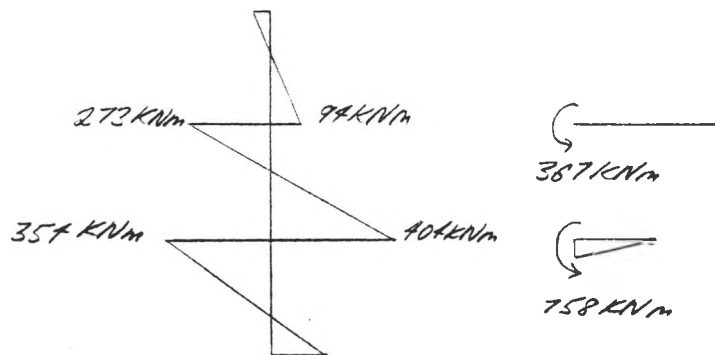
$$F.E.M. \text{ beam } BE \sim \frac{5 \times 28.7 \times 13.5}{16} + \frac{1.1 \times 13.5^2}{12} = 390 \text{ kNm}$$

$$F.E.M. \text{ beam } CF \sim 532 + 368 \times 0.615 = 758 \text{ kNm}$$

$$K_{BA} = K_{BC} = K_{CB} = K_{CD} = K_{CE} = \frac{E \times 38700}{470}$$

$$K_{BE} = \frac{E \times 27300}{1350}$$

Hence from a moment distribution analysis
the moments are ~





DESIGN EXAMPLE

Column Design

J. V.R.

Max column moment = 407 kNm

Without calculating the full axial loads and other cases rigorously, based on a similar 7 storey building analysis, assume 50% of the column capacity resists axial loads.

Hence PMR req'd = $\frac{407}{0.5} = \underline{808 \text{ kNm}}$

PMR of 305 UC158 grade 50 = 911 kNm > 808 kNm ∴ OK

USE 305x305 UC158 grade 50



Job No.	Sheet 15 of	Rev.
Job Title	DESIGN EXAMPLE	
Subject	Main Beam Construction Condition	
Client	Made by	Date
	Checked by	Date

MAIN BEAM CONSTRUCTION CONDITION
 (non-composite)

Loading -

slit 3

Dead - slab = 2.33 kN/m^2

∴ Dead load from secondary beam
 $= (2.33 \times 3.375 + 0.3 \times 6.0) \times 6.0 = \underline{49 \text{ kN}}$

cl 2.2.3

Construction load = 0.5 kN/m^2

cl 2.3.2

∴ Imposed load from secondary beam
 $= 0.5 \times 3.375 \times 6.0 = \underline{10.1 \text{ kN}}$

slit 3

Main beam s.w.l = $\underline{0.75 \text{ kN/m}}$

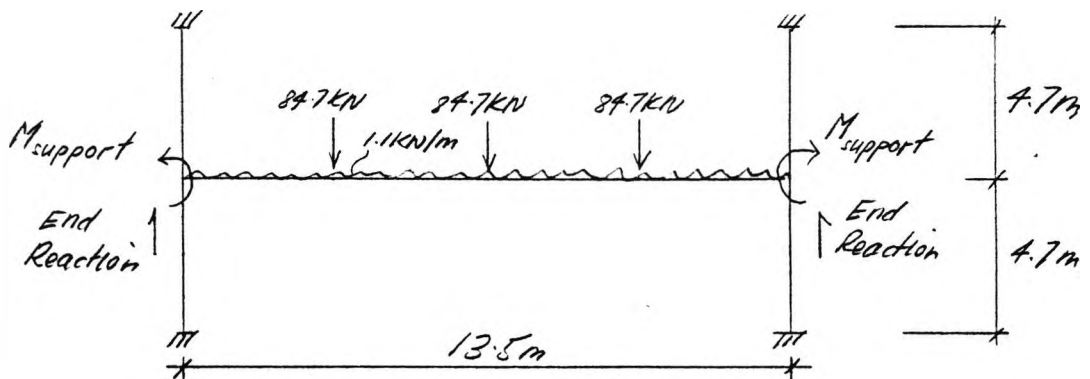
Check Ultimate Limit State -

Design load from secondary beam
 $= 1.4 \times 49 + 1.6 \times 10.1 = \underline{87.7 \text{ kN}}$

Design s.w.l load = $1.4 \times 0.75 = \underline{1.1 \text{ kN/m}}$

B35950
 pt. 1
 Fig 11

Using the substitute frame -





Job No.	Sheet 16 of	Rev.
Job Title	DESIGN EXAMPLE	
Subject	Main Beam Construction Condition	
Client	Made by J.W.R.	Date
	Checked by	Date

Fixed End Moment ~

$$= \frac{5 \times 84.7 \times 13.5}{16} + \frac{1.1 \times 13.5^2}{12} = 374 \text{ kNm}$$

ref
Haunched
Beam
Design Guide

Let the column stiffness parameter, $\phi_c = \frac{I_{col} \times L}{I_{beam} \times h}$

$$\therefore \text{at the construction stage } \phi_c = \frac{38700 \times 13.5}{27300 \times 4.7} = 4.07$$

Hence it can be shown that $M_{support}$

— 11 —
(p. 44)

$$= \frac{4\phi_c}{(4\phi_c + 1)} \times \text{FEM} = \frac{4 \times 4.07}{(4 \times 4.07 + 1)} \times 374 = \underline{\underline{352 \text{ kNm}}}$$

The maximum free bending moment, M_0

$$= \frac{84.7 \times 13.5}{2} + \frac{1.1 \times 13.5^2}{8} = 597 \text{ kNm}$$

\therefore The maximum sagging moment

$$= 597 - 352 = \underline{\underline{245 \text{ kNm}}}$$

$$\text{End Reaction} = (84.7 \times 3 + 1.1 \times 13.5) \times 0.5 = \underline{\underline{134 \text{ kN}}}$$

slt 11

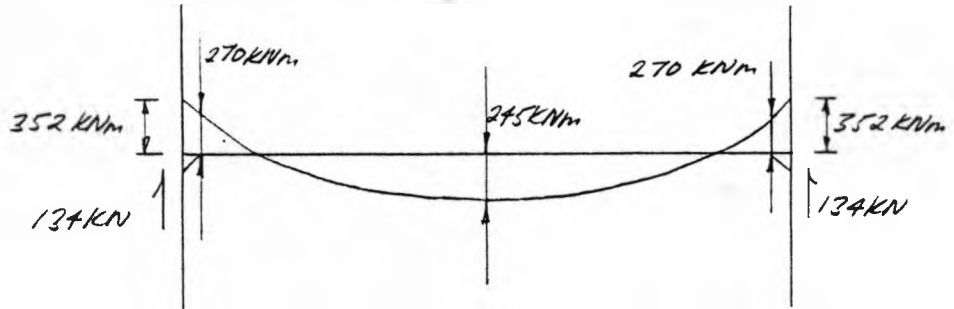
$$\text{haunch length} = 0.815 \text{ m}$$

\therefore Haunch toe moment

$$= 352 + \frac{1.1 \times 0.815^2}{2} - 134 \times 0.815 = \underline{\underline{270 \text{ kNm}}}$$



Job No.	Sheet 17 of	Rev.
Job Title	DESIGN EXAMPLE	
Subject	Main Beam Construction Condition	
Client	Made by J.W.K.	Date
	Checked by	Date



Since main beam $PMR = 532 \text{ kNm} > 270 \text{ kNm}$, 245 kNm
section is adequate

For stability check, see later (sh 22)



Job No.	Sheet 12 of	Rev.
Job Title	DESIGN EXAMPLE	
Subject	Main Beam Elastic Properties	
Client	Made by J.W.R.	Date
	Checked by	Date

MAIN BEAM ELASTIC COMPOSITE PROPERTIES

B.3.1

2nd moment of area (uncracked section) ~

$$I_g = I_x + \frac{B_e (D_s - D_p)^3}{12 \alpha_e} + \frac{A B_e (D_s - D_p) (D + D_s + D_p)^2}{2 \{A \alpha_e + B_e (D_s - D_p)\}}$$

cl 4.1

α_e = modular ratio

for light weight concrete, put $\alpha_e = \frac{2}{3} \times 10 + \frac{1}{3} \times 25 = 15$

$$\begin{aligned} \therefore I_g &= 27300 + \frac{2363 (130 - 51)^3}{12 \times 15 \times 10^4} \\ &\quad + \frac{95 \times 10^2 \times 2363 (130 - 51) (413 + 130 + 51)^2}{2 \{95 \times 10^2 \times 15 + 2363 (130 - 51)\}} \times 10^4 \end{aligned}$$

$$\underline{I_g = 75470 \text{ cm}^4}$$

B.4.1

position of neutral axis ~ (positive moments)

$$\frac{(D_s - D_p)^2 B_e}{(D + 2D_p) \alpha_e} = \frac{(130 - 51)^2 \times 2363}{(413 + 2 \times 51) \times 15} = 1909 \text{ mm}^2$$

$A = 95 \times 10^2 > 1909$ \therefore n.a. lies in steel member (case 2)

$$\begin{aligned} \therefore y_g &= \frac{A \alpha_e (D + 2D_s) + B_e (D_s - D_p)^2}{2 \{A \alpha_e + B_e (D_s - D_p)\}} \\ &= \frac{95 \times 10^2 \times 15 (413 + 2 \times 130) + 2363 (130 - 51)^2}{2 \{95 \times 10^2 \times 15 + 2363 (130 - 51)\}} \\ &= \underline{168 \text{ mm}} \text{ below top of concrete} \end{aligned}$$



Job No.	Sheet 19 of	Rev.
Job Title	DESIGN EXAMPLE	
Subject	Main Beam Serviceability Conditions	
Client	Made by J.W.R.	Date
	Checked by	Date

Hence modulus for top of concrete

$$Z_g = I_g d_e / y_g = \frac{75470 \times 10^4 \times 15}{168 \times 10^3} = \underline{\underline{67387 \text{ cm}^3}}$$

modulus of bottom steel flange

$$Z_s = I_g / (D + D_s - y_g) = \frac{75470 \times 10^4}{(413 + 130 - 168) \times 10^3} = \underline{\underline{2013 \text{ cm}^3}}$$

MAIN BEAM SERVICEABILITY CONDITIONS

(a) Non-composite state ~

Loading ~ Unfactored, non-superimposed dead

Dead ~ slab = 2.3 kN/m²

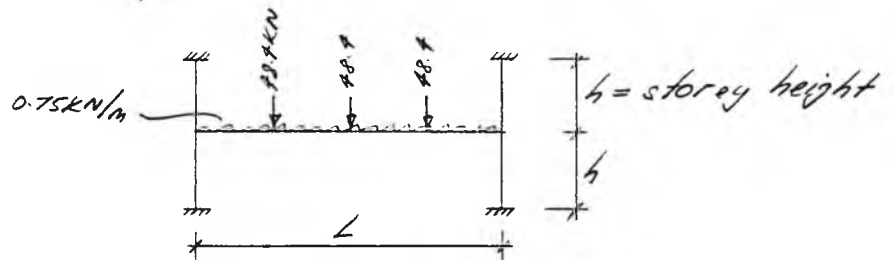
Dead load from secondary beam

$$= (2.3 \times 3.375 + 0.33 \times 6.0) \times 6.0 = 48.4 \text{ kN}$$

∴ Fixed End Moment (from tables)

$$= \frac{5 \times 48.4 \times 13.5}{16} + \frac{0.75 \times 13.5^2}{12} = 216 \text{ kNm}$$

By assuming a sub frame thus ~



As before,

the end moment is given by

$$M_{\text{support}} = \text{F.E.M} \times \frac{\pm \phi_c}{(\pm \phi_c + 1)} \quad \text{where } \phi_c = \frac{I_{\text{COL}} \times L}{I_{\text{BEAM}} \times h}$$

and I_{COL} & I_{BEAM} are the respective moments of area

sht 3



Job No.	Sheet 20 of	Rev.
Job Title	DESIGN EXAMPLE	
Subject	Main Beam Serviceability Conditions	
Client	Made by J.W.R.	Date
	Checked by	Date

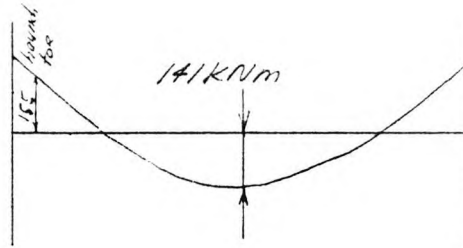
$$\text{non-composite } \phi_c = \frac{32700 \times 135}{27300 \times 4.7} = 4.07$$

$$M_{\text{support}} = \frac{216 \times 4 \times 4.07}{(4 \times 4.07 + 1)} = \underline{203 \text{ kNm}}$$

Maximum free bending moment, M_0

$$= \frac{48.4 \times 13.5}{2} + \frac{0.75 \times 13.5^2}{8} \text{ S.W.B.} = 344 \text{ kNm}$$

$$\text{Hence maximum positive} = 344 - 203 = \underline{141 \text{ kNm}}$$



2.4.3

check stress at mid-span only ~

stress in top & btm flange at mid-span

$$= \frac{141 \times 10^6}{1320 \times 10^3} = \underline{107 \text{ N/mm}^2}$$

(b) composite state ~

Loading ~

Live = 4.7 kN/m²

Dead (superimposed only) ~

ceiling and services = 0.5 kN/m²

raised floor = 0.2 kN/m²

5.4 kN/m²

sheet 5



Job No.	Sheet 21 of	Rev.
Job Title DESIGN EXAMPLE		
Subject Main Beam Serviceability Conditions		
Client	Made by J.U.R.	Date
	Checked by	Date

sheet 19

Design load from secondary beams

$$= 5.4 \times 3.375 \times 6.0 = 109.4 \text{ kN}$$

$$F.E.M = \frac{5 \times 109.4 \times 13.5}{16} = 462 \text{ kNm}$$

$$\text{As before, } M_{\text{support}} = F.E.M \times \frac{4\phi_c}{(4\phi_c + 1)}$$

$$\text{but } \phi_c = \frac{I_{\text{col}} \cdot L}{I_{\text{beam}} \cdot h} \quad (\text{composite state})$$

$$= \frac{38700 \times 13.5}{75470 \times 4.7} = 1.473$$

$$\therefore M_{\text{support}} = \frac{462 \times 4 \times 1.473}{(4 \times 1.473 + 1)} = 395 \text{ kNm}$$

To allow for cracking in the hogging regions ie its effect on the section properties, and for slight yielding that may occur at the haunch toe, a reduction of 10% in the end moment is considered.

$$M_{\text{support}(10)} = 0.9 \times 395 = \underline{\underline{355 \text{ kNm}}}$$

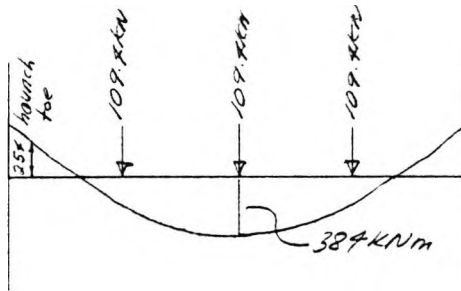
$$M_0 \text{ (maximum free b.m)} = \frac{109.4 \times 13.5}{2} = 739 \text{ kNm}$$

Hence max positive b.m

$$= 739 - 355 = \underline{\underline{384 \text{ kNm}}}$$



Job No.	Sheet 22 of	Rev.
Job Title	DESIGN EXAMPLE	
Subject	Main Beam Serviceability Conditions	
Client	Made by J.W.K.	Date
	Checked by	Date



sheet 19

$$\text{stress in top of concrete} = \frac{384 \times 10^6}{67384 \times 10^3} = 5.7 \text{ N/mm}^2$$

$$\text{permissible concrete stress} = 0.5 f_{cu} = 15 \text{ N/mm}^2 > 5.7 \text{ N/mm}^2$$

concrete stress satisfactory

$$\text{stress in bottom steel flange} = \frac{384 \times 10^6}{2013 \times 10^3} = 190 \text{ N/mm}^2$$

$$\begin{aligned} \text{Total stress (non-comp + comp) in btm flange} \\ = 107 + 190 = 297 \text{ N/mm}^2 < 355 \text{ N/mm}^2 \end{aligned}$$

sheet 20

steel stress satisfactory

$$(\text{NB haunch toe b.m.} = 155 + 257 = 409 \text{ kNm} < 532 \text{ kNm (M}_c\text{)}) \text{ } \underline{\text{OK}}$$

MAIN BEAM SERVICEABILITY DEFLECTIONS

(a) Imposed Live Load only - composite state

sheet 5

Design load from secondary beams

$$= 4.7 \text{ kN/m}^2 \times 3.375 \times 6.0 = 95.2 \text{ kN}$$

$$\text{F.E.M} = \frac{5 \times 95.2 \times 13.5}{16} = 402 \text{ kNm}$$

$$M_{\text{support}} = \frac{\text{F.E.M} \times 4\phi_c}{(4\phi_c + 1)}$$

sheet 21

$$= \frac{402 \times 4 \times 1.473}{(4 \times 1.473 + 1)} = 343 \text{ kNm}$$



Job No.	Sheet 23 of	Rev.
Job Title DESIGN EXAMPLE		
Subject Main Beam Serviceability Conditions		
Client	Made by J.L.R.	Date
	Checked by	Date

sht 21

As before, in the composite state reduce M_{end} by 10% for cracking etc

$$\therefore M_{support(10)} = 343 \times 0.9 = \underline{309 \text{ kNm}}$$

$$M_0 (\text{maximum free b.m.}) = \frac{95.2 \times 13.5}{2} = 643 \text{ kNm}$$

cl 6.1.3.5

For a symmetric load case, the mid-span deflection, δ_c can be found from

$$\delta_c = \delta_0 \left[1 - 0.6 (M_1 + M_2) / M_0 \right]$$

where δ_0 = deflection at mid-span of a simply supported beam subject to the same loading

$$= \frac{19 \times 95.2 \times 13.5^3 \times 10^9}{324 \times 205 \times 75470 \times 10^6} = 74.9 \text{ mm}$$

$$\therefore \delta_c = 74.9 \left[1 - 0.6 (309 + 309) / 643 \right] = \underline{31.7 \text{ mm}}$$

since full interaction provided, no further increase in δ_c

$$\text{Hence } \text{span} / \delta_c = \frac{13500}{31.7} = 426$$

but for brittle finishes, recommended limit is 380

since 426 > 380, live load serviceability deflection OK



Job No.		Sheet 24 of	Rev.
Job Title <i>DESIGN EXAMPLE</i>			
Subject <i>Main Beam Serviceability Conditions</i>			
Client	Made by <i>J.W.R.</i>	Date	
	Checked by	Date	

sht 20

(b) Dead Load (non-superimposed) - non-composite state

As before, $M_{\text{support}} = 203 \text{ kNm}$, $M_0 = 344 \text{ kNm}$

$$\text{and } \delta_0 = \frac{19 \times 48.4 \times 13.5^3 \times 10^9}{384 \times 205 \times 27300 \times 10^4} + \frac{5 \times 0.75 \times 13.5^4 \times 10^9}{384 \times 205 \times 27300 \times 10^4} = 111 \text{ mm}$$

$$\text{Hence } \delta_c = 111 \left[1 - 0.6 \frac{(203 + 203)}{344} \right] = \underline{32.4 \text{ mm}}$$

$$\text{Span}/\delta_c = \frac{13500}{32.4} = 417 \sim \text{say } \underline{OK}$$

(Assuming a limit of 250 or 50mm whichever critical)



Job No.	Sheet 25 of	Rev.
Job Title	DESIGN EXAMPLE	
Subject	FLOOR Dynamic Sensitivity	
Client	Made by J.W.K.	Date
	Checked by	Date

DYNAMIC SENSITIVITY

Natural frequency of floor ~

consider secondary beam, for a beam loaded with a UDL

$$f = \frac{\pi}{2} \sqrt{\frac{g \cdot E_s \cdot I_c}{w \cdot L^4}}$$

where $g = 9.81 \text{ m/s}^2$, $L = \text{span} = 8.0 \text{ m}$

$E_s = \text{young's mod of steel} = 205 \times 10^6 \text{ kN/m}^2$

$w = \text{inertia load} = \text{dead} + \text{super dead} + 10\% \text{ imposed}$

ref
Design
Guide on
the Vibration
of Floors
by SCI
ch 5.1

(ch 4)

$$= (3.03 + 5 \times 0.1) \times 3.375 = 11.9 \text{ kN/m}$$

$$+ \text{Swb} = \underline{0.3 \text{ kN/m}}$$

$$\underline{\underline{12.2 \text{ kN/m}}}$$

$I_c = \text{composite 2nd moment of area using an effective width and the short term modulus}$
(= 10 for light wt. concrete)

B3750
pt 31
Table 1

App B3.1

$$I_c = I_x + \frac{B_e (D_s - D_p)^2}{12 \alpha_e} + \frac{A_f B_e (D_s - D_p) (D + D_s + D_p)^2}{4 (A_{f,e} + B_e (D_s + D_p))}$$

$$\text{but } B_e = \frac{8.0}{f} = 1.5$$



Job No.	Sheet 26 of	Rev.
Job Title	DESIGN EXAMPLE	
Subject	Floor Dynamic Sensitivity	
Client	Made by J.L.I.R.	Date
	Checked by	Date

$$\begin{aligned} \therefore I_c &= 4440 \times 10^4 + \frac{1500(130-51)^2}{12 \times 10} \\ &+ \frac{40 \times 10^2 \times 1500(130-51)(252+130+51)}{\{40 \times 10^2 + 1500(130-51)\}^2} \\ &= 23193 \text{ cm}^4 = 23193 \times 10^{-8} \text{ m}^4 \end{aligned}$$

$$\therefore f = \frac{\pi}{2} \sqrt{\frac{9.81 \times 205 \times 10^6 \times 23193 \times 10^{-8}}{12.2 \times 6^3}} = \underline{\underline{8.5 \text{ Hz}}}$$

consider natural frequency of slab ~

ref
SCI
Vibrations
Design
Guide
p35

In the absence of detailed calc,

$$\text{take } I_c = 1 \times 10^{-5} \text{ m}^4$$

$$\text{but } w = 3.03 + 5 \times 0.1 = 3.53 \text{ kN/m}$$

\(\therefore\) natural frequency based on 1m width,

$$f = \frac{\pi}{2} \sqrt{\frac{9.81 \times 205 \times 10^6 \times 1 \times 10^{-5}}{3.53 \times 3.275^3}} = \underline{\underline{10.4 \text{ Hz}}}$$

consider natural frequency of main beam ~

using inertia load deflection method

$$f = \frac{18}{\sqrt{\delta_{sw}}} \text{ where } \delta_{sw} = \text{max deflection due to inertia load}$$

as before, inertia load = dead + superdead + 0.1 \(\times\) imposed



Job No.	Sheet 27 of	Rev.
Job Title	DESIGN EXAMPLE	
Subject	Floor Dynamic Sensitivity	
Client	Made by J.W.K.	Date
	Checked by	Date

sht 19

loads from secondary beam

dead = 48.7 kN

superimposed dead = $0.7 \times 6.0 \times 3.375 = 14.2 \text{ kN}$

0.1x imposed = $0.1 \times 47 \times 6.0 \times 3.375 = 9.5 \text{ kN}$

72.1 kN

s.wt of main beam = 0.75 kN/m

Fixed End Moment = $\frac{5 \times 72.1 \times 13.5}{18} + \frac{0.75 \times 13.5^2}{12}$

= 316 kNm

sht 21

$M_{\text{support}} = \frac{\text{FEM} \times 4 \times 1.473}{(4 \times 1.473 + 1)} = 270 \text{ kNm}$

max free b.m, $M_0 = \frac{72.1 \times 13.5}{2} + \frac{0.75 \times 13.5^2}{2} = 504 \text{ kNm}$

As before, the mid-span deflection is given by

sht 23

$f_c = f_0 (1 - 0.6 (M_1 + M_2) / M_0)$

but $f_0 = \frac{19 \times 72.1 \times 13.5^3 \times 10^9}{32 \times 205 \times 75 \times 470 \times 10^4} + \frac{5 \times 0.75 \times 13.5^4 \times 10^9}{38 \times 205 \times 75 \times 470 \times 10^4} = 58.8 \text{ mm}$

$\therefore f_c = 58.8 \left(1 - \frac{0.6 \times 2 \times 270}{504} \right) = 21 \text{ mm}$

$\therefore f = \frac{18}{1.21} = 3.9 \text{ Hz} > 3.0 \text{ Hz} \therefore \text{OK}$

Vibrations
Design
Guide
ch 5.1

combined (floor) frequency is given by

$\frac{1}{10.4^2} + \frac{1}{8.5^2} + \frac{1}{3.9^2} = \frac{1}{f_0^2}$

$\therefore f_0 = 2.7 \text{ Hz} > 3.0 \text{ Hz} \therefore \text{floor frequency OK}$



Job No.	Sheet 22 of	Rev.
Job Title	DESIGN EXAMPLE	
Subject	Floor Dynamic Sensitivity	
Client	Made by J.W.K.	Date
	Checked by	Date

Vibrations
Design
Guide

ch 7.6

7.6

Table 7.1

Dynamic Response Factor ~

$$\text{for } f_0 < 7\text{Hz}, R = \frac{68000 C_f}{m \cdot S \cdot L_{\text{eff}} \cdot G}$$

where $m = \text{inertia floor mass (Kg/m}^2\text{)}$

$$= \left[\frac{12.2}{3.375} + \frac{0.75 \cdot 5.66}{6} \right] \times \frac{10^3}{9.81} = 381 \text{ Kg/m}^2$$

take $G = 0.03$ for open plan, well furnished floor.

for $3.0\text{Hz} < f_0 < 7\text{Hz}$, put $C_f = 0.7$

Floor Layout is case (3), $\therefore s = w = 12.5\text{m}$

$L_{\text{eff}} \sim$

main beam relative flexibility

$$= \frac{1}{f_{\text{main beam}}^2} \bigg/ \frac{1}{f_0^2} = \frac{1}{39^2} \bigg/ \frac{1}{35^2} = 0.805 > 0.6$$

$$\therefore L_{\text{eff}} = L^* = 3.8 \left[\frac{E \cdot I_b}{m \cdot b \cdot f_0^2} \right]^{\frac{1}{4}} > L (= 6.0\text{m})$$

The second moment of area of the secondary beam, I_b was found to be $19 \times 10^{-5} \text{m}^4$

$b = \text{secondary beam spacing} = 3.375\text{m}$

$$\therefore L_{\text{eff}} = 3.8 \left[\frac{205 \times 10^9 \times 19 \times 10^{-5}}{381 \times 3.375 \times 3.5^2} \right]^{\frac{1}{4}} = 26.8\text{m} > L_{\text{max}}, \text{ say,}$$

where $L_{\text{max}} = \text{building length in direction of secondary beams}$



Job No.	Sheet 27 of	Rev.
Job Title	DESIGN EXAMPLE	
Subject	Floor Dynamic Sensitivity	
Client	Made by J.W.R.	Date
	Checked by	Date

ref
SCI
Vibrations
Design
Guide
ch. 7.6

— " —
Table 7.2

∴ put $L_{eff} = 26.8m$

$$\text{hence } R = \frac{68000 \times 0.7}{381 \times 135 \times 26.8 \times 0.03} = \underline{\underline{6.6}}$$

Acceptance criteria -

for a general office, R should be ≤ 8

since $6.6 < 8$,

dynamic sensitivity satisfactory



Job No.	Sheet 30 of	Rev.
Job Title <i>DESIGN EXAMPLE</i>		
Subject <i>Main Beam Shear Connection Design</i>		
Client	Made by <i>J.W.R.</i>	Date
	Checked by	Date

MAIN BEAM SHEAR CONNECTION
(at ultimate loads)

Connector capacity for positive moments

$$Q_p = 0.8 Q_k \times K$$

Q_k for 19mm ϕ stud, 100mm high and $f_{cu} = 30 \text{ N/mm}^2$

$$Q_k = 100 \text{ kN} \times 90\% \text{ (for lightweight concrete)} = 90 \text{ kN}$$

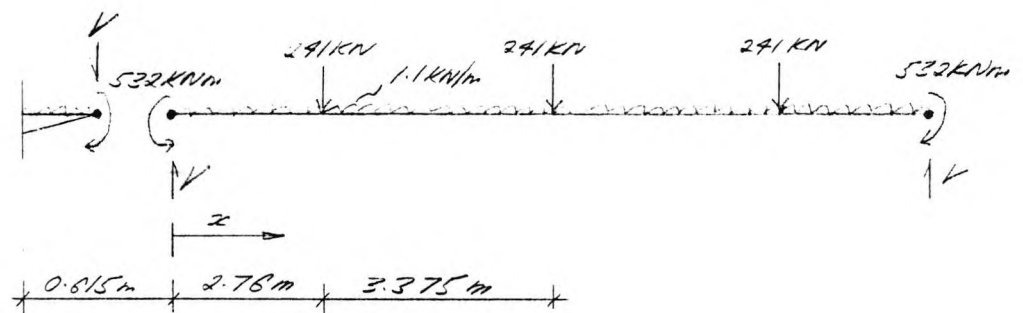
for ribs running parallel to the beam,

$$\frac{b_r / D_p}{\text{profile depth}} = \frac{\text{average trough width}}{\text{profile depth}} = \frac{110}{51} = 3.2 > 1.5$$

\therefore take $K=1$

$$\text{and } Q_p = 0.8 \times 90 = \underline{72 \text{ kN}}$$

Length of sagging region ~



$$V = \frac{3 \times 241 + 1.1 (13.5 - 2 \times 0.615)}{2} = 388 \text{ kN}$$



Job No.	Sheet 31 of	Rev.
Job Title DESIGN EXAMPLE		
Subject Main Beam Shear Connection Design		
Client	Made by J.W.R.	Date
	Checked by	Date

Moment under 1st point load ~

$$M_{oc} = 532 + \frac{1.1 \times 2.76^2}{2} - 368 \times 2.76 = -479 \text{ kNm}$$

st 10

M_x at centre = -921 kNm

Point of contraflexure ~

$$532 + \frac{1.1x^2}{2} - 368x = 0$$

$$\therefore 0.55x^2 + 368x + 532 = 0$$

$$x = \frac{368 \pm \sqrt{368^2 - 4 \times 0.55 \times 532}}{2 \times 0.55}, \therefore x = 1.75 \text{ m}$$

\therefore length of sagging region

$$= 13.5 - 2(0.615 + 1.75) = \underline{9.37 \text{ m}}$$

Number of connectors required for full interaction = $(R_c \text{ or } R_s) / 72$, whichever less

st 9

$$\text{Hence } n_c = \frac{2520}{72} = 35, \text{ say } 36 \text{ each side, but}$$

$$\text{try equal spacing} = \frac{9370}{2 \times 36} = 130 \text{ mm}$$

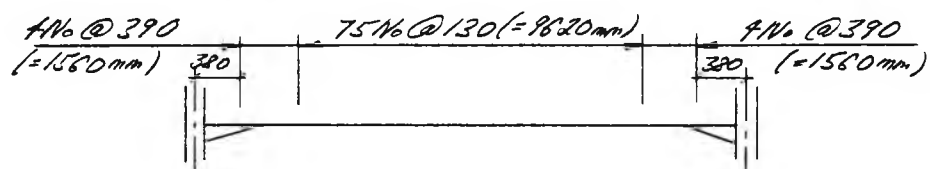
cl 5.7.2.1

check min spacing ~ $5d = 5 \times 19 = 95 \text{ mm} < 130 \text{ mm}$

check max spacing in hogging region

$$\sim 4d_s = 4 \times 130 = 520 \text{ mm}$$

\therefore provide connectors as follows ~



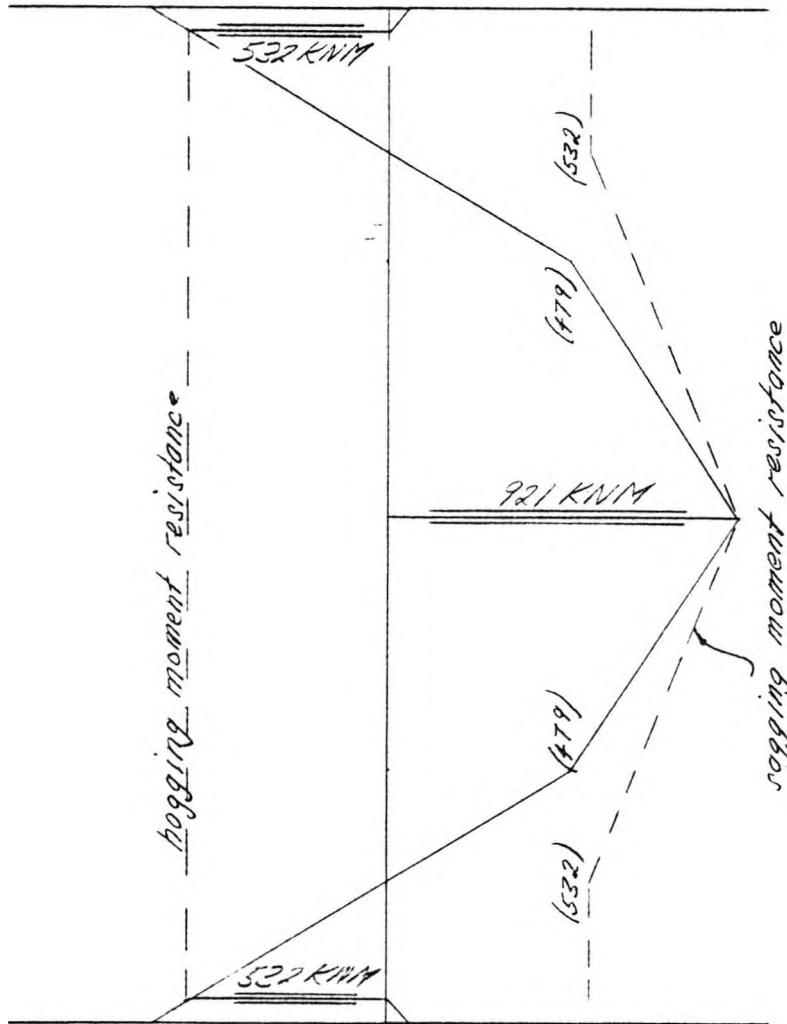
The Steel Construction Institute



Silwood Park Ascot Berks SL5 7QN
 Telephone: (0344) 23345
 Fax: (0344) 22944

CALCULATION SHEET

Job No.	Sheet 32 of	Rev.
Job Title <i>DESIGN EXAMPLE</i>		
Subject <i>Main Beam Shear Connection Design</i>		
Client	Made by <i>J.W.R.</i>	Date
	Checked by	Date



MAIN BEAM PLASTIC DESIGN MOMENTS AND RESISTANCES



Job No.	Sheet 33 of	Rev.
Job Title <i>DESIGN EXAMPLE</i>		
Subject <i>Main Beam Lateral Stability</i>		
Client	Made by <i>J.W.R.</i>	Date
	Checked by	Date

MAIN BEAM LATERAL STABILITY

(a) Construction condition (non-composite)

(i) hogging moment region ~ check length between column and outer secondary beam

check $\bar{M} \leq M_b$ where $\bar{M} = m \cdot M_A$

put $m=1$, assume the maximum moment occurs at the haunch toe and that the haunch is at yield throughout its length

sht 16

Haunch toe moment = $M_H = 270 \text{ kNm} = \bar{M}$

BS5950

Find $\lambda_{LT} = n \cdot u \cdot r \cdot c \cdot \lambda$, hence P_b , then $M_b = S_x \cdot P_b$

pt.1
4.2.1.5
& 6.3.3

Use method of BS5950 pt.1 chapt.6.3.3 because it allows for tapered sections and has a generalised method for calculating 'n'. Clearly 'r' should not be calculated by assuming lateral restraint to the tension flange in this case because with the decking spanning parallel to the main beam, little restraint is provided

pt.1
6.3.6.1

$n_t \sim$

For simplicity and to be conservative, assume

$N_1 \rightarrow N_2$ are stresses and $M_1 \rightarrow M_2$ are p_y . Also assume that the stress varies linearly between the haunch



Job No.	Sheet 34 of	Rev.
Job Title	DESIGN EXAMPLE	
Subject	Main Beam Lateral Stability	
Client	Made by J.V.R.	Date
	Checked by	Date

sht 17

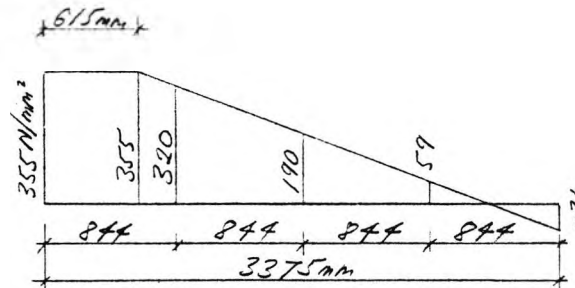
and the outer secondary beam.

Moment at outer secondary beam

$$= 352 - 134 \times 3.375 + \frac{1.1 \times 3.375^2}{2} = -94 \text{ kNm}$$

$$\text{flange stress} = \frac{94 \times 10^6}{1320 \times 10^3} = -71 \text{ N/mm}^2$$

stress diagram ~



$$\text{Then } \frac{M_1}{M_2} = 1.0 = \frac{M_E}{M_L}, \quad \frac{M_2}{M_3} = \frac{320}{355} = 0.9 = \frac{M_4}{M_5}$$

$$\text{and } \frac{M_3}{M_4} = \frac{190}{355} = 0.535, \quad \frac{M_4}{M_5} = \frac{59}{355} = 0.166$$

$$\frac{M_5}{M_5} < 0 \quad \therefore \frac{M_5}{M_5} = 0$$

$$\text{Hence } n_L = \sqrt{\frac{1}{12} \left\{ 1.0 + 3 \times 0.9 + 4 \times 0.535 + 3 \times 0.166 + 0 + 2 \frac{0.9 - 1.0}{0.9} \right\}}^{\frac{1}{2}}$$

$$\therefore n_L = 0.727$$

u ~ take properties at haunch toe $\therefore u = 0.881$



Job No.	Sheet 35 of	Rev.
Job Title	DESIGN EXAMPLE	
Subject	Main Beam Lateral Stability	
Client	Made by J.W.R.	Date
	Checked by	Date

BS5950
pt 1
4.3.7.5

$v \sim$ assume no restraint to tension flange and for properties at haunch toe, with equal flanges,

$$N=0.5, \lambda = L_E / I_y = \frac{1.0 \times 3375}{40.3} = 83.7$$

pt 1
Table 14

$$\lambda / \lambda_c = \frac{83.7}{27.6} = 3.03 \quad \therefore v = 0.91$$

pt 1
6.2.3

$$C \sim = 1 + \frac{3}{(x-9)} (R-1) q^{\frac{2}{3}}$$

$$R=2, q = \frac{0.615}{3.275} = 0.182$$

$$\therefore C = 1 + \frac{3}{27.6-9} (1) \times 0.182^{\frac{2}{3}} = 1.07$$

pt 1
Table 11

$$\text{Hence } \lambda_{LT} = 0.727 \times 0.881 \times 0.91 \times 1.07 \times 83.7 = 52.2$$

$$\therefore p_b = 287 \text{ N/mm}^2$$

$$\text{and } M_1 = \frac{1500 \times 287}{10^3} = \underline{\underline{426 \text{ kNm}}}$$

since 426 kNm > 270 kNm, hogging stability OK

(iv) sagging region ~ (considered since beam assumed unrestrained along top flange)

check between centre and outer secondary beams ~

For simplicity, take $m=1$ and $n=1$

$$\text{hence } \bar{M} = \text{max span b.m} = 295 \text{ kNm}$$

$$\text{but } \lambda_{LT} = n.u.v.\lambda = 1.0 \times 0.881 \times 0.91 \times 83.7 = 67$$

$$\therefore p_b = 232 \text{ N/mm}^2$$

sht 17

pt 1
Table 11



Job No.	Sheet 32 of	Rev.
Job Title DESIGN EXAMPLE		
Subject Main Beam Lateral Stability		
Client	Made by J.L.R.	Date
	Checked by	Date

$$\therefore M_b = \frac{1500 \times 232}{10^3} = \underline{348 \text{ kNm}}$$

since 348 kNm > 245 kNm, sagging stability OK

(b) Ultimate In-Service condition (composite)
hogging moment region (only since compression
flange fully restrained in sagging region in this state)

A hinge occurs at the haunch toe which is assumed
to be fully restrained by two full depth web
stiffeners providing torsional and lateral rigidity
in conjunction with the cutting flange and floor
slab.

Hence check between haunch toe and outer
secondary beam.

check $\frac{\bar{M}}{M_b} \leq 1$, where $\bar{M} = m_f \cdot M_a$

put $m_f = 1$ as before, hence find $\lambda_{TE} = 116.4 \text{ U.V.E. c. } \lambda$

This elastic check is valid despite the hinge
at one end since it is more onerous than the plastic
check and because the spread of plasticity away
from the hinge is limited by the rapid decrease
in moment.

pt 1
G.2(a)

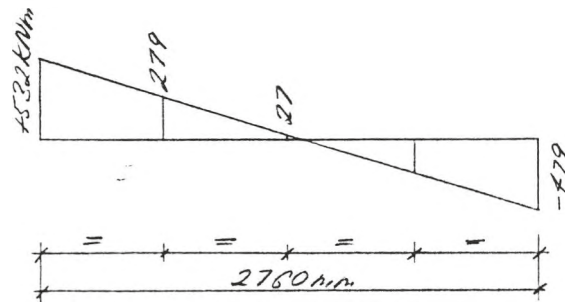
pt 1
G.3.3



Job No.	Sheet 37 of	Rev.
Job Title	DESIGN EXAMPLE	
Subject	Main Beam Lateral Stability	
Client	Made by J.W.H.	Date
	Checked by	Date

$n_L \sim$ For simplicity assume a linear b.m diagram between restraints.

b.m. diagram \sim



$$\frac{M_1}{M_1} = 1.0 = \frac{M_4}{M_4}, \quad \frac{M_2}{M_2} = \frac{27.9}{53.2} = 0.527 = \frac{M_5}{M_5}, \quad \frac{M_3}{M_3} = \frac{27}{53.2} = 0.051$$

$$\frac{M_4}{M_4} = \frac{M_5}{M_5} = 0$$

$$\therefore n_L = \sqrt{\frac{L}{12} \left[1.0 + 3 \times 0.527 + 4 \times 0.051 + 0 + 2(0.527 - 1) \right]}$$

$$\therefore n_L = 0.98$$

$$u = 0.881$$

$n_L \sim$ assuming lateral and torsional restraint is provided to the tension flange by the slab

$$\text{then } n_L = \frac{1}{\left\{ 1 + \frac{1}{40} \left(\frac{L}{2} \right)^2 + \frac{1}{16} \left(\frac{L}{D} \right)^3 \frac{I_w \cdot L_n}{I_y} \right\}^{\frac{1}{2}}}$$

compare $L = 2760 \text{ mm}$ with $L_{cr} = 3.74 I_y^{0.25} (D/t_f)^{0.75}$

$$\therefore L_{cr} = 3.74 (1540 \times 10^4)^{0.25} (10.8/9.7)^{0.75} = 3907 \text{ mm}$$

since $L < L_{cr}$, $L_n = L$

Ref
Hunched
Composite
Beam
Design Guide



Job No.	Sheet 3 rd of	Rev.
Job Title	DESIGN EXAMPLE	
Subject	Main Beam Lateral Stability	
Client	Made by	Date
	Checked by	Date

$$I_w = \frac{t^3}{12} = \frac{9.7^3}{12} = 76 \text{ mm}^4, \quad \lambda = \frac{2760}{40.3} = 68.5$$

$$\gamma_{lx} = \frac{68.5}{27.6} = 2.48, \quad \frac{I_w \cdot L_n}{I_y} = \frac{76 \times 2760}{1540 \times 10^4} = 0.013$$

$$\therefore \eta_x = \frac{1}{\left\{ 1 + \frac{1}{40} (2.48)^2 + \frac{1}{16} \left(\frac{2760}{412.8} \right)^2 \times 0.013 \right\}^{\frac{1}{2}}} = 0.85$$

$$c \approx c = 1.0$$

$$\therefore \lambda_{TR} = 0.48 \times 0.881 \times 0.85 \times 1.0 \times 68.5 = 27.6$$

Since $27.6 < 30$, $p_b = p_y$, hence $M_b = M_p = 532 \text{ kNm} = \bar{M}$

∴ no additional restraint required

pt 1
Table 11



Job No.	Sheet 37 of	Rev.
Job Title	DESIGN EXAMPLE	
Subject	Main Beam Longitudinal Shear Check	
Client	Made by J.W.R.	Date
	Checked by	Date

MAIN BEAM LONGITUDINAL SHEAR CHECK

Applied shear from shear connectors (sagging region only since hogging region non-composite) ~

c/5.6.2

$$v = N Q_p / s = 1 \times 72 / 0.13 = 554 \text{ kN/m}$$

For no transverse reinforcement, the resistance of the concrete flange is given by

5.6.3

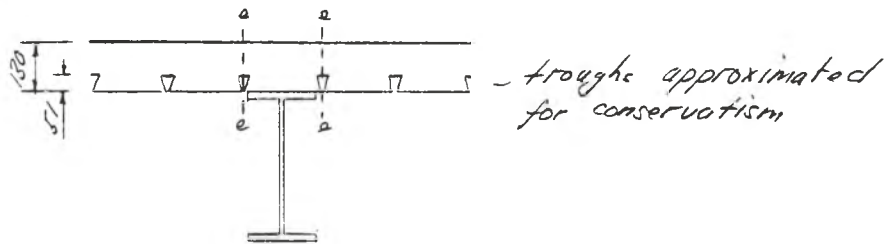
$$v_r = 0.03 \eta A_{cv} f_{cu} + v_p$$

Ignore contribution of sheeting because of edge laps

$$\therefore v_p = 0$$

Area of critical concrete planes, $A_{cv} \sim$

Fig 7(d)



$$A_{cv} = 2(130 - 51) = 158 \text{ mm}^2/\text{mm}$$

$$\therefore v_r = 0.03 \times 0.8 \times 158 \times 30 \times \frac{10^3}{10^3} = 114 \text{ kN/m}$$

check limit of flange resistance ~

$$= 0.8 \eta A_{cv} \sqrt{f_{cu}} + v_p = 0.8 \times 0.8 \times 158 \sqrt{30} \times \frac{10^3}{10^3} = 554 \text{ kN/m}$$



5.6.3

∴ Transverse steel must resist $557 - 117 = 440 \text{ kN/m}$

∴ $440 \times 10^3 = 0.7 A_{sv} f_y$, put $f_y = 460 \text{ N/mm}^2$

∴ $A_{sv} = \frac{440 \times 10^3}{0.7 \times 460} = 1388 \text{ mm}^2$

But for two failure planes, $A_{sv} = 2A_t$

hence $A_t = 683 \text{ mm}^2/\text{m}$

But fire mesh = $193 \text{ mm}^2/\text{m}$, ∴ additional required

= $683 - 193 = 490 \text{ mm}^2/\text{m}$

Try T16's @ 390 ctrs ~

$A_{sv} = \frac{\pi \times 16^2}{4} \times \frac{1000}{390} = 516 \text{ mm}^2/\text{m} > 490 \text{ mm}^2/\text{m}$ ∴ OK

Curtailment ~

Resistance of mesh alone = $\frac{0.7 \times 2 \times 193 \times 460}{10^3} = 127 \text{ kN/m}$

Resistance of mesh + concrete = $127 + 117 = 238 \text{ kN/m}$

Try staggered reinf arrangement ~

hence resistance of T16's @ 780

= $\frac{0.7 \times 2 \left(\frac{516}{2}\right) \times 460}{10^3} = 166 \text{ kN/m}$

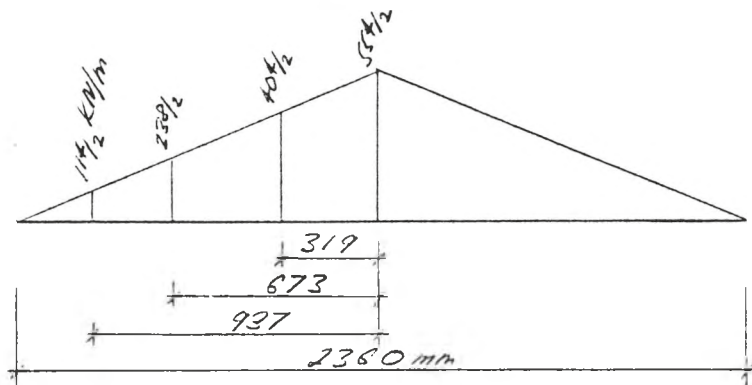
∴ Resistance of concrete + mesh + T16's @ 780

= $117 + 127 + 166 = 407 \text{ kN/m}$

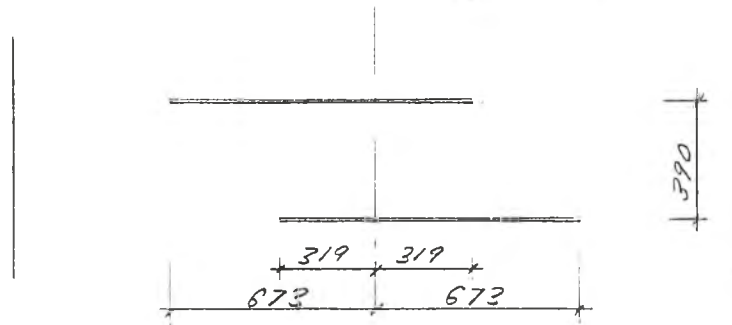


Job No.	Sheet 1 of	Rev.
Job Title <i>DESIGN EXAMPLE</i>		
Subject <i>Main Beam Longitudinal Shear Check</i>		
Client	Made by <i>J.L.R.</i>	Date
	Checked by	Date

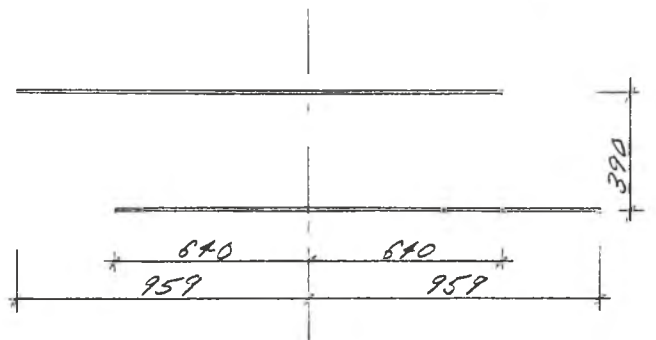
Hence shear force diagram for the slab is ~



Reinforcement arrangement ignoring anchorage ~



By considering the more onerous of adding 12ϕ for nominal end anchorage and 40ϕ for full end anchorage, the minimum lengths are thus



Hence provide T16's x 1600Lg @ 390 ctrs staggered at 640 mm from slab centre-line

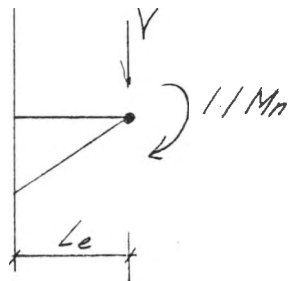


Job No.	Sheet 42 of	Rev.
Job Title	DESIGN EXAMPLE	
Subject	Haunch and Haunch Connection Design	
Client	Made by J.L.K.	Date
	Checked by	Date

HAUNCH AND HAUNCH CONNECTION DESIGN

To be conservative, haunch is designed to remain elastic when haunch toe moment = $1.1 M_n$, where M_{nc} = hinge moment resistance.

ref sht 30



$$\begin{aligned} \text{Design moment} &= 1.1 M_n + Y \cdot L_e \\ &= 1.1 \times 532 + 368 \times 0.615 \\ &= \underline{\underline{816 \text{ KNm}}} \end{aligned}$$

Try total haunch depth, $D_h = 2D$, ie 810mm

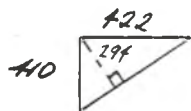
The elastic haunch strength, M_{he} is given approximately by

ref
Haunched
Beam
Design
Guide

$$\frac{M_{he}}{M_s} = 0.17 \left(\frac{D_h}{D} \right)^2 + 0.7 \left(\frac{D_h}{D} \right) \text{ where } M_s = M_p \text{ steel beam}$$

$$\therefore M_{he} = \left[0.17(2)^2 + 0.7(2) \right] \times 532 = 1107 \text{ KNm}$$

Since $1107 \text{ KNm} > 816 \text{ KNm}$, \therefore 810mm depth OK
check whether cutting can be made from beam section
cutting length, L_c , = $615 - \frac{327}{2} - 30 \text{ pt(say)} \approx 222 \text{ mm}$



$$\text{check } 413 - 16 - 10_{\text{cut(say)}} = 387 \text{ mm} > 294 \text{ mm} \therefore \text{OK}$$

Use 40 x 422 dp cutting ex 408 x 178 UBF grade 50



Job No.		Sheet 43 of	Rev.
Job Title DESIGN EXAMPLE			
Subject Haunch and Haunch Connection Design			
Client	Made by	Date	
	Checked by	Date	

Connection Design ~

sh 42

Design moment = 816 kNm

ref
BS 5950

Try M27 Grade 8.8 bolts

p 1
6.3.6.1

Tension capacity $P_t = p_t \cdot A_t = \frac{450 \times 353}{10^3} = 159 \text{ kN}$

—
6.3.2

Shear capacity $P_s = p_s \cdot A_s = \frac{375 \times 353}{10^3} = 132 \text{ kN}$

minimum spacing down web is limited by strength of web such that

$$e_{\min} \times t_w \times p_y = 2 \times \text{bolt force}$$

$$\therefore e_{\min} \times 9.7 \times 355 = 2 \times 159 \times 10^3$$

$$\therefore e_{\min} = 92 \text{ mm} = \text{min spacing}$$

Try an 2 bolt tension group with a 4 bolt shear group.

sh 42

Shear capacity = $4 \times 132 = 528 \text{ kN} > 368 \text{ kN} \therefore \text{OK}$

ref
Haunched
Beam
Design
Guide

The following bolt force profile and moment capacity has been calculated by solving the equilibrium equations - see over



Job No.	Sheet 75 of	Rev.
Job Title DESIGN EXAMPLE		
Subject Haunch and Haunch Connection Design		
Client	Made by J.W.K.	Date
	Checked by	Date

ref
Haunched
Beam Design
Guide
P.70

End plate ~ design by yield line analysis

Consider top 4 bolts, yield line pattern in Design Guide

$$a = 70\text{mm}, b = 50\text{mm}, c = 70 - 10/2 = 65\text{mm}$$

$$\text{check } 1.7b = 85\text{mm} > a \quad \therefore \text{OK}$$

$$n = (300 - 140) / 2 = 80\text{mm}$$

$$\text{check } c + 1.4b + a = 65 + 70 + 70 = 205\text{mm} > 0.5B_e \quad \therefore \text{OK}$$

The plate moment of resistance, m_p is given by

$$F \leq 2m_p \left(\frac{a+b}{c} + \frac{c+n}{b} \right) = \left(\frac{70+50}{65} + \frac{65+80}{50} \right) = 9.5m_p$$

Now $F = 159\text{KN}$ and try G43 plate with modulus

$\frac{t^2}{5}$ /unit width (to allow for prying uncertainties)

$$\therefore \frac{t^2}{5} \times 265 \times 9.5 \geq 159 \times 10^3$$

$$\therefore t \geq \sqrt{\frac{159 \times 10^3 \times 5}{265 \times 9.5}} \quad \text{ie } t \geq \underline{17.8\text{mm}}$$

— 11 —

Consider 3rd row of bolts ~ yield line pattern in Guide

$$e = 100\text{mm}, m = 64\text{mm}$$

$$F \leq \frac{2m_p \cdot e}{m} = \frac{2m_p \cdot 100}{64} = 3.1m_p$$

$$\text{but } F = 137\text{KN}, \therefore t \geq \sqrt{\frac{137 \times 10^3 \times 5}{265 \times 3.1}} \quad \text{ie } t \geq \underline{28.8\text{mm}}$$

USE 30mm thick plate G43



Job No.	Sheet 75 of	Rev.
Job Title JELMAN EXAMPLE		
Subject Haunch and Haunch Connector Design		
Client	Made by J.W.R.	Date
	Checked by	Date

ref
BS5950
pt 1
Table 38

Beam to End plate welds ~

weld design strength p_w using E43 electrode
= 215 N/mm²

Top flange weld ~

min leg req'd for fillet weld = $\frac{F \times 159 \times 10^3}{2 \times 180 \times 215 \times 0.7} = 11.7 \text{ mm}$

Provide 12mm F.W to top flange

Beam web weld ~

— " —
cl 6.6.5.1

min leg to achieve web strength assuming weld
strength = 265 N/mm² (E43 30thk plate)

$$= \frac{9.7}{2 \times 0.7} \times \frac{355}{265} = 9.3 \text{ mm}$$

but for $F = 159 \text{ kN}$, check bolt load spread
= $2 \times 70 \times \tan 60^\circ = 242 \text{ mm} > 100 \text{ mm}$ vertical spacing

$$\therefore \text{min leg} = \frac{2 \times 159 \times 10^3}{2 \times 0.7 \times 100 \times 265} = 8.6 \text{ mm}$$

find limiting bolt force for nominal 8mm F.W

$$= \frac{6}{8.6} \times 159 = 111 \text{ kN} < 114 \text{ kN}$$

ref sbt 44

Provide 10mm f.w to top 300mm of beam web
and 8mm f.w to remainder



Job No.	Sheet 17 of	Rev.
Job Title DESIGN EXAMPLE		
Subject Haunch and Haunch Connection Design		
Client	Made by J.W.R.	Date
	Checked by	Date

Cutting flange to end plate weld -

to be conservative,

provide full strength butt weld

Cutting web to beam flange weld -

sheet 12

$$\text{cutting length, } L_c = 722\text{mm} \quad \therefore L_c = \frac{722}{412.8} \approx D$$

$$\text{toe angle, } \theta = \tan^{-1}(410/412.8) = 44.2^\circ$$

$$\text{haunch depth ratio, } h_o/D = (412.8 + 410)/412.8 \approx 2$$

ref
JWR's
PhD thesis

\therefore use design method referred to.

stress in beam flange just beyond haunch toe,

$$\sigma = p_y = 355\text{N/mm}^2$$

max design shear stress, τ , at toe

$$= \sigma(0.12 \tan \theta + 0.2)$$

$$= 355(0.12 \times \frac{410}{722} + 0.2) = 112\text{N/mm}^2$$

(based on effective weld thickness = web thickness)

ref
BS5950
pt. 1
6.6.5.1

but, design strength of E 43 electrode = 215 N/mm²

and cutting web thickness = 9.7mm

$$\therefore \text{min throat thickness req'd} = \frac{112 \times 9.7}{215} = 5.1\text{mm}$$



Job No.	Sheet 72 of	Rev.
Job Title DESIGN EXAMPLE		
Subject Haunch and Haunch Connection Design		
Client	Made by J.W.R.	Date
	Checked by	Date

for 2x6mm fillet welds ~

$$\text{throat thickness} = 2 \times 6 \times 0.7 = 8.4 \text{ mm} > 5.1 \text{ mm}$$

~ provide symmetric 6mm f. welds

Cutting toe weld ~

Design force = $0.7 F_0$, where F_0 = force in beam flange at haunch toe

$$\therefore \text{design force} = \frac{0.7 \times 355 \times 179.7 \times 16.0}{10^3} = 719 \text{ kN}$$

minimum leg length for a one-sided fillet weld using a E43 electrode

$$= \frac{719 \times 10^3}{179.7 \times 215 \times 0.7} = 26.9 \text{ mm} !$$

by inspection,

provide a full strength butt weld

ref
J.W.R.
PhD thesis



Job No.	Sheet 49 of	Rev.
Job Title DESIGN EXAMPLE		
Subject Column Stiffening Check:		
Client	Made by J.V.R.	Date
	Checked by	Date

COLUMN STIFFENING CHECKS

Column flange bending ~

Using yield line analysis, assume that the combined axial and bending stress based on linear interaction

$> p_y$, hence the interaction factor μ on the horizontal components of yield line strength (where $\mu = 1 - (\frac{p}{p_y})^2$) is less than zero.

\therefore neglect horizontal components of yield lines

Consider 2nd row of bolts, yield line pattern in Design Guide assuming tension stiffeners

for $\mu=0$, the condition is given for a single bolt force $F \leq 2m_p' \frac{(f+0.5e)}{m'}$

where $f = 50 + \frac{(10-12)}{2} = 52\text{mm}$, $e=100\text{mm}$, $F=159\text{KN}$

also $m' = 70 - \frac{15.7}{2} = 62\text{mm}$

take the plastic modulus of the column flange

$m_p' = \frac{t^2}{5} \cdot p_y$, for grade 43 end plate ~

$$\therefore 67 \sqrt{\frac{159 \times 10^3 \times 5}{345} \cdot \frac{62}{2(52+0.5 \times 100)}} = \underline{26.5 \text{ mm}}$$

ref
Haunched
Beam
Design
Guide
p.74

— " —



Job No.	Sheet 50 of	Rev.
Job Title <i>DESIGN EXAMPLE</i>		
Subject <i>Column Stiffening Checks</i>		
Client	Made by <i>J.L.R.</i>	Date
	Checked by	Date

ref
Haunched
Beam
Design
Guide
P 76

Consider 3rd row of bolts, yield line pattern in Design Guide

the condition is $F \leq \frac{2m_p \cdot c}{m'}$, $F = 137 \text{ kN}$

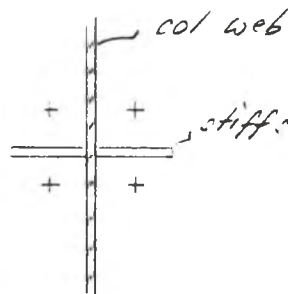
$$\therefore t \geq \sqrt{\frac{137 \times 10^3 \times 5 \cdot 82}{345 \cdot 2 \times 100}} = \underline{\underline{26.8 \text{ mm}}}$$

The former check is critical but although 26.7mm > 25.0mm (flange thickness), say no further stiffening required

Column tension stiffeners ~

provide tension stiffeners between top two rows of bolts to ensure equalisation of bolt forces at ultimate loads.

NR col web unlikely to be critical since normally thicker than beam web



Try grade F3 stiffeners, assume each stiffener attracts 10% bolt load.



Job No.	Sheet 51 of	Rev.
Job Title	DESIGN EXAMPLE	
Subject	Column Stiffening Checks	
Client	Made by J.W.R.	Date
	Checked by	Date

$$\therefore \text{min area per stiffener req'd} = \frac{159 \times 10^3}{275} = 578 \text{ mm}^2$$

but provide 100x10thk full depth stiffeners: 6x2

min leg length for weld to web

$$= \frac{159 \times 10^3}{(327 - 2 \times 25) \times 215 \times 0.7} = 38 \text{ mm}$$

but provide 6mm f.w.

column compression zone ~

bearing check on load from cutting flange ~

bearing load = 1151 kN

$$\text{capacity} = (b_1 + n_2) t P_{yw}$$

b_1 = cutting flange thickness + 2x plate thickness

$$= 16 + 2 \times 25 = 66 \text{ mm}$$

n_2 = 2x 2.5x (col flange thickness + root radius)

$$= 2 \times 2.5 (25 + 152) = 201 \text{ mm}$$

$$\therefore \text{capacity} = \frac{(66 + 201) \times 15.7 \times 375}{10^3} = 1746 \text{ kN} > 1151 \text{ kN} \quad \text{OK}$$

buckling check ~

$$\text{capacity } P_w = (b_1 + n_1) t p_c$$

$$n_1 = \frac{2 \times 327}{2} = 327 \text{ mm}$$

ref
BS5950
pt 1
Table 36

clt 11

ref
BS5950
pt 1
cl 7.5.3

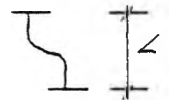
— " —
cl 7.5.2.1



Job No.	Sheet 52 of	Rev.
Job Title	DESIGN EXAMPLE	
Subject	Column Stiffening Check:	
Client	Made by J.W.R.	Date
	Checked by	Date

p_c ~ although no lateral restraint at this level
it is in close proximity to the floor slab

∴ assume the following condition



$$L_E = 1.2L$$

$$\lambda = \frac{1.2 \times 2.5d}{0.7} = \frac{1.2 \times 2.5 \times 15.7}{0.7} = 67$$

$$\therefore p_c = 270 \text{ N/mm}^2$$

$$\therefore p_w = \frac{(66 + 327) \times 15.7 \times 270}{10^3} = 1666 \text{ KN} > 1151 \text{ KN} \text{ : OK}$$

However to provide torsional restraint to the
column flange and hence through the haunch flange
to the haunch too,

provide 100 x 10 thick full depth stiffeners G.F.3

Column shear panel ~

$$\text{shear load } F_v = 1151 \text{ KN}$$

$$\text{shear capacity } P_v = 0.6 p_y A_v$$

$$= \frac{0.6 \times 15.7 \times 327.2 \times 345}{10^3} = 1063 \text{ KN}$$

since $1151 \text{ KN} > 1063 \text{ KN}$, web is inadequate and
doubler plates are required

$$\text{limit force in web to } 0.6 P_v = 0.6 \times 1063 = 638 \text{ KN}$$

$$\therefore \text{doubler plate thickness} = \frac{(1063 - 638) \times 10^3}{0.6 \times 255 \times 327.2}$$

provide 6mm thick web doubler plate



Job No.	Sheet 53 of	Rev.
Job Title	DESIGN EXAMPLE	
Subject	Haunch Toe Web Stiffener Design	
Client	Made by J.W.R.	Date
	Checked by	Date

BEAM WEB STIFFENING AT HAUNCH TOE

ref
J.W.R.
PhD Thesis

Total design force in web stiffeners

$$= F_0 \sqrt{(1 - \cos \theta) / 3}$$

$$= \frac{355 \times 179.7 \times 15}{10^3} \sqrt{(1 - 0.717) / 3}$$

$$= 312 \text{ kN}$$

Sheet:
47 & 48

min area for bearing ~ (grade 43 stiffs)

$$= \frac{0.8 F_x}{P_y} = \frac{0.8 \times 312 \times 10^3}{275} = 910 \text{ mm}^2$$

R35950
pt 1
4.5.4.2

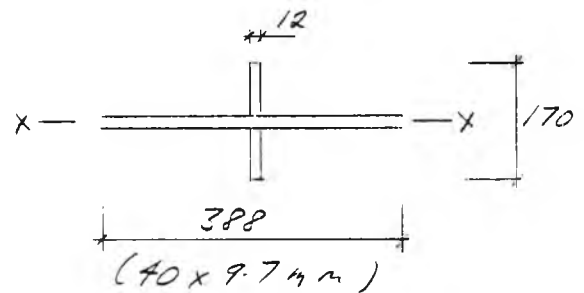
try 2 No. 80x12 thick g.43 stiffs ~

$$\text{area} = 2 \times 80 \times 12 = 1920 \text{ mm}^2 > 910 \text{ mm}^2$$

stiffener buckling check -

4.5.4.1

effective section



$$I_{xx} \approx \frac{12 \times 170^3}{12} = 4913 \times 10^3 \text{ mm}^4$$

$$A = 1920 + 9.7 \times 388 = 5689 \text{ mm}^2$$

$$t_{xy} = \sqrt{\frac{I}{A}} = \sqrt{\frac{4913 \times 10^3}{5689}} = 29.7 \text{ mm}$$

The
Steel Construction
Institute



Silwood Park Ascot Berks SL5 7QN
Telephone: (0344) 23345
Fax: (0344) 22944

CALCULATION SHEET

Job No.	Sheet 54 of	Rev.
Job Title <i>DESIGN EXAMPLE</i>		
Subject <i>Haunch Top Web Stiffener Design</i>		
Client	Made by <i>J.W.R.</i>	Date
	Checked by	Date

$$\frac{L_e}{r_{xx}} = \frac{361}{29.7} = 12.2, \text{ clearly OK}$$

∴ provide 2 No. 80x12 thick stiffeners G. 42